

# **A comparison of different test and analysis methods for asphalt fatigue**

Cinzia Maggiore

Thesis submitted to the University of Nottingham for the degree of  
Doctor of Philosophy

December 2014

*Nothing in life is to be feared,  
it is only to be understood.  
Now is the time to understand more,  
so that we may fear less.*

**Marie Skłodowska-Curie**

# Abstract

Flexural fatigue is one of the main failure modes in asphalt mixtures and flexible pavement structures, so a good prediction of the fatigue life of the pavement will help to develop and improve pavement design procedures. Fatigue is a process of cumulative damage and one of the major causes of cracking in asphalt pavements. Various factors affect the fatigue behaviour such as: the method of construction (compaction), the loading (axle loads, modes and patterns), the rest periods (healing effect), the material characteristics, and finally traffic and environmental variables (temperature, ageing, healing, etc.).

The primary research goal of this project is to understand better the fatigue phenomenon in asphalt materials. Several approaches such as phenomenological approach, fracture mechanics, dissipated energy methods have been developed in research. After reviewing and critiquing the current literature about fatigue in pavement engineering, this research project focused on dissipated energy approaches because they take into account the evolution of the material during a fatigue test; a comparison between the traditional method (phenomenological approach) and several dissipated energy methods was made by using statistical analysis. The findings from the literature review showed a lack of statistical analyses when different sets of data, and therefore regression lines, are compared. Therefore, the second goal of this research project has been to introduce statistical knowledge to pavement engineering by presenting a wider range of techniques for the analysis of different data sets. Due to lack of information in pavement engineering, statistics was involved in this study. Statistics includes the design of biological experiments, the collection, the analysis and the interpretation of data; understanding and introducing the appropriate technique to analyse fatigue data in pavement engineering was one of the main challenges in this project. Commonly, multiple comparisons are made by employing the *Student t test*; depending on the data and on the hypothesis there is a high chance to get a mistaken answer, and therefore a mistaken analysis and findings. This

thesis presents several multiple comparison procedures that properly suits comparison of several sets of fatigue data in different situations.

Statistical analysis showed that, although regression lines of different sets of data look different (graphically regression lines do not match between each other), in many cases they are characterised by the same slope and elevation: that means they could be represented by the same fatigue regression line (statistically the findings are the same when different methods are used). This was the case when different dissipated energy approaches were compared with the traditional approach ( $N_f, 50$ ); dissipated energy methods graphically show different fatigue life values because the definition of failure is different for each method; statistically in the majority of cases the different methods are giving a similar answer: that is the transition point from micro to macro cracking. Thus, a phenomenological failure criterion still represents an easy and quick way to determine the failure point.

Further research investigation involved the understanding of fatigue testing machines; do they give the same answer in terms of fatigue? This project gives an answer comparing simple flexural tests (such as 2 Point Bending and 4 Point Bending) with diametral fatigue tests (such as Indirect Tensile Fatigue Test). In the first category, the stress or the strain is applied with sinusoidal waveform until the specimen reaches the failure point; this kind of test is also known as a *pure* fatigue test. In the second category, the stress or the strain is applied using pulsating loads in a diametral direction; it tends to underestimate fatigue life in asphalt pavements because the test is characterised by an accumulation of permanent deformation during a test. Of course, different categories of tests give different answers (fatigue life values); so which one best represents the real world?

The main innovative contribution of this thesis is the development of a new fatigue test: Indirect Tensile Fatigue Test (ITFT) in strain controlled mode. It is a simple fatigue test with widespread use in the United Kingdom due to the fact that it is a simple test, easily suitable for cylindrical specimens manufactured in the laboratory or cored from a flexible pavement; this is one of the reasons why it is often used by civil engineering firms to characterise the stiffness and fatigue properties of asphalt materials mostly for construction and maintenance sites.

Researchers usually tend to use strain control mode to evaluate mixes for thin pavements (thickness of asphalt layers less than 50 mm); stress control mode for thicker and relatively stiffer structures (thickness of asphalt layers greater than 150 mm). Currently, the Indirect Tensile Test characterises the behaviour of asphalt material under repeated constant load; so no ITFT data obtained in strain control mode exists. To overcome this lack, the ITFT was developed in strain control mode; this allows comparing of results between simple flexural tests and diametral tests also in strain control mode. Results show that fatigue lives obtained by means of the ITFT are smaller than fatigue lives obtained by means of either 2PB or 4PB, this is due to the accumulation of permanent deformation during the ITFT; however ITFT results are reliable and statistically not different from 4PB results.

It is true that pure fatigue does not really exist in real life; failure is a more complicated phenomenon. Thus, developing ITFT in strain control mode could reduce the gap between research in the laboratory (where pure fatigue tests often are used) and in the field (where experience showed that quick and simple tests are preferred by civil engineering consultancy). As researchers, we should not forget that the first aim is always to describe and understand the reality and flexural fatigue is still one of the main failure modes in pavements. As pavement engineers, we should not forget that the first aim is to design a more efficient pavement and in order to do that we would need a laboratory machine that better describes reality; the ITFT is a very good link between research and reality.

Numerical quantification of the repeatability and reproducibility of the ITFT in strain control mode needs to be obtained in order for the test method to become a full national standard. Further testing of unusual and new mixtures is required to ensure that the ITFT can be applicable to all mixture types. Also, there are many areas this research could be developed such as size effect, temperature effects, but mostly varying the loading time and rest time in the ITFT to better understand the influence of healing for this test.

# Acknowledgement

I would like to thank you the European Commission and the Marie Curie Action – Research Fellowship Programme for funding this project and contribute to the success of it. Particular thanks go to partners involved in TEAM (Training in European Asset management) Project.

Great thanks go to Prof. Gordon Airey for his excellent, patient and enthusiastic supervision and to Dr. James Grenfell whose knowledge and expertise were important and very supporting in this study.

I am grateful to all those who contribute to the development of the ITFT in strain control mode. Particular thanks go to Dr. Andrea Cocurullo who donates significant and valuable time, expertise and data to the project. Thank you very much for your friendship, very precious to me.

Thank you to IFSTTAR that hosted me for few months during the project. Special thanks go to Dr. Paul Marsac and Dr. Jean Micheal Piau who made my time in Nantes warding in so many different ways.

Big thanks go to Richard, Lawrence, Nancy, Jon, Martin and Mick for their support in the laboratory. It would not be the same without your support and help.

Warm hearted thanks go to every researcher, academic and staff at NTEC. You made my PhD experience the best I could ever possibly dreamt.

Finally (but not least) thanks to my wonderful family, Marta, Grazia and Mimmo for your encouragement, love and support that have got me where I am.

# Declaration

The research reported in this thesis was conducted at the University of Nottingham, Department of Civil Engineering, Nottingham Transportation Engineering Centre (NTEC) between May 2010 and April 2014.

I declare that the work is my own and has not be submitted for a degree at another university.

Cinzia Maggiore

Nottingham

December 2014

# Contents

Abstract .....	iii
Acknowledgement .....	vi
Declaration .....	vii
Contents .....	viii
List of Figures .....	xii
List of Tables .....	xxi
List of Publications .....	xxii
Introduction.....	1
1.1 The history of the paved roads .....	1
1.2 Typical pavement structure .....	2
1.3 Critical stress and strain in flexible pavement.....	4
1.4 Flexural Fatigue.....	5
1.5 Objectives and methodology .....	7
Literature review about fatigue .....	9
2.1 Different approaches to characterise fatigue behaviour .....	9
2.1.1 Phenomenological approach .....	9
2.1.2 Fracture mechanics .....	12
2.1.3 Dissipated Energy concepts .....	16
2.2 Dissipated Energy approaches.....	21
2.3 Factors affecting fatigue in asphalt mixtures .....	31
2.4 Healing .....	34
2.4.1 Mechanism of healing.....	34
2.4.2 Healing in literature.....	35
2.5 Laboratory fatigue testing .....	38
2.5.1 Considering healing in fatigue tests .....	40

2.6	Summary.....	41
2.7	List of variables .....	43
Applying statistics to fatigue test data.....		46
3.1	Simple linear regression.....	46
3.2	Testing the significance of a regression: Fisher and Student t tests .....	49
3.3	Confidence interval, confidence bands and prediction bands in regressions 52	
3.4	Testing the adequacy of a linear model.....	54
3.5	Sample size .....	55
3.6	Comparing simple linear regressions .....	55
3.7	Summary.....	61
3.8	List of variables .....	61
Experimental Program.....		63
4.1	Introduction .....	63
4.2	Materials .....	63
4.3	Mixing and compaction .....	65
4.4	Specimen cutting .....	66
4.5	Volumetric characteristics .....	66
4.6	Storage.....	67
4.7	Testing machines.....	67
4.8	List of variables .....	70
2 Point Bending Test .....		72
5.1	Introduction .....	72
5.2	Trapezoidal Specimens .....	74
5.2.1	Gluing of Trapezoidal Specimens.....	75
5.3	Test results .....	76
5.3.1	10mm DBM .....	76
5.3.2	20mm DBM .....	88

5.4	Summary.....	101
4	Point Bending Test .....	103
6.1	Introduction .....	103
6.2	Prismatic specimens .....	105
6.3	Calibration of the testing machine .....	107
6.4	Test results .....	114
6.4.1	10mm DBM .....	114
6.5	Summary.....	128
	Indirect Tensile Fatigue Test .....	130
7.1	Introduction .....	130
7.2	Cylindrical specimens.....	130
7.3	Indirect tension to cylindrical specimen - IT-CY .....	131
7.4	Indirect Tension Fatigue Test (ITFT) .....	136
	Equipment 136	
7.5	ITFT in strain control mode .....	139
7.6	Test results .....	143
7.6.1	Fatigue life: initial strain calculation.....	143
7.6.2	Fatigue life: dissipated energy.....	148
7.6.3	Fatigue life: healing .....	150
7.6.4	Fatigue life: permanent deformation.....	162
7.7	ITFT and other fatigue tests .....	163
7.8	Summary.....	168
	Conclusions and future work .....	171
8.1	Conclusions .....	171
8.2	Future work.....	176
	References .....	180
	Appendix A .....	1

Measurement of resistance to fatigue using Two Point bending test (2PB) in strain controlled mode. ....	2
Measurement of resistance to fatigue using Four Point bending test (4PB) in strain controlled mode. ....	16
Measurement of resistance to fatigue using Indirect Tensile Fatigue Test (ITFT) in strain controlled mode.....	44
Appendix B .....	1
Data for 10mm DBM.....	1
Data for 20mm DBM.....	12

# List of Figures

Figure 1 Cross section of a Roman road (Encyclopaedia Britannica, no date)	1
Figure 2 Cross sections of John McAdam (Encyclopaedia Britannica, no date)	2
Figure 3 Rigid and Flexible Pavement Load Distribution (Pavement Interactive, no date)	3
Figure 4 Stress and Strain in a flexible pavement	5
Figure 5 Common crack patterns (Colombier, 1997)	6
Figure 6 Alligator Cracking.	6
Figure 7 Pothole.	6
Figure 8 Typical da/dN versus $\Delta K$ curve.	14
Figure 9 Response of elastic, viscous and viscoelastic material under constant stress loading (Hamed, 2010)	17
Figure 10 Elastic and viscoelastic behaviour under loading and unloading conditions (Rowe, 1996)	18
Figure 11 Hysteresis loop	18
Figure 12 Phase lag between the applied load and the measured strain	19
Figure 13 DE versus load cycle for different loading modes (Rowe, 1996)	20
Figure 14 Changing of the hysteresis loop during a fatigue test (at 20°C, 15Hz; at 160 $\mu\epsilon$ ; on 10mm DBM)	21
Figure 15 CDE versus cycles to failure using 2PB in strain controlled mode at 20°C, at 15 and 25Hz (10mm DBM)	23
Figure 16 Evolution of $\psi$ during stress and strain controlled tests (Van Dijk, 1975 and Van Dijk and Visser, 1977)	24
Figure 17 DER vs Number of cycles during a fatigue test undertaken in strain controlled mode at 190 $\mu\epsilon$ , 10°C, 25 Hz on 20mm DBM	25
Figure 18 DER vs Number of cycles during a fatigue test undertaken in stress controlled mode at 1500 kPa, 10°C, 25 Hz on 20mm DBM	26
Figure 19 ER for a strain control test using stress control criteria (Rowe, 1996)	27

Figure 20 The variation of RDEC with Load cycles obtained from 2PB test undertaken in strain control mode at $180 \mu\epsilon$ , at $20^{\circ}\text{C}$ and 25 Hz on 10mm DBM .....	28
Figure 21 $\Delta A$ against number of cycles during a fatigue test for the 10mm DBM .....	31
Figure 22 The effect of rest periods during a fatigue test (Castro and Sanchez, 2006) .....	33
Figure 23 PV-RP curve on a log-log scale (Sutharsan, 2010) .....	36
Figure 24 Healing test: DCSE plotting versus time (Kim and Roque, 2006) ..	37
Figure 25 <i>Pavement Fatigue Carrousel</i> in Nantes, France.....	40
Figure 26 Test with and without rest (Castro and Sanchez, 2006) .....	41
Figure 27 Optimum rest period value (Castro and Sanchez, 2006).....	41
Figure 28 Best-fit regression line between the fatigue life $N_f,50$ and the strain level applied $\epsilon$ .....	48
Figure 29 Slope of linear regression line .....	49
Figure 30 Confidence bands related to the best fitted regression line of a sample data.....	54
Figure 31 Gradation curve 10 mm DBM .....	64
Figure 32 Gradation curve .....	65
Figure 33 Mixing according to BS EN 12697-35: 2004.....	66
Figure 34 Compacting according to BS EN 12697-33: 2003 .....	66
Figure 35 Representation of complex modulus .....	69
Figure 36 Trapezoidal specimen .....	72
Figure 37 Glued specimen .....	72
Figure 38 2PB equipment at IFSTTAR .....	73
Figure 39 2PB equipment at the University of Nottingham .....	73
Figure 40 Stress in the 2PB specimen .....	74
Figure 41 Fractured specimen.....	74
Figure 42 Jig for sawing trapezoidal specimens from compacted asphalt mixture slabs. ....	74
Figure 43 Coring and trimming procedure .....	75
Figure 44 Geometry of trapezoidal specimens: BS EN 12697-24: 2004. ....	75
Figure 45 Jig for gluing trapezoidal specimens to two point bending apparatus end plates.....	76

Figure 46 Stiffness testing machine at IFSTTAR.....	77
Figure 47 Isotherm curves (frequency sweeps).....	78
Figure 48 Isochrones curves (temperature sweeps).....	79
Figure 49 Master curve at a reference temperature of 15°C.....	80
Figure 50 Phase angle at different temperatures.....	81
Figure 51 Fatigue life at 20°C – 10 mm DBM.....	83
Figure 52 Fatigue life at 10°C - 10 mm DBM.....	83
Figure 53 Fatigue life at 15 Hz - 10 mm DBM.....	84
Figure 54 Fatigue life at 25 Hz - 10 mm DBM.....	84
Figure 55 Fatigue lives obtained by means of Energy Ratio (Pronk) and traditional methods .....	85
Figure 56 Fatigue lives obtained by means of Energy Ratio (Rowe) and traditional methods .....	85
Figure 57 Fatigue lives obtained by means of RDEC (Shen) and traditional methods.....	86
Figure 58 RDEC at 20°C at two different frequencies (15 and 25Hz).....	87
Figure 59 RDEC at 15Hz at two different temperatures (10 and 20°C) .....	88
Figure 60 RDEC at 25Hz at two different temperatures (10 and 20°C) .....	88
Figure 61 Isotherm curves (frequency sweeps).....	90
Figure 62 Isochrones curves (temperature sweeps).....	91
Figure 63 Phase angle at different temperatures for 20mm DBM.....	92
Figure 64 Master curve at a reference temperature of 10°C (20mm DBM) ...	93
Figure 65 Fatigue life at 10°C and 25 Hz in both stress and strain control mode (20 mm DBM) .....	94
Figure 66 Unique regression line for fatigue life data at 10°C and 25 Hz in both stress and strain control mode.....	94
Figure 67 RDEC at 10°C and 25 Hz in both stress and strain control mode .	95
Figure 68 Fatigue lives obtained by means of Dissipated Energy Ratio (Pronk) and traditional methods in strain control mode .....	97
Figure 69 Fatigue lives obtained by means of Energy Ratio (Pronk) and traditional methods in stress control mode .....	97
Figure 70 Fatigue lives obtained by means of Energy Ratio (Rowe) and traditional methods in strain control mode .....	98

Figure 71 Fatigue lives obtained by means of Energy Ratio (Rowe) and traditional methods in stress control mode .....	98
Figure 72 Fatigue lives obtained by means of RDEC (Shen) and traditional methods in strain control mode.....	99
Figure 73 Fatigue lives obtained by means of RDEC (Shen) and traditional methods in stress control mode.....	99
Figure 74 Isotherm curves at 10 °C (10 and 20mm DBM data) .....	100
Figure 75 Phase angle at 10°C (10 and 20mm DBM data) .....	100
Figure 76 Fatigue lives for 10 and 20mm DBM .....	101
Figure 77 Clumped specimen.....	103
Figure 78 4 PB equipment at the University of Nottingham .....	104
Figure 79 Load and strain amplitude for the 4PB .....	105
Figure 80 4PB Coring and trimming procedure .....	105
Figure 81 Different beam heights for the 4PB .....	106
Figure 82 Geometry of prismatic specimens: BS EN 12697-24: 2004.....	107
Figure 83 Section of aluminium beam .....	108
Figure 84 Longitudinal profile of aluminium beams .....	108
Figure 85 Small, medium and large beam size configurations .....	109
Figure 86 Stiffness versus frequency. Aluminium beam.....	109
Figure 87 Phase angle versus frequency. Aluminium beam.....	110
Figure 88 Stiffness versus frequency before calibration (20mm DBM) .....	111
Figure 89 Phase angle versus frequency before calibration (20mm DBM)..	112
Figure 90 Stiffness versus frequency after calibration (20mm DBM).....	112
Figure 91 Phase angle versus frequency after calibration (20mm DBM).....	113
Figure 92 Stiffness versus frequency after calibration (10mm DBM).....	113
Figure 93 Phase angle versus frequency after calibration (10mm DBM).....	114
Figure 94 Isotherm curve at 10°C (2PB and 4PB data) .....	115
Figure 95 Phase angle at 10°C (2PB and 4PB data).....	115
Figure 96 Fatigue life at 10°C and 25 Hz in strain control mode (10 mm DBM) .....	116
Figure 97 Fatigue lives obtained by means of Dissipated Energy Ratio (Pronk) and traditional methods .....	117
Figure 98 Fatigue lives obtained by means of Energy Ratio (Rowe) and traditional methods .....	117

Figure 99 Fatigue lives obtained by means of RDEC (Shen) and traditional methods.....	118
Figure 100 PV- Nf, 50 relationship obtained by 4PB and 2PB.....	119
Figure 101 Healing test: 10,000 cycles for each loading time stage and 10,000 cycles for each rest time stage .....	120
Figure 102 Example of healing test (10,000 cycles of loading time and 10,000 cycles of rest time).....	121
Figure 103 Number of cycles (Nf,50 and Nf,30) for different loading times (constant rest time).....	122
Figure 104 Number of cycles (Nf,50 and Nf,30) for different resting times (constant loading time) .....	122
Figure 105 Variation in stiffness at different rest time periods (fixed loading time = 10,000 pulses) .....	123
Figure 106 Variation in dissipated energy at different rest time periods (fixed load time = 10,000 pulses) .....	124
Figure 107 Variation in phase angle at different rest time periods (fixed load time = 10,000 pulses) .....	124
Figure 108 Variation in stiffness at different load time periods (fixed rest time = 10,000 pulses).....	125
Figure 109 Variation in dissipated energy at different load time periods (fixed rest time = 10,000 pulses) .....	126
Figure 110 Variation in phase angle at different load time periods (fixed rest time = 10,000 pulses) .....	126
Figure 111 Healing Ratio for different load time periods (fixed rest time = 10,000 cycles) .....	127
Figure 112 Healing Ratio for different rest time periods (fixed load time = 10,000 cycles) .....	128
Figure 113 Coring and trimming procedure .....	131
Figure 114 Cylindrical specimen (10mm DBM) .....	131
Figure 115 IT-CY Stiffness Modulus test.....	132
Figure 116 Frame for measuring horizontal diametral deformation .....	132
Figure 117 Stress pulse applied.....	133
Figure 118 Strain waveform recorded.....	133
Figure 119 Stiffness versus air void content (10mm DBM).....	135

Figure 120 Stiffness results for 10mm DBM mixture with 100 pen bitumen (10mm DBM) .....	135
Figure 121 ITFT apparatus.....	136
Figure 122 Indirect Tension Fatigue Test .....	137
Figure 123 Mechanism of failure in stress control mode .....	137
Figure 124 Fatigue tests in stress control mode at 10 and 20°C (10mm DBM) .....	138
Figure 125 Recoverable deformation (10 mm DBM) .....	139
Figure 126 Failure in strain control mode .....	140
Figure 127 Fatigue life in strain control mode at 10°C (10mm DBM).....	140
Figure 128 Signals for a bending test and the ITFT.....	141
Figure 129 Dissipated energy for a bending test and the ITFT.....	141
Figure 130 Stress-strain hysteresis loop for a single pulse in ITFT (10mm DBM) .....	142
Figure 131 Calculation of Dissipated Energy.....	143
Figure 132 Initial strain amplitude EN 12697-24:2004.....	144
Figure 133 Initial strain amplitude EN 12697-26:2004.....	145
Figure 134 Initial resilient strain amplitude EN 12697-24:2012 .....	145
Figure 135 Fatigue life obtained in stress and strain control modes (20mm DBM) .....	146
Figure 136 Fatigue life obtained in stress and strain control modes (10mm DBM) .....	147
Figure 137 Fatigue lives obtained by means of Dissipated Energy Ratio (Pronk) and traditional methods.....	149
Figure 138 Fatigue lives obtained by means of Energy Ratio (Rowe) and traditional methods .....	149
Figure 139 Fatigue lives obtained by means of RDEC (Shen) and traditional methods.....	150
Figure 140 Healing test: 10,000 pulse for each loading time stage and 10,000 pulse for each rest time stage.....	151
Figure 141 Example of healing test (10,000 pulses of loading time and 10,000 pulses of rest time) .....	152
Figure 142 Number of cycles (Nf,50 and Nf,30) for different rest times (constant loading time = 5000 consecutive pulses) .....	153

Figure 143 Number of cycles ( $N_f,50$ and $N_f,30$ ) for different rest times (constant loading time = 15000 consecutive pulses) .....	153
Figure 144 Number of cycles ( $N_f,50$ and $N_f,30$ ) for different loading times (constant rest time = 10,000 consecutive pulses).....	154
Figure 145 Number of cycles ( $N_f,50$ and $N_f,30$ ) for different loading times (constant rest time = 15,000 consecutive pulses).....	154
Figure 146 Number of cycles ( $N_f,50$ ) plotted vs different loading times considering two constant rest times (10,000 and 15,000 pulses) .....	155
Figure 147 Number of cycles ( $N_f,50$ ) plotted vs different rest times considering two constant load times (5,000 and 10,000 pulses).....	155
Figure 148 Stiffness ratio for different rest times when load time is constant (5,000 pulses).....	157
Figure 149 Dissipated Energy for different rest times when load time is constant (5,000 pulses) .....	157
Figure 150 Total vertical deformation for different rest times when load time is constant (5,000 pulses) .....	158
Figure 151 Stiffness ratio for different load times when rest time is constant (10,000 pulses).....	158
Figure 152 Dissipated Energy for different load times when rest time is constant (10,000 pulses) .....	159
Figure 153 Total vertical deformation for different load times when rest time is constant (10,000 pulses) .....	159
Figure 154 Linear relationship between total vertical deformation and number of pulses for different rest times when load time is constant (5,000 pulses)	160
Figure 155 Healing Ratio for different load time periods (fixed rest time = 10,000 pulses).....	161
Figure 156 Healing Ratio for different rest time periods (fixed load time = 10,000 pulses).....	162
Figure 157 Permanent vertical deformation depending on the mode of loading .....	163
Figure 158 Permanent horizontal deformation depending on the mode of loading.....	163

Figure 159 Fatigue life obtained in strain control mode, at 10°C by means of 2PB, 4PB and ITFT according to the phenomenological method (Nf,50) for the 10mm DBM.....	164
Figure 160 Fatigue life obtained in strain control mode, at 10°C by means of 2PB, 4PB and ITFT according to the Dissipated Energy Ratio (Pronk) for the 10mm DBM.....	165
Figure 161 Fatigue life obtained in strain control mode, at 10°C by means of 2PB, 4PB and ITFT according to the Energy Ratio (Rowe) for the 10mm DBM .....	165
Figure 162 Fatigue life obtained in strain control mode, at 10°C by means of 2PB, 4PB and ITFT according to the RDEC (Shen) for the 10mm DBM .....	166
Figure 163 Varying rest time in ITFT .....	179

# List of Tables

Table 1 SS, DF and MS (Zar, J.H. 2010).....	51
Table 2 0/10 mm size DBM specification.....	64
Table 3 0/20 mm size DBM specification.....	64
Table 4 Experimental work for 10mm DBM .....	70
Table 5 Experimental work for 20mm DBM .....	70
Table 6 Dimensions of the specimens: BS EN 12697-24: 2004. ....	75
Table 7 Comparison between temperatures and frequencies .....	82
Table 8 DE method comparison by using Dunnett's test .....	86
Table 9 RDEC: temperature comparison at 15 and 25 Hz .....	87
Table 10 Comparison between stress and strain mode of loading .....	94
Table 11 DE method comparison by using Dunnett's test – 20mm DBM @25Hz and 10°C .....	96
Table 12 Dimensions of the specimens: BS EN 12697-24: 2004. ....	107
Table 13 Dimensions of aluminium specimens.....	107
Table 14 Phase compensation .....	111
Table 15 DE method comparison by using Fisher test .....	118
Table 16 RDEC: 2PB-4PB comparison at 10°C and 25 Hz .....	119
Table 17 Loading times and rest times (in number of cycles).....	120
Table 18 Strain control fatigue life vs stress control fatigue life – 10mm DBM .....	148
Table 19 DE method comparison by using Dunnett's test .....	150
Table 20 Loading times and rest times (in number of pulses) .....	151
Table 21 ITFT, 2PB and 4PB – Phenomenological approach (Nf,50)– Tukey's Test .....	167
Table 22 ITFT, 2PB and 4PB – DER approach – Tukey's Test.....	167
Table 23 ITFT, 2PB and 4PB –ER approach – Tukey's Test .....	167
Table 24 ITFT, 2PB and 4PB –RDEC approach – Tukey's Test .....	168
Table 25 Specimen dimensions (EN 12697-24: 2004) .....	177

## List of Publications

Maggiore, C., Airey, G., Grenfell, J. and Collop, A. (2012). Evaluation of fatigue life using dissipated energy methods. 7<sup>th</sup> RILEM International Conference on cracking in pavements. RILEM Bookseries Volume 4, pp 643-652. Delft, The Netherlands

Maggiore, C., Airey, G., Marsac, P. and Grenfell, J. (2012). A dissipated energy comparison to evaluate fatigue resistance using 2 PB test. Journal of Traffic and Transportation Engineering (English Edition)., 1(1), 49-54. ISSN 2095-7564 CN 61-1494/U. February 2014.

Maggiore, C. Airey, G. Di Mino, G. Marsac, P. and Di Liberto, M (2012). Fatigue resistance: is it possible having a unique response?. Proceeding of the 3<sup>rd</sup> Workshop on 4PB – Four Point Bending, Davis, California, USA. September 2012.

Maggiore, C. Di Mino, G., Di Liberto, M., Airey, G. and Collop, A. (2012). Mechanical characterization of dry asphalt rubber concrete for base layers by means of the four bending points tests. Proceeding of the 3<sup>rd</sup> Workshop on 4PB – Four Point Bending, Davis, California, USA. September 2012.

Di Mino, G., Di Liberto, M., Maggiore, C. and Noto, S. (2012). A dynamic model of ballasted rail track with bituminous sub-ballast layer. Proceeding of SIIV (Societa Italiana Infrastrutture Viarie) 5<sup>th</sup> International Congress on Sustainability of road infrastructure. Volume 53, pp366-378. Rome, Italy. October 2012.

Maggiore, C., Airey, G. and Grenfeel, J. (2013). Evaluation of different fatigue failure criteria for asphalt material using laboratory tests. Proceeding of the 2<sup>nd</sup> Conference on Sustainable Asphalt, MESAT 2012. Sharja, Middle East. February 2013.

Maggiore, C. and Airey, G. (2013). Evaluation of stiffness and fatigue using 2 Point Bending and Indirect Tensile Fatigue tests. Proceeding of 2013 Airfield

and highway pavement conference. Volume 1, pp. 1030-1039. Publisher: American Society of Civil Engineers, ISBN (print): 978-0-7844-1300-5. June 2013.

# CHAPTER 1

## Introduction

### 1.1 The history of the paved roads

The Romans were famous for their roads. They built roads so that the army could march from one place to another and they tried to build the roads as straight as possible, so that the army could take the shortest route. In general there were 3 layers. The first layer of large stones was covered by a second layer of smaller stones, then a top layer of gravel or small stones (see Figure 1).

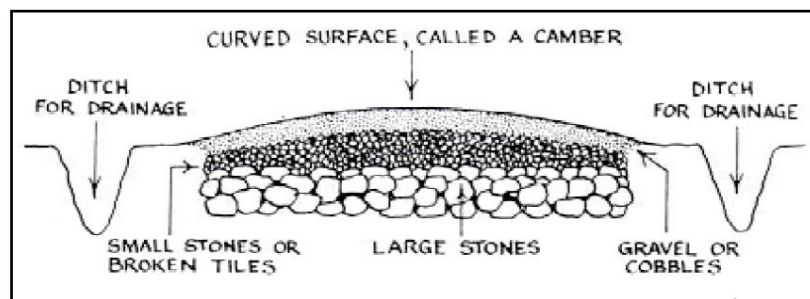


**Figure 1** Cross section of a Roman road (Encyclopaedia Britannica, no date)

Modern roads were the result of the work of a French and two Scottish engineers, Pierre Marie Tresaguet (1716-1796), Thomas Telford (1757-1834) and John Loudon McAdam (1756-1836). Among these three engineers, John Loudon McAdam was the most important in the English road construction design. He designed roads using well compacted broken angular stones, smaller than the previous designs, laid in symmetrical, tight patterns and covered with small stones to create a hard surface (see Figure 2). This course could reduce the stresses on the subgrade to an acceptable level, provided the subgrade was kept relatively dry and drained. The strength and stiffness of the course of compacted angular stone came from the mechanical interlock that developed between individual pieces of stone; this principal is still used in the modern road construction. McAdam's design, called "macadam roads," spread very quickly across the world and it provided a great advancement in road construction (Lay, 2009).

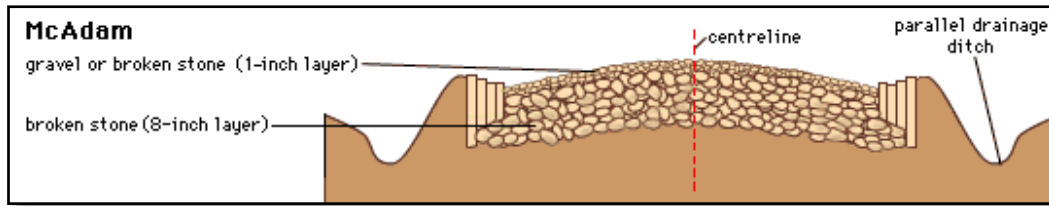


**Figure 2** Cross sections of John McAdam (Encyclopaedia Britannica, no date)

Over time McAdam's road construction provided the cheapest pavement, but its unbound surface was difficult to maintain and was usually either slippery or dusty as a consequence of water. Thus, roads at the turn of the 20th century were largely inadequate for the demands about to be placed on them by the newly developed automobile and truck. As vehicle speeds increased rapidly, the available friction between road and tyre became critical for accelerating, braking, and cornering, thus much stronger and tougher materials were required. All those problems were solved by the introduction of bituminous materials or asphalt mixtures. Bitumen is defined as a black, sticky, highly viscous, liquid or semi-solid material; asphalt material is made up of a mixture of coarse and fine aggregate, bound together by bitumen. Nowadays road construction involves combinations of asphalt layers between the surface and the ground. Each layer has a specific role and its own mechanical properties strictly related with its thickness, thus the pavement design (Hunter, 2000).

## 1.2 Typical pavement structure

Different types of pavement are commonly used in the construction of roadways. There are three generic classes of pavement based on the structural performance and layered structure; these are:

- Rigid Pavement,
- Flexible Pavement, and
- Composite pavement (rigid pavement overlaid with an asphalt layer).

Rigid pavements are usually composed of a surface layer, made up of slabs of concrete (PQC), a base course that provides a stable base for the surface course and assists in drainage; the base course sits on a sub-base course, usually more flexible than the previous two layers. As the name implies, a rigid pavement deflects very little under loading due to the high modulus of

elasticity of their surface course and tends to distribute the load over a wide area of sub-grade (see Figure 3). Rigid pavements tend to have higher construction costs and lower maintenance costs; however the main advantage is its durability.

In a flexible pavement, the main structural layer is the road base, which is usually covered by a base course, directly underneath the wearing course. The main role of the wearing course is to ensure safety and comfort to the driver/vehicle and waterproofing. Wearing course and base course are part of the surfacing (or bituminous layers) and their main role is to spread the wheel load in order to not overstress the layers below. The foundation is composed of the sub-base and the capping and it is laying on the sub-grade. The foundation is usually highly stressed (mostly during the construction phase) and it is made by granular materials and soil.

Wheel load stresses are transmitted to the lower layers by grain-to-grain transfer through the points of contact in the granular structure. The wheel load is transferred from a small area on the surface of the pavement, at high stress level, and in to a larger area at the bottom of the pavement, at lower stress level. For this reason the strength of each layer is different: the strongest material (least flexible) is in the top layer and the weakest material (most flexible) is in the lowest layer (Mallick and El-Korchi, 2009), See Figure 3.

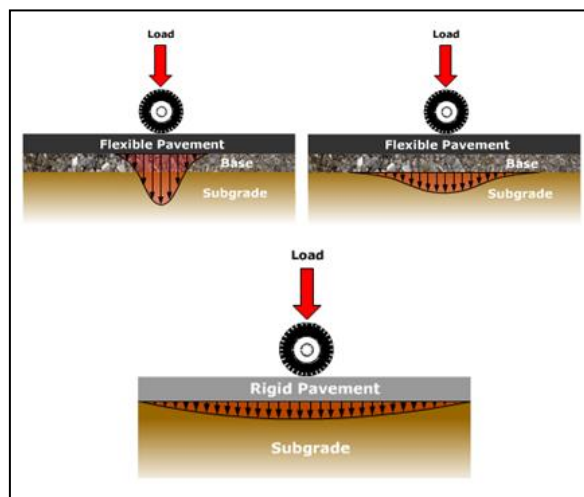


**Figure 3** Rigid and Flexible Pavement Load Distribution (Pavement Interactive, no date)

Flexible pavements normally consist of the following layers:

- Surface course (20-50 mm).
- Binder course (50-80 mm).
- Base course (200 mm or more).
- Sub-base course (about 150 mm).
- Subgrade or existing soil.

### **1.3 Critical stress and strain in flexible pavement**

Repetitive moving wheel loads cause different kinds of distress in flexible pavements (see Figure 4). There are two main kind of distress located in two critical different locations:

- Vertical compressive strain at the top of the sub-grade due to the vehicle weight, which can cause sub-grade deformation resulting in permanent deformation at the pavement surface.
- Horizontal tensile strain or stress at the bottom of the asphalt layers due to vehicle weight, motion, braking and curving motion, which can cause fracture of the bituminous layer.

Pavements do not fail suddenly; they gradually deteriorate until they lose their serviceability. The two major kinds of failure of asphalt in a pavement are: fatigue cracking, caused by excessive horizontal tensile strain at the bottom of the asphalt layer, and rutting, caused by excessive vertical compressive strain on top of the sub-grade. In the design of an asphalt pavement, it is necessary to investigate these critical stresses and strains and design the right thickness to avoid them. Fatigue cracking is a phenomenon which occurs in pavements due to repeated applications of traffic loads. Permanent deformation or rutting is a manifestation of depressions that form in the wheel path.

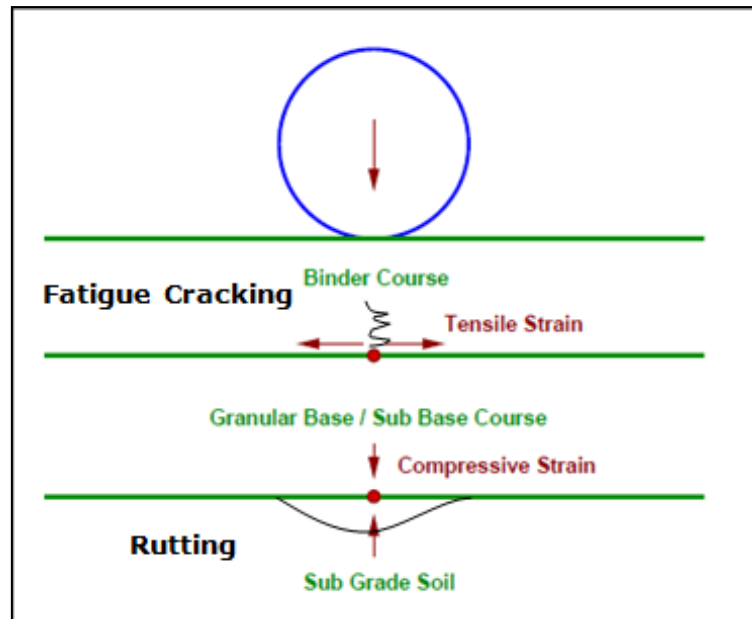


**Figure 4** Stress and Strain in a flexible pavement

## 1.4 Flexural Fatigue

Flexural fatigue is one of the main failure modes of flexible pavement structures.

From a mechanical point of view, the mechanism of fatigue can be divided into two parts: the first one is the occurrence of tensile stress/strain in the base layer; the second one is the repetitive occurrence of such tensile stress/strain under traffic repetitions. The repetition of the tensile stress/strain causes the accumulation of micro damage in the bottom of the base layer that, over time, results in the break between the aggregate and the binder, thus generating more or less deep cracks. In other words if a beam is subjected to load, the beam would tend to assume a convex downward shape, with tensile stress/strain in the bottom part and compressive stress/strain in the top one. Since the asphalt pavement has viscoelastic behaviour, it recovers when the load is removed. At the end of this first cycle there is part of the strain that is recovered and a small part that is permanent. Under the next load the pavement undergoes the same cycle. Ultimately the pavement will fail due to damage accumulation (Mallick and El-Korchi, 2009).

Physically speaking, micro cracking originates at the bottom of an asphalt concrete layer caused by horizontal tensile strain; this compromises the contact between the aggregate skeleton and the binder (particle-to-particle

contacts). Furthermore the water trapped in the cracks and the repeated loading leads to a decrease in the strength of the mixtures and micro cracking starting to propagate towards the layers above and leading to pavement collapse. This phenomenon is called Bottom-Up Cracking (Thom, 2008).

Depending on the type of road structure, the materials and the progress of deterioration, cracks can take different orientations and patterns. They usually are parallel to the direction of vehicle travel (longitudinal cracking) or perpendicular to the direction of travel (transverse cracking). They, also, can be single breaks in the pavement or double, branched or interlaced (Colombier, 1997). As shown in Figure 5, longitudinal cracks, over time, may be connected to transversal cracks to form a pattern of blocks (block cracking) or small polygons (alligator cracking).

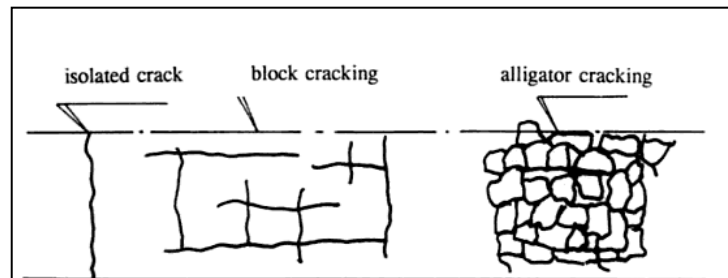


**Figure 5** Common crack patterns (Colombier, 1997)

All cracks allow the water to enter in the pavement structure, thus the final degradation due to this phenomenon is the development of potholes as shown in Figure 6 and Figure 7.



**Figure 6** Alligator Cracking.



**Figure 7** Pothole.

## **1.5 Objectives and methodology**

This project is part of the Marie Curie Initial Training Network: TEAM - Training in European Asset Management, funded under the Seventh Framework Programme (FP7) by the European Commission that deals with Training in European Asset Management. The TEAM proposal exploits the benefits of new sensor and processing technologies, methodologies, models and algorithms to monitor the condition and safety of transport infrastructure. Partners of the TEAM are: University College Dublin (UCD), ROC Systemtechnik, University of Nottingham (UoN), Institut Francais des Sciences et Technologies des Transports, de l'Amenagement et des Reseaux (IFSTTAR), Ecole Polytechnique Federal de Lausanne (EPFL), Ramboll, ABM Contruction, Trinity College Dublin (TCD) and the Forum of European National Highway Research Laboratories (FEHRL). The TEAM project comprises several work packages; this research project was developed under the pavement service life optimisation work package and it was based 80% at the University of Nottingham and 20% at IFSTTAR. The topic of the project is fatigue in asphalt materials.

Flexural fatigue is one of the main failure modes in asphalt mixtures and flexible pavement structures, so a good prediction of the fatigue life of the pavement will help to develop and improve pavement design procedures.

The primary research goal of this project is to understand better the fatigue phenomenon in asphalt materials. Several approaches such as phenomenological approach, fracture mechanics, dissipated energy methods have been developed in research. This project focuses on the phenomenological and different dissipated energy methods to describe fatigue because dissipated energy is strongly related to fatigue; it changes during a fatigue test: it increases during a stress control test; it decreases during a strain control test. Therefore a deep literature review about the fatigue phenomenon and fatigue failure in asphalt materials was undertaken.

The second main aim of this research project was choosing different fatigue testing machines to collect data. Three main tests were chosen: 2 Point Bending (2PB), 4 Point Bending (4PB) and Indirect Tensile Fatigue Test

(ITFT). 4PB test was chosen because is widely used in the world; 2PB was chosen because an exchange with IFSTTAR was planned during this project. IFSTTAR is the French institution where 2PB was designed and developed for pavement research. The novelty of the research project is the development of a new fatigue test: the ITFT in strain control mode. ITFT is a more practical test and very often chosen by engineering consultancies. Undertaking the ITFT in strain control mode represents a big chance to better link research and pavement design and reduce the existing gap between the two.

To investigate the differences between various fatigue methods, various materials, various fatigue tests, and statistical comparisons were involved in the project. Due to lack of information in pavement engineering, a deep literature review on statistics was involved in this study. In general, statistics includes the design of experiments, the collection, the analysis and the interpretation of data; understanding and introducing the appropriate technique to analyse fatigue data in pavement engineering was one of the main challenges in this project. Several techniques are presented in this thesis.

The University of Nottingham recently (September 2012) bought a new 4PB test where different prismatic size specimens could be tested. One of the aims was to calibrate the test to ensure a good performance and reliable results.

Healing is one of the factors that most influences fatigue performance in asphalt materials. Not many testing machines are suitable to set up a rest time after a load cycle, and this includes 2PB; thus, healing tests were undertaken by means of 4PB and ITFT in strain control mode. 4PB does not allow undertaking healing tests; therefore a modification in the software was necessary to build a new healing test to evaluate the effects of healing during a fatigue test.

Finally, writing fatigue testing procedures for the new ITFT test in strain control mode, as well as 2PB and 4PB tests, was the final aim of this project to help future researchers.

## CHAPTER 2

# Literature review about fatigue

The purpose of this chapter is to review the literature about fatigue in asphalt materials. This literature review consists of four parts; the first part describes different approaches to evaluate fatigue such as phenomenological approach, fracture mechanics approach and dissipated energy approach. This project focuses more on the dissipated energy concepts; so a description of several dissipated energy methods is presented in the second part of this chapter. The main topic in the third part is to identify the common factors affecting fatigue in asphalt mixtures like environmental and loading conditions, rest period, material characteristics, etc.

Healing is one of the factors that most influences fatigue performance in asphalt materials. A literature review on the mechanism of healing and its relation with fatigue is presented in this chapter.

Finally, different laboratory fatigue tests and the two main modes of loading (control stress and control strain) are presented in the fourth part.

### **2.1 Different approaches to characterise fatigue behaviour**

It has been generally accepted that fatigue is a process of cumulative damage and one of the major causes of cracking in asphalt concrete pavement. Three approaches are usually used in characterising fatigue behaviour: the phenomenological approach; the fracture mechanics approach; and the energy-based approach.

#### **2.1.1 Phenomenological approach**

The fatigue characteristics of asphalt mixtures can be expressed as relationships between the initial stress or strain and the number of load repetitions; the relationship usually is not derived from a theoretical analysis of pavement mechanics (Hamed, 2010).

Depending on the mode of loading, results from fatigue tests are typically formulated as follows (Shen, 2007):

$$N_f = A \left( \frac{1}{\varepsilon} \right)^b \quad \text{in strain control mode} \quad \text{Equation 1}$$

$$N_f = C \left( \frac{1}{\sigma} \right)^d \quad \text{in stress control mode} \quad \text{Equation 2}$$

Where:

- $N_f$  = Number of cycle to failure,
- $\varepsilon$  ,  $\sigma$  = Tensile strain or stress repeatedly applied, and
- A, b, C, d = Material coefficients, derived by fitting the data from laboratory testing.

Usually researchers tend to use the controlled strain mode because the results tend to be independent of the temperature; this does not happen for the controlled stress mode. When the controlled strain mode is considered, it is easier plotting and comparing the results of the same material for different temperatures.

Pell suggested the following observed relationship between the tensile strain at the bottom of the asphalt concrete layer ( $\varepsilon_t$ ) and the number of load applications to crack appearance in the pavement ( $N_f$ ):

$$N_f = K_1 \left( \frac{1}{\varepsilon_t} \right)^{K_2} \quad \text{Equation 3}$$

in which  $K_1$  and  $K_2$  are the intercept and the slope respectively, determined by linear regression (Pell, 1967 and 1987).

Afterwards many researchers stated that in controlled strain laboratory tests the stiffer mixtures generally have shorter fatigue life; thus, they introduced the stiffness modulus into the fatigue relation to absorb temperature and loading time effects (Monismith et al., 1985):

$$N_f = K_1 \left( \frac{1}{\varepsilon_t} \right)^{K_2} \left( \frac{1}{E_0} \right)^{K_3} \quad \text{Equation 4}$$

Where:

- $N_f$  = number of cycles to failure,
- $\varepsilon_t$  = tensile strain at the bottom of the asphalt layer,

- $E_0$  = initial asphalt mix stiffness, and
- $K_1$ ,  $K_2$  and  $K_3$  are regression constants obtained from laboratory testing.

To account for strain variations, Miner's hypothesis of damage has been used (Miner, 1945). Miner's hypothesis is represented as a relative damage factor where the crack will occur when the sum of the damage factors equals one. Miner's linear law of cumulative damage in conventional asphalt pavement design is given as follow:

$$D = \sum_i^T \frac{n_i}{N_i} = 1 \quad \text{Equation 5}$$

Where:

- $D$  = damage,
- $T$  = number of periods,
- $n_i$  = number of load applications during a period  $i$ , and
- $N_i$  = the ultimate number of load applications the pavement could carry.

To use Miner's approach,  $N_i$  is determined from the fatigue equation (Equation 4).

In those first models there are always some coefficients that need to be determined:  $K_1$ ,  $K_1$  and  $K_3$  as shown in the equation 3 and equation 4. These parameters represent the material properties of the mixture and they are experimentally determined through the fatigue tests. Different researchers found different values for these coefficients; the typical range for  $K_2$  values is between 3 and 6 (Barenberg and Thompson, 1992). It is not possible to establish a range for the  $K_1$  coefficient, because it varies by several orders of magnitude. In any case, the two coefficients ( $K_1$  and  $K_2$ ) seem to be highly correlated and the relation suggested from some researchers (Pell and Cooper, 1975) is:

$$K_2 = -0.313 \log K_1 + 0.5 \quad \text{Equation 6}$$

Mode of loading, testing temperature and asphalt content has a more significant effect on the  $K_1$ - $K_2$  relation than asphalt type, air voids levels and aggregate gradations (Ghuzlan and Carpenter, 2002).

Although widely used, the traditional phenomenological approach does not provide a mechanism of damage accumulation in the mixture under the repetitive load. Furthermore, the accumulated damage is treated as linear in the strain-fatigue life relationship, which has been found to be incorrect mostly at low strain/damage condition (Carpenter et al., 2003). The phenomenological approach is also material and loading dependent.

### 2.1.2 Fracture mechanics

Fracture mechanics relates fatigue life of asphalt mixtures to the cracking mechanism. Asphalt materials are not homogenous (the hypothesis in the phenomenological approach) but they are characterised by pre-existing internal flaws (microcracks) in the form of air voids, surface irregularities and internal defects; cracking is considered to develop progressively through three stages: crack initiation, crack propagation, and failure. The first phase is characterised by the formation and growth of pre-existing microcracks. During crack propagation, the cracks start to propagate at a given state of stress and reach critical dimensions and pattern until they reach the failure. The number of load repetitions at which the rate of crack growth increases is designated as the fatigue life of the mixture (Khatakk and Baladi, 2013).

A simple and well-known method for predicting fatigue crack propagation (this stage consumes most of the fatigue life) is the power law described by Paris and Erdogan (1963), and it is also known as the Paris law. The equation represents the first application of fracture mechanics to fatigue and it relates the increase in crack length per load cycle ( $da/dN$ ) to the stress intensity factor ( $\Delta K$ ) (Paris and Erdogan, 1963). The relationship is the following one:

$$\frac{da}{dN} = C(\Delta K)^m \quad \text{Equation 7}$$

Where:

- $da/dN$  = crack growth rate,

- $\Delta K = \Delta K_{\max} - \Delta K_{\min}$  is the range of the stress intensity factor (the difference between the stress intensity factor at maximum and minimum loading),
- C and m = material constants, precisely C is the intercept and m is the slope on the log-log plot of da/dN versus  $\Delta K$  (see Figure 8).

K is the crack tip stress intensity factor and a simple model to identify K for finite plates is:

$$K = \sigma Y \sqrt{\pi a} \quad \text{Equation 8}$$

Where:

- $\sigma$  = uniform tensile stress perpendicular to the crack tip,
- Y = is a function depending on the specimen geometry and the crack (Masad et al., 2008).

If K is known, it is possible to obtain  $\Delta K$ , considering  $\Delta\sigma$  which is the range of cyclic stress amplitude.

$$\Delta K = \Delta\sigma Y \sqrt{\pi a} \quad \text{Equation 9}$$

Substituting this equation in the Paris law, the differential equation can be solved via separation of variables and subsequent integration.

$$\int_0^{N_f} dN = \int_{a_i}^{a_c} \frac{da}{C(\Delta\sigma Y \sqrt{\pi n})^m} = \frac{1}{C(\Delta\sigma Y \sqrt{\pi n})^m} \int_{a_i}^{a_c} a^{-\frac{m}{2}} da \quad \text{Equation 10}$$

$$N_f = \frac{2 \left( a_c^{\frac{2-m}{2}} - a_i^{\frac{2-m}{2}} \right)}{(2-m)C(\Delta\sigma Y \sqrt{\pi n})^m} \quad \text{Equation 11}$$

Where:

- Nf = number of load cycles to fracture,
- $a_c$  = critical length at which instantaneous fracture will occur,
- $a_i$  = initial crack length at which fatigue crack growth starts for the given stress range  $\Delta\sigma$ .

Equation 10 represents a straight line on the log-log plot of da/dN versus  $\Delta K$  and thus describes region II (see Figure 8) of the fatigue rate curve. The

limitation of the Paris law is that it is only capable of describing data in region II. If the data shows a threshold (region I) or an accelerated growth (region III) the Paris law cannot effectively describe these regions.

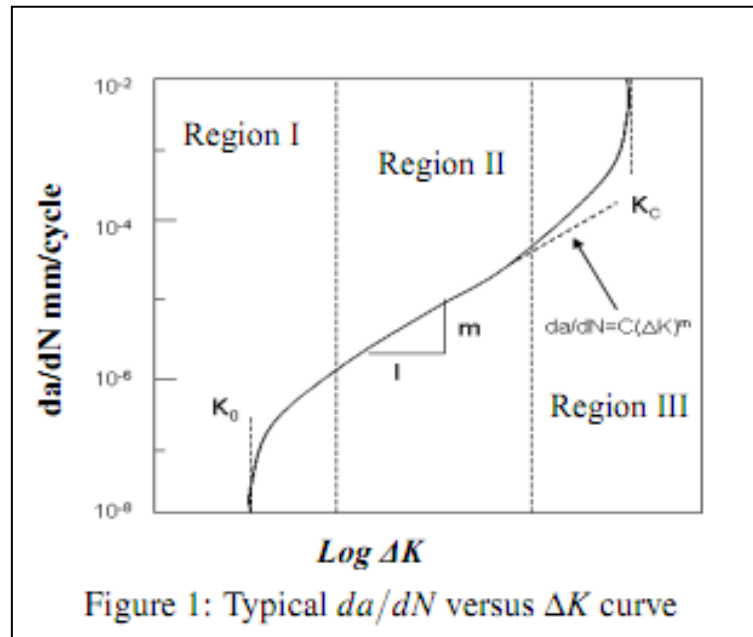


**Figure 8** Typical  $da/dN$  versus  $\Delta K$  curve.

Later work proposed a different relationship, adding more terms in the Paris law as follows (Majidzadeh et al., 1971):

$$\frac{dc}{dN} = A_1 K^2 + A_2 K^4 \quad \text{Equation 12}$$

Where:

$$\bullet \quad A_1 10^{10} = 7.02 + 77.9 \left( \frac{1000 \sigma_t}{E^*} \right)^2 - 6.09 \left( \frac{K_{IC}}{1000} \right)^3 \quad \text{Equation 13}$$

$$\bullet \quad A_2 10^{16} = 31.36 + 1132.4 \left( \frac{1000 \sigma_t}{E^*} \right)^3 - 43.32 \left( \frac{K_{IC}}{1000} \right)^3 \quad \text{Equation 14}$$

- $\sigma_t$  = tensile stress,
- $E^*$  = complex modulus, and
- $K_{IC}$  = fracture toughness.

Different researchers have tried to better define the “A” value (Molenaar, 1983). Molenaar, in his PhD thesis in 1983, estimated the “A” value from laboratory tests as follows:

$$\log A = 4.389 - 2.5 \log(E\sigma_t m) \quad \text{Equation 15}$$

Where:

- E = stiffness modulus of the asphalt mixture,
- $\sigma_t$  = tensile stress,

Lytton also incorporating field effects expressed the “A” value as follows:

$$\log A = 4.389 - 2.5 \log(K\sigma_t m) \quad \text{Equation 16}$$

Where:

- K = coefficient determined through field calibration, and
- $\sigma_t$  = tensile stress.

In general, fracture mechanics can be divided into two main groups: linear elastic fracture mechanics (LEFM) and nonlinear fracture mechanics (NLFM). It has been shown that in LEFM the intensity of the stress field near the crack is measured by means of the “stress intensity factor” and it is a linear function of the stress, the crack length and the structure’s geometry. In addition the LEFM describes fracture behaviour well for brittle materials and asphalt is a brittle material at low temperatures.

Since LEFM cannot satisfactorily characterize the cracking and failure of asphalt materials, different nonlinear models have been developed to better simulate stable crack growth. In particular, two approaches have been used to evaluate the nonlinear response: the compliance approach and the R-Curve approach (Mamlouk and Mobasher, 2004). The compliance approach is generally limited to defining the condition of crack instability; in particular it allows measurement of the energy release rate and of the stress intensity factor. The R-Curve approach, instead, evaluates the fracture resistance of the material at different crack lengths providing more insight of the crack propagation phenomenon.

Even if fracture mechanics is a good method to describe the crack propagation in asphalt materials, it has still some gaps concerning crack initiation and failure.

### **2.1.3 Dissipated Energy concepts**

Asphalt is a viscoelastic material, thus it dissipates energy under mechanical work (loading and relaxation). Its mechanical behaviour depends on the temperature and loading conditions; it has an elastic behaviour under low temperatures and short loading time conditions; it has a viscous behaviour under high temperatures and long loading time conditions. Figure 9 shows the behaviour of asphalt when a constant load is applied on it. The elastic material (a) is characterised by a complete recovery to the original position when the load is removed; in the viscous material (b) the strain increases over time and there will be a permanent deformation when the load is removed; in the viscoelastic material the strain increases over time and, when the load is removed, it tends to the original position but it still maintains a residual deformation on it (Suthersan, 2010, Hamed, 2010).

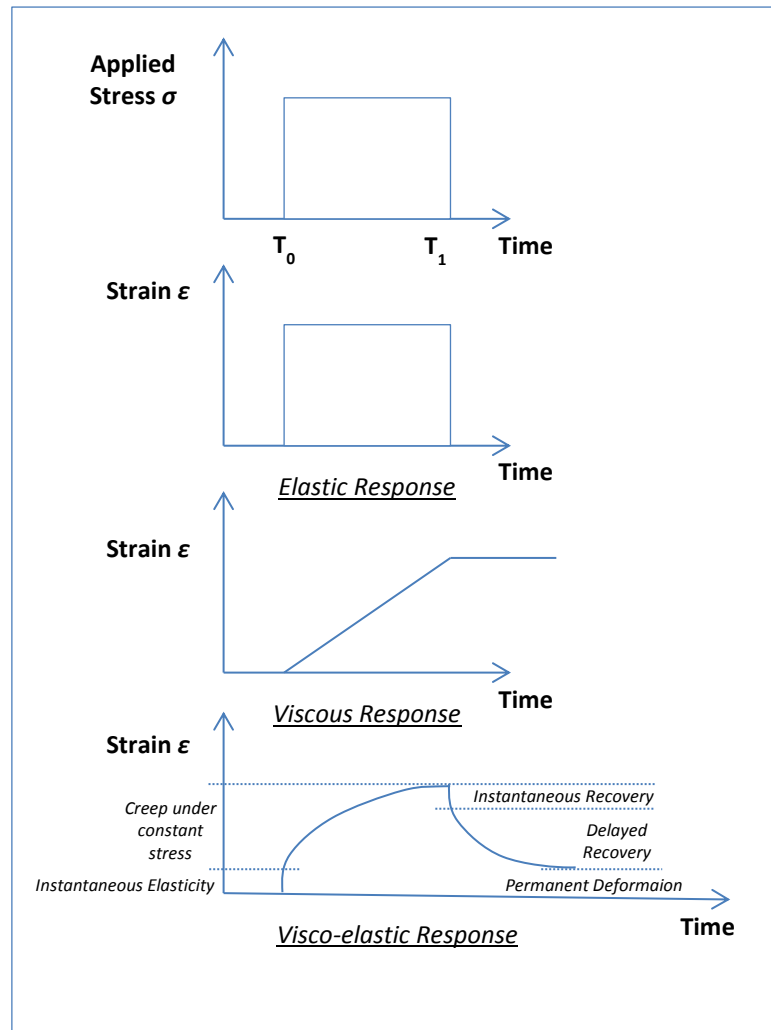


**Figure 9** Response of elastic, viscous and viscoelastic material under constant stress loading (Hamed, 2010)

Energetically, in an elastic material the energy is stored in the system when the load is applied, all the energy is recovered when the load is removed; in this case the unloading and the loading curves coincide. Viscoelastic materials are characterised by a hysteresis loop because the unloaded material traces a different path to that when loaded (phase lag is recorded between the applied stress and the measured strain); in this case the energy is dissipated in the form of mechanical work, heat generation, or damage (see Figure 10, Figure 11 and Figure 12).

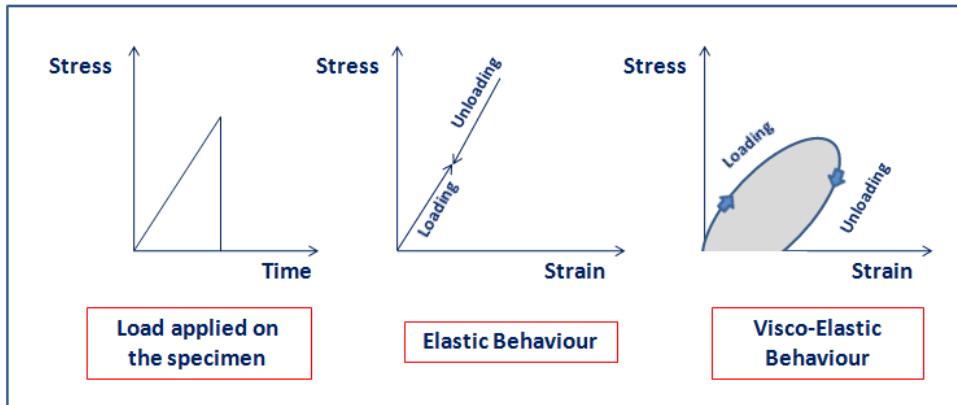


**Figure 10** Elastic and viscoelastic behaviour under loading and unloading conditions  
(Rowe, 1996)

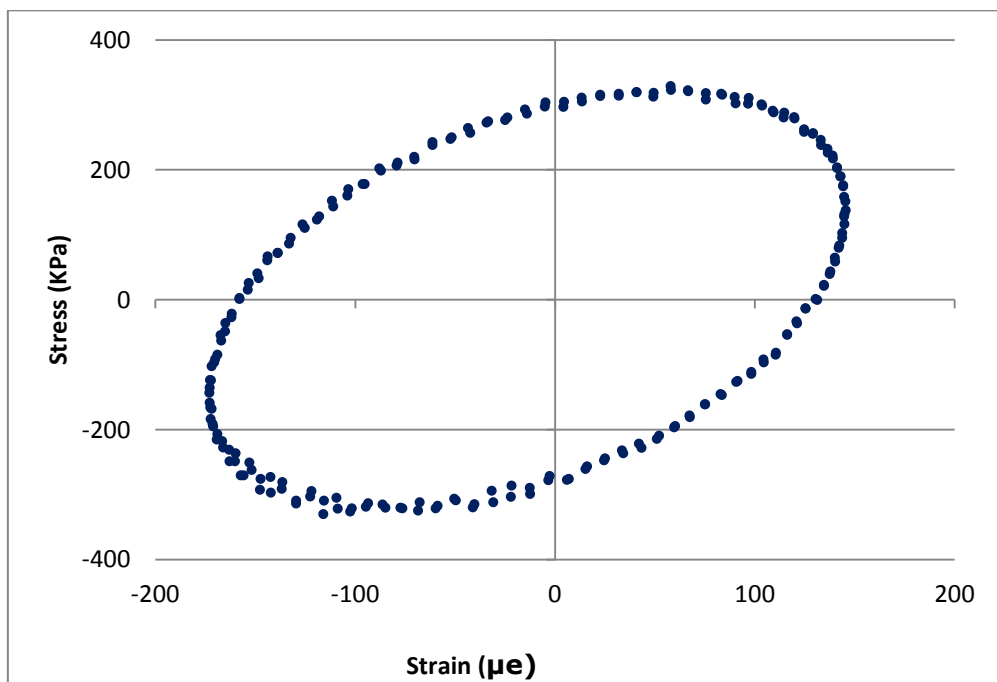


**Figure 11** Hysteresis loop

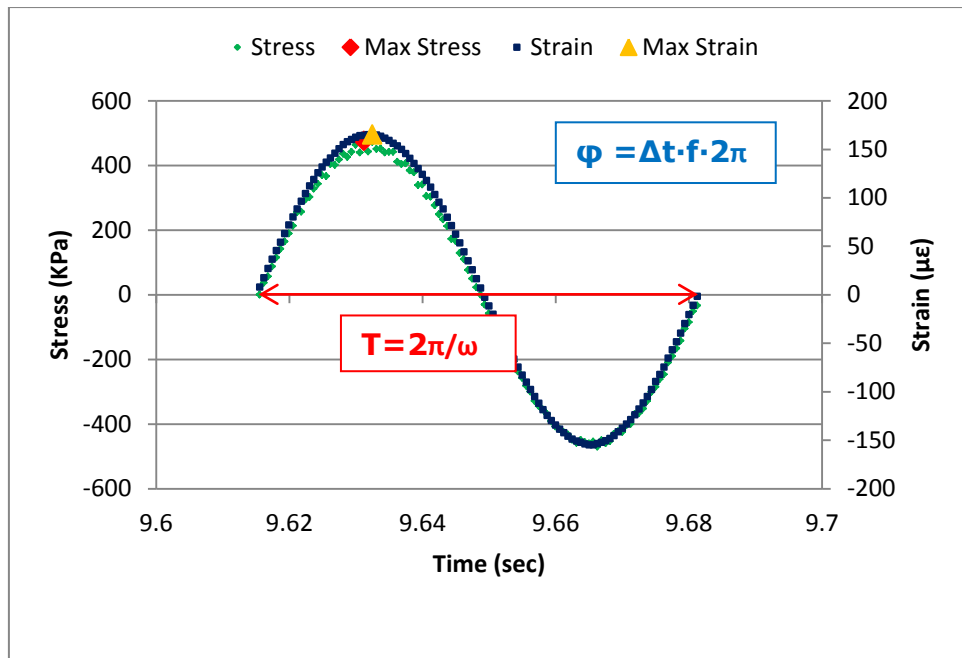


**Figure 12** Phase lag between the applied load and the measured strain

The area of the hysteresis loop represents the dissipated energy in a load cycle and the following equation can be used to calculate its value in a linear viscoelastic material:

$$W_i = \pi \sigma_i \varepsilon_i \sin \varphi_i \quad \text{Equation 17}$$

Where:

- $W_i$  = Dissipated energy in cycle  $i$ ,
- $\sigma_i$  = stress level in cycle  $i$ ,
- $\varepsilon_i$  = strain level in cycle  $i$ , and
- $\varphi_i$  = phase angle in cycle  $i$ .

During a fatigue test, the stiffness reduces, the fatigue process starts and microcracks are induced in the material; therefore the dissipated energy,  $W$ , varies per loading cycle and it, usually, increases for controlled stress tests and it decreases for controlled strain tests, as shown in Figure 13 (Rowe, 1996).

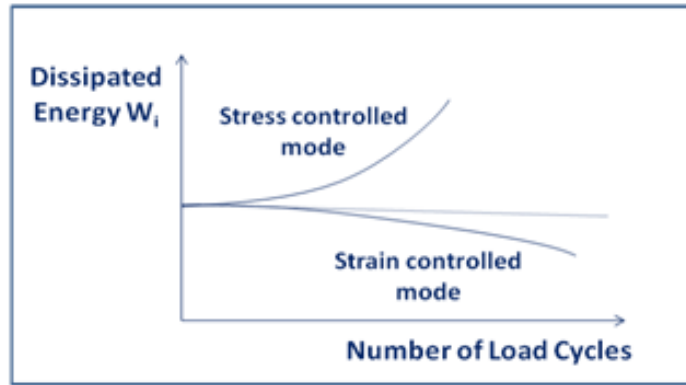


**Figure 13** DE versus load cycle for different loading modes (Rowe, 1996)

The hysteresis loop and the stress and strain sinusoidal waveforms start to change (see Figure 14); microcracks generate discontinuities in the stress-strain path; in the beginning the waveforms are smooth and well defined, then they start to deform (first failure: cracking) and in the end they are flat (fatigue failure) (Al-Katheen and Shenoy, 2004). In addition the dissipated energy is history dependent, i.e. the energy dissipated in a cycle depends on the energy dissipated in the previous cycle (Shen and Carpenter, 2007).

Some researchers (Ghuzlan and Carpenter, 2000; Ghuzlan and Carpenter, 2001; Shen and Carpenter, 2007 and Shen, 2007) believe that in order to have damage in the material there should be a change in the hysteresis loop, and thus a change in dissipated energy. Since the dissipated energy is path dependent, it is a parameter well related to the damage accumulation in a specimen.

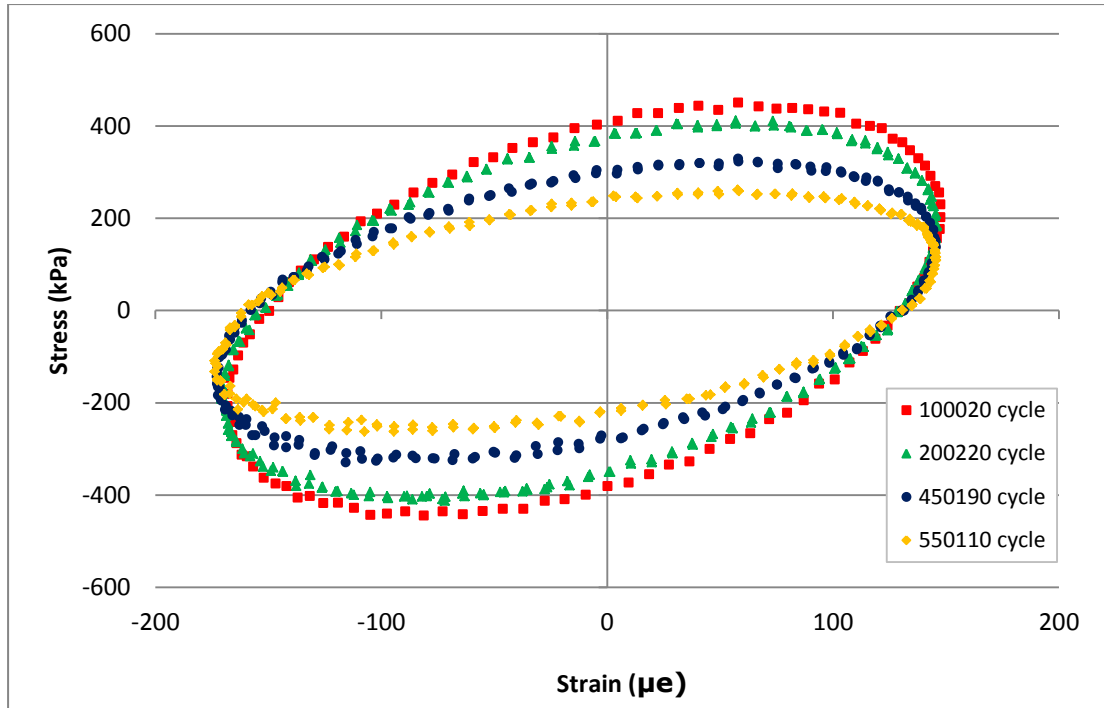


**Figure 14** Changing of the hysteresis loop during a fatigue test (at 20°C, 15Hz; at 160 µε; on 10mm DBM)

## 2.2 Dissipated Energy approaches

In the literature, several dissipated energy based methods exist. In following sections, a description and analysis of some dissipated energy methods is reported.

### Initial Dissipated Energy (IDE) approach

The initial dissipated energy is the dissipated energy measured at initial loading cycles, usually measured at the 50th cycle from the beginning of the fatigue test.

Different researchers (Rowe, 1993; Shen and Carpenter, 2007; SHRP-A-404, 1994; Baburamani, 1999) have showed that the initial dissipated energy is a factor that affects the fatigue in asphalt mixtures, thus it could be a good parameter to describe the fatigue behaviour of pavements. The SHRP-A-404 Project developed the following surrogate fatigue model to relate the fatigue life to the initial dissipated energy:

$$N_f = 2.365e^{0.069W_0} (W_0)^{-1.882} \quad \text{Equation 18}$$

$$W_0 = 0.25\pi\varepsilon_0^2 \cdot (E_0 \sin \varphi_0) \quad \text{Equation 19}$$

Where:

- $N_f$  = the fatigue life,
- $W_0$  = the initial dissipated energy at the 50<sup>th</sup> cycle, and
- VFB = the percentage void filled with binder.

Other researchers (Shen, 2007) have found out that the initial dissipated energy approach is not appropriate for fatigue tests that are taken under low strain levels.

### **Cumulative Dissipated Energy (CDE) approach**

The cumulative dissipated energy is the total energy dissipated by the material during the fatigue test; in particular it is the sum of all areas within the stress-strain hysteresis loop for every cycle until failure, relating the fatigue behaviour to both initial and final cycles. Van Dijk was one of the earliest researchers that applied the dissipated energy concepts to study fatigue in asphalt mixtures. To better describe fatigue behaviour in asphalt mixes, Van Dijk led a laboratory campaign of bending tests (i.e. two and three point bending tests) undertaken under a different range of temperature (between 10 and 40°C) and several frequencies (between 10 and 50 Hz). Based on past investigations (i.e. Heukelom and Quedeville in 1971), he calculated the total dissipated energy per unit volume given by the following summation:

$$W_{fat} = \sum_{i=1}^n W_i \quad \text{Equation 20}$$

Where:  $W_i$  is the dissipated energy at  $i^{\text{th}}$  cycle using the mean values for stress, strain and phase angle. Van Dijk in 1975 determined a unique equation that relates the total dissipated energy to the number of cycles to failure for the different loading conditions as follows:

$$W_{fat} = A(N_f)^z \quad \text{Equation 21}$$

Where:

- $W_{fat}$  = the cumulative dissipated energy to failure,
- $N_f$  = the number of load cycle to failure, and
- $A, z$  = the mixture dependent constants (experimentally determined).

The relationship seems to be independent of the mode of loading, temperature and rest periods; but it is very material dependent (Van Dijk, 1975 and Van Dijk and Visser, 1977).

Figure 15 shows cumulative dissipated energy (CDE) versus cycles to failure obtained by using a 2PB fatigue test in strain controlled mode at 20°C and 15 and 25 Hz; for a higher fatigue life of the mix more energy is dissipated.

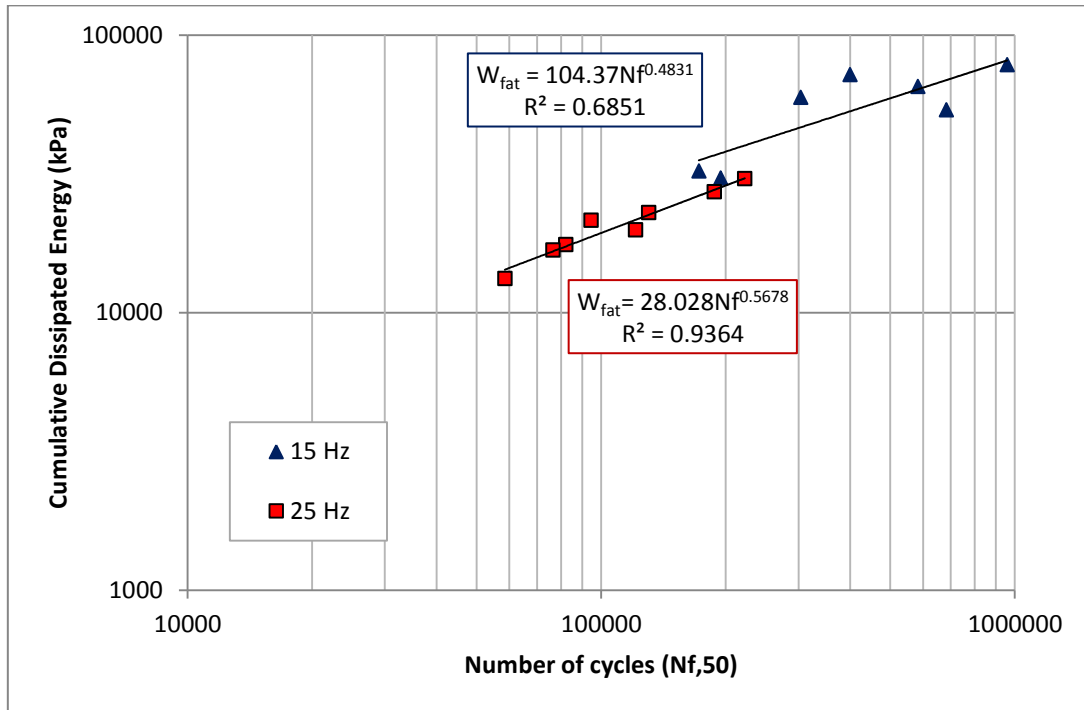


**Figure 15** CDE versus cycles to failure using 2PB in strain controlled mode at 20°C, at 15 and 25Hz (10mm DBM)

Van Dijk developed his research and he introduced an energy ratio  $\psi$  that related loading mode and the mixture properties (stress, strain and phase angle).  $\psi$  is the ratio between the initial cumulative dissipated energy  $\Sigma W_{initial}$  and the total dissipated energy  $\Sigma W_{fat}$  :

$$\Psi = \frac{\Sigma W_{initial}}{\Sigma W_{fat}} \quad \text{Equation 22}$$

Where:  $W_{initial} = N_f \cdot \pi \cdot \sigma_0 \cdot \varepsilon_0 \cdot \sin \varphi_0$  and  $N_f$  is the total number of cycles to failure (subscript “0” indicates the initial values of the material characteristics).

Since the dissipated energy decreases in a controlled strain test, the ratio “ $\psi$ ” was found to be greater than 1 for controlled strain tests; since the dissipated energy increases in a controlled stress test, the ratio “ $\psi$ ” was found to be less

than 1 for controlled stress tests; therefore  $\psi$  is dependent on the type of test and the mix stiffness as shown in Figure 16 (Van Dijk 1975; Van Dijk and Visser, 1977; Rowe, 1996 and Shen, 2007).

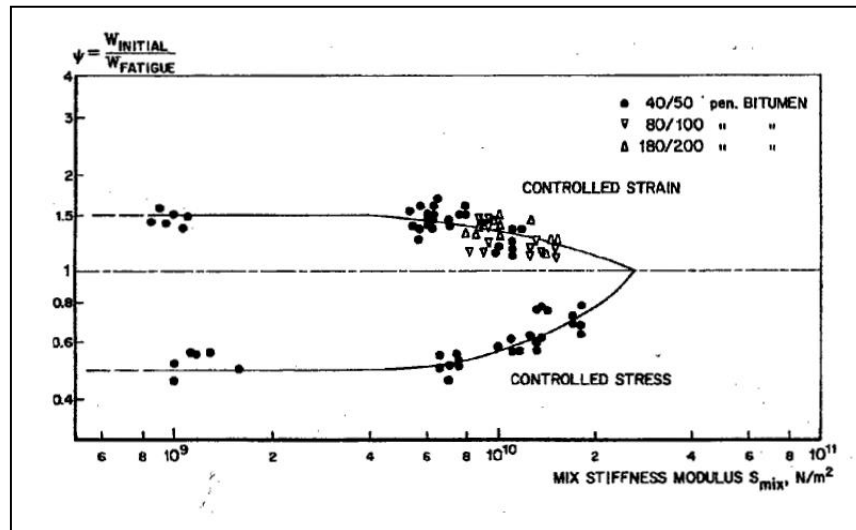


**Figure 16** Evolution of  $\psi$  during stress and strain controlled tests (Van Dijk, 1975 and Van Dijk and Visser, 1977)

CDE is not a good parameter to describe the fatigue phenomenon in asphalt materials; it does not distinguish the amount of DE due to damage rather than viscoelasticity. Also, Equation 21 is not unique; it was found that it changes depending on the mode of loading frequency and temperature. The same result was found by SHRP-A-404 1994 for stress controlled tests (SHRP-A-404, 1994).

### **Dissipated Energy Ratio approach**

Some researchers in 1989 proposed a new dissipated energy method based on the determination of the dissipated energy ratio (DER) defined as follows:

$$DER = \frac{W_i}{\Sigma W_i} \quad \text{Equation 23}$$

Where:  $W_i$  is the dissipated energy at the cycle  $i$ ,  $W_i = N_f \cdot \pi \cdot \sigma_i \cdot \varepsilon_i \cdot \sin \phi_i$ ,  $\Sigma W_i$  is the accumulated dissipated energy up to the cycle  $n$  (Hopman et al., 1989; Pronk and Hopman, 1990; Pronk, 1995).

Pronk suggested a new definition of fatigue life  $N_1$  based on the idea that a difference between the energy needed for the creation of micro cracks and the energy needed for the growth of these cracks exists.  $N_1$  represents the

point where the widening of hair cracks starts and the creation of crack network develops until failure (Pronk, 1999).

In order to obtain  $N_1$ , it is necessary to plot DER versus number of cycles. If the specimen is tested in strain controlled mode, the DER will be a straight line with a rapid increase after a certain number of cycles,  $N_1$  (see Figure 17). If the specimen is tested in stress controlled mode, the DER will be a straight line with a rapid decrease after a certain number of cycles,  $N_1$  (see Figure 18).  $N_1$  is determined graphically and it is the point at which data deviates from the straight line.

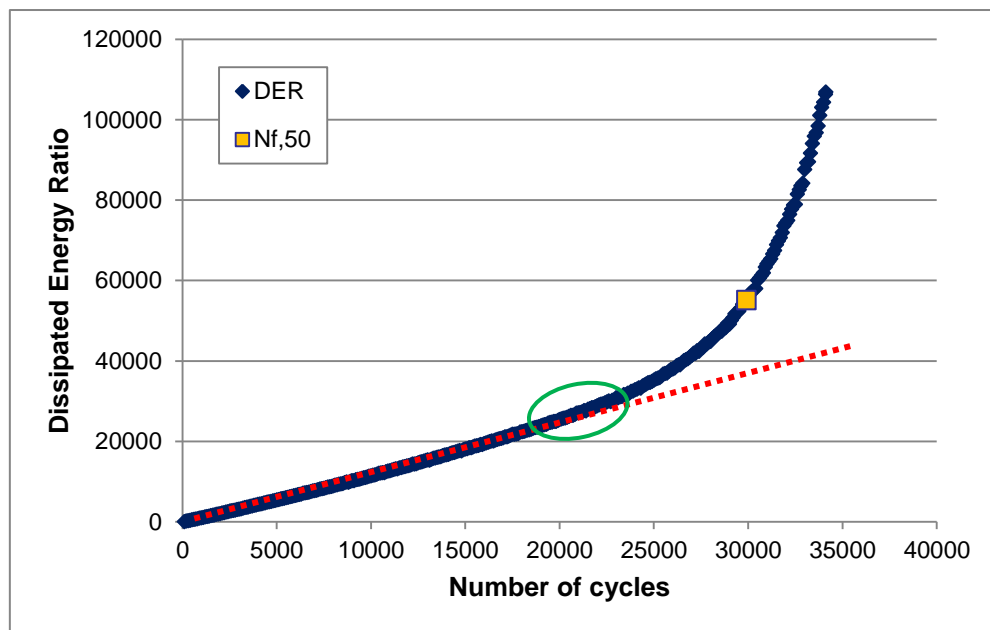


**Figure 17** DER vs Number of cycles during a fatigue test undertaken in strain controlled mode at  $190\mu\epsilon$ ,  $10^\circ\text{C}$ , 25 Hz on 20mm DBM

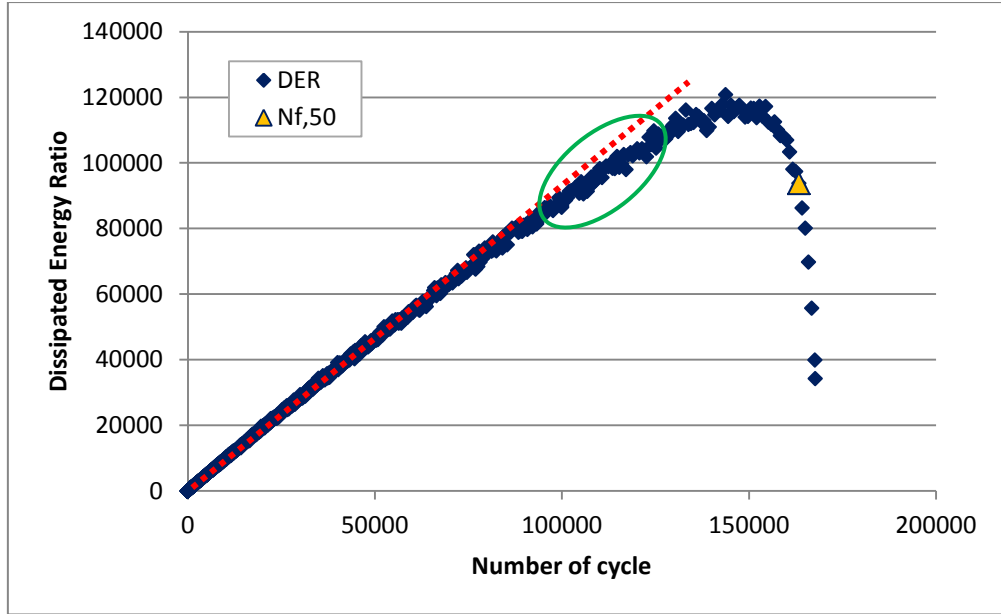


**Figure 18** DER vs Number of cycles during a fatigue test undertaken in stress controlled mode at 1500 kPa, 10°C, 25 Hz on 20mm DBM

The determination of  $N_1$  is subjective and is dependent on the mode of testing.

### **Energy Ratio approach**

Energy ratio (ER) was developed from previous works such as Van Dijk and Visser (1975) and Pronk (1990). ER is the ratio between the product of the initial dissipated energy  $W_0$  multiplied by the number of load cycles  $n$ , and the dissipated energy at the  $i^{th}$  cycle, as calculated in the following expression:

$$ER = \frac{n \cdot W_0}{W_i} \quad \text{Equation 24}$$

The ER can be written as:

$$ER = \frac{n \cdot (\pi \cdot \sigma_0 \cdot \varepsilon_0 \cdot \sin \varphi_0)}{\pi \cdot \sigma_i \cdot \varepsilon_i \cdot \sin \varphi_i} \quad \text{Equation 25}$$

For strain controlled tests, the strain level remains constant during the test and if the stress is replaced by the product of strain  $\varepsilon$  and modulus  $E^*$ , Equation 25 can be rewritten as follows:

$$ER = \frac{n \cdot (\pi \cdot \varepsilon_0^2 \cdot E_0^* \cdot \sin \varphi_0)}{\pi \cdot \varepsilon_i^2 \cdot E_i^* \cdot \sin \varphi_i} \quad \text{Equation 26}$$

For stress controlled tests, the stress level remains constant during the test and if the strain is replaced by the ratio between stress  $\sigma$  and modulus  $E^*$ , Equation 25 can be rewritten as follows:

$$ER = \frac{n \cdot \left( \pi \cdot \frac{\sigma_0^2}{E_0^*} \cdot \sin \varphi_0 \right)}{\pi \cdot \frac{\sigma_i^2}{E_i^*} \cdot \sin \varphi_i} \quad \text{Equation 27}$$

Removing constant terms and considering that the change of  $\sin \varphi_i$  is smaller compared to the change in  $E^*$ , the Equation 26 and Equation 27 can be written as follows (Rowe, 1993 and Rowe, 1996):

$$ER_\varepsilon = \frac{n}{E_i} \quad \text{for strain controlled test} \quad \text{Equation 28}$$

$$ER_\sigma = n \cdot E_i \quad \text{for stress controlled test} \quad \text{Equation 29}$$

The number of cycles to failure,  $N_1$ , corresponds to the formation of sharp cracks.  $N_1$  is determined by plotting ER against the number of cycles for both controlled strain and stress tests.  $N_1$  is the number of cycles at which a change in behaviour of the curve is underlined; for a controlled strain test  $N_1$  coincides with the point where the slope of ER- $N_f$  deviates from a straight line; for a controlled stress test,  $N_1$  coincides with the peak of the curve ER- $N_f$ . The same author plotted data from strain control test using the criteria developed for stress control test; in this case, data shows a further stage of behaviour due to the crack slowly propagating through the specimen as the stress decreases during a fatigue test (see Figure 19).

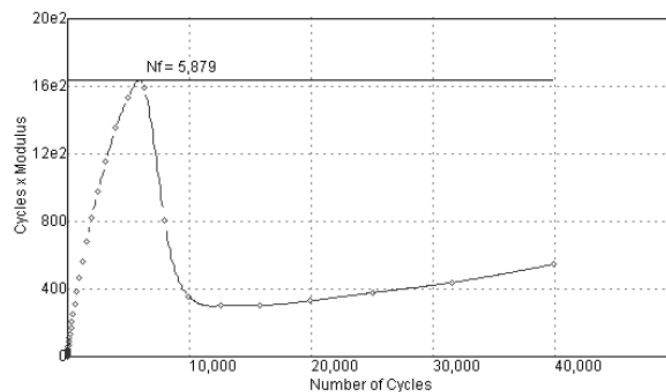


**Figure 19** ER for a strain control test using stress control criteria (Rowe, 1996)

### Ratio of Dissipated Energy Change Approach

Since the dissipated energy is history dependent and, in order to accumulate damage there should be a change in dissipated energy value, some researchers (Ghuzlan and Carpenter, 2000; Carpenter et al. 2003 and Shen and Carpenter, 2007) have suggested the Ratio of Dissipated Energy Change, *RDEC* as a parameter to describe fatigue in asphalt materials. The same researchers believed that the *RDEC* is a true indicator of damage because it is able to eliminate the other forms of dissipated energy due to mechanical work or heat generation; so it can be considered a good parameter to describe the fatigue process in asphalt, and is calculated with the following expression:

$$RDEC = \frac{W_{n+1} - W_n}{W_n} \quad \text{Equation 30}$$

Where:

- *RDEC* = ratio of the dissipated energy change per load cycle,
- $W_n$  = dissipated energy produced in load cycle  $n$ , and
- $W_{n+1}$  = dissipated energy produced in load cycle  $n+1$ .

Figure 20 shows the variation of the *RDEC* with load cycles, and is representative of fatigue behaviour (Shen, 2007).

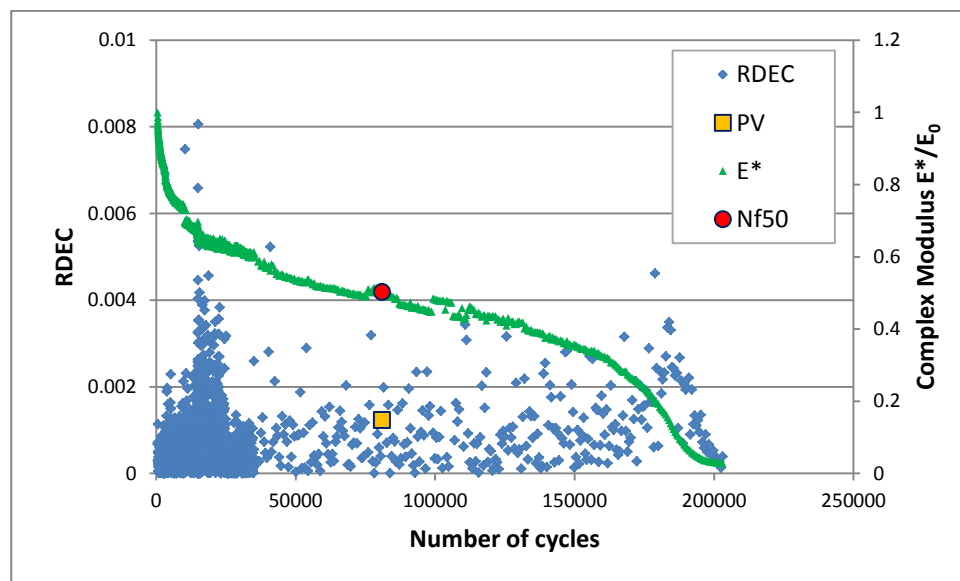


**Figure 20** The variation of *RDEC* with Load cycles obtained from 2PB test undertaken in strain control mode at  $180 \mu\epsilon$ , at  $20^\circ\text{C}$  and 25 Hz on 10mm DBM

The RDEC, after a rapid decreasing (stage I), reaches a plateau stage in which there is constant energy value being turned into damage (stage II); finally the RDEC rapidly increases until true fatigue failure (stage III).

$N_{f50}$  is the typical failure criterion used by many researchers (Tayebaldi et al., 1993) and it corresponds to the 50% initial stiffness reduction and this value was defined as the Plateau Value (PV). Ghuzlan found that the Plateau Value is load dependent for different mixtures and it is mixture dependent for different load levels, and moreover he believed that the PV is a good parameter to obtain a unique relationship for fatigue life (Ghuzlan and Carpenter, 2001).

The procedure to obtain the PV from laboratory fatigue tests, suggested by Shen and Carpenter in 2007, is (Shen, 2007):

- Obtaining the dissipated energy relationship for each loading cycle (a fitting process may be needed to obtain a best relationship);
- Calculation of the parameter  $RDEC_a$ , the average ratio of dissipated energy change between two loading cycles ( $W_a$ ,  $W_b$ ) divided by the number of cycles between the two cycles (a, b):

$$RDEC_a = \frac{W_a - W_b}{W_a \cdot (b - a)} \quad \text{Equation 31}$$

- If the regressed dissipated energy curve vs. loading cycle follows the power law ( $Ax^k$ ), the average RDEC can be simplified and calculated by the following equation:

$$RDEC = \frac{1 - \left(1 + \frac{100}{a}\right)^k}{100} \quad \text{Equation 32}$$

where k is the exponential slope of the regressed dissipated energy curve versus loading cycle.

- Calculation of the PV parameter at normal strain level (200-1000  $\mu\epsilon$ ); the PV can be calculated with the following expression:

$$PV = \frac{1 - \left(1 + \frac{100}{N_{f,50}}\right)^k}{100} \quad \text{Equation 33}$$

where k is the exponential slope of the regressed dissipated energy curve vs. loading cycle, and  $N_{f50}$  is the failure point.

By means of a statistical approach and laboratory fatigue tests, the same researchers (Ghuzlan and Carpenter, 2000; Carpenter et al., 2003; Shen, 2007; Carpenter and Shen, 2005) verified that the PV- $N_f$  relationship is unique for different loading modes, mixture types and testing conditions. In other words the relationship is valid for different mixture types, loads, strains, frequencies and rest periods. The relationship, between the Plateau Value (PV) and the fatigue life at 50% stiffness reduction ( $N_f$ ), is reported as:

$$PV = cN_f^d \quad \text{Equation 34}$$

The value of the constants c and d were determined experimentally (Shen and Carpenter 2007).

According to Ghuzland and Carpenter (2000), Ghuzland and Carpenter (2003), and Shen and Carpenter (2007) failure corresponds to the transition point at which RDEC starts to increase dramatically (transition point between the second and the third stage) and this can be considered as the true failure point (macro-cracking propagation initiates), defined as  $N_{fm}$  (Shen and Lu, 2010).

In order to obtain  $N_{fm}$ , the difference between the area under the dissipated energy curve (SDE) and the trapezoidal area (AT) obtained by linearly connecting the initial dissipated energy and the dissipated energy at cycle n, has be calculated. AT and SDE are calculated as follows:

$$AT = \frac{(DE_0 + DE_n) \cdot n}{2} \quad \text{Equation 35}$$

$$SDE = \sum_0^n DE \quad \text{Equation 36}$$

Where  $DE_0$  is initial dissipated energy, calculated as the average value of the DE between the cycle 100<sup>th</sup> and 500<sup>th</sup> to take into account the variation of the

data;  $DE_n$  is the dissipated energy produced in load cycle  $n$ , and  $n$  is the number of load cycles. The difference is:

$$\Delta A = |AT - SDE| \quad \text{Equation 37}$$

By plotting  $\Delta A$  against the number of cycles, it is possible to obtain  $N_{fm}$  as the peak value of the curve as shown in Figure 21.

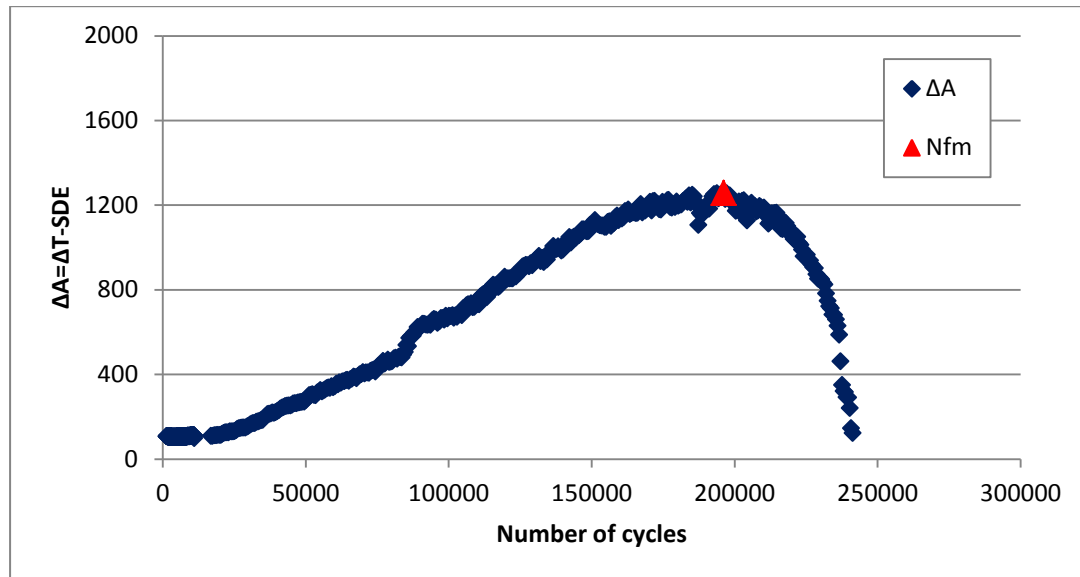


**Figure 21**  $\Delta A$  against number of cycles during a fatigue test for the 10mm DBM

### 2.3 Factors affecting fatigue in asphalt mixtures

Various factors affect the fatigue behaviour such as: the method of specimen construction (compaction), the loading (axle loads, modes and patterns), the rest periods (healing effect), the material characteristics, traffic and environmental variables (temperature, ageing, healing, etc.). In theory, construction variables and material characteristics can be controlled, but load and environmental variables can change significantly.

This project focuses more attention on the healing phenomenon, thus the effects of including rest periods, in asphalt materials.

#### Traffic Loading

Traffic loading is one of the main inputs in the design procedure (others are subgrade strength and temperature). Usually it is convenient to convert every real traffic load (wheel loads of various magnitudes and repetitions) into an equivalent number of a standard axle loading – ESAL (equivalent 80 kN single axle load) (HRB, 1962). Several loading waveforms are used to simulate

traffic loading in the laboratory; the most common is the sinusoidal: it approximates more realistically the traffic load expected in the field. Loading frequency and duration influence the fatigue life; increasing the frequency or decreasing the duration of load pulse increases the stiffness, thus the fatigue life increases (Read, 1996).

### **Temperature**

Pavement temperatures are affected by air temperatures as well as precipitation, wind speed, and solar radiation. Also, annual, seasonal, and daily variations in temperature and precipitation have large influences on pavement service life. For flexible pavements, temperature has an effect on the stiffness of the bituminous layers. Asphalt concrete becomes stiffer at lower temperatures and softer at higher temperatures and exhibits different material characteristics at different temperatures. Stiffness of a general asphalt layer seems to decrease by about three times when the temperature increases by ten degrees, which means that temperature influences the fatigue behaviour of asphalt material (Ongel, A. and Harvey, J. 2004).

### **Rest Period**

Usually, a fatigue test is carried out through a dynamic test with continuous loading cycles without any rest. To better simulate what in the reality happens (elapsing time between two successive axles of the same or different vehicles), it could be helpful introduce a rest period between successive load cycles.

Many researchers (SHRP-A-404, 1994, De La Roche and Riviere, 1997, Baburamani, 1999, Si et al. 2002a, Si et al. 2002b, Kim et al. 2003, Kim and Roque, 2006, Castro and Sanchez, 2006 and Shen and Carpenter, 2007) have demonstrated an increases in the fatigue life when a rest period is introduced during a fatigue test. In particular, the improving in fatigue life is shown in Figure 22.

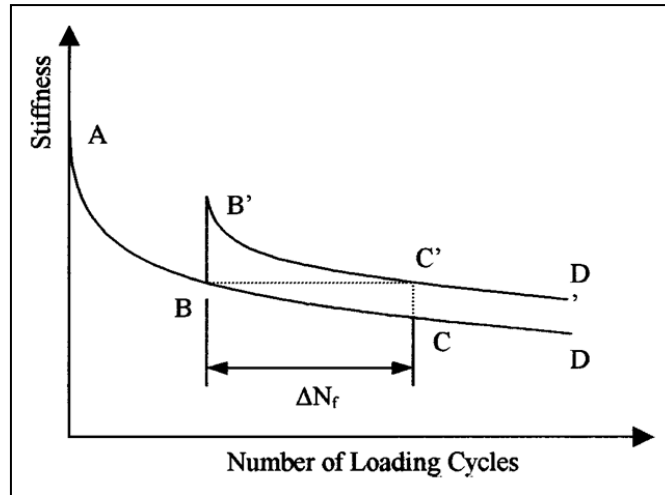


**Figure 22** The effect of rest periods during a fatigue test (Castro and Sanchez, 2006) During a fatigue test, the stiffness modulus decreases (curve ABD); when a rest period is considered during the test, the stiffness modulus recovers; healing is taking place during the rest. So, after the rest, when the load is applied again on the specimen the stiffness modulus decreases again (curve B'C'D').

### **Material characteristics**

In general, for continuously graded mixes, the two primary factors influencing fatigue life are: the asphalt content and the air void content (aggregate type seems to have less influence). The increase of asphalt content will increase the fatigue resistance of the mixture. The decrease of air void content (compaction level) will increase the fatigue resistance; also in this case it should comply with the permanent deformation requirements (Read, 1996).

### **Ageing**

Another factor that can influence the fatigue life in asphalt material is: ageing or hardening. Usually ageing is a phenomenon linked with the bituminous binder and is manifested as an increase in viscosity of the bitumen and consequential stiffening of the mixture. Ageing is primarily associated with the loss of volatile components and oxidation of the bitumen in the process of asphalt mixture construction (short-term ageing) and progressive oxidation of the in-place material in service (long-term ageing). Both phenomena can change the fatigue resistance in asphalt mixtures (Raad et al., 2001 and Airey, 2003).

## **2.4 Healing**

Since 1970, the healing of asphalt mixtures has been considered a very important phenomenon, responsible for the difference between the laboratory and the field experience in fatigue behaviour. Healing in asphalt mixtures has been analysed by few researchers and its connection to fatigue behaviour is still far from clear. Thus, more research and more tests should be done to better improve this knowledge.

### **2.4.1 Mechanism of healing**

Kim et al (1990) considers two different mechanisms for healing occurring simultaneously in an asphalt pavement. The first one is the chemical healing in microcrack and macrocrack faces; the second one is the relaxation of stresses due to the viscoelastic behaviour proper of an asphalt mixture (Kim et al., 1990, Kim et al.1991). The same researchers have evaluated the effects of the two healing mechanisms during rest periods in cyclic uniaxial tests. They have considered the nonlinear viscoelastic correspondence principle, including pseudostrain concepts, to evaluate the mechanisms separately, transforming a viscoelastic problem into an elastic one by means of a constitutive model. In the end they believe the stress increase after a rest period is due to the chemical healing and viscoelastic behaviour of asphalt. They also believe that the chemical healing has a strong influence on the evaluation of fatigue life; in particular they noticed that the aliphatic chains in the binder influence the chemical healing, by means of chemical analyses. The chemical analysis, however, was not fully understood by the authors, so the same researchers believe that more testing is necessary to better understand chemical healing and its influence in fatigue life.

According to some researchers (Bhasin et al, 2009, Little and Bhasin, 2008) healing is a “two step” process in asphalt: viscoelastic recovery and healing in asphalt material. The first one occurs also when the stress or strain is too low to damage the material and recovery is due to the rearrangement of molecules in the material. Healing occurs only for high levels of stress that generate damage, and it is due to the wetting and intrinsic healing processes occurring across a crack interface.

## 2.4.2 Healing in literature

Several researchers (Little et al., 2001, Lytton et al., 1993, Si et al., 2002b, Shen, 2007) have used different ways to quantify and characterise the impact of healing occurring during rest periods in fatigue.

Some researchers (Lytton et al., 1993) used a shift factor to include the effects of healing in the evaluation of fatigue life from laboratory tests. Generally laboratory fatigue life ( $N_{lab}$ ) is multiplied by a shift factor (SF), in order to obtain fatigue life in the field ( $N_{field}$ ):

$$N_{field} = N_{lab} \times SF \quad \text{Equation 38}$$

There are many values for the SF but, Lytton et al. defined it as the results of three individual processes occurring in the material: healing, residual stresses and resilient dilatation. In particular, for the healing processes SF has the following expression:

$$SF_h = 1 + \alpha(t_r)^b \quad \text{Equation 39}$$

Where:

- $SF_h$  is the shift factor due to the healing process,
- $t_r$  is the rest period,
- $a$  and  $b$  are the healing coefficient and the exponent respectively.

For the same researchers the  $SF_h$  varies between 1 and 10, for other researchers (Bhasin et al., 2009) the  $SF_h$  can be between 1.09 and 2.7 for a 30 seconds rest period.

Previously, the Ratio of Dissipated Energy Change (RDEC) approach was presented (Carpenter and Shen, 2006 and Carpenter and Shen, 2007). In this approach the researchers have quantified the healing effects by considering the reduction of PV due to the rest periods in a fatigue test. In this way the healing effect can be included in the PV prediction model as shown in the following equation:

$$PV_h = PV_{w/0} \times \text{healing\_factor} \quad \text{Equation 40}$$

Where:

- $PV_h$  is the PV value considering healing, and

- $PV_{w/o}$  is the PV value not considering healing.

In this case the healing factor is evaluated based only on the influence of the rest periods. Later, the same researchers were able to rewrite the equation above, considering the laboratory fatigue behaviour based on energy principles, as follows:

$$PV_h = PV_{w/o} \times (RP+1)^{slope} \quad \text{Equation 41}$$

Where  $(RP+1)^{slope}$  is the healing factor and the slope represents the healing rate for a particular mixture (Shen, 2007).

The healing rate is the gradient of the relation between PV and rest period (RP) on a log-log scale and it represents the energy recovery per unit of rest time; see Figure 23 (Carpenter and Shen, 2006 and Sutharsan, 2010).

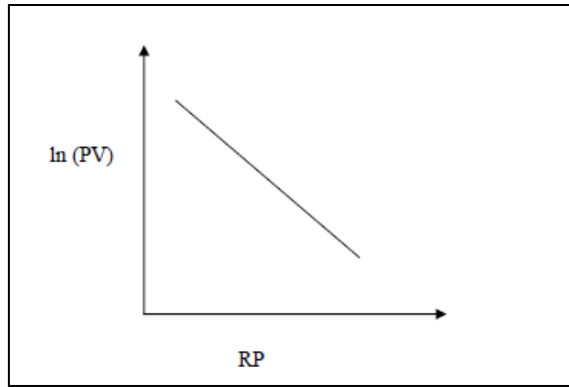


**Figure 23** PV-RP curve on a log-log scale (Sutharsan, 2010)

The researchers believed that the healing rate is not affected by the duration of rest period.

Kim and Roque (2006) have analysed the healing effect of four asphalt mixtures and they have considered the dissipated creep strain energy (DCSE) recovered per unit of time to better understand healing in asphalt.

DCSE is the absorbed energy that damages the material (Kim and Roque, 2006). They undertook several creep tests in order to obtain the parameters necessary to express the accumulated DCSE as the following expression:

$$\frac{DCSE}{cycle} = \frac{1}{20} \sigma_{AVE} [\sigma_{AVE} D_1 m(100)]^{m-1} \quad \text{Equation 42}$$

Where:

- $\sigma_{AVE}$  is the average stress applied,

- $D_1$  and  $m$  are material properties

To consider the healing effect the same researchers considered the plot of DCSE versus time and they noticed that healing is not linear; the rate of healing reduced with time and is proportional to the DCSE applied. See Figure 24.

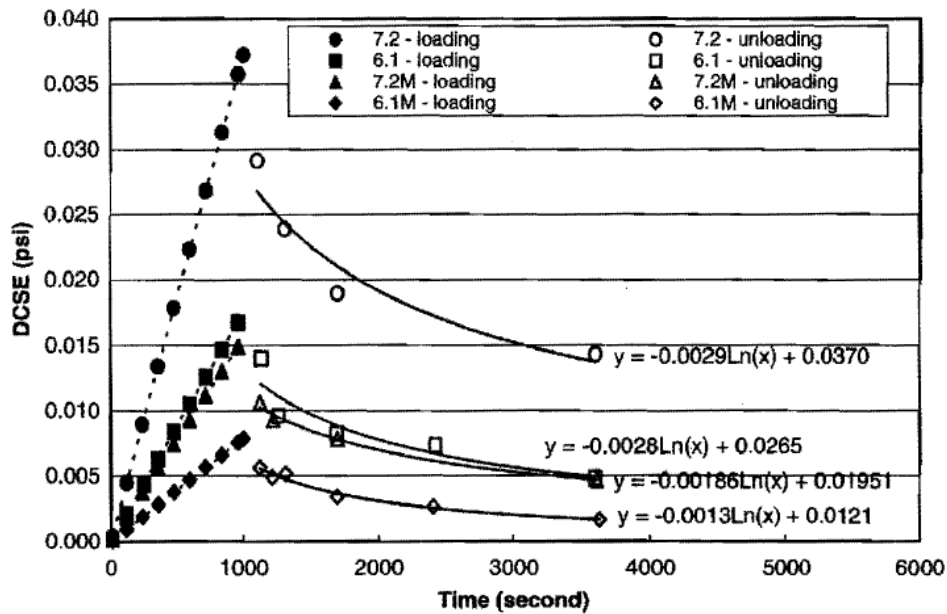


**Figure 24** Healing test: DCSE plotting versus time (Kim and Roque, 2006)

They considered the normalized DCSE (DCSE divided by the total DCSE) to define the healing properties of a material, and it seems to be affected by the binder content and temperature. Healing rate increases when the binder content is low; healing rate increases when the temperature increases (Kim and Roque, 2006).

Daniel and Kim (2001) have compared the healing potential of two asphalt mixtures, during a fatigue test (3 Point bending test) by means of a non-destructive method based on the stress wave propagation. In particular they analysed the fatigue damage growth in the material demonstrating the different healing potential of the two materials and evaluating the effects of rest periods and temperature. The researchers (Daniel and Kim, 2001) evaluated several methods to compare the healing potential in the two mixtures:

- Percent Increase (PI) in the number of cycles to failure. This is the difference between the number of cycles of a fatigue test with or without a rest period.

$$PI = \frac{N_{f,healing} - N_f}{N_f} \quad \text{Equation 43}$$

- Damage Indicator (DI). This is the ratio between the number of cycles that a specimen has reached at a particular rest period and the number of cycles to failure.

$$DI = \frac{N_{at\_a\_particular\_rest\_time}}{N_{f,healing}} \quad \text{Equation 44}$$

- Horizontal Increase (HI). This is the ratio between the number of cycles reached during three rest periods and the number of cycles to failure.

$$HI = \frac{\Delta N_{f,1} + \Delta N_{f,2} + \Delta N_{f,3}}{N_{f,healing}} \quad \text{Equation 45}$$

- Comparison of the decreasing and increasing of the flexural stiffness before and after a rest period.

All four methods have shown that the stiffness modulus was decreasing as the temperature increases and it was increasing during rest periods as microcracks heal; the higher temperatures seem to encourage healing in asphalt mixtures (Daniel and Kim, 2001 and Kim et al., 2003).

## 2.5 Laboratory fatigue testing

Researchers have brought forward their research projects by means of several fatigue tests. Below some general categories of the most used test methodologies over the past are presented (Rao Tangella et al., 1990).

### Simple Flexural

The stress or the strain is applied with sinusoidal waveform until the specimen reaches the failure point. So the mathematical results will be expressed linking the number of cycles to failure to the stress or strain level. In simple flexural tests, usually a prismatic beam (or a trapezoidal beam) is subjected sinusoidally to a load under center-point or third-point configuration;

### **Supported Flexural**

The stress or strain is directly related to the number of cycles to failure (fatigue life). The specimen (beam or circular slab) is supported in several ways to simulate in-situ stress and modes of loading conditions. In this type of test there is a better simulation of the field conditions, but at the same time it is more time consuming, more costly and more complex than other kinds of fatigue test

### **Direct axial**

In this kind of test, the stress (usually conducted in the controlled stress mode of loading) is applied using sinusoidal or pulsating loads in a uniaxial manner to the specimen (circular or rectangular shape). Different types of this kind of tests are: tension (uniaxial tensile tests without stress reversal), compression (uniaxial compressive tests without stress reversal) and tension-compression tests (uniaxial tensile and compressive loading tests).

### **Traixial**

This test is similar to the previous one but in this case the test is characterised by specimens (cylindrical shape) subjected to a sinusoidal axial stress with confinement. One of the main advantages is that this test simulates the loading conditions in the field very well, even if this test seems be time consuming.

### **Diametral**

Also in this kind of test, the stress or the strain is applied using pulsating loads in a diametral direction. It is an indirect tensile fatigue test - ITFT, usually, conducted on cylindrical specimens by means of a compressive load. In this way, a uniform tensile stress perpendicular to the load and along the vertical diametral plane is developed. Even if it is a simple test that can also be performed on field cores it tends to underestimate the fatigue life of the mixture, due to accumulation of permanent deformations during the test.

### **Fracture Tests**

The main characteristic is that for this kind of test the user considers fracture mechanics principles to predict the fatigue life of the mixture under testing. The fatigue crack growth usually considers three main stages: crack initiation, stable crack propagation and failure. This kind of test is able to explain and

represent the crack propagation stage very well, but it is not able to quantify the crack initiation and the failure stages.

### **Wheel-tracking tests**

The stress or the strain is related to the number of load applications or to the amount of cracking in the specimen/slab. In the laboratory a wheel tracking machine is used, a loaded wheel (with a pneumatic tire) moved back and forth over a specimen. Of course one of the limitations of this test is the speed of the rolling wheel and sometimes rutting could be more significant than fatigue. However it is a good simulation of the field conditions.

For the full-scale arrangements a good example is the *Pavement fatigue carousel* in Nantes, France (see Figure 25). It is composed of a central tower and four arms, usually ended with different configurations of loads (single or twinned wheels on simple or tandem axle or single wheel on a triple axle).



**Figure 25** *Pavement Fatigue Carousel* in Nantes, France

Certainly this kind of test can do an excellent simulation of the field conditions, but the initial investment cost and the annual maintenance cost is very high.

This project involved the use of 2 Point Bending test (2PB), 4 Point Bending test (4PB) and Indirect Tensile Fatigue test (ITFT). Also, a new test was developed: Indirect Tensile Fatigue test in strain control mode. An in-depth description for each test used in this project is presented in Chapters 5, 6 and 7.

#### **2.5.1 Considering healing in fatigue tests**

To better understand and quantify the healing effects in asphalt material, researchers usually consider rest periods during a fatigue test.

Depending on the way the material is allowed to rest, there are two different types of test (see Figure 26):

- With rest intervals: the fatigue test is stopped during a rest interval and, at the end of it, it is continued until the next rest interval;
- With intermittent loads: each loading cycle is followed by a rest period; usually this kind of test reflects the true traffic load better than the previous one and the duration of the rest period is a multiple of the loading cycle duration (Castro and Sanchez, 2006).

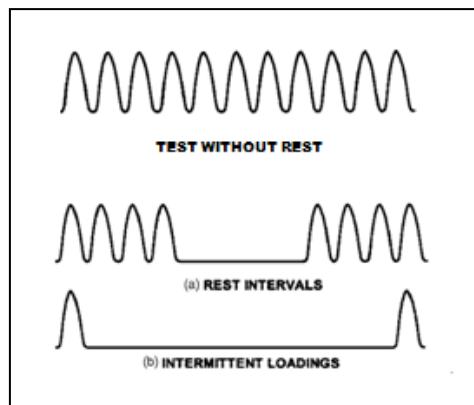


**Figure 26** Test with and without rest (Castro and Sanchez, 2006)

Many researchers have noticed that introducing a rest period during a fatigue test, results in a recovery of the stiffness modulus value, thus the fatigue life increases. Of course this increase is caused by the healing that takes place during the rest periods. Fatigue life, however, does not seem to increase for rest periods greater than ten times the loading time (Castro and Sanchez, 2006, Bonnaure et al., 1983, Di Benedetto et al., 1997, Raithby and Sterling, 1972). So the conclusion is that the optimum rest period value is around ten times the loading time (See Figure 27).

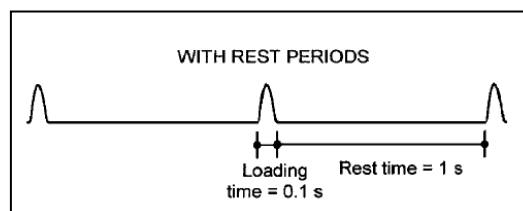


**Figure 27** Optimum rest period value (Castro and Sanchez, 2006)

## 2.6 Summary

This chapter presents an in-depth literature review about fatigue. Several fatigue methods exist in the literature such as phenomenological approach

(that is also the traditional approach used to analyse fatigue), fracture mechanics approach and dissipated energy approach. This project chose to focus more on the dissipated energy methods; thus the dissipated energy concepts related to asphalt materials are described and several methods in this area are presented.

Among all them, three in particular have been chosen to analyse fatigue data: the Dissipated Energy Ratio (DER) by A. Pronk, the Energy Ratio (ER) by G. Rowe, and the Ratio of Dissipated Energy Change (RDEC) by S. Carpenter and S. Shen. Those were chosen because a strong correlation between the changing of dissipated energy and fatigue damage has previously been found. Many other dissipated energy methods do not distinguish the amount of DE due to damage rather than viscoelasticity or heating phenomena and they strongly depend on loading and environmental conditions.

The chapter has also reviewed the different factors affecting fatigue life in asphalt pavement such as temperature, material characteristics, traffic loading, etc.

One of the purposes of this project is to include rest periods during a fatigue test, thus better understand how healing is correlated to fatigue. A literature review about healing phenomenon has been presented. The main reason to do that is because in Pavement Design some of these factors are considered already such as temperature, traffic loading and material resistance. Influence of rest period is not taken into consideration yet, although loading in the field is not applied continuously but rest periods happen in real asphalt pavements. To better understand fatigue behaviour, three different testing machines are involved in this project: 2 Point Bending, 4 Point Bending and Indirect Tensile Fatigue test. 2PB and 4PB are flexural fatigue tests; ITFT is a diametral test. ITFT is a common test used by different civil engineering and construction companies for pavement design purposes. As part of the project an exchange with the French Institution IFSTTAR in Nantes was planned to get knowledge about the 2PB. 4PB test and ITFT tests were, instead, undertaken at the University of Nottingham. The same loading and environmental conditions were chosen to undertake tests on the same material. A key point

of this project is the development of the ITFT in strain control mode to be able to compare results with the flexural fatigue tests mainly used in research.

## 2.7 List of variables

- $N_f$  is the Number of cycle to failure,
- $\varepsilon$  is the tensile strain
- $\sigma$  is the tensile stress
- A, b, C, d are material coefficients, derived of fitting the data from laboratory testing.
- $\varepsilon_t$  is the tensile strain at the bottom of the asphalt layer,
- $E_0$  is the initial stiffness modulus (at the 50th cycle);
- $K_1$ ,  $K_2$  and  $K_3$  are regression constants obtained from laboratory testing.
- D is the damage,
- T is the number of periods,
- $n_i$  is the number of load applications during a period I;
- $N_i$  is the the ultimate number of load applications the pavement could carry.
- PI is the Penetration Index of the bitumen,
- E is the stiffness of the mixture.
- $E^*$  is the complex modulus.
- $V_b$  is the percentage of bitumen by volume in the layer;
- $V_a$  is the percentage of aggregate by volume in the layer;
- $V_v$  is the percentage of air voids by volume in the layer;
- C is the correction factor;
- $\mu\varepsilon_t$  is the tensile microstrain;
- $E^*$  is the complex modulus;
- VFB is the percentage of voids filled with bitumen;
- $\varepsilon_0$  is initial tensile strain;
- $\delta$  is the phase angle;
- $da/dN$  is the crack growth rate;

- $\Delta K$  is the range of the stress intensity factor;
- $C$  and  $m$  are material constants: the intercept and the slope on the log-log plot of  $da/dN$  versus  $\Delta K$ ;
- $Y$  is a function depending on the specimen geometry and the crack;
- $a_c$  is the critical length at which instantaneous fracture will occur;
- $a_i$  is the initial crack length at which fatigue crack growth starts for the given stress range  $\Delta\sigma$ ;
- $K_{IC}$  is the fracture toughness;
- $\sigma_t$  is the tensile stress;
- $W_i$  is the Dissipated energy in cycle  $i$ ;
- $\sigma_i$  is the stress level in cycle  $i$ ;
- $\varepsilon_i$  is the strain level in cycle  $i$ ;
- $\varphi_i$  is the phase angle in cycle  $i$ ;
- IDE is the Initial Dissipated Energy method;
- $W_0$  is the initial dissipated energy (at the 50th cycle);
- CDE is the Cumulative Dissipated energy method
- $\Sigma W_{fat}$  is the cumulative dissipated energy to failure,
- $\Sigma W_{initial}$  is the initial cumulative dissipated energy ;
- DER is the Dissipated Energy Ratio method;
- $\Sigma W_i$  is the accumulated dissipated energy up to the cycle  $n$ ;
- $N_1$  is the number of cycle to failure (in both DER and ER methods);
- ER is the Energy Ratio method;
- $N$  is the number of cycle;
- $\sigma_0$  is the initial stress level (at the 50th cycle);
- $\varepsilon_0$  is the initial strain level (at the 50th cycle);
- $\varphi_0$  is the initial phase angle (at the 50th cycle);
- RDEC is the Ratio Dissipated Energy Change method;
- $W_n$  is the dissipated energy produced in load cycle  $n$ ;
- $W_{n+1}$  is the dissipated energy produced in load cycle  $n+1$ ;

- $k$  is the exponential slope of the regressed dissipated energy curve versus loading cycle;
- $PV$  is the plateau value;
- $N_{f50}$  is the number of cycle that corresponds to the 50% initial stiffness reduction;
- $Ax^k$  is the power law;
- $P_{asp}$  is the percentage by weight of asphalt (aggregate basis);
- $G_{asp}$  is the specific gravity of asphalt;
- $G_{agg}$  is the specific gravity of aggregate;
- $MF$  is the mode factor;
- $\Psi$  is the energy ratio of the initial dissipated energy;
- $N_{field}$  is the fatigue life in the field,
- $N_{lab}$  is the laboratory fatigue life;
- $SF$  is the shift factor;
- $t_r$  is the rest period;
- $PV_h$  is the  $PV$  value considering healing;
- $PV_{w/o}$  is the  $PV$  value not considering healing;
- $DCSE$  is the absorbed energy that damages the material;
- $PI$  is the Percentage Increase in the number of cycles;
- $DI$  is the Damage Indicator;
- $HI$  is the Horizontal Increase.

## CHAPTER 3

# Applying statistics to fatigue test data

Statistics is necessary to organize, analyse, and interpret numerical information from data. Descriptive statistics involves methods of organising and summarising information from data. Inferential statistics involves methods of using information from a sample to draw conclusions about the population.

In this project, an in-depth study in statistics was done to compare different fatigue lines obtained from different loading conditions, different fatigue methods and different laboratory tests. This chapter shows the statistical background necessary to understand what statistical test is more appropriate depending on the initial hypothesis to compare data.

**Note:** a population is a group of measurements about which a researcher wishes to draw conclusions; a sample is a subset of all the measurements in the population and it is usually random. If the population is very small, it may be reasonable to consider the whole population as the sample (sample=population). A variable is a characteristic of the single measurement.

### 3.1 Simple linear regression

A regression represents a relationship between two variables. The term simple refers to the simplest kind of regression, one in which only two variables are considered; the term linear refers to the relationship between the two variables being a straight line. One of the two variables is usually a dependent variable and the other one is independent. In an experiment, the dependent variable is studied in order to analyse how and if it varies when the independent variable changes. Fatigue data are usually pairs of experimental data where the independent variable is the strain level ( $\epsilon$ ) applied and the dependent variable is the number of cycles to failure ( $N_f$ ).

The simplest relationship between two variables in a population is the simplest linear regression (equation for a straight line) as follows:

$$Y_i = a + bX_i \quad \text{Equation 46}$$

Where:  $Y_i$  is the dependent variable,  $X_i$  is the independent variable,  $a$  and  $b$  are population parameters and they represent the intercept and slope respectively.

Usually, researchers collect several pairs of experimental data and there may be considerable variability; thus the traditional procedure is to plot them in a log-log chart ( $\epsilon$ ,  $N_f$ ) and to determine what is commonly called the “best-fit line” (the equation of the fatigue line by using the best-fit regression line). That means that, after plotting the pairs of data, a unique relationship between the two variables is determined using the concept of the least squares. The method of the least square is an approach to minimise the sum of the squared residuals (a residual is the difference between the experimental data and the fitted value provided by the best-fit regression); in other words, the least square approach considers the deviation of each experimental point from the best-fit line. The best-fit line is the regression line that has the minimum value of the sum of the squares of these deviations for all the experimental data.

The distribution of fatigue life ( $N_f$  values) is usually unknown, but it is common to assume that the logarithms of the fatigue lives are normally distributed and the variance of log life is constant over the entire range of the independent variables used in testing (that is the strain level applied  $\epsilon$ ). Thus, in order to have a straight line, fatigue life is usually represented in a log-log plot (ASTM E739-10). See Figure 28.

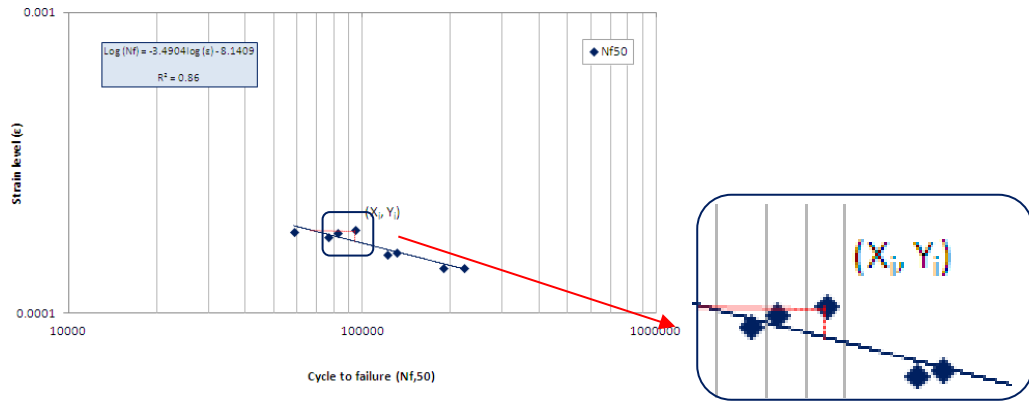


**Figure 28** Best-fit regression line between the fatigue life  $Nf,50$  and the strain level applied  $\epsilon$ .

Considering a sample of  $n_i$  data, the slope  $b$  of the regression line is estimated by means of the following equation:

$$b = \frac{\sum xy}{\sum x^2} = \frac{\sum (X_i - \bar{X}) \cdot (Y_i - \bar{Y})}{\sum (X_i - \bar{X})^2} = \frac{\sum X_i Y_i - \frac{(\sum X_i) \cdot (\sum Y_i)}{n}}{\sum X_i^2 - \frac{(\sum X_i)^2}{n}} \quad \text{Equation 47}$$

Where:

- $X_i$  and  $Y_i$  are the abscissa and the ordinate, respectively, of experimental data point;
- $\bar{X}$  and  $\bar{Y}$  are the average values of the  $n$  abscissa and  $n$  ordinate of the data set;
- $\sum xy$  is the sum of cross products;
- $\sum x^2$  is the sum of squares;
- $b$  is the slope of the best fitted-line regression.

In Equation 47, the denominator is always positive; the numerator can be positive, negative, or zero; thus the value of  $b$  can vary from  $-\infty$  to  $+\infty$  as shown in Figure 29.

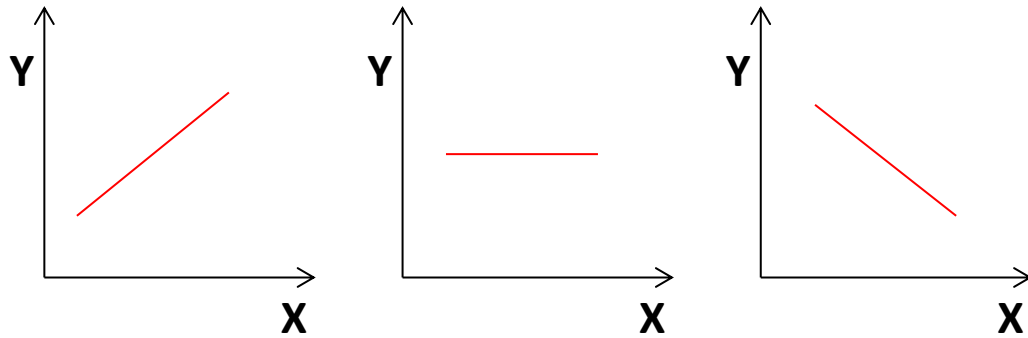


**Figure 29** Slope of linear regression line

The intercept  $a$  is the height of the line that means that mathematically it represents the average value of  $y$  when  $x$  equals zero. It is determined by means of the following:

$$\bar{Y} = a + b\bar{X} \Rightarrow a = \bar{Y} - b\bar{X} \quad \text{Equation 48}$$

In the case of fatigue life of a material, it is always assumed that fatigue lives are log-normally distributed and the variance of log life is constant over the entire range of the independent variable used in testing (ASTM E739-10).

### **3.2 Testing the significance of a regression: Fisher and Student t tests**

Once the linear regression line is determined, it is necessary to analyse the variance of testing data (ANOVA) that examines the several sources of variation among all the data in an experiment by determining the sum of squares.

The aim of ANOVA is to test appropriate hypotheses about the values determined on a chosen data set. Usually a null hypothesis  $H_0: \beta=0$  and an alternative hypothesis,  $H_A: \beta \neq 0$ , are set up. If there is a probability (usually greater the level of significance for example 5%) that the calculated  $\beta$  could have come from sampling a population with  $\beta=0$ , the  $H_0$  is rejected and the alternative hypothesis is true. In order to proceed, several quantities have to be defined (see Table 1) and calculated such as:

- Total SS. The total sum of squares of deviations of  $Y_i$  values from the mean value  $\bar{Y}$ .

$$TotalSS = \sum (Y_i - \bar{Y})^2 = \sum y^2 \quad \text{Equation 49}$$

- Regression SS. The linear regression sum of squares that determines the variability of the  $Y_i$  values because they are in a linear regression.

$$regressionSS = \sum (\hat{Y}_i - \bar{Y})^2 = \frac{(\sum xy)^2}{\sum x^2} = b \cdot \sum xy \quad \text{Equation 50}$$

The regression SS is equal to the total SS only if the data points fall on the regression line.

- Residual SS. The residual sum of squares corresponds to the errors.

$$residualSS = \sum (Y_i - \hat{Y}_i)^2 = totalSS - regressionSS \quad \text{Equation 51}$$

- Degree of freedom (DF). The number of variables that are free to vary. The DF associated with the total variability of  $Y_i$  is shown in Equation 52; the DF associated with the variability of  $Y_i$  due to the regression is always 1 in the case of simple linear regression. The residual DF is calculated by means of the equation (Equation 53).

$$totalDF = n - 1 \quad \text{Equation 52}$$

$$residualDF = totalDF - regressionDF = n - 2 \quad \text{Equation 53}$$

- Means sum of squares (MS) or *variance*. The mean squared deviation from the mean and is calculated by taking the sum of squared differences from the mean and dividing by the degree of freedom (Equation 54). The residual mean square is also written as  $s_{Y.X}^2$  to denote the variance of Y after taking into account the dependence of Y on X. The square root of  $s_{Y.X}^2$  is called standard error of estimate.

$$MS = \frac{SS}{DF} \quad \text{Equation 54}$$

**Table 1** SS, DF and MS (Zar, J.H. 2010)

Source of Variation	SS	DF	MS
Total	$\sum y^2$	n-1	
Linear regression	$\frac{(\sum xy)^2}{\sum x^2}$	1	$\frac{regressionSS}{regressionDF}$
Residual	$totalSS - regressionSS$	n-2	$\frac{residualSS}{residualDF}$

In order to test the null hypothesis, it is necessary to consider the Fisher analysis of variance. Fisher introduced the concepts of comparing the variance among groups to the variance within groups. So the F-test, that is the ratio between the means of squares of the regression and the errors (residual MS), is calculated as follows:

$$F = \frac{regressionMS}{residualMS} \quad \text{Equation 55}$$

The computed value is then compared to a critical value that is  $F_{\alpha(1),v_1,v_2} = F_{\alpha(1),(k-1),(N-k)}$ . In general, it represents the value of F at the one-tailed significance level  $\alpha$  and with numerator degree of freedom of  $v_1=k-1$  (regression DF) and denominator degree of freedom of  $v_2=N-k$  (residual DF); where k is the number of groups considered. If  $|F| \geq F_{\alpha(1),v_1,v_2}$  then the hypothesis  $H_0$  is rejected.

The residual mean square is also written as  $s_{Y.X}^2$  to denote the variance of Y after taking into account the dependence of Y on X. The square root of  $s_{Y.X}^2$  is called *standard error of estimate*. It indicates the accuracy with which the fitted regression predicts the dependence of Y on X. The proportion of the total variation in Y is called the coefficient of determination  $R^2$ , often used as a measure to indicate the goodness of a fitted line to the data (or as the precision of regression).  $R^2$  is calculated as follows:

$$R^2 = \frac{regressionSS}{totalSS} \quad \text{Equation 56}$$

Another way to test the null hypothesis is to use the Student's t test. It is usually applied when the data are normally distributed and the aim is to determine if two set of data are significantly different from each other. In general the t value is calculated as:

$$t = \frac{(\text{parameter\_estimate} - \text{parameter\_value\_hypothesized})}{\text{standard\_error\_parameter\_estimate}} \quad \text{Equation 57}$$

If we consider the two-tailed previous hypothesis  $H_0:\beta=0$  and  $H_A:\beta\neq 0$ , the t parameter can be calculated as:

$$t = \frac{b - \beta}{s_\beta} \quad \text{Equation 58}$$

Where  $S_\beta$  is the variance of b equal to  $s_b = \sqrt{\frac{s_{y.X}^2}{\sum x^2}}$  and b is the estimated value of  $\beta$ .

The computed value of t is then compared to a critical value, that is  $t_{\alpha(2),v}$ . It represents the value of t at the two-tailed significance level  $\alpha$  and with degree of freedom of v ( $v = n-1$ ). If  $|t| \geq t_{\alpha(2),v}$  then the hypothesis  $H_0$  is rejected.

For the two-tailed hypothesis  $H_0:\beta=0$ , either t or F may be used, obtaining the same results.

### 3.3 Confidence interval, confidence bands and prediction bands in regressions

A confidence interval gives an estimated range of values which is likely to include all the data according to a certain confidence level (usually 95%), in other words it represents the level of certainty about an estimated value. The precision of the estimated parameter is proportional to the width of the confidence interval: a wide interval may indicate that more data should be included in order to have more confident estimation. Assuming that the estimator is normally distributed and the variance of log-normal distribution is constant, the confidence intervals for  $a = \hat{\alpha}$  and  $b = \hat{\beta}$  are given by:

$$\hat{\alpha} \pm t\sigma \left[ \frac{1}{n} + \frac{\bar{X}^2}{\sum_{i=1}^n (X_i - \bar{X})^2} \right]^{\frac{1}{2}} \quad \text{Equation 59}$$

$$\hat{\beta} \pm t\sigma \left[ \sum_{i=1}^n (X_i - \bar{X})^2 \right]^{\frac{1}{2}} \quad \text{Equation 60}$$

Where t is the value of the t distribution that depends on the confidence level chosen (usually 95%) and the degree of freedom ( $v=n-2$ ).

Confidence bands represent the uncertainty in an estimate of a curve or function based on limited data. It gives a visual sense of how well data define the best-fit curve. The confidence bands are defined by a lower and an upper curve by the following equations:

$$\alpha + \beta X \pm \sqrt{2F}\sigma \left[ \frac{1}{n} + \frac{(X - \bar{X})^2}{\sum_{i=1}^n (X_i - \bar{X})^2} \right]^{\frac{1}{2}} \quad \text{Equation 61}$$

where F is the value of the F distribution that depends on the confidence level chosen (usually 95%), the degree of freedom of  $v_1$  (regression DF) and the degree of freedom of  $v_2$  (residual DF). As shown in Figure 30, the dashed hyperbolic lines are the confidence bands relating to the best fitted line of  $\epsilon$ -Nf data. The confidence bands represent the boundaries of all possible linear regression lines relating to a certain set of data. Considering a 95% significance level, it means that the upper and lower confidence curves enclose the true best fitted line with 95% of confidence, leaving a 5% chance that the true regression line is outside the boundaries.

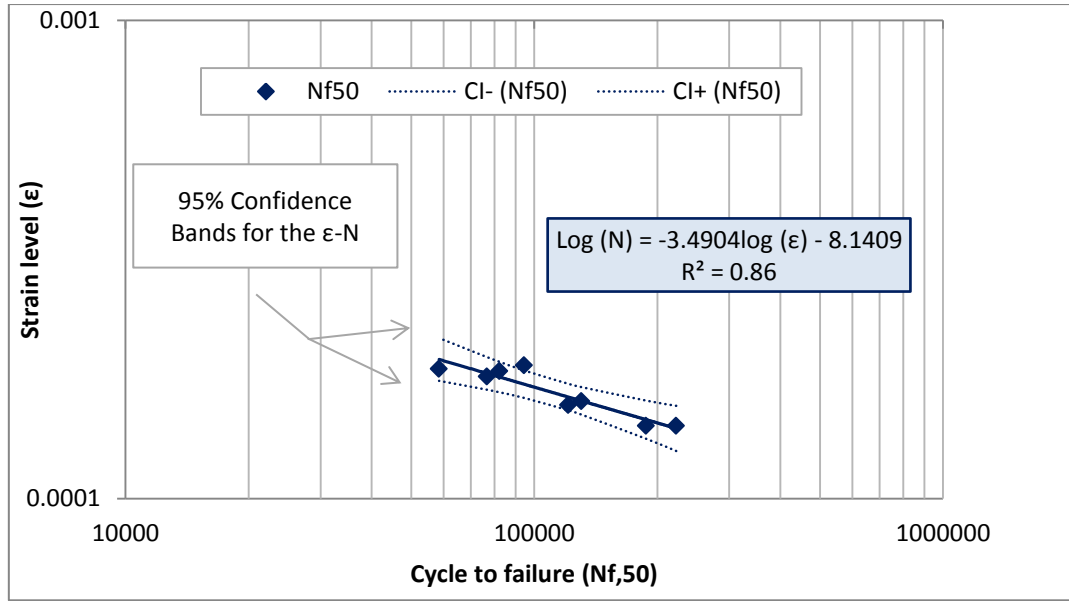


**Figure 30** Confidence bands related to the best fitted regression line of a sample data.

In contrast, prediction bands represent the area in which future data points are expected to fall. They take into account the uncertainty in the true position of the fitted curve and the scatter of data around the fitted curve. For this reason they are always wider than confidence bands (Little, 1975).

### 3.4 Testing the adequacy of a linear model

There may happen to be more than one observed value of fatigue life  $N_f$  ( $Y_i$ ), for a certain strain level  $\epsilon$  ( $X_i$ , where  $I$  is  $\geq 3$ ). In this case, it is necessary to verify the linearity based on the F distribution. Assuming that fatigue tests are conducted at  $\epsilon$  different strain levels of  $X$  and  $m_i$  replicate values of  $Y$  are observed at each  $X_i$ . In order to verify the linearity, a computed value  $L$  has to be calculated by means of the following equation:

$$L = \frac{\sum_{i=1}^{\epsilon} m_i \cdot (\hat{Y}_i - \bar{Y}_i)^2 / (\epsilon - 2)}{\sum_{i=1}^{\epsilon} \sum_{j=1}^{m_i} (Y_{ij} - \bar{Y}_i)^2 / (N - \epsilon)} \quad \text{Equation 62}$$

where  $Y_{ij}$  is the log life of the  $j^{\text{th}}$  replicate specimen tested at  $i^{\text{th}}$  level of strain ( $X_i$ ), and where  $N$  is the total number of specimens tested  $N = \sum_{i=1}^{\epsilon} m_i$ .

After that, the L value has to be compared with the critical value F for the significance level chosen  $F_{\alpha(1),v_1,v_2}$ . Note: significance level is defined as the probability in percent of incorrectly rejecting the hypothesis of linearity when there is indeed a linear relationship between X and Y (ASTM E739-10).  $F_{\alpha(1),v_1,v_2}$  represents the value of F at the one-tailed significance level  $\alpha$  (i.e. 95%) and with numerator degree of freedom of  $v_1$  (regression DF =  $\epsilon - 2$ ) and denominator degree of freedom of  $v_2$  (residual DF =  $N - \epsilon$ ). If  $|L| \geq F_{\alpha(1),v_1,v_2}$  then the hypothesis of linearity is rejected.

### **3.5 Sample size**

According to the American standards (ASTM E739-10), the minimum number of specimens necessary for obtaining the regression line depends on the type of test conducted. In the case of this thesis the planned kind of test is related with research and development testing and for this reason the minimum number suggested is between 6 and 12. In the case of design and reliability data the minimum number suggested is between 12 and 24.

### **3.6 Comparing simple linear regressions**

It may happen that several samples of fatigue data have to be fitted, that means several best fitted regression lines will be obtained. An interesting thing to do is to compare different regression lines, this may mean either comparing different materials at the same loading and environmental conditions or different fatigue approaches for the same material (or both!). In order to verify difference between regressions, the slopes and the intercepts of different regressions have to be compared to understand if they are either significantly different or not. In order to proceed the first thing to know is how many regression lines (k) have to be compared: if  $k = 2$  then the Student's t test will be involved in the analysis, if  $k \geq 2$  than a multiple analysis has to be done using the analysis of covariance (ANCOVA) and different kinds of tests.

#### **Comparing two regression lines**

Comparing two different regression lines means to evaluate if the slopes and the elevations of the two regression lines are significantly different.

In the case of the slopes, the hypotheses are:

- $H_0: \beta_1 = \beta_2$
- $H_A: \beta_1 \neq \beta_2$ .

Student's t test is considered by determining the t function as follows (ASTM: E739-10):

$$t = \frac{b_1 - b_2}{S_{b_1 - b_2}} \quad \text{Equation 63}$$

$$S_{b_1 - b_2} = \sqrt{\frac{(S_{Y \cdot X}^2)_\alpha}{(\sum x^2)_1} + \frac{(S_{Y \cdot X}^2)_\alpha}{(\sum x^2)_2}} \quad \text{Equation 64}$$

$$(S_{Y \cdot X}^2)_\alpha = \frac{(\text{residualSS})_1}{(\text{residualDF})_1} + \frac{(\text{residualSS})_2}{(\text{residualDF})_2} \quad \text{Equation 65}$$

Where  $b_1$  and  $b_2$  are regression coefficients,  $S_{b_1 - b_2}$  is the standard error of the difference between regression coefficients,  $(S_{Y \cdot X}^2)_\alpha$  is the pooled residual mean square; the subscripts 1 and 2 refer to the two regression lines. The critical value of t is  $t_{\alpha(2),v}$  and it represents the value of t at the two-tailed significance level  $\alpha$  and with degree of freedom of  $v$  equal to the sum of the two residual degrees of freedom  $v = (n_1 - 2) + (n_2 - 2) = n_1 + n_2 - 4$ . If  $|t| \geq t_{\alpha(2),v}$  then the hypothesis  $H_0$  is rejected. The next step might be to calculate the point where the two lines intersect ( $X_I, Y_I$ ) by using the following equation:

$$X_I = \frac{a_2 - a_1}{b_1 - b_2} \quad \text{Equation 66}$$

$$Y_I = a_1 + b_1 X_I \quad \text{Equation 67}$$

If the hypothesis of equality is not rejected ( $H_0: \beta_1 = \beta_2$ ), the two regression lines are parallel and a common regression coefficient  $b_c$  can be determined as follows:

$$b_c = \frac{(\sum xy)_1 + (\sum xy)_2}{(\sum x^2)_1 + (\sum x^2)_2} \quad \text{Equation 68}$$

In the case of the elevation, the hypotheses are:

- $H_0$ : the two regression lines have the same elevation
- $H_A$ : the two regression lines do not have the same elevation

The Student's t test is considered also in this case, but first several quantities for the common regression have to be calculated as follows:

- Sum of squares of X,  $A_c = (\sum x^2)_1 + (\sum x^2)_2$
- Sum of crossproducts,  $B_c = (\sum xy)_1 + (\sum xy)_2$  :
- Sum of squares of Y,  $C_c = (\sum y^2)_1 + (\sum y^2)_2$  :
- Residual SS,  $SS = C_c - \frac{B_c^2}{A_c}$  :
- Residual DF,  $DF_c = n_1 + n_2 - 3$  :
- Residual MS,  $MS_c = (S_{Y.X}^2)_c = \frac{SS_c}{DF_c}$  :

Then, the t value can be calculated by using the following expression:

$$t = \frac{(\bar{Y}_1 - \bar{Y}_2) - b_c(\bar{X}_1 - \bar{X}_2)}{\sqrt{(S_{Y.X}^2)_c \left[ \frac{1}{n_1} + \frac{1}{n_2} + \frac{(\bar{X}_1 - \bar{X}_2)^2}{A_c} \right]}} \quad \text{Equation 69}$$

The critical value of t is  $t_{\alpha(2),v}$  and it represents the value of t at the two-tailed significance level  $\alpha$  and with degree of freedom of v equal to  $DF_c$ . If  $|t| \geq t_{\alpha(2),v}$  then the hypothesis  $H_0$  is rejected, which means that the two regression lines are parallel but does not have the same vertical position on a graph. In this case, the two regressions can be written as follows:

$$Y_i = a_1 + b_c X_i \quad \text{Equation 70}$$

$$Y_i = a_2 + b_c X_i \quad \text{Equation 71}$$

If  $|t| \leq t_{\alpha(2),v}$  then the hypothesis  $H_0$  is not rejected, which means that the two regression lines are parallel and have the same elevation. In this case, a unique regression equation can be determined as follows:

$$Y_i = a_c + b_c X_i \quad \text{Equation 72}$$

Where  $a_c$  is the common regression intercept defined as:

$$a_c = \bar{Y}_p - b_c \bar{X}_p \quad \text{Equation 73}$$

Where  $\bar{Y}_p$  and  $\bar{X}_p$  are the pooled sample means obtained by:

$$\bar{X}_p = \frac{n_1\bar{X}_1 + n_2\bar{X}_2}{n_1 + n_2} \quad \text{Equation 74}$$

$$\bar{Y}_p = \frac{n_1\bar{Y}_1 + n_2\bar{Y}_2}{n_1 + n_2} \quad \text{Equation 75}$$

### **Comparing more than two regression lines**

When more regression lines have to be compared, there could be misunderstanding trying to apply two-sample t tests to all possible pairs of samples. In this case an error could be made and the probability of incorrectly rejecting at least one of the hypotheses is:

$$1 - (1 - \alpha)^C \quad \text{Equation 76}$$

$$C = \frac{k(k-1)}{2} \quad \text{Equation 77}$$

Where C is the number of possible different pair combination of k samples. As the number of samples increases, the probability of committing at least one type I error by using two-sample t tests increases.

Thus, in case k regression lines have to be compared, the first thing to verify is that the k sampled populations do not have the same slope. The hypothesis of equality between slopes of different regressions is usually tested with the analysis of covariance (ANCOVA). The hypotheses are:

- $H_0: \beta_1 = \beta_2 = \dots = \beta_k$
- $H_A: \beta_1 \neq \beta_2 \neq \dots \neq \beta_k$

Several calculations necessary to compare the k slopes have to be calculated as follows:

- $\sum x^2, \sum y^2, \sum xy$ , for each regression k;
- Residual SS and residual DF, for each regression k;
- Pooled residual sum of squares  $SS_p = \sum_{i=1}^k SS_i$  ;
- Pooled residual degree of freedom  $DF_p = \sum_{i=1}^k (n_i - 2)$ ;

- Common residual sum of squares  $SS_c = C_c - \frac{B_c^2}{A_c}$ , where  $A_c = \sum_{i=1}^k A_i$ ,

$$B_c = \sum_{i=1}^k B_i \text{ and } C_c = \sum_{i=1}^k C_i ;$$

- Common residual degree of freedom  $DF_c = \sum_{i=1}^k n_i - k - 1$ ;

Thus, the F test is considered using the following expression:

$$F = \frac{\left( \frac{SS_c - SS_p}{k - 1} \right)}{\frac{SS_p}{DF_p}} \quad \text{Equation 78}$$

The computed value is then compared to a critical value that is  $F_{\alpha(1),v1,v2}$ . If  $|F| \leq F_{\alpha(1),v1,v2}$  then the hypothesis  $H_0$  is not rejected, which means that the slopes are not significantly different and a common regression coefficient can be determined as:

$$b_c = \frac{\sum_{i=1}^k (\sum xy)_i}{\sum_{i=1}^k (\sum x^2)_i} \quad \text{Equation 79}$$

If  $|F| \geq F_{\alpha(1),v1,v2}$  then the hypothesis  $H_0$  is rejected, which means that the slopes are not all equal and the next step will be a multiple comparison to understand which of the k regression slopes differ from which others. Two different tests could be used:

- *Tukey test*. This test is usually used to compare each possible pair of slopes in the group of k regressions.
- *Dunnett's test*. This test is usually used to compare each slope to a "control" slope chosen *a priori* before the analysis.

The Tukey test is similar to the t test, apart from the corrections that have to be considered due to the fact that a probability of making a type I error exists (when a multiple analysis is made). Considering two regressions A and B of the groups of k regressions, the test q is calculated as follows:

$$q = \frac{b_B - b_A}{SE} \quad \text{Equation 80}$$

Where:

$$SE = \sqrt{\frac{(S_{Y.X}^2)_p}{2} \left[ \frac{1}{(\sum x^2)_B} + \frac{1}{(\sum x^2)_A} \right]} \quad \text{Equation 81}$$

The degree of freedom is the pooled residual DF. The critical value is  $q_{\alpha, v, k}$  where  $\alpha$  is the significance level,  $v$  is the residual pooled degree of freedom and  $k$  is the number of regressions in the group.

If  $\sum x^2$  is the same for regressions A and B, the standard error is:

$$SE = \sqrt{\frac{(S_{Y.X}^2)_p}{\sum x^2}} \quad \text{Equation 82}$$

In contrast, in Dunnett's method, a regression is chosen to be the "control" regression. All the other regressions are compared to the control one. In Dunnett's test the value SE is expressed as follows:

$$SE = \sqrt{\frac{(S_{Y.X}^2)_p}{2} \left[ \frac{1}{(\sum x^2)_A} + \frac{1}{(\sum x^2)_{Control}} \right]} \quad \text{Equation 83}$$

And the critical value is  $q'_{\alpha, v, k}$  where  $\alpha$  is the significance level (in this case either one-tailed or two-tailed hypothesis can be tested),  $v$  is the residual pooled degree of freedom and  $k$  is the number of regressions in the group.

In both cases, if the values calculated ( $q_{\alpha, v, k}$  and  $q'_{\alpha, v, k}$ ) are greater than the critical values, then the hypotheses are rejected. In contrast, if the hypotheses are not rejected then a multiple comparison between the elevations has to be made using either the Tukey test or Dunnett's test (Dunnett, C.W. 1964 and Dunnett, C.W. 1964). The test for the Tukey test is:

$$q = \frac{(\bar{Y}_A - \bar{Y}_B) - b_c (\bar{X}_A - \bar{X}_B)}{SE} \quad \text{Equation 84}$$

Where:

$$SE = \sqrt{\frac{(S_{Y.X}^2)_p}{2} \left[ \frac{1}{n_B} + \frac{1}{n_A} + \frac{(\bar{X}_A - \bar{X}_B)^2}{(\sum x^2)_B + (\sum x^2)_A} \right]} \quad \text{Equation 85}$$

If Dunnett's test is used then the expression for SE is the following:

$$SE = \sqrt{(S_{Y.X}^2)_c \left[ \frac{1}{n_A} + \frac{1}{n_{Control}} + \frac{(\bar{X}_A - \bar{X}_{Control})^2}{(\sum x^2)_A + (\sum x^2)_{Control}} \right]} \quad \text{Equation 86}$$

### 3.7 Summary

This chapter has presented the statistical background necessary to understand which statistical test is more appropriate depending on the initial hypothesis to compare different sets of data. In this project, fatigue lines have been obtained by calculating the slope and the intercept for each set of data. Comparisons between different fatigue methods have then been made by using the Dunnett test considering the phenomenological approach as a "control method". Comparisons between different tests were made by using the Tukey test considering each possible pair of fatigue lines.

### 3.8 List of variables

- $\epsilon$  is the strain level;
- $N_f$  is the fatigue life;
- $Y_i$  is the dependent variable;
- $X_i$  is the independent variable;
- $\alpha$  is a population parameter and it represents the intercept;
- $\beta$  is a population parameter and it represents the slope;
- $n(X_i, Y_i)$  is a data point;
- $X_i$  and  $Y_i$  are the abscissa and the ordinate, respectively, of experimental data point;
- $\bar{X}$  and  $\bar{Y}$  are the average values of the  $n$  abscissa and  $n$  ordinate of the data set;
- $\Sigma xy$  is the sum of cross products;
- $\Sigma x^2$  is the sum of squares;

- $b$  is the slope of the best fitted-line regression;
- $k$  is groups of data ( $n_i$ );
- $N$  is the total number of data in all  $k$  groups;
- $H_0$  is the null hypothesis;
- $H_A$  is the alternative hypothesis;
- Total SS is the total sum of squares of deviations  $Y_i$  values from the mean value  $\bar{Y}$  ;
- Regression SS is the linear regression sum squares;
- Residual SS is the residual sum of squares;
- DF is the degree of freedom;
- $v_1$  is regression DF;
- $v_2$  is residual DF;
- MS is the means sum of squares or variance;
- $s_{Y.X}^2$  is the residual mean of square, also known as standard error;
- $F_{\alpha(1),v_1,v_2}$  represents the Fisher test;
- $R^2$  is the coefficient of determination;
- $t_{\alpha(2),v}$  is the Student t test;
- $\hat{\alpha}$  and  $\hat{\beta}$  are the confidence interval;
- $m_i$  represent the replication of a value of  $Y$ ;
- $L$  is a parameter to verify the linearity;
- $Y_{ij}$  is the log life of the  $j^{\text{th}}$  replicate specimen tested at  $i^{\text{th}}$  level of strain ( $X_i$ );
- $N$  is the total number of specimens;
- $(S_{Y.X}^2)_\alpha$  is the pooled residual mean square of regression line;
- ANCOVA is the analysis of covariance;
- $q$  is Tukey test;
- $q'$  is Dunnett test.

## CHAPTER 4

# Experimental Program

### 4.1 Introduction

Fatigue cracking occurs due to repeated applications of tensile stress and strain. There are different ways of carrying out fatigue tests in the laboratory, thus there are different ways to simulate reality. Mostly bending tests such as 2 point bending (2PB) and 4 point bending (4PB) tests are used in pavement research; sometimes, the equipment and the testing procedures are relatively complex and the preparation of specimens (trapezoidal for the 2PB and prismatic for the 4PB) is time consuming. Consequently, such pure fatigue test methods are usually confined to a research laboratory.

An attractive alternative is the Indirect Tensile Fatigue Test (ITFT). It is a simple fatigue test method; no special specimen preparation techniques are necessary and it is easily suitable for cylindrical specimens manufactured in the laboratory or cored from a flexible pavement. Currently, it is only possible to carry out ITFT in control stress mode. In this project, the development of ITFT in strain control mode was developed; also, dissipated energy concepts were included in the software. Results were compared with other pure fatigue testing methods such as 2PB and 4PB.

A disadvantage of this testing machine is the accumulation of permanent deformation; thus the ITFT is not a pure fatigue testing machine (does not measure fatigue behaviour directly), especially at high temperature when the viscoelastic behaviour is more pronounced.

### 4.2 Materials

Two different materials were used in this project: a 10 mm Dense Bitumen Macadam (DBM) and a 20 mm DBM. The aggregate types used are:

- porphyritic andesite (Aggregate Industries' Bardon Hill quarry) for the 20mm DBM,
- crushed limestone (Ivonbrook Quarry) for the 10mm DBM.

The mixture design for the asphalt mixtures was based on a 0/20 and 0/10 mm size course according to BS 4987-1: 2005.

Two different penetration bitumen grades from the same crude source (Venezuelan) were used for the project:

- 40 pen bitumen,
- 100 pen bitumen.

The grading specification for the 10 mm DBM is reported in Table 2 whereas the design gradation curve is shown in Figure 31.

Four lines are presented: the upper, the lower limits and the mid-point curve from the British Standards and the aggregate gradation (BS-4987-2005).

**Table 2** 0/10 mm size DBM specification

Test sieve aperture size (mm)	Passing sieve (% by mass)
14	100
10	85-100
6.3	30-60
2	10-30
0.063	2-7

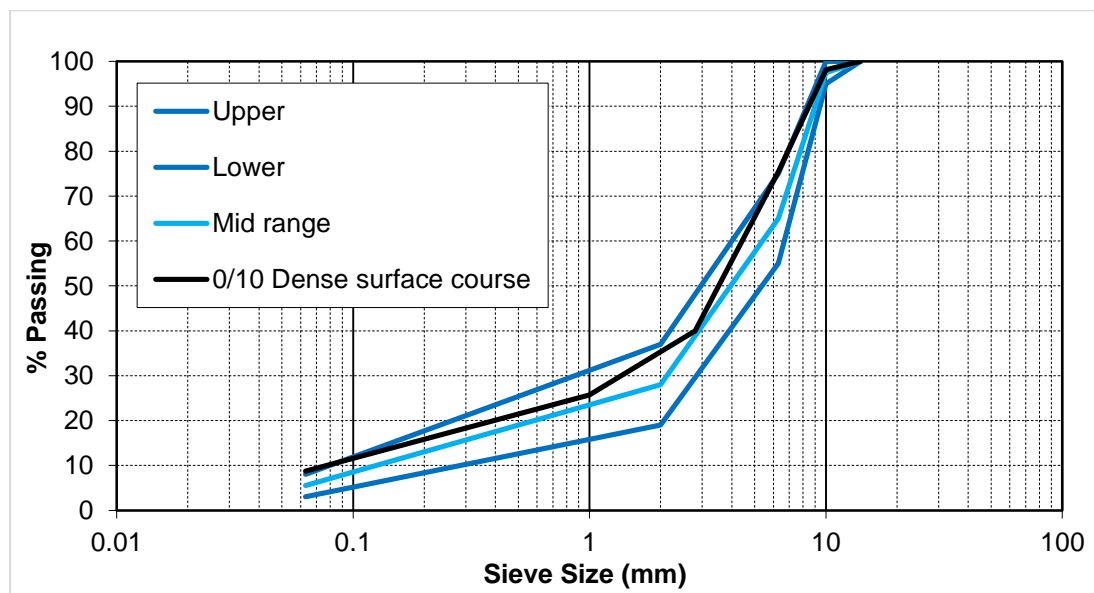


**Figure 31** Gradation curve 10 mm DBM

The grading specification for the 20 mm DBM is reported in Table 3 whereas the design gradation curve is shown in Figure 32.

**Table 3** 0/20 mm size DBM specification

Test sieve aperture size (mm)	Passing sieve (% by mass)
31.5	100
20	95-100
14	65-85
10	52-72
6.3	38-56
1	20-40
0.25	6-20
0.063	2-9

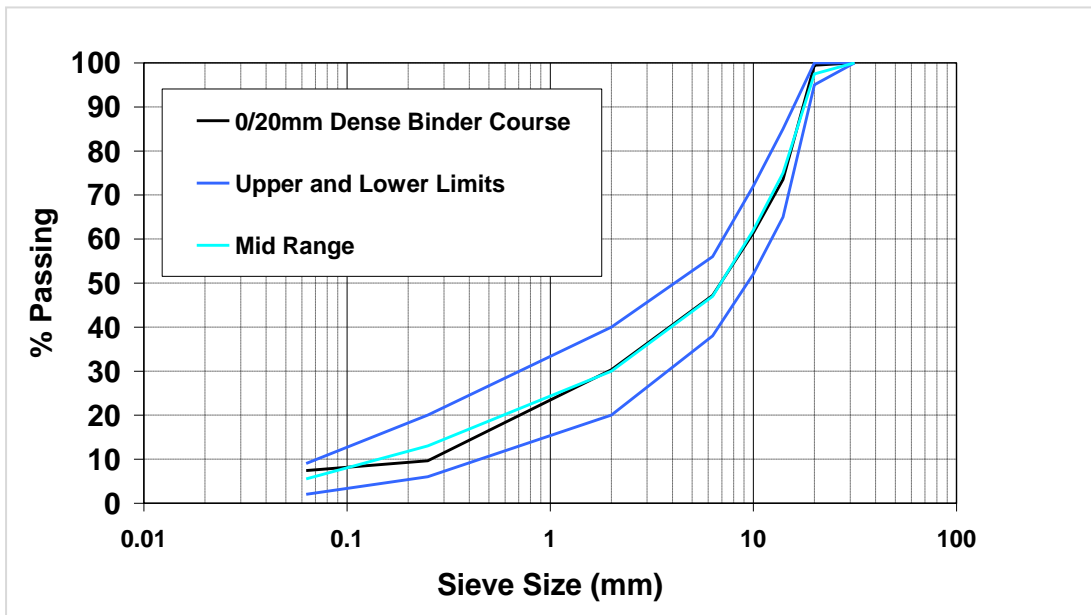


**Figure 32** Gradation curve

Both mixtures, 10mm DBM and 20mm DBM, were chosen because they are typical of those used in pavement design, often as base and binder layers.

### 4.3 Mixing and compaction

The procedures chosen for the production of the control asphalt mixtures, in terms of laboratory mixing and compaction by roller compactor, conform to BS EN 12697-35: 2004 and BS EN 12697-33: 2003 respectively. Once the aggregates, bitumen and filler are uniformly mixed and the temperature before compaction is within the specified range, a calculated amount of hot mixture is poured into pre-heated square moulds (305 mm by 305 mm) and compacted to the required slab thickness in order to achieve the desired air void content (see Figure 33 and Figure 34).



**Figure 33** Mixing according to BS EN 12697-35: 2004



**Figure 34** Compacting according to BS EN 12697-33: 2003

#### **4.4 Specimen cutting**

Each testing machine requires different specimen shape (see Section 5.2, 6.2 and 7.2).

#### **4.5 Volumetric characteristics**

After the specimens are trimmed, they are placed on absorbent paper and allowed to dry out at room temperature.

The dimensions of each specimen are measured and the specimens are then tested for bulk density as detailed in BS EN 12697-6: 2003. The bulk densities are used together with the maximum theoretical densities, which were determined on loose mix samples by the volumetric procedure BS EN 12697-5: 2009, to calculate the actual percentage of air voids of each test specimen according to BS EN 12697-8: 2003.

The target void content was  $4\pm 1\%$  for the 10mm DBM; it was  $6\pm 1\%$  for the 20mm DBM. See Appendix B for bulk density and air void content details.

Note: cylindrical specimens (20mm DBM only) have a higher air void content. Those specimens (even if out of the target air void range) were used for calibrating the ITFT in strain control; some results are presented to show the difference between ITFT in strain and stress control mode. Due to a big difference in air void content those results were not compared with the 2PB results.

#### **4.6 Storage**

The cored and cut specimens were then stored at room temperature on one of their flat faces for up to two weeks from compaction and then stored in a dry atmosphere at a temperature of 5°C to prevent distortion. Specimens were only removed from this controlled environment to be conditioned and tested at the required temperature.

#### **4.7 Testing machines**

As shown in Chapter 2, different testing machines exist in order to describe fatigue behaviour in asphalt materials. In this project, three different testing machines were involved: 2 Point Bending test (2PB), 4 Point Bending test (4PB) and Indirect Fatigue Tensile test (ITFT). Each of them is described in the following sections.

The 2 Point Bending test is widely used for measuring fatigue resistance and stiffness for asphaltic paving materials. For this laboratory activity, fatigue tests were performed at IFSTTAR, the French institute of science and technology for transport, development and networks, in Nantes (France) and at the University of Nottingham (United Kingdom). Regarding the 10mm DBM material, fatigue tests were carried out at two different temperature (10 and 20°C) and two different frequencies (15 and 25 Hz). Regarding the 20mm DBM material, fatigue tests were carried out in both strain and stress control mode at 10 °C and 25 Hz.

The 4 Point Bending test is the most used fatigue test in the United States. The tests were performed with a servo-hydraulic testing system at the University of Nottingham. Only the 10mm DBM material was tested at 10 °C and 25 Hz. Healing tests were performed at different rest time periods and different loading time periods.

The Indirect Tension test is a simple fatigue test widespread in the United Kingdom due to the fact that it is a simple test, easily suitable for cylindrical specimens manufactured in the laboratory or cored from a flexible pavement.

For each testing machine involved in this project, stiffness modulus and fatigue resistance were obtained.

### **Stiffness modulus**

Stiffness modulus is the absolute value of the complex modulus, that relates stress to strain under a continuous sinusoidal loading in the frequency domain for linear visco-elastic materials (Maggiore, C. at al. 2012, Pais J. at al. 2009, Di Benedetto, H., 2001).

The complex modulus (at any given temperature) is defined as the ratio of the amplitude of the sinusoidal stress (at any given time and load frequency) and sinusoidal strain (at the same time and frequency) as follows:

$$E^* = \frac{\sigma(t)}{\varepsilon(t)} = \frac{\sigma_0 \cdot \text{sen}(\omega t)}{\varepsilon_0 \cdot \text{sen}(\omega t - \varphi)} = \frac{\sigma_0}{\varepsilon_0} \cdot e^{i\varphi} = |E^*| \cdot e^{i\varphi} \quad \text{Equation 87}$$

Where:

- $|E^*|$  is stiffness modulus;
- $\sigma_0$  is the peak (maximum) stress;
- $\varepsilon_0$  is the peak (maximum) strain;
- $\omega = 2\pi f$  is the angular velocity;
- $f$  is the load frequency;
- $\varphi$  is the phase angle that represents the lag time between stress and strain;
- $t$  is the time;
- $i$  is the imaginary unit.

The complex modulus (see Figure 35) can also be defined as (EN 12697:24):

$$E^* = |E^*| \cdot (\cos \varphi + i \cdot \text{sen} \varphi) = E_1 + iE_2 \quad \text{Equation 88}$$

The real component  $E_1$  (see Equation 89) represents the elastic behaviour of the material while the imaginary component  $E_2$  (see Equation 90) describes the viscous behaviour. They are defined as follows:

$$E_1 = |E^*| \cdot \cos \varphi \quad \text{Equation 89}$$

$$E_2 = |E^*| \cdot \sin \varphi \quad \text{Equation 90}$$

Stiffness modulus  $|E^*|$  (the absolute value of the complex modulus) and the phase angle  $\varphi$  (phase lag between stress and strain waveforms) can be calculated as:

$$|E^*| = \sqrt{(E_1^2 + E_2^2)} \quad \text{Equation 91}$$

$$\varphi = \arctg(E_2 / E_1) \quad \text{Equation 92}$$

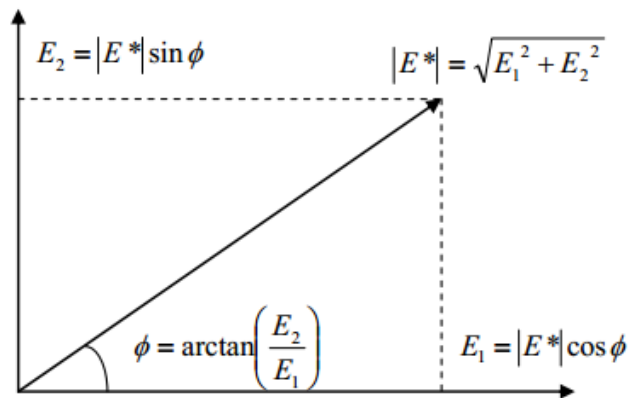


**Figure 35** Representation of complex modulus

According to the standard BS EN 12697-26:2004, the two components can be expressed in general terms by the following expressions:

$$E_1 = \gamma \times \left( \frac{F}{z} \times \cos \varphi + \frac{\mu}{10^3} \times \omega^2 \right) \quad \text{Equation 93}$$

$$E_2 = \gamma \times \left( \frac{F}{z} \times \sin \varphi \right) \quad \text{Equation 94}$$

Where:

- $\gamma$  is the form factor as a function of specimen size and shape;
- $\mu$  is the mass factor, a function of the mass of the specimen (M in grams) and the mass of the movable parts (m in grams), that influence the resultant force by their inertial effects;
- $F$  is the applied force;
- $z$  is the displacement.

Depending on the type of test and the shape of the specimens,  $\gamma$  and  $\mu$  have different expressions.

The stiffness modulus provides important information about the linear viscoelastic behaviour of that particular mix over a wide range of temperature and loading frequencies. A deeper study about fatigue was undertaken during the exchange at IFSTTAR, in Nantes by means of the 2 Point Bending test.

Thus, stiffness tests were included in the laboratory plan in this project.

### **Fatigue resistance**

A summary of the tests undertaken is shown in Table 4 and

Table 5.

The dissipated energy methods used to compare sets of data are: DER by Pronk, ER by Rowe and RDEC by Carpenter and Shen. These three methods were chosen because they relate fatigue life with the change in dissipated energy during a fatigue test.

**Table 4** Experimental work for 10mm DBM

<b>Fatigue test</b>	<b>Temperature</b>	<b>Frequency</b>	<b>Healing</b>	<b>Mode of loading</b>
2PB	10-20°C	15-25Hz	NA	Strain control
4PB	10°C	25Hz	Yes	Strain control
ITFT	10-20°C	NA	Yes	Strain and stress control

**Table 5** Experimental work for 20mm DBM

<b>Fatigue test</b>	<b>Temperature</b>	<b>Frequency</b>	<b>Healing</b>	<b>Mode of loading</b>
2PB	10°C	25Hz	NA	Strain and stress control
ITFT	10°C	NA	Yes	Strain and stress control

## **4.8 List of variables**

- 2PB is 2 Point Bending;
- 4PB is 4 Point Bending;
- ITFT is Indirect Tensile fatigue Test;
- DBM is Dense Bitumen Macadam;
- pen is penetration;

- $\rho$  is the bulk density of specimen (in  $1000\text{kg/m}^3$ );
- $\rho_w$  is the bulk density of specimen ( $1000\text{kg/m}^3$ );
- $m_1$  is the mass of dry specimen in the air unsealed;
- $m_2$  is the mass of dry specimen in the air sealed in foil;
- $m_3$  is the mass of in the water, sealed in foil;
- $\rho_{sm}$  is the relative density of the aluminium foil ( $1603 \text{ kg/m}^3$ );
- $\rho_{max}$  is the maximum theoretical density of the mixture (in  $1000\text{kg/ m}^3$ );
- $p_A$  is the proportion of aggregates in the mixture in percent;
- $\rho_A$  is the particle density of aggregate (in  $1000\text{kg/m}^3$ );
- $p_B$  is the proportion of binder in the mixture in percent;
- $\rho_B$  is the density of binder (in  $1000\text{kg/m}^3$ );
- $P_{target}$  is the target density;
- $V_{m.target}$  is the target air void content;
- $V_m$  is the air voids content of the mixture in percent;
- IFSTTAR is the French institute of science and technology for transport, development and networks;
- $|E^*|$  is complex modulus;
- $\sigma_0$  is the peak (maximum) stress;
- $\varepsilon_0$  is the peak (maximum) strain;
- $\omega = 2\pi f$  is the angular velocity;
- $f$  is the load frequency;
- $\phi$  is the phase angle that represents the lag time between stress and strain;
- $t$  is the time;
- $i$  is the imaginary unit;
- $\gamma$  is the form factor as function of specimen size and shape;
- $\mu$  is the mass factor, function of the mass of the specimen ( $M$  in grams) and the mass of the movable parts ( $m$  in grams), that influence the resultant force by their inertial effects;
- $F$  is the applied force;
- $z$  is the displacement.

## CHAPTER 5

# 2 Point Bending Test

### 5.1 Introduction

The test consists of applying a continuous sinusoidal waveform at the top of a trapezoidal specimen. The specimen is glued to metal plates at the top and at the bottom (see Figure 36 and Figure 37). The specimen is mounted as a vertical cantilever and sinusoidal constant displacement is applied at the top of the specimen, while the bottom base is fixed.



**Figure 36** Trapezoidal specimen



**Figure 37** Glued specimen

Usually four specimens were tested for each strain level at IFSTTAR; two specimens for each strain level at the University of Nottingham. Figure 38 shows the 2PB equipment at IFSTTAR. Figure 39 shows the 2PB equipment at the University of Nottingham.

During a fatigue test, the fracture (failure) usually occurs at 1/3 of the height of the specimen from the bottom, where the tensile stress is a maximum (see Figure 40 and Figure 41) (BS-EN 12697-24, 2004; BS-EN 12697-26, 2004).

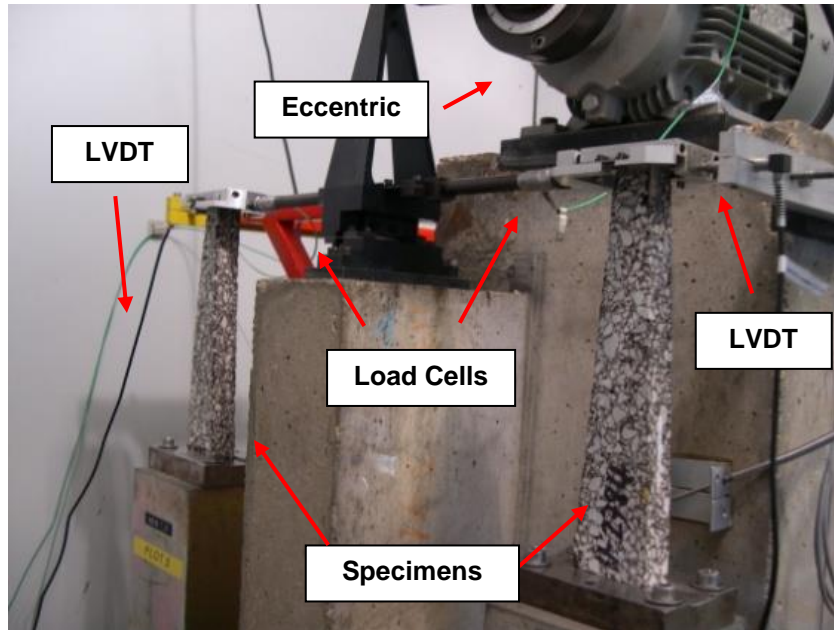


Figure 38 2PB equipment at IFSTTAR

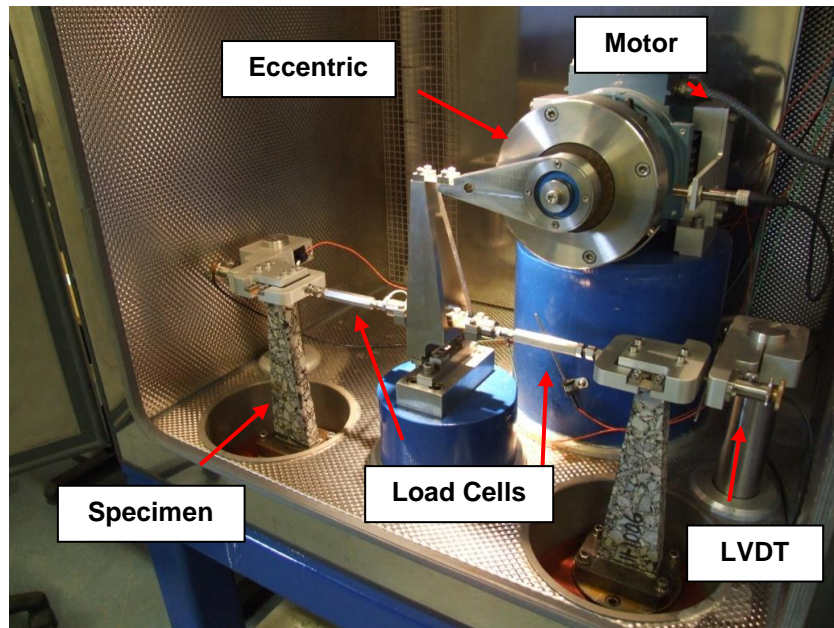
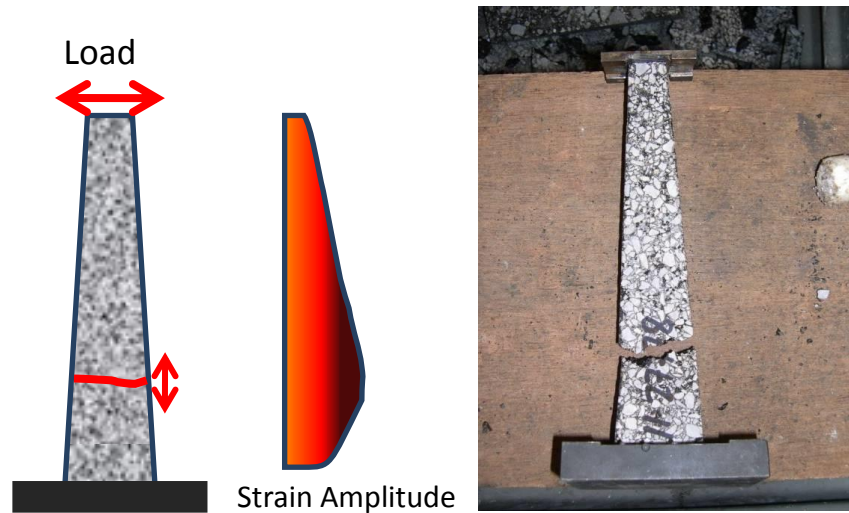


Figure 39 2PB equipment at the University of Nottingham



**Figure 40** Stress in the 2PB specimen

**Figure 41** Fractured specimen

The initial stiffness is usually chosen between the 50<sup>th</sup> and the 100<sup>th</sup> load application. Traditionally, a fatigue test ends when the stiffness has decreased to half of its initial value (Rowe, 1993; SHRP-A-404, 1994).

## 5.2 Trapezoidal Specimens

Trapezoidal test specimens are manufactured from slabs using a masonry saw and a purpose-built clamping device (see Figure 42).

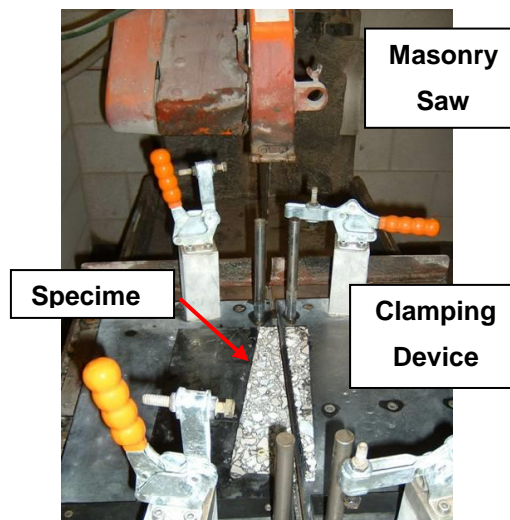


**Figure 42** Jig for sawing trapezoidal specimens from compacted asphalt mixture slabs.

The procedure consists of sawing the specimens along horizontal planes in the direction of compaction. Using this procedure it is possible to produce 10 specimens per slab (see Figure 43).

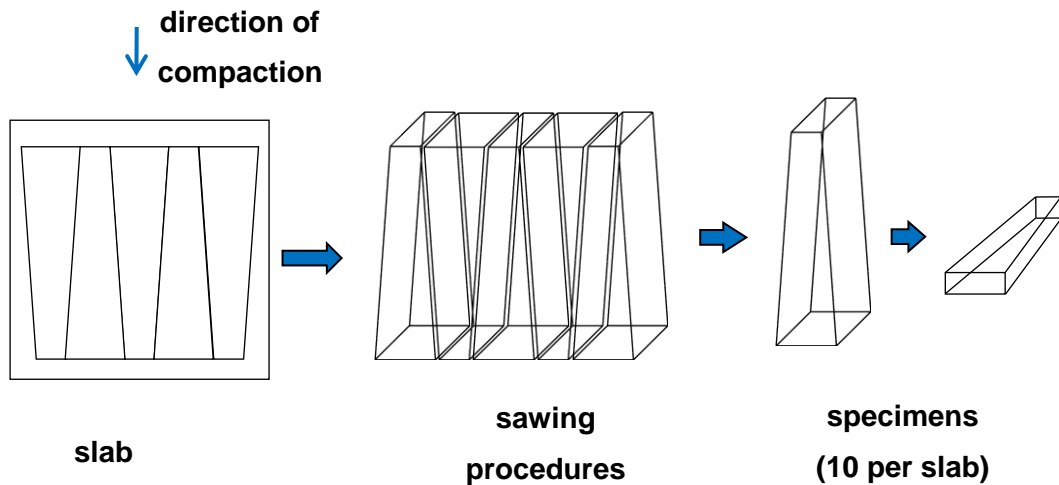


**Figure 43** Coring and trimming procedure

The dimensions required for a 20 mm and a 10 mm size DBM, according to BS EN 12697-24: 2004, are reported in Figure 44 and Table 6.

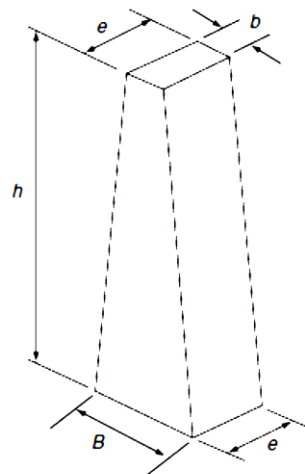


**Figure 44** Geometry of trapezoidal specimens: BS EN 12697-24: 2004.

**Table 6** Dimensions of the specimens: BS EN 12697-24: 2004.

Dimensions of the Specimens	Type of Mixture	
	$14 < D \leq 20$ mm	$D \leq 14$ mm
$B$	$70 \pm 1$ mm	$56 \pm 1$ mm
$b$	$25 \pm 1$ mm	$25 \pm 1$ mm
$e$	$25 \pm 1$ mm	$25 \pm 1$ mm
$h$	$250 \pm 1$ mm	$250 \pm 1$ mm

### 5.2.1 Gluing of Trapezoidal Specimens

The trapezoidal specimens are bonded to steel end plates using epoxy resin to enable them to be fitted to the test apparatus. This operation is carried out

on a special jig to ensure the correct specimen positioning on the base during the resin hardening process (in accordance to the European specification BS EN 12697-24: 2004) as shown in Figure 45. The glue film is kept as thin as possible and the resin is allowed to harden for a minimum period of 24 hours prior to testing.



**Figure 45** Jig for gluing trapezoidal specimens to two point bending apparatus end plates

2 Point bending tests were carried out at IFSTTAR in Nantes. The trapezoidal specimens were manufactured at the University of Nottingham and then shipped to Nantes in order to ensure the consistency in manufacturing specimens (materials, mixing, compaction, coring, etc.).

## 5.3 Test results

### 5.3.1 10mm DBM

#### Stiffness modulus

According to the standards BS EN 12697:26:2004, the form ( $\gamma$ ) and the mass factor ( $\mu$ ) for a trapezoidal specimen are expressed as:

$$\gamma = \frac{12h^3}{e(B-b)^3} \left[ \left( 2 - \frac{b}{2B} \right) \frac{b}{B} - \frac{3}{2} - \ln \frac{b}{B} \right] \quad \text{Equation 95}$$

$$\mu = 0.135M + m \quad \text{Equation 96}$$

Stiffness test were carried out at 7 different temperatures (-10, 0, 10, 15, 20, 30 and 40°C) and 6 different frequencies (1, 3, 10, 25, 30 and 40 Hz). Four different specimens were tested at the same time (see Figure 46).



**Figure 46** Stiffness testing machine at IFSTTAR

In order to understand the effect of the frequency on the modulus of the mixture a frequency sweep was considered and isotherm curves were obtained (Figure 47). Also, temperature sweeps were considered in order to evaluate the effect of the temperature on the stiffness modulus. See Figure 48. As expected, the stiffness modulus decreases when the temperature increases (and the effect of temperature is amplified at lower frequencies); it decreases when frequency decreases (and the effect is amplified at higher temperatures). Asphalt pavements tend to fail in permanent deformation when they are subjected to slow moving traffic; they tend to fail in fatigue when they are subjected to faster traffic during their life (Hunter, R.N., 2000).

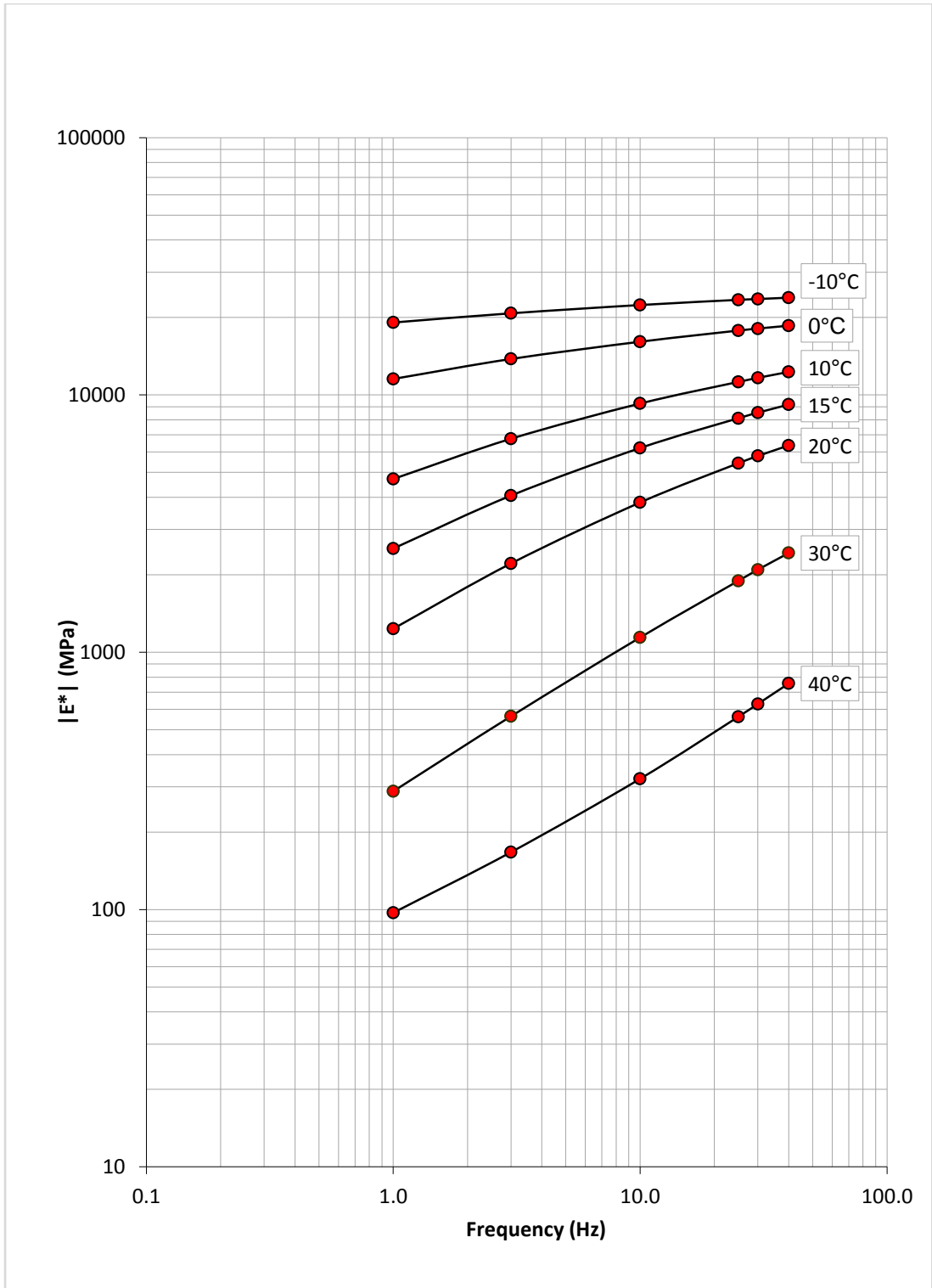
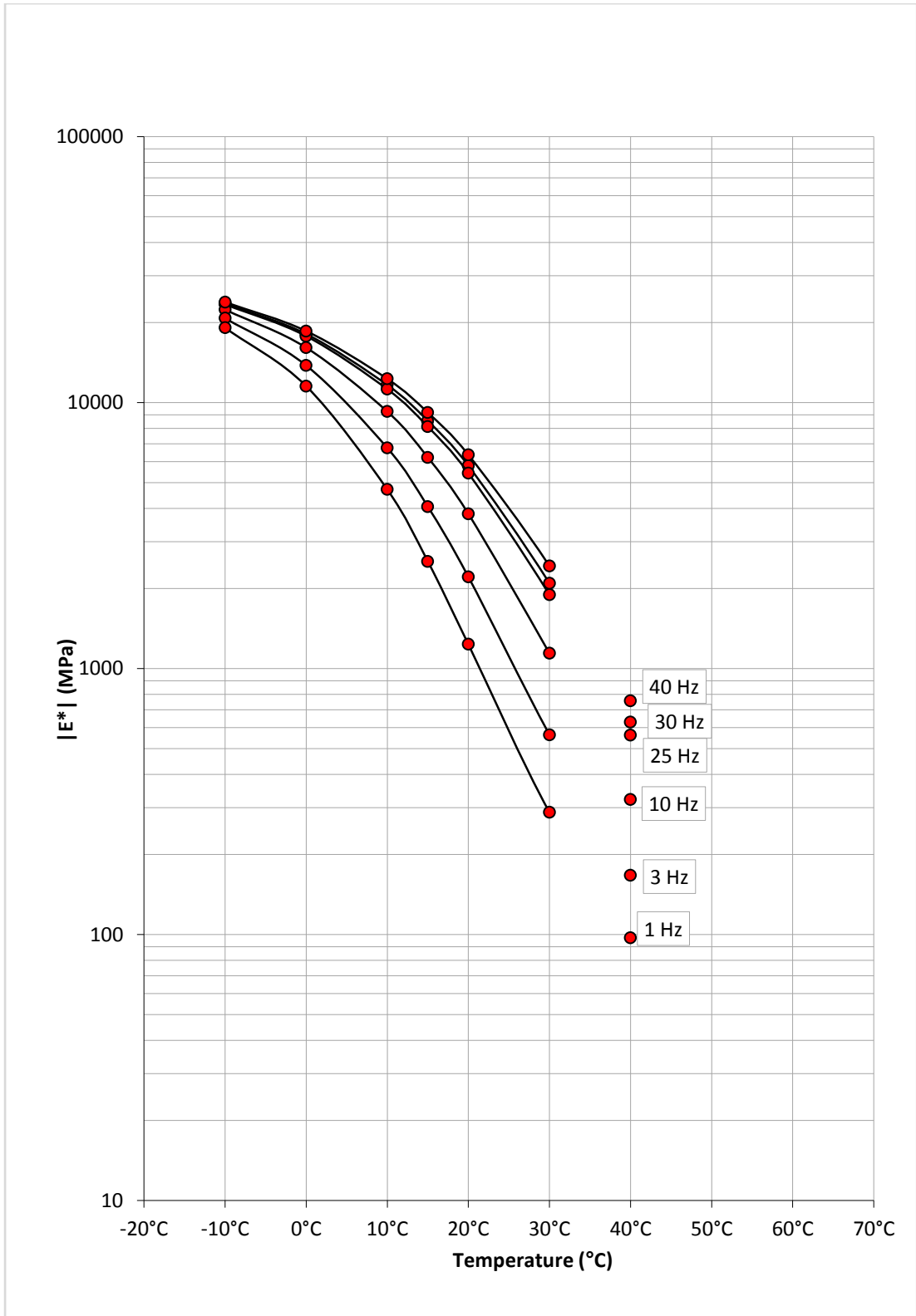


Figure 47 Isotherm curves (frequency sweeps)



**Figure 48** Isochrones curves (temperature sweeps)

Although temperature and frequency sweeps give a good indication of the material behaviour, researchers express both data sets on a single axis (usually frequency) by means of the Time/Temperature superposition principle.

This involves undertaking different frequency sweeps at different temperatures and then shifting each of the curves until they lie on the same plan as the curve chosen *a priori* as a reference curve. This is called a master curve and the reference temperature is 15°C (see Figure 49). Master curves help to understand the behaviour of the mixture at higher and lower frequencies (also outside of the measured ranges).

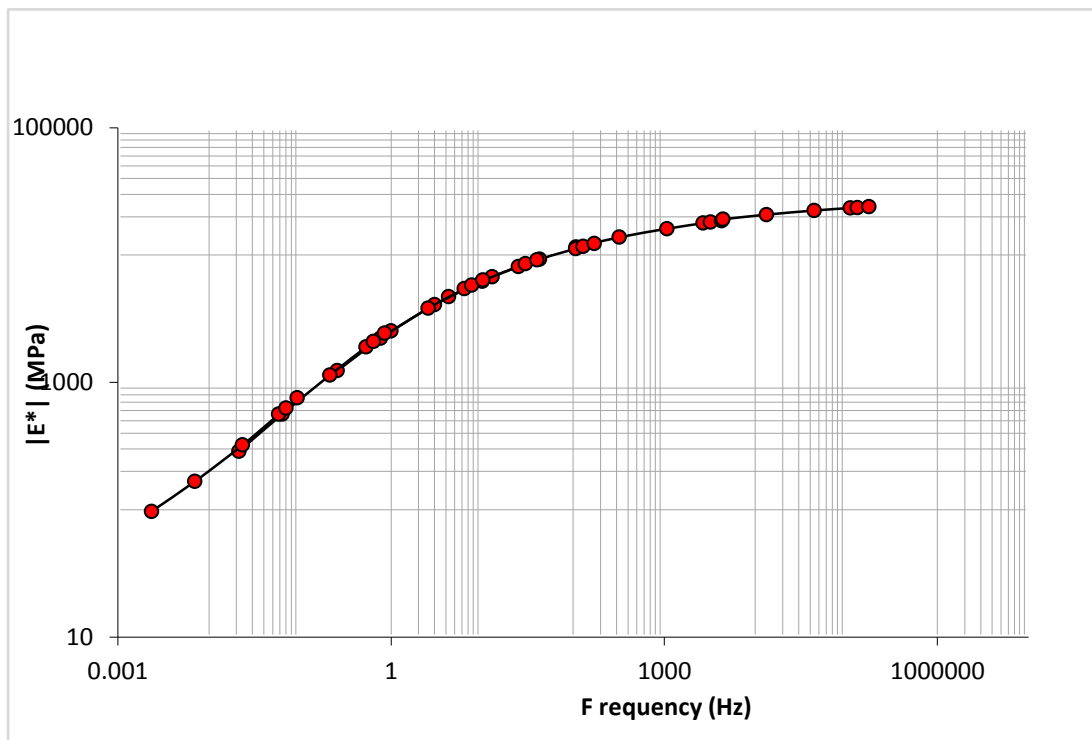


**Figure 49** Master curve at a reference temperature of 15°C

Generally phase angle increases when stiffness decreases or when temperature increases (this is not true at temperature as high as 40 °C). Higher values of phase angle indicate a tendency towards more viscous behaviour, whilst lower values indicate more elastic response (see Figure 50).

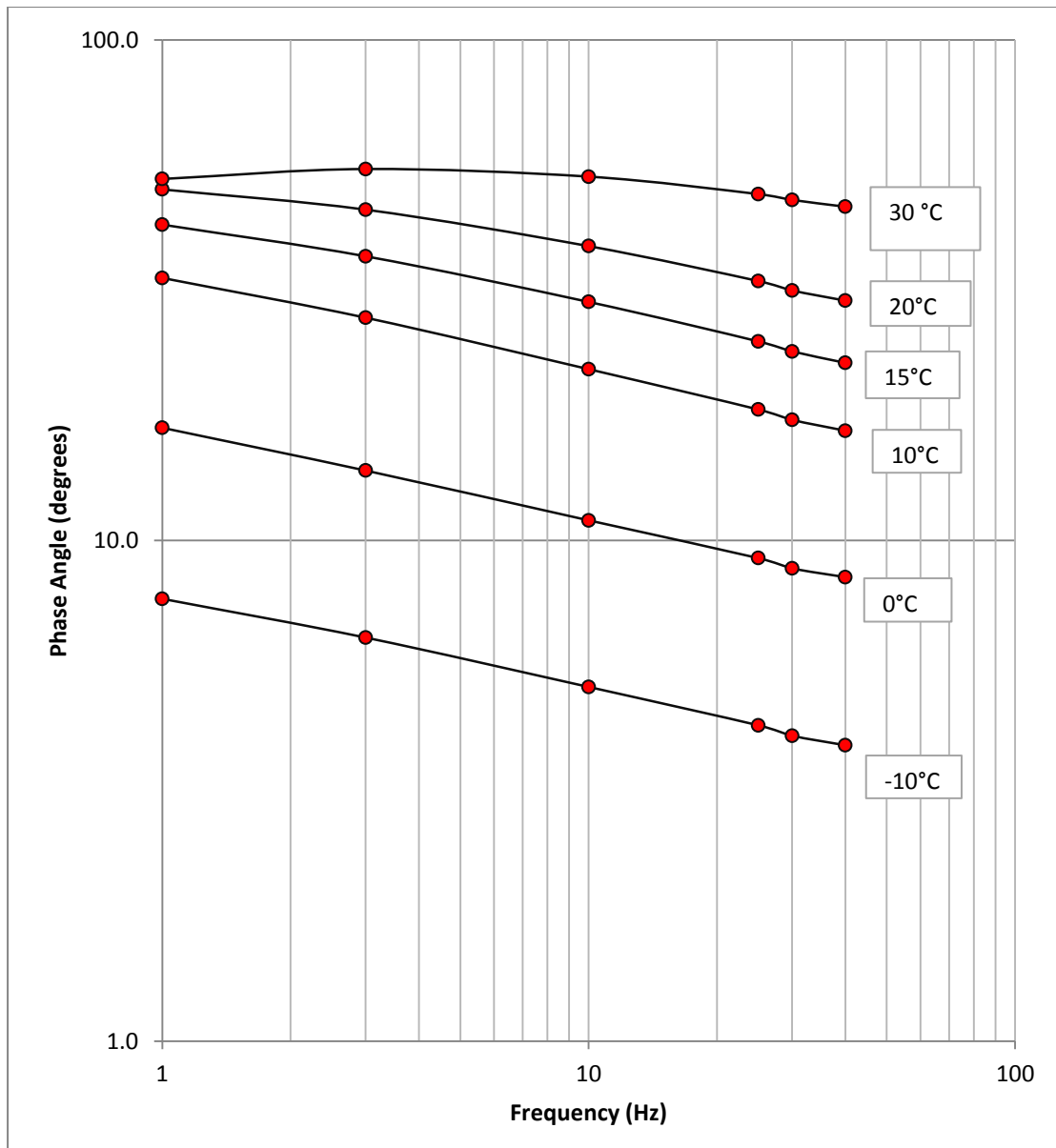


**Figure 50** Phase angle at different temperatures

The phase angle increases when the temperature increases (and the effect of temperature is amplified at lower frequencies); it decreases when frequency increases. This can be easily explained by the fact that the lower the temperature the more elastic behaviour is exhibited; whilst at higher temperatures asphalt materials demonstrate a more viscous behaviour.

### **Fatigue**

Fatigue tests were carried out in strain control mode at constant temperature and frequency;

Two different temperatures (10°C and 20°C) and two different frequencies (15Hz and 25Hz) were used in the test program.

Figure 51 shows fatigue life at two different frequencies at 20°C. Figure 52 shows fatigue life at two different frequencies at 10°C. Figure 53 shows fatigue life at two different temperatures at 15 Hz. Figure 54 shows fatigue life at two different temperatures at 25 Hz. Regression lines were calculated for each case and then compared using the *t test*; results are shown in Table 7.

**Table 7** Comparison between temperatures and frequencies

Cases	Slope	Elevation	Result
15-25Hz @20°C	$t=5.65 > t_{0.05(2),11}=2.201$	-	Regressions are different
15-25Hz @10°C	$t=1.59 < t_{0.05(2),22}=2.074$	$t=0.68 < t_{0.05(2),21}=1.318$	Regressions have same slopes and elevations = Unique equation
10-20°C @15Hz	$t=1.76 < t_{0.05(2),19}=2.093$	$t=0.72 < t_{0.05(2),19}=2.093$	Regressions have same slopes but not elevations
10-20°C @25Hz	$t=4.08 > t_{0.05(2),16}=2.120$	-	Regressions are different

Fatigue data are characterised by different regression lines for different frequencies (15 and 25 Hz) and different temperatures (10 and 20 °C). Asphalt material has a more elastic behaviour at lower temperatures or at higher frequencies and fatigue life is strongly influenced by stiffness modulus; stiffness increases when temperature decreases, it increases when frequencies increases. During a fatigue test in strain control mode, the specimen is subjected to a higher stress at lower temperatures or higher frequencies therefore fatigue life decreases.

Statistically it was found that regression lines at 15 and 25 Hz are the same at 10 °C and different at 20°C; this is explained by the fact that the chosen material is characterised by a soft binder (100 pen), this underlines the effects of temperature on fatigue life: it increases at higher temperatures. For this particular case, a unique equation that characterises fatigue data was obtained. A similar scenario was obtained when frequency increases (at 25Hz).

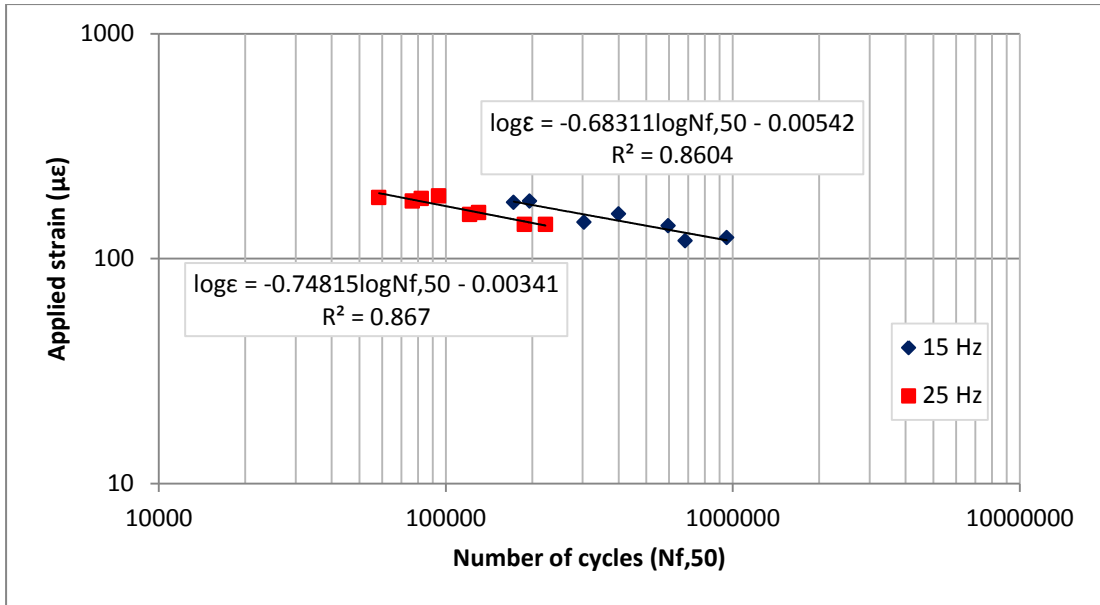


**Figure 51** Fatigue life at 20°C – 10 mm DBM

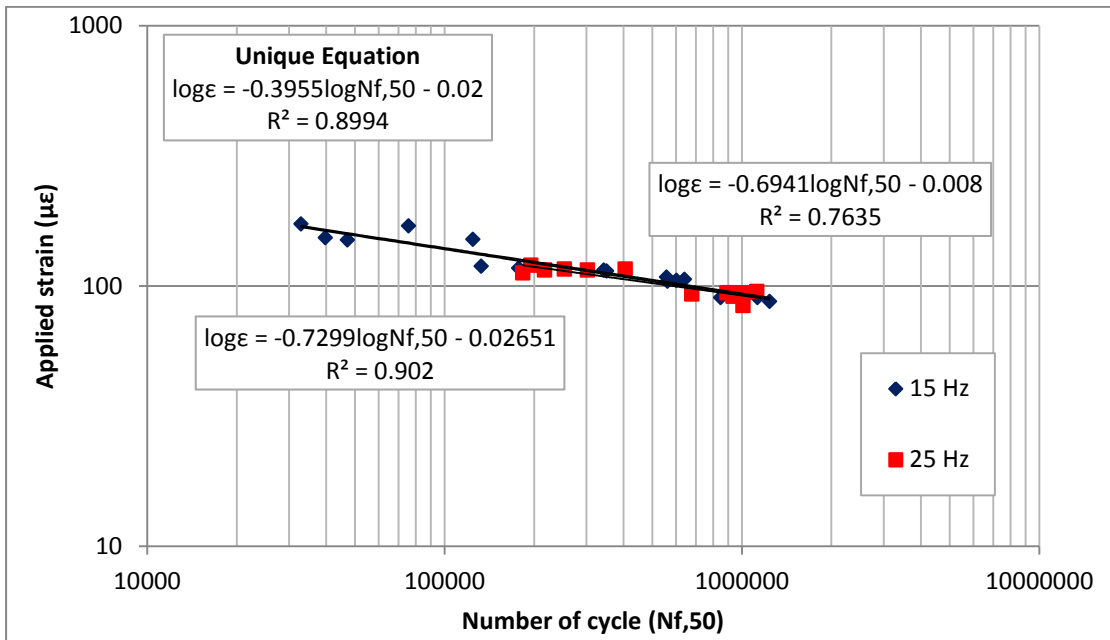


**Figure 52** Fatigue life at 10°C - 10 mm DBM

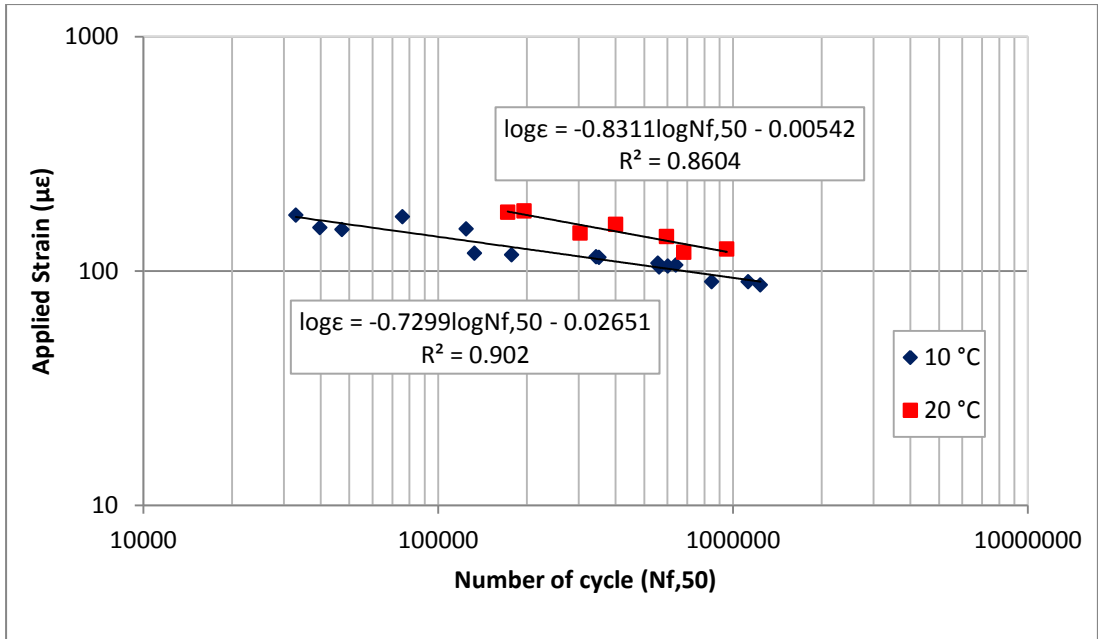


**Figure 53** Fatigue life at 15 Hz - 10 mm DBM

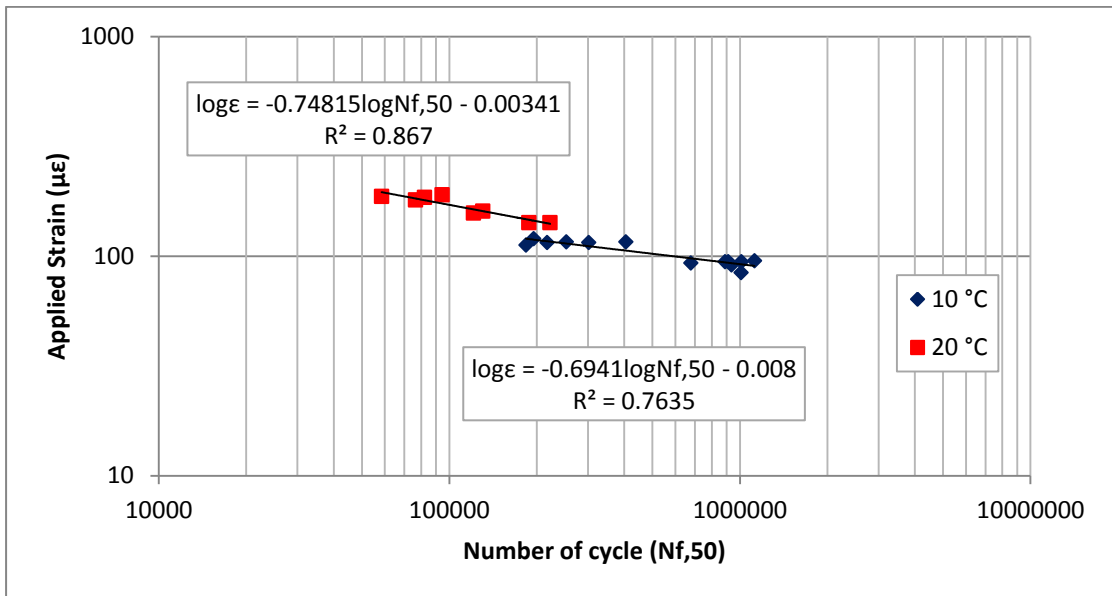
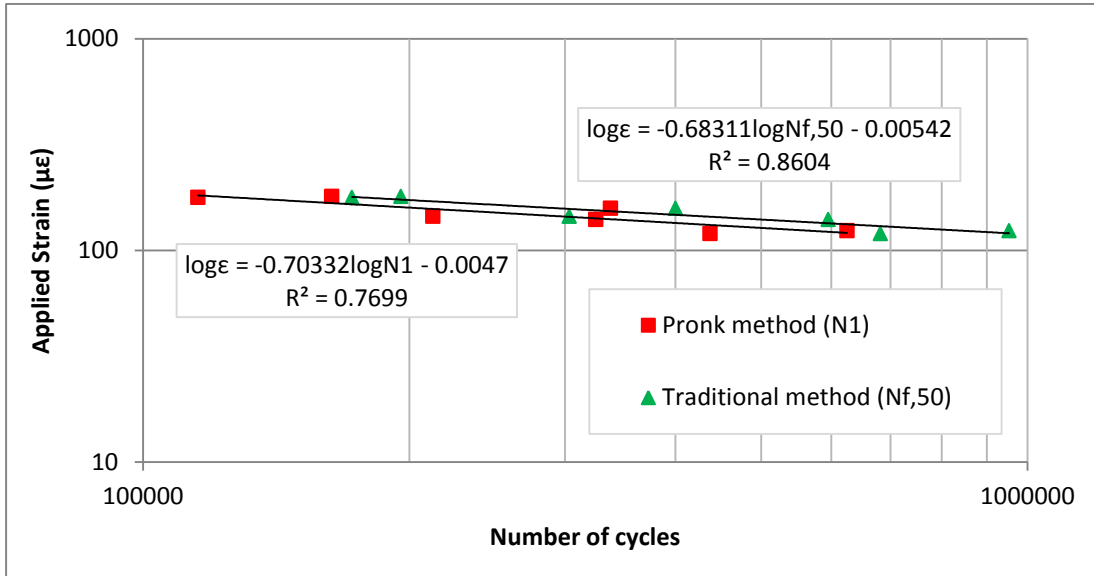


**Figure 54** Fatigue life at 25 Hz - 10 mm DBM

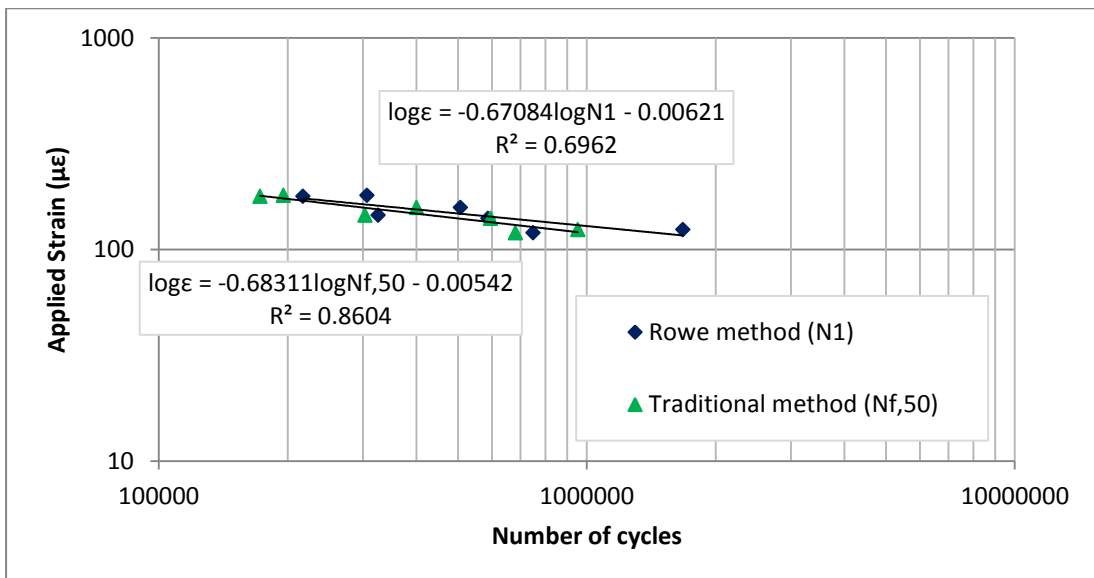
Dissipated energy methods were analysed and compared for the different temperatures and frequencies; in particular the criteria chosen were: traditional method ( $Nf,50$ ), Dissipated Energy Ratio ( $N1$  Pronk), Energy Ratio ( $N1$  Rowe) and RDEC method ( $Nfm$ ).

Figure 55, Figure 56 and Figure 57 show the fatigue lives obtained from the different dissipated energy methods at 20°C and 15 Hz. As it can be noticed, the Energy Ratio method by Pronk generates fatigue life values smaller than the traditional method (see Figure 55). The same method reviewed by Rowe

generates fatigue lives larger than the traditional method (see Figure 56). The third method used in this paper was RDEC; Nfm was calculated and the results show that Nfm values are slightly larger than Nf,50 values at lower strain levels, the values almost coincide at higher strain levels (see Figure 57).



**Figure 55** Fatigue lives obtained by means of Energy Ratio (Pronk) and traditional methods



**Figure 56** Fatigue lives obtained by means of Energy Ratio (Rowe) and traditional methods

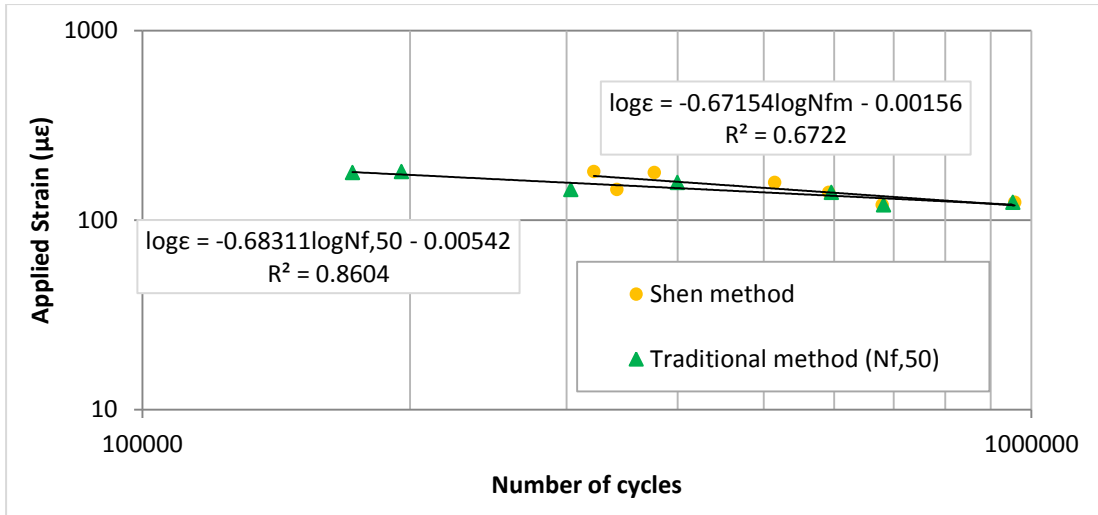


**Figure 57** Fatigue lives obtained by means of RDEC (Shen) and traditional methods. Regression lines were calculated for each case and then compared by using the appropriate statistical method. Statistically, first the hypothesis of equality between slopes of different regressions was tested with the analysis of covariance (ANCOVA); the hypothesis is  $H_0: \beta_1 = \beta_2 = \dots = \beta_k$  and it was rejected for a significance level of 0.1. Therefore, Dunnett's test was used for a multiple comparison considering Nf,50 as the control fatigue line; regression lines obtained from different dissipated energy methods statistically are not different from Nf,50; they are different for a significance level of 0.01 (considering a smaller significance level means a smaller probability to make a mistake). Results are shown in Table 8. The same behaviour was noticed for the test results undertaken at 20°C and 25 Hz.

**Table 8** DE method comparison by using Dunnett's test

Case	Slope	Elevation	Results
Nf,50 - DER - ER - Nfm	$F=2.84 < F_{0.05(1),3,20}=3.1$	$F=7.6 > F_{0.05(1),3,20}=3.1$	Regressions do not have same elevations for a significance level $\alpha=0.05$
	$F=2.84 > F_{0.1(1),3,20}=2.3$	-	Regressions are not all the same for a significance level $\alpha=0.01$
Nf,50 - DER	$q'=1.5 < q'_{0.05(1),20,3}=2.5$	$q'=1.4 < q'_{0.05(1),20,3}=2.5$	Regressions are the same for a significance level $\alpha=0.05$
Nf,50 - ER	$q'=0.98 < q'_{0.05(1),20,3}=2.5$	$q'=0.8 < q'_{0.05(1),20,3}=2.5$	Regressions are the same for a significance level $\alpha=0.05$
Nf,50 - Nfm	$q'=0.92 < q'_{0.05(1),20,3}=2.5$	$q'=0.2 < q'_{0.05(1),20,3}=2.5$	Regressions are the same for a significance level $\alpha=0.05$

Regarding the Ratio of Dissipated Energy Change approach, a comparison between different temperatures and different frequencies was done. The

plateau value is correlated with a number of fatigue cycles to failure by using Equation 34 (see Paragraph 2.2). The value of the constants  $c$  and  $d$  were determined experimentally. The coefficient  $d$  varies from -0.80 and -1.60 according to Shen (2007). It can be seen from the experimental curve that the fit line, of the experimental data at 20°C and both 15 and 25 Hz, is characterised by a coefficient  $d$  equal to -1.048 (see Figure 58).

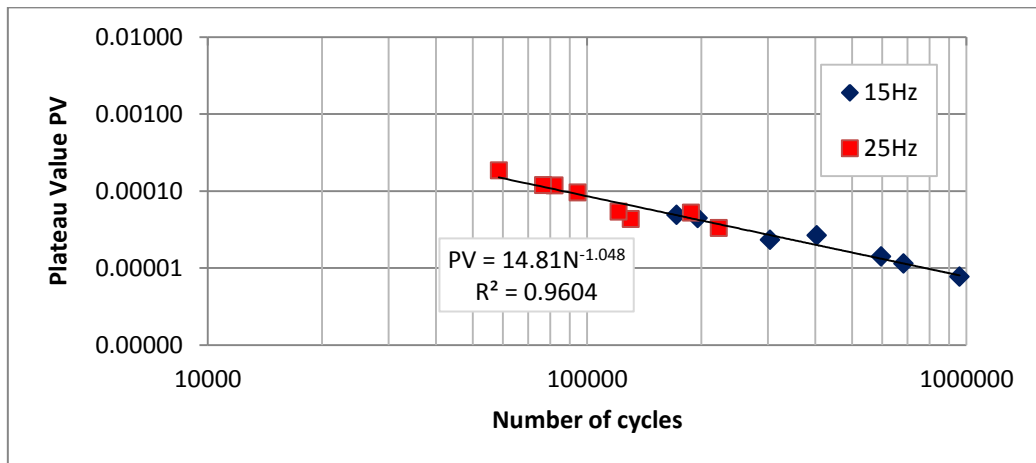


**Figure 58** RDEC at 20°C at two different frequencies (15 and 25Hz)

The same behaviour was noticed for the test results undertaken at 10°C.

Fatigue data have a different behaviour when different temperatures are compared at constant frequency: Figure 59 and Figure 60 show the data at 15 and 25 Hz. Also in this case, regression lines were calculated for each case and then compared using the  $t$  test; results are shown in Table 9.

**Table 9** RDEC: temperature comparison at 15 and 25 Hz

Cases	Slope	Elevation	Result
10-20°C @ 15Hz	$t=5.62 > t_{0.05(2),19}=2.093$	-	Regressions are different
10-20°C @ 15Hz	$t=10.09 > t_{0.05(2),18}=2.101$	-	Regressions are different

It is not possible to get a unique relationship when RDEC is used at different temperatures.

Only two temperatures and two frequencies were tested so more research would be needed to confirm those results.

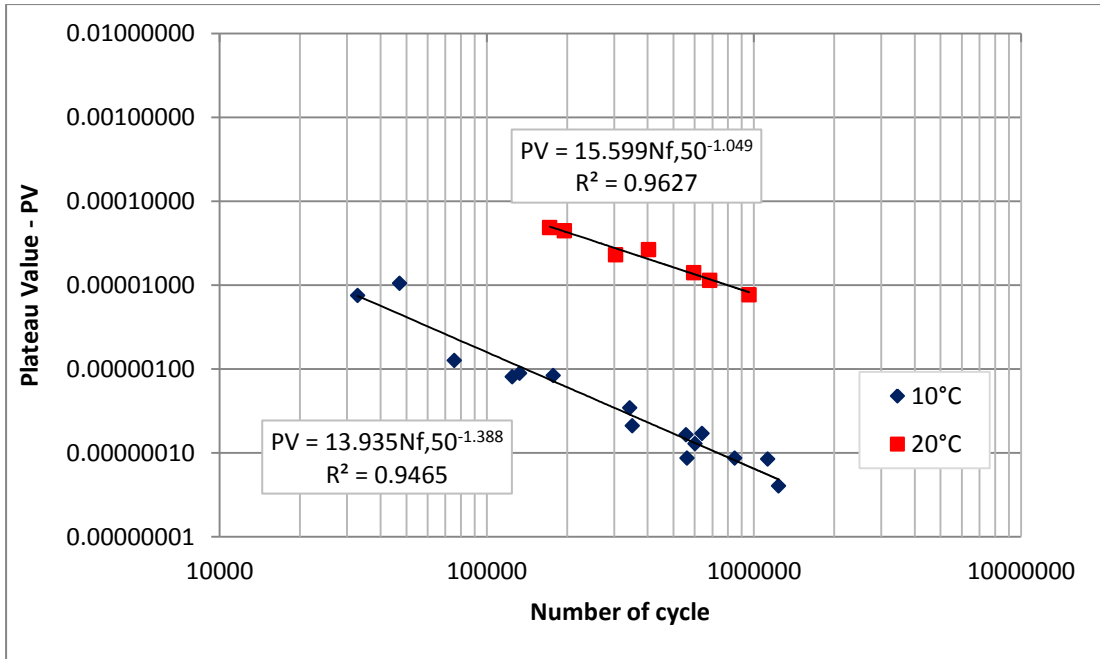


**Figure 59** RDEC at 15Hz at two different temperatures (10 and 20°C)

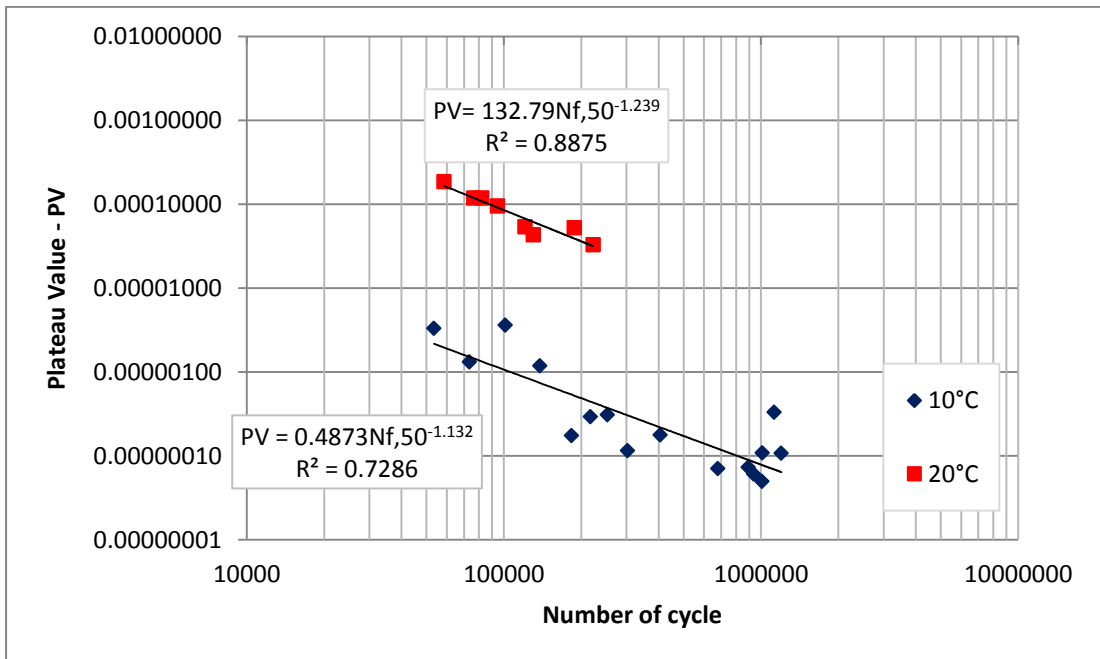


**Figure 60** RDEC at 25Hz at two different temperatures (10 and 20°C)

### 5.3.2 20mm DBM

#### Stiffness modulus

Stiffness tests were carried out at 11 different temperatures (-20, -15, -10, -5, 0, 5, 10, 15, 20, 25 and 30°C) and 8 different frequencies (1, 2, 5, 10, 15, 20, 25 and 30 Hz). Two different specimens were tested at the same time and in

this case the experimental work was undertaken at the University of Nottingham (see Figure 39).

Also for this material, a frequency sweep and a temperature sweep were obtained (see Figure 61 and Figure 62).

As for the previous material, the stiffness modulus decreases when the temperature increases (and the effect of temperature is amplified at lower frequencies); it decreases when frequency decreases (and the effect is amplified at higher temperatures).

The evolution of phase angle at different temperatures is shown in Figure 63; stiffness modulus master curve is shown in Figure 64. Phase angle became unstable at lower temperature and higher frequency; one reason may be that the testing machine is not stiff enough at lower temperature and higher frequency compared to the stiffness of the specimen; therefore it becomes unstable.

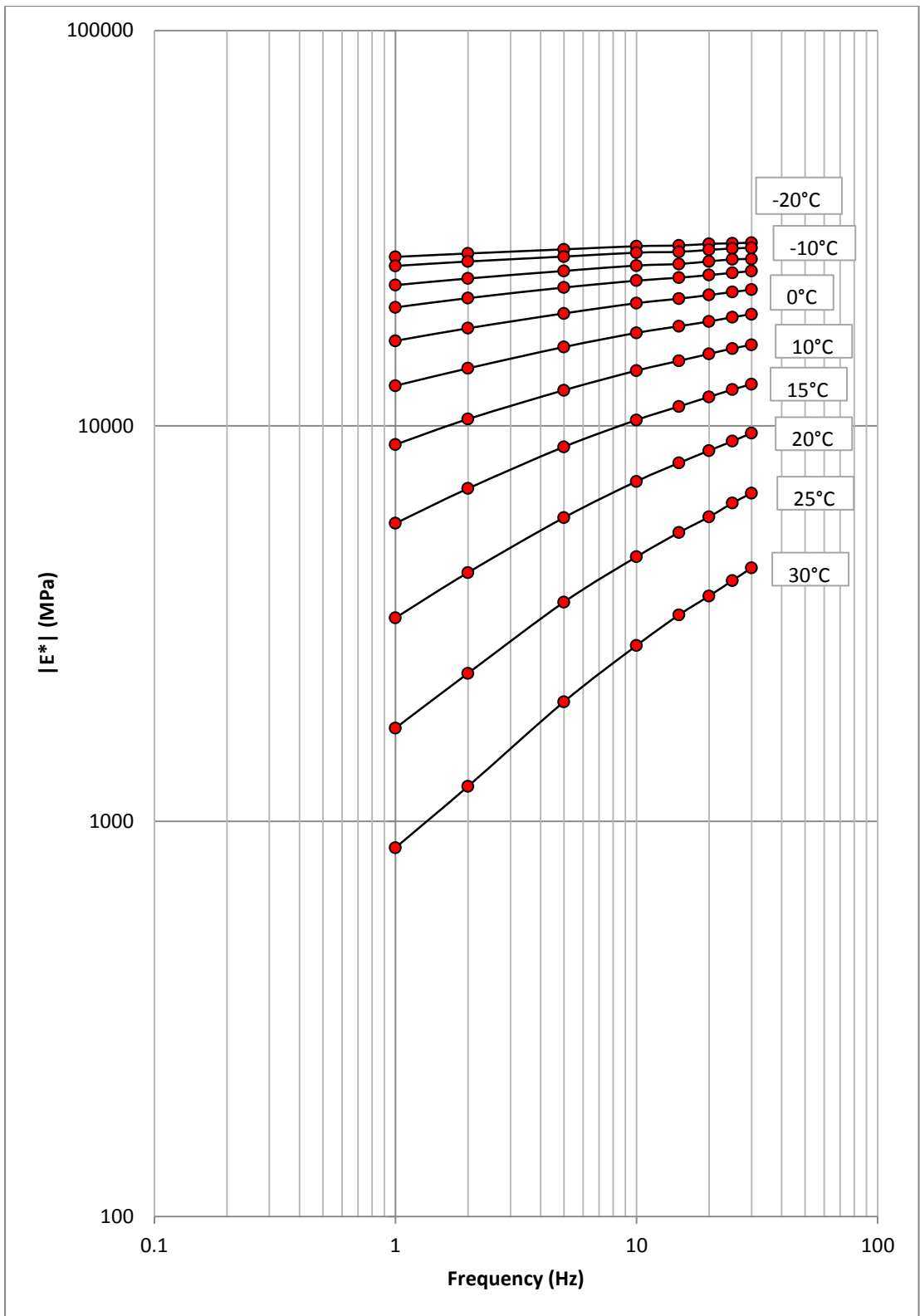


**Figure 61** Isotherm curves (frequency sweeps)

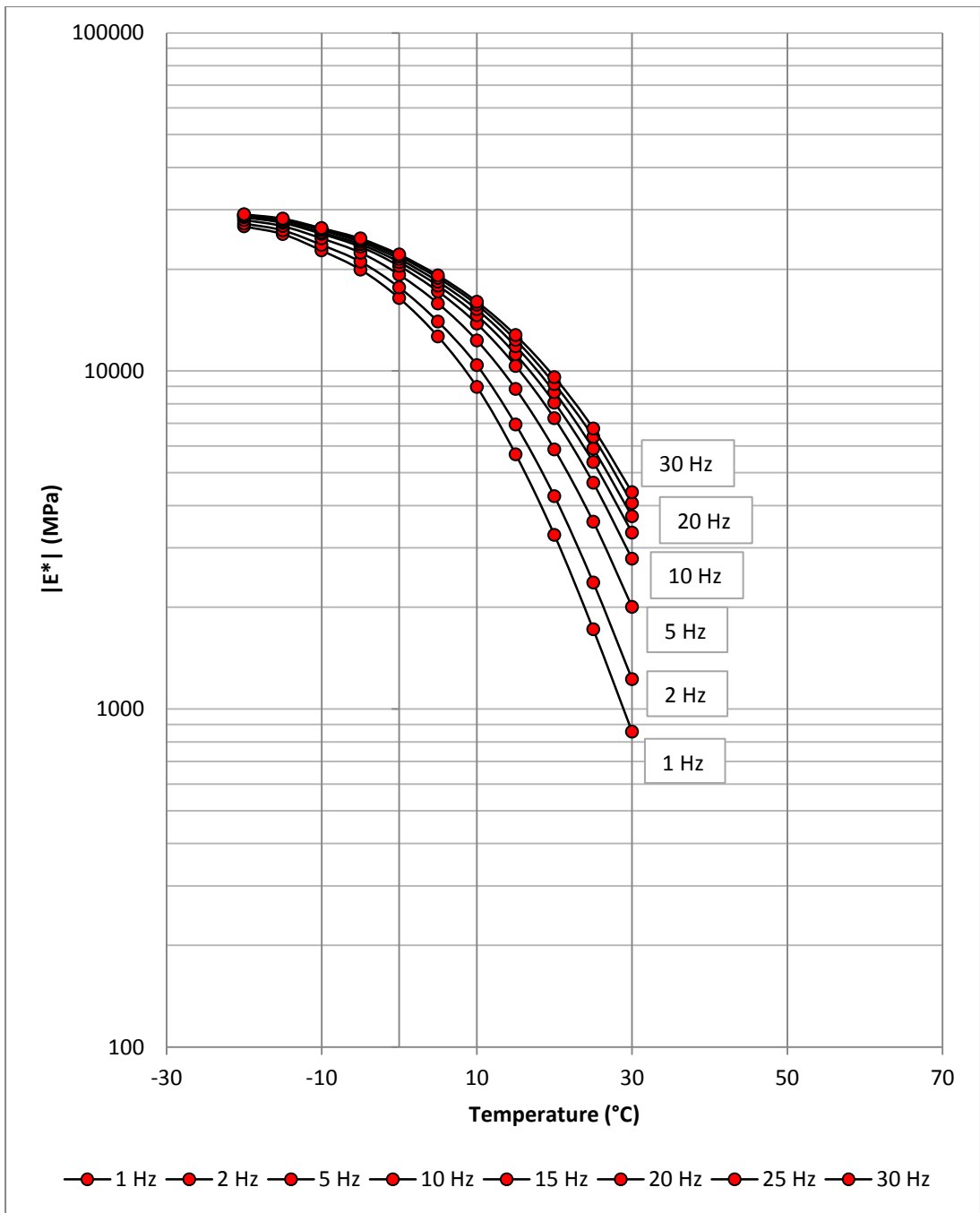


**Figure 62** Isochrones curves (temperature sweeps)

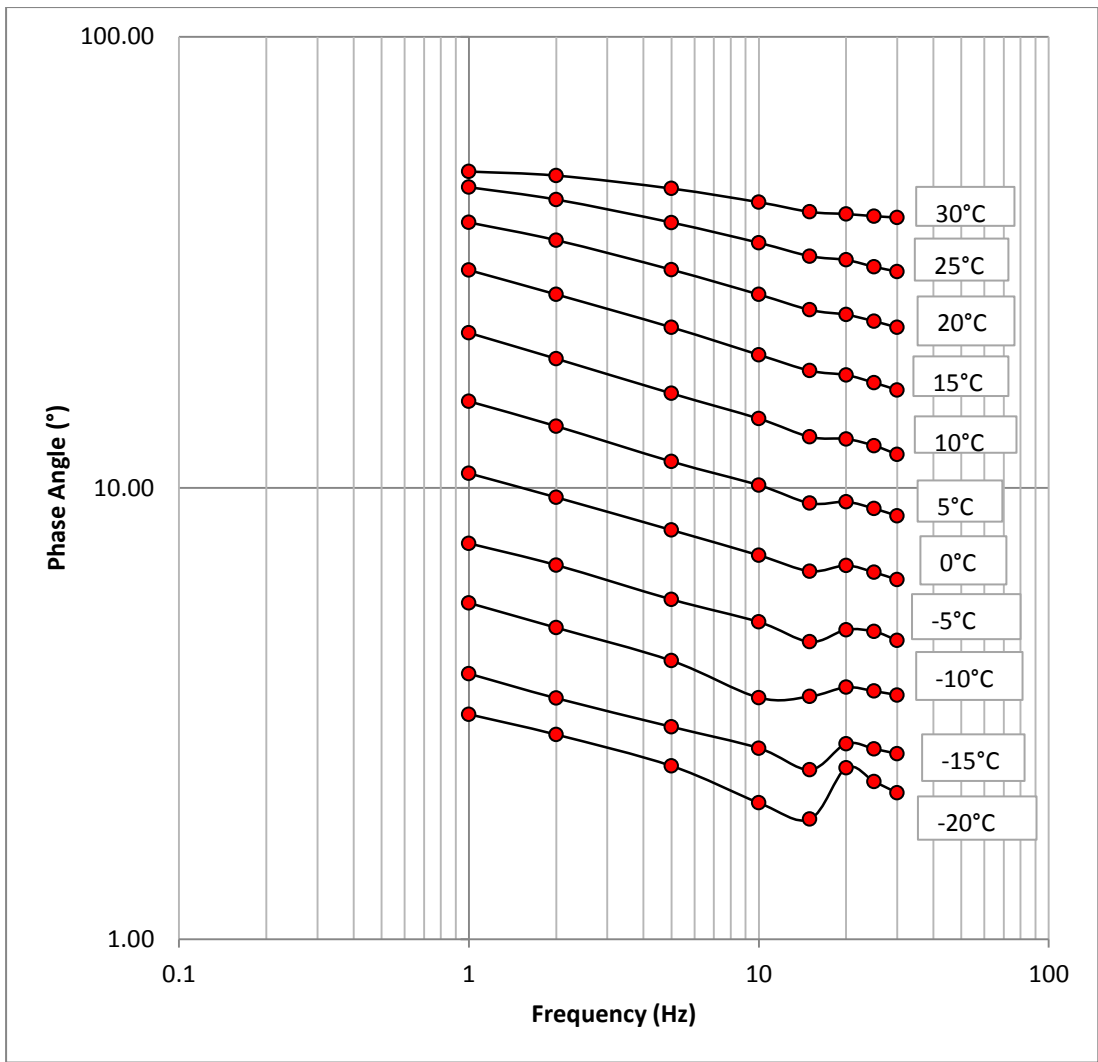


**Figure 63** Phase angle at different temperatures for 20mm DBM

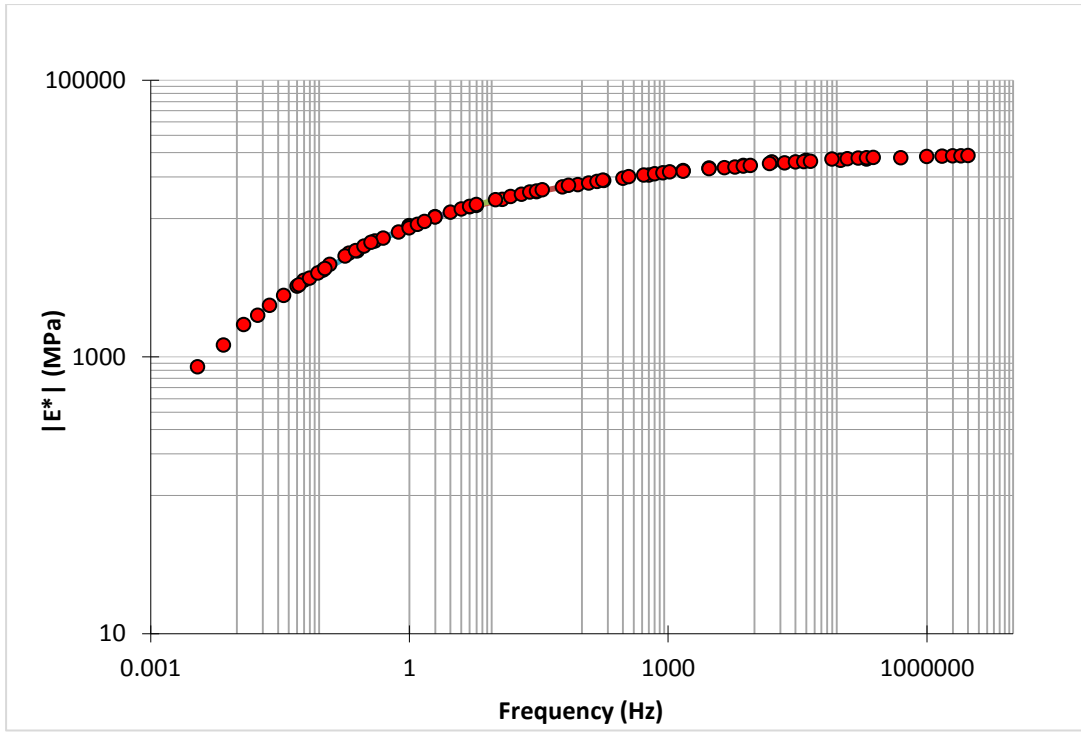


**Figure 64** Master curve at a reference temperature of 10°C (20mm DBM)

### **Fatigue**

Fatigue tests were carried out in both strain and stress control mode at 10°C and 25 Hz. Strain levels used for testing were from 80  $\mu\epsilon$  to 190  $\mu\epsilon$ ; stress levels from 1150 kPa to 1750 kPa. Regression lines were calculated for each mode of loading and then compared using the *t test*, to make a right comparison initial strain was calculated for each test undertaken in stress control mode (see Figure 65). Another comparison between the two modes of loading was made using the RDEC approach. In this first case, the regression lines have the same slope and same elevation, thus a unique relationship could be found as shown in Figure 66;  $R^2$  decreases though. In the second case (RDEC), the regression lines are different; thus this method is not independent on the mode of loading (see Figure 67). Results are shown in Table 10.

**Table 10** Comparison between stress and strain mode of loading

Case	Slope	Elevation	Result
Nf,50 (Strain-stress control mode)	$t=0.63 < t_{0.05(2),14}=2.145$	$t=0.42 < t_{0.05(2),14}=1.76$	Regressions are not different
PV (Strain-stress control mode)	$t=4.33 > t_{0.05(2),14}=2.145$	-	Regressions are different

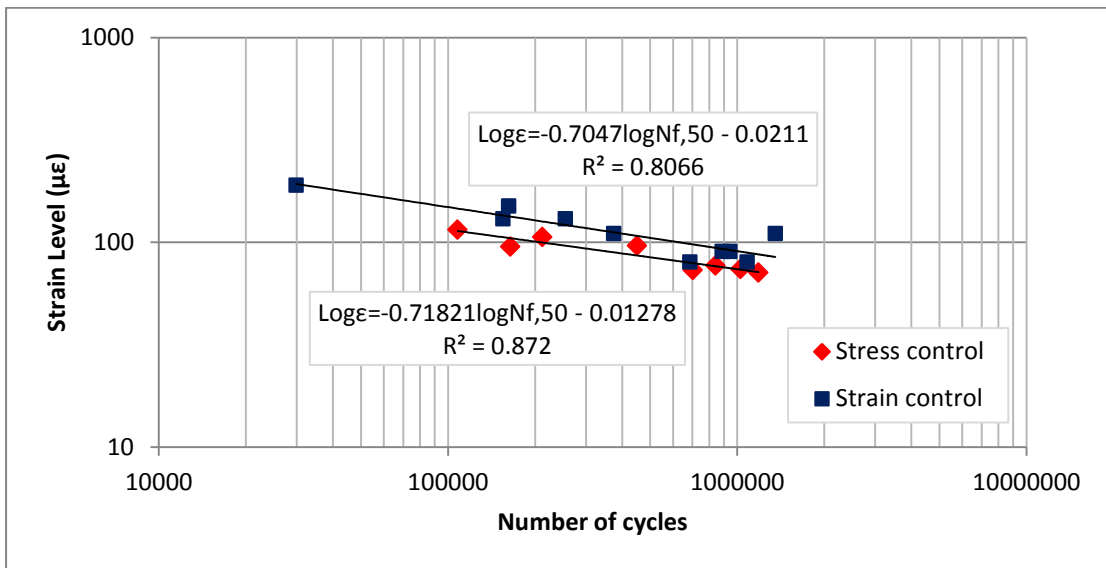


**Figure 65** Fatigue life at 10°C and 25 Hz in both stress and strain control mode (20 mm DBM)

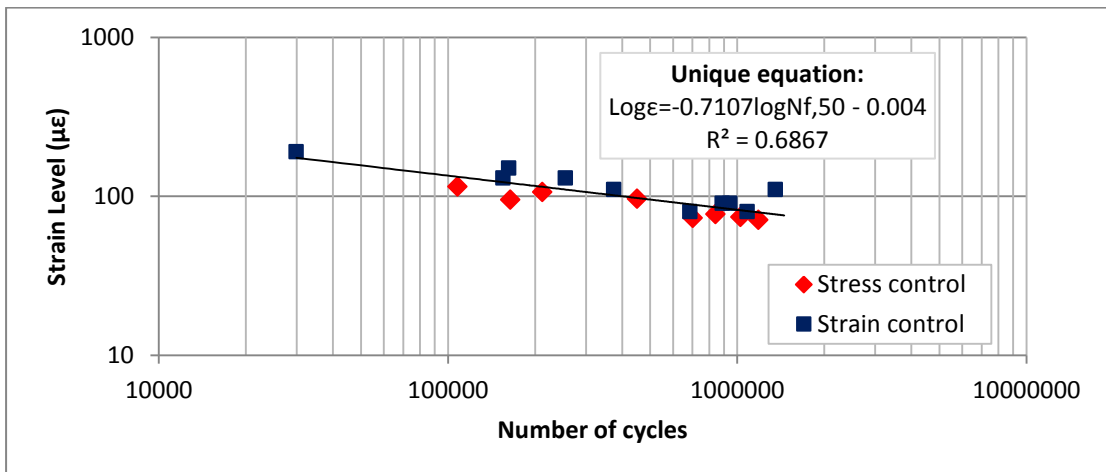


**Figure 66** Unique regression line for fatigue life data at 10°C and 25 Hz in both stress and strain control mode

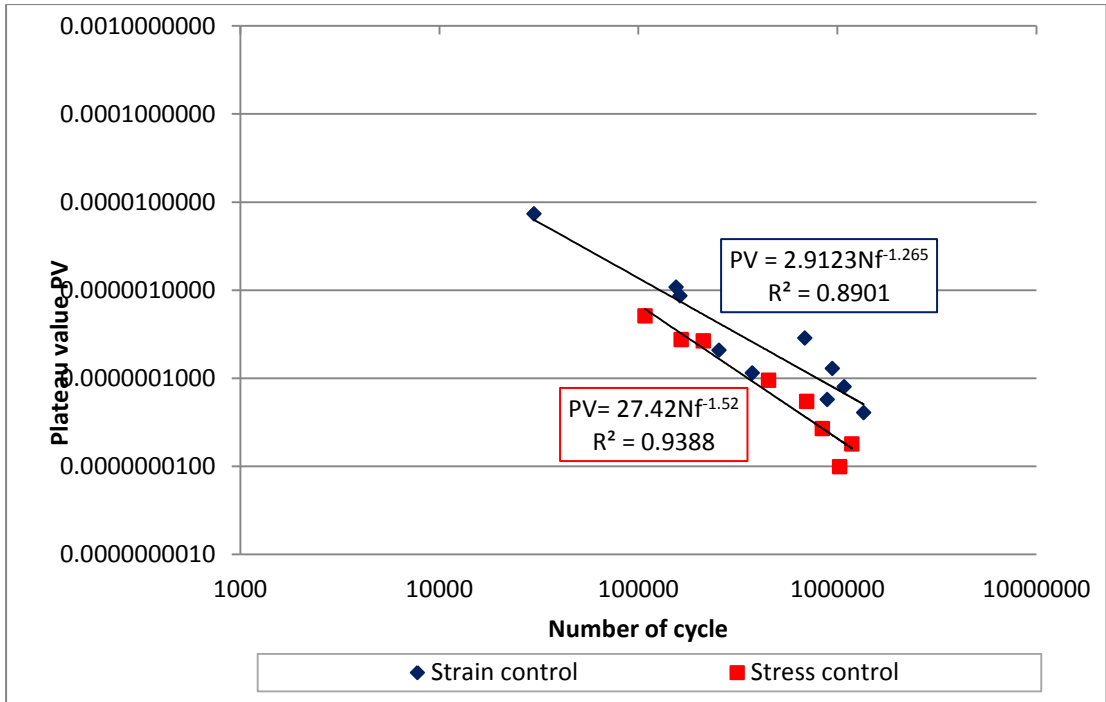


**Figure 67** RDEC at 10°C and 25 Hz in both stress and strain control mode

Dissipated energy methods were analysed and compared for the different modes of loading; in particular the criteria chosen were: traditional method (Nf,50), Dissipated Energy Ratio (N1 Pronk), Energy Ratio (N1 Rowe) and RDEC method (Nfm).

Figure 68, Figure 69, Figure 70, Figure 71, Figure 72 and Figure 73 show the fatigue lives obtained from the different dissipated energy methods at 10°C and 25 Hz in both modes of loading. As for the 10mm DBM, in strain control mode, the DER (by Pronk) method generate fatigue life values smaller than the traditional method; although fatigue values are different, there is no difference between the two methods if the trend lines are compared in stress control mode. DER is strictly related to the stiffness evolution; unlike the 10mm DBM, DER shows smaller values than Nf,50; this is due to the stiffness of the material: 20mm DBM is characterised by higher stiffness values than 10mm DBM.

The last method considered was Shen's method (Nfm); also in this case, the fatigue curves are slightly different in both strain and in stress control mode.

**Table 11** DE method comparison by using Dunnett's test – 20mm DBM @25Hz and 10°C

<b>Strain</b>	<b>Slope</b>	<b>Elevation</b>	<b>Results</b>
Nf,50 - DER - ER - Nfm	$F=1.88 < F_{0.05(1),3,32}=2.9$	$F=11.6 > F_{0.05(1),3,32}=2.9$	Regressions have same slopes but elevations for a significance level $\alpha=0.05$
Nf,50 - DER	$q'=1.1 < q'_{0.05(1),32,4}=2.46$	$q'=1.3 < q'_{0.05(1),32,4}=2.46$	Regressions are the same for a significance level $\alpha=0.05$
Nf,50 - ER	$q'=0.4 < q'_{0.05(1),32,4}=2.46$	$q'=0.4 < q'_{0.05(1),32,4}=2.46$	Regressions are the same for a significance level $\alpha=0.05$
Nf,50 - Nfm	$q'=0.6 < q'_{0.05(1),32,4}=2.46$	$q'=0.6 < q'_{0.05(1),32,4}=2.46$	Regressions are the same for a significance level $\alpha=0.05$
<b>Stress</b>	<b>Slope</b>	<b>Elevation</b>	<b>Results</b>
Nf,50 - DER - ER - Nfm	$F=1.02 < F_{0.05(1),3,24}=3.01$	$F=2.39 < F_{0.05(1),3,24}=3.01$	Regressions have same slopes and elevations for a significance level $\alpha=0.05$
Nf,50 - ER	$q'=0.39 < q'_{0.05(1),24,3}=2.01$	$q'=0.44 < q'_{0.05(1),24,3}=2.01$	Regressions are the same for a significance level $\alpha=0.05$
Nf,50 - DER	$q'=0.31 < q'_{0.05(1),24,3}=2.01$	$q'=0.36 < q'_{0.05(1),24,3}=2.01$	Regressions are the same for a significance level $\alpha=0.05$
Nf,50 - Nfm	$q'=0.26 < q'_{0.05(1),24,3}=2.01$	$q'=0.35 < q'_{0.05(1),24,3}=2.01$	Regressions are the same for a significance level $\alpha=0.05$

Statistically, regression lines are slightly different in strain control mode; they are not different in stress control mode. Dunnett's test was used for the multiple comparison of the difference between the dissipated energy methods for fatigue lives obtained in strain and stress control modes (see Table 11).

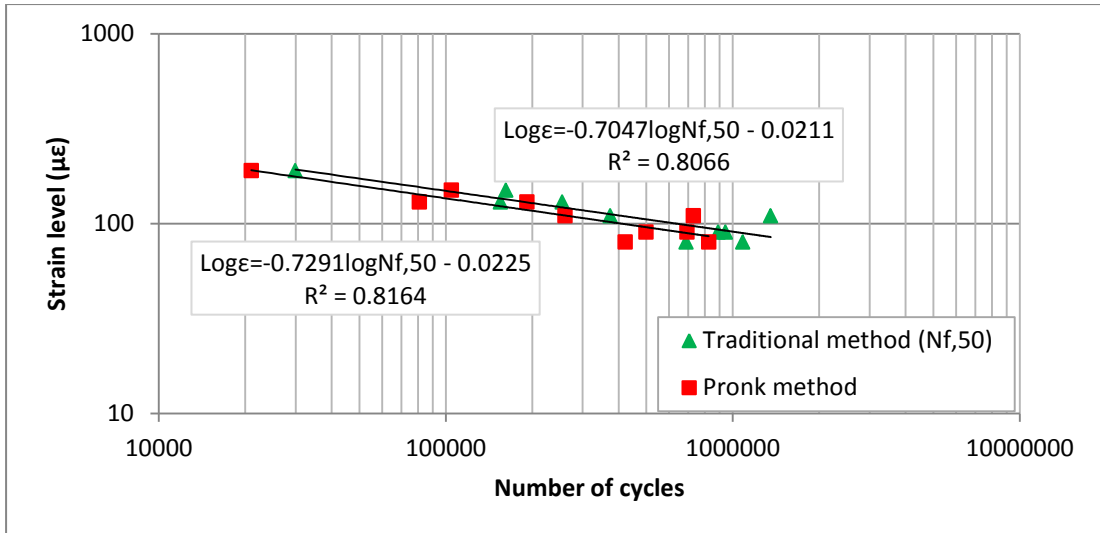


**Figure 68** Fatigue lives obtained by means of Dissipated Energy Ratio (Pronk) and traditional methods in strain control mode

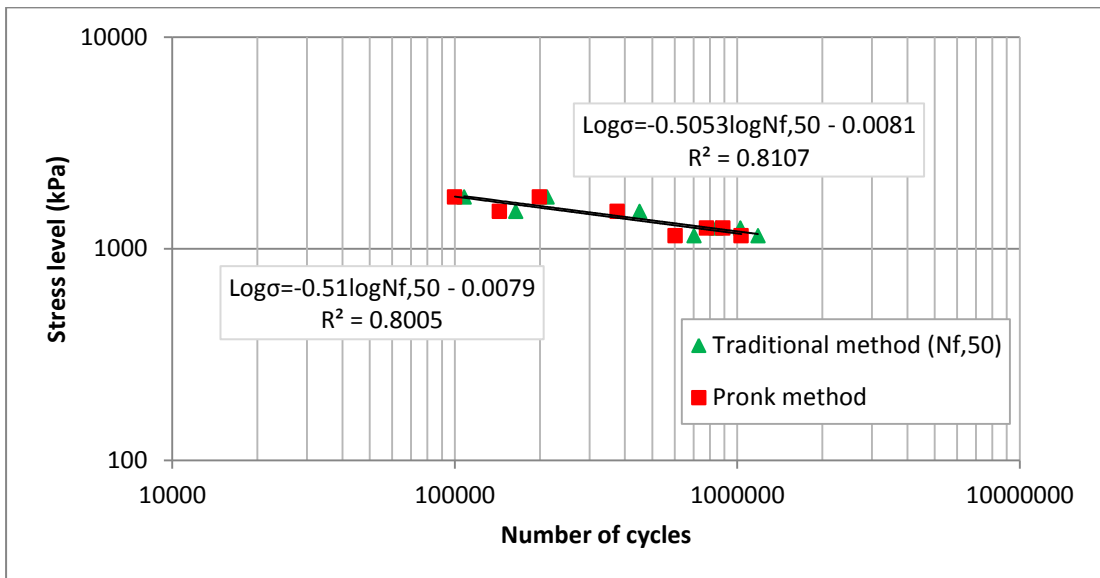


**Figure 69** Fatigue lives obtained by means of Energy Ratio (Pronk) and traditional methods in stress control mode

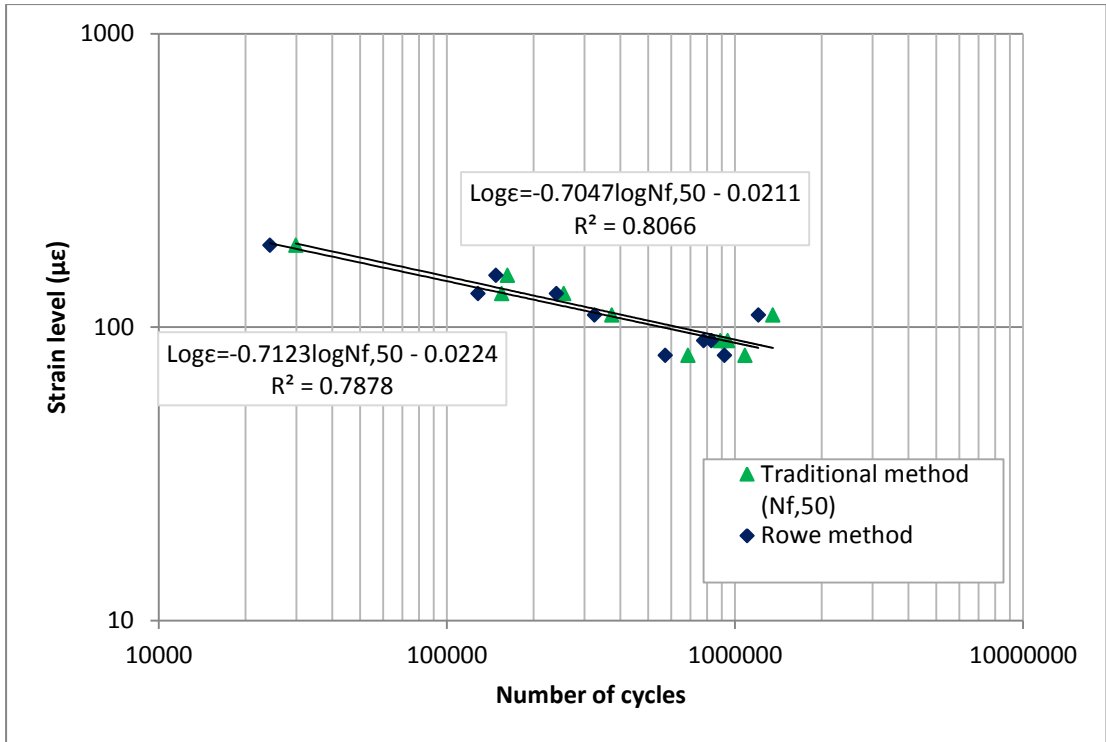


**Figure 70** Fatigue lives obtained by means of Energy Ratio (Rowe) and traditional methods in strain control mode

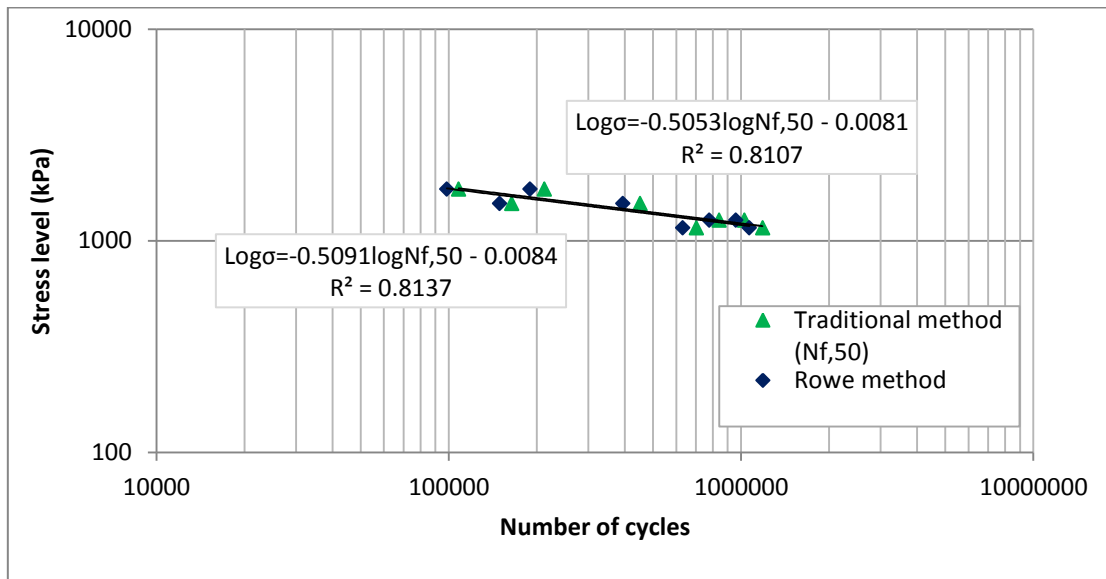


**Figure 71** Fatigue lives obtained by means of Energy Ratio (Rowe) and traditional methods in stress control mode

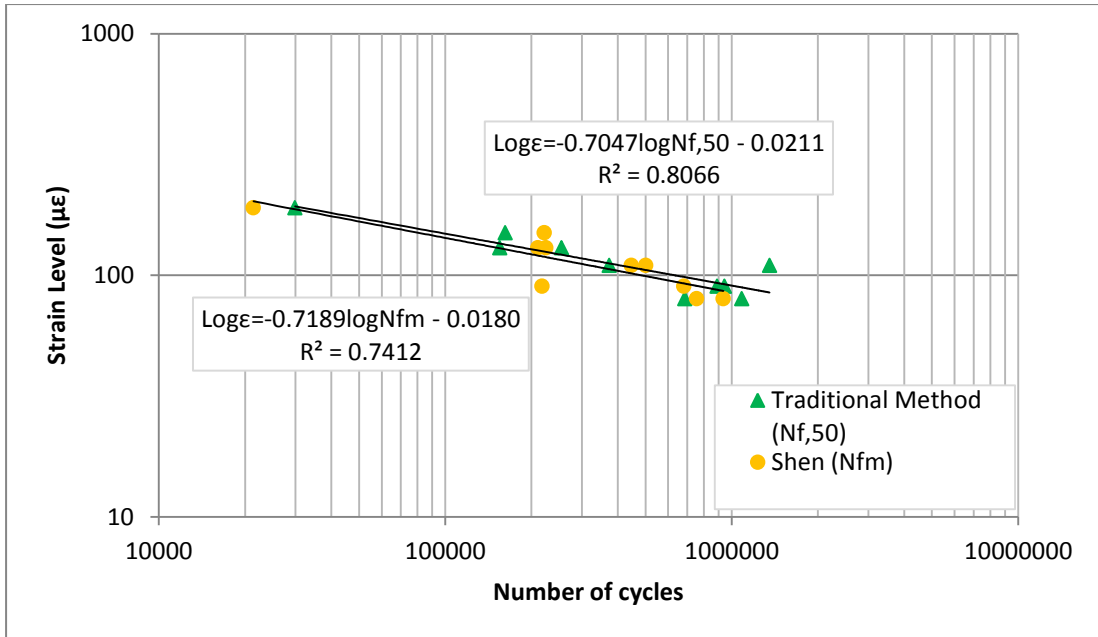


**Figure 72** Fatigue lives obtained by means of RDEC (Shen) and traditional methods in strain control mode

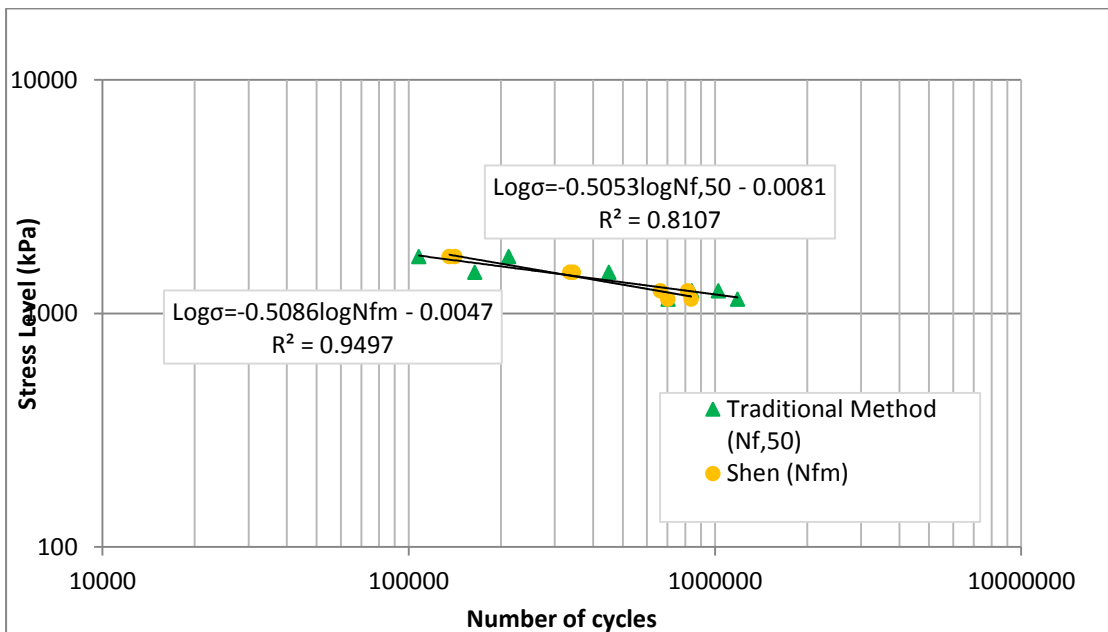


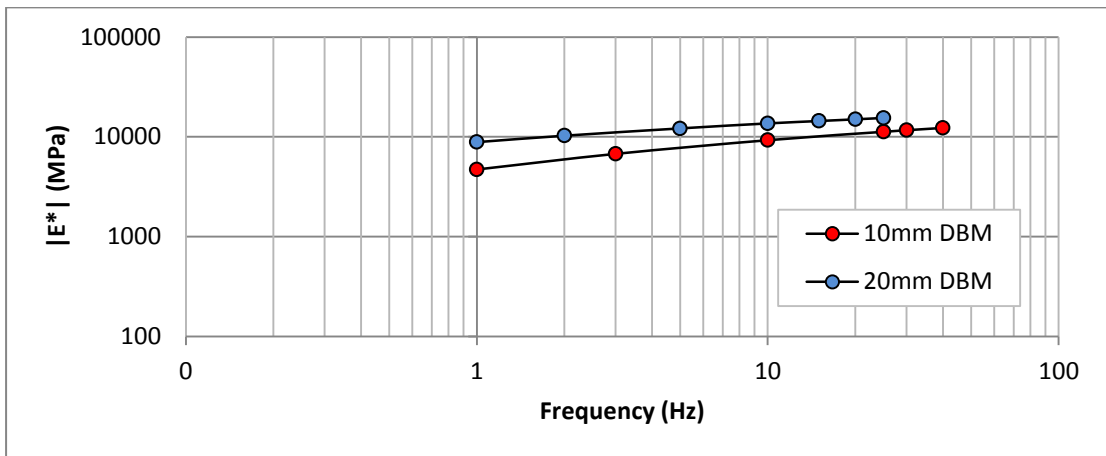
**Figure 73** Fatigue lives obtained by means of RDEC (Shen) and traditional methods in stress control mode

**Comparison between 10mm DBM and 20mm DBM**

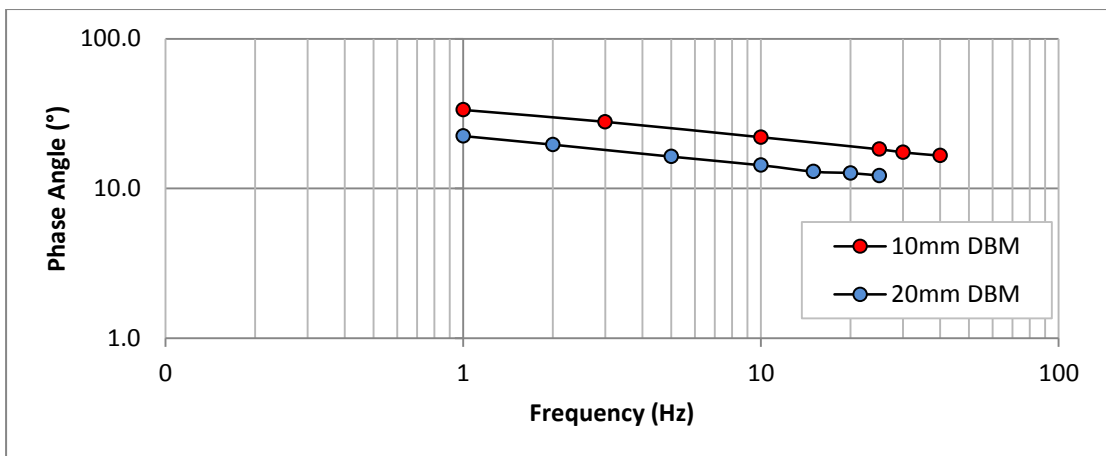
A comparison in terms of stiffness, phase angle and fatigue was made between the two materials.

Figure 74 and Figure 75 show the isotherm curve and the phase angle at 10°C for both materials.

10mm DBM is characterised by lower stiffness values and higher phase angle values; one of the reasons is the lower penetration bitumen for the 10mm DBM (the material tends to be characterised a more viscous behaviour). A comparison in terms of fatigue between the two materials was also done. As can be seen from Figure 76, there is only a small difference between the two regression lines.



**Figure 74** Isotherm curves at 10 °C (10 and 20mm DBM data)



**Figure 75** Phase angle at 10°C (10 and 20mm DBM data)

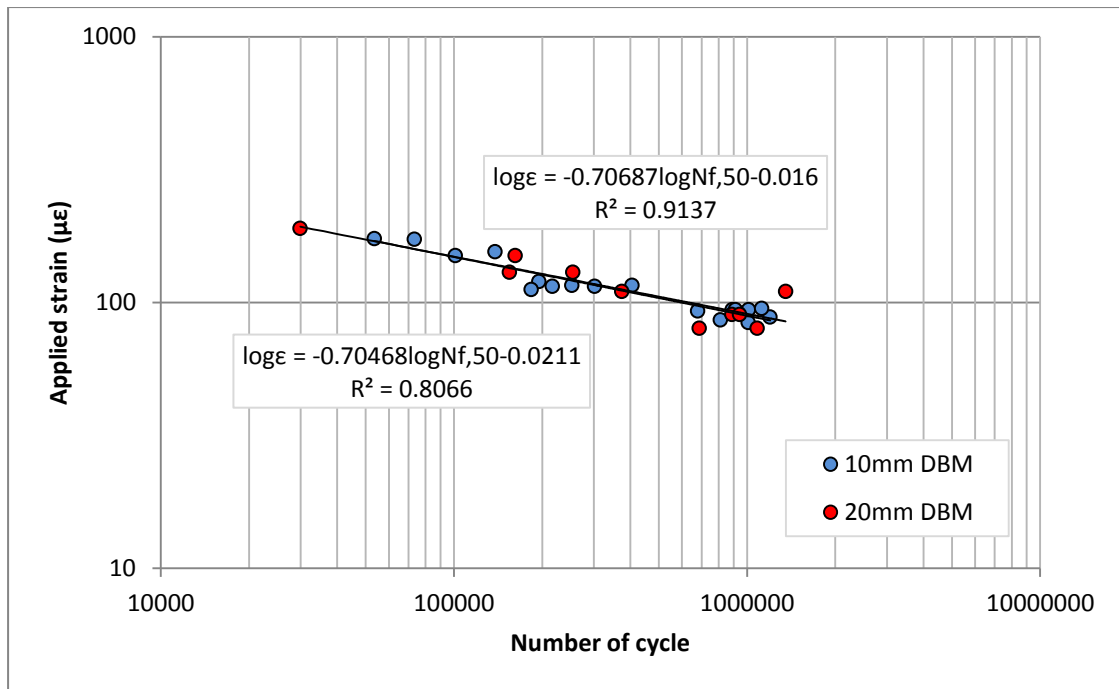


**Figure 76** Fatigue lives for 10 and 20mm DBM

## 5.4 Summary

The 2 Point Bending (2PB) test is described in this chapter. A detailed description of the test, the production of trapezoidal specimens and configuration of the machine is presented. Two materials were tested: 10mm DBM and 20mm DBM.

For the 10mm DBM the following conclusions can be drawn:

- In terms of fatigue, graphically, data are characterised by different regression lines for different frequencies (15 and 25 Hz) and different temperatures (10 and 20 °C). Statistically it was found that regression lines at 15 and 25 Hz are the same at 10 °C and different at 20°C; this is explained by the fact that the chosen material is characterised by a soft binder (100 pen), this underlines the effects of temperature on fatigue life: it increases at higher temperatures. A similar scenario was obtained when frequency increases (at 25Hz).
- A comparison between different dissipated energy methods (Pronk, Rowe and Shen' methods) was made. Statistically, Dunnett's test was used for a multiple comparison considering Nf,50 as the control fatigue line; regression lines obtained from different dissipated energy methods statistically are not different from Nf,50. Regarding the RDEC method, PV-

Nf,50 relationship was found to be unique for data obtained at different frequencies; if different temperatures are compared, it was found that data have different behaviour, therefore the RDEC is not dependent on temperature (only two temperatures and two frequencies were tested so more research would be needed to confirm these results).

For the 20mm DBM the following conclusions can be drawn:

- A comparison between different modes of loading was made. Statistically, regression lines were calculated for each mode of loading and then compared using the *t test* according Nf,50 and RDEC method. In the first case, the regression lines have the same slope and same elevation, thus a unique relationship could be found; in the second case (RDEC), the regression lines are different; thus it was found that this method is not independent of the mode of loading.
- In terms of DE, statistically, Dunnett's test was used for the multiple comparison and results show that DE methods give the same fatigue values in both strain and stress control mode.

A comparison between the two materials was also made. The two materials show a similar behaviour in terms of fatigue although the 10mm DBM is characterised by a softer binder and it shows smaller values of stiffness.

## CHAPTER 6

# 4 Point Bending Test

### 6.1 Introduction

The test consists of applying a continuous sinusoidal waveform at the top of a prismatic specimen by means of two load points (inner clamps). The specimen is restrained at four points by means of four clamps: the two outside remain static (they can only shift horizontally), the two inner clamps deflect according to the strain/stress applied. Free translation and rotations are allowed at all loads and reactions points. See Figure 77.

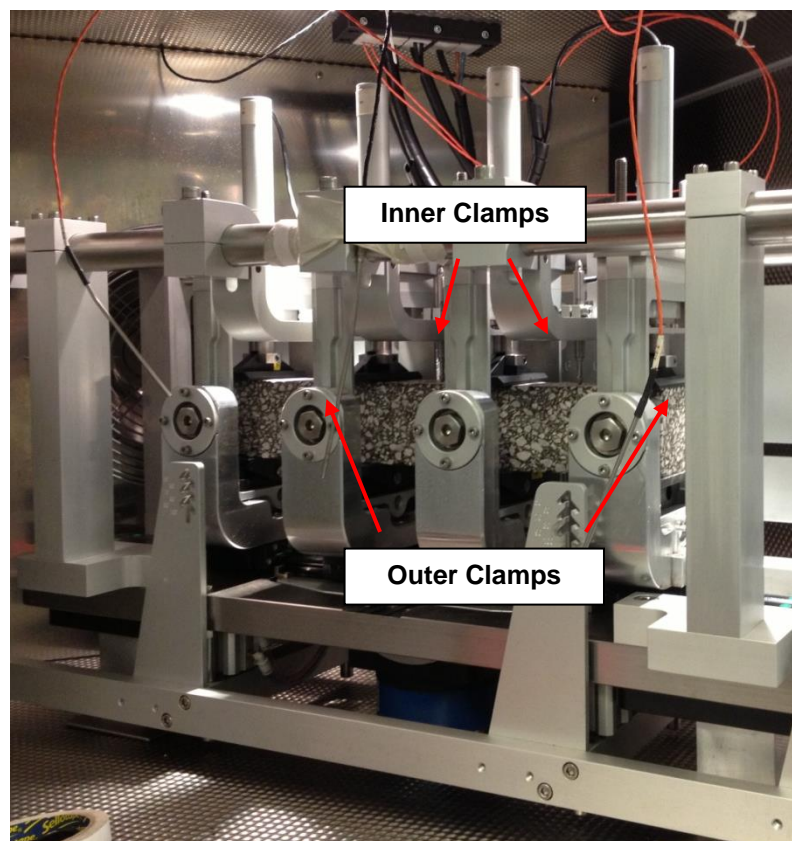


**Figure 77** Clumped specimen

The deformation of the specimen is measured at the bottom between the two inner clamps (BS-EN 12697-24, 2004; BS-EN 12697-26, 2004). Deformation is calculated by means of three LVDTs (Linear Variable Differential Transformers) located in three different points (see Figure 78). Total

deformation is given by Equation 97:

$$D = \left[ LVDT_1 - \left( \frac{LVDT_2 + LVDT_3}{2} \right) \right] \times 2 \quad \text{Equation 97}$$

$$D = \left[ D_1 + \Delta\varepsilon - \left( \frac{D_2 + \Delta\varepsilon + D_3 + \Delta\varepsilon}{2} \right) \right] \times 2 \quad \text{Equation 98}$$

$$D_2 = D_3 = \frac{1}{2} D_1 \quad \text{Equation 99}$$

$$D = \left[ D_1 + \Delta\varepsilon - \left( \frac{\frac{D_1}{2} + \Delta\varepsilon + \frac{D_1}{2} + \Delta\varepsilon}{2} \right) \right] \times 2 = \left( D_1 + \Delta\varepsilon - \frac{D_1}{2} - \Delta\varepsilon \right) \times 2 = D_1 \quad \text{Equation 100}$$

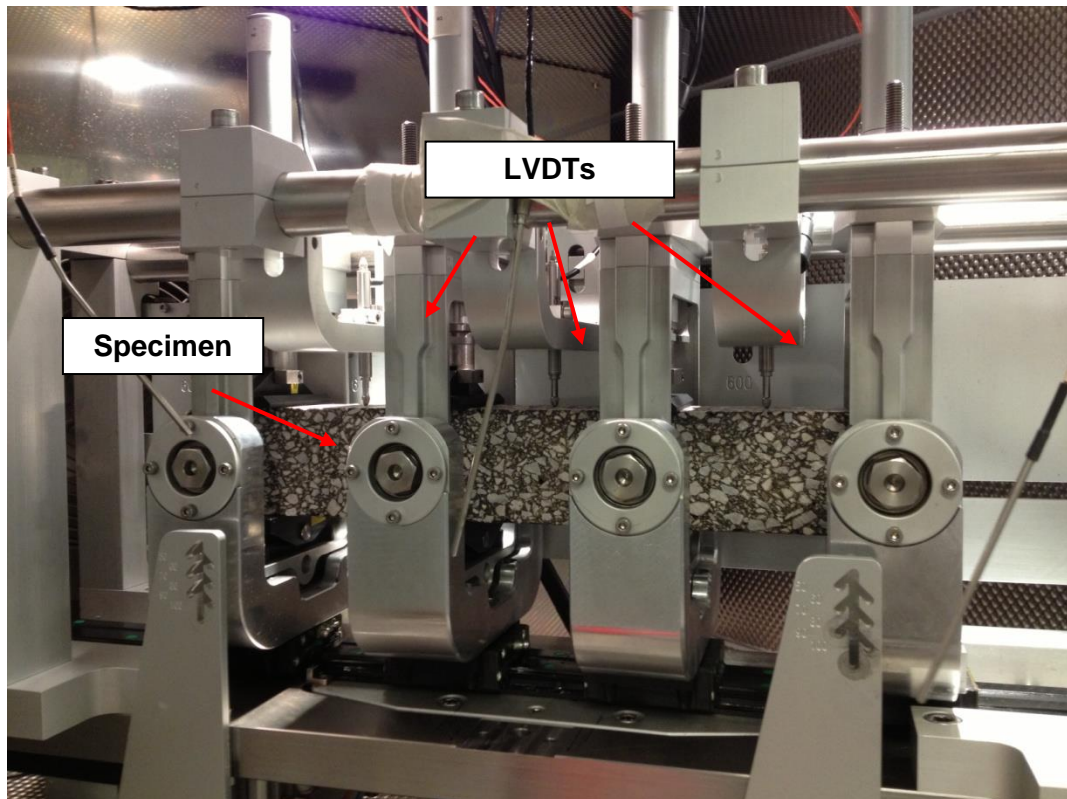


**Figure 78** 4 PB equipment at the University of Nottingham

This test simulates very well a pavement fatigue failure under traffic loading because repeated loading causes tension in the bottom zone of the specimen, cracking will initiate and then propagate to the top zone until failure; fracture usually occurs in the area of constant maximum value of bending moment between the two inner clamps (See Figure 79).

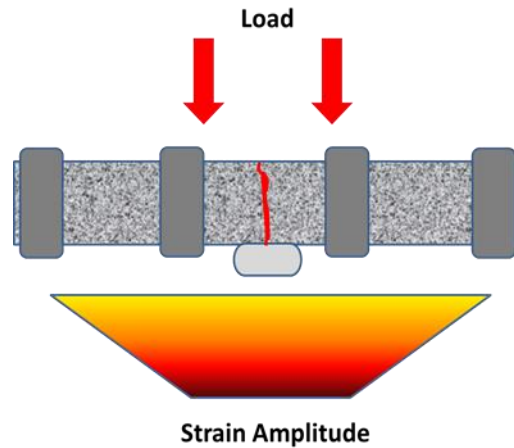


**Figure 79** Load and strain amplitude for the 4PB

In this type of test free lateral translation are permitted to prevent internal stresses developing in the specimen.

In the 4 point bending test, initial stiffness is usually chosen between the 50<sup>th</sup> and the 100<sup>th</sup> load application. Conventionally, fatigue failure is the moment when the stiffness has decreased to half of its initial value (SHRP-A-404, 1994; Di Benedetto et al. 1997; Shen, 2007).

## 6.2 Prismatic specimens

Prismatic test specimens are manufactured from the large slabs.

The procedure consists of sawing the specimens along horizontal planes in the direction of compaction. Using this procedure it is possible to produce 10 specimens per slab (see Figure 80).

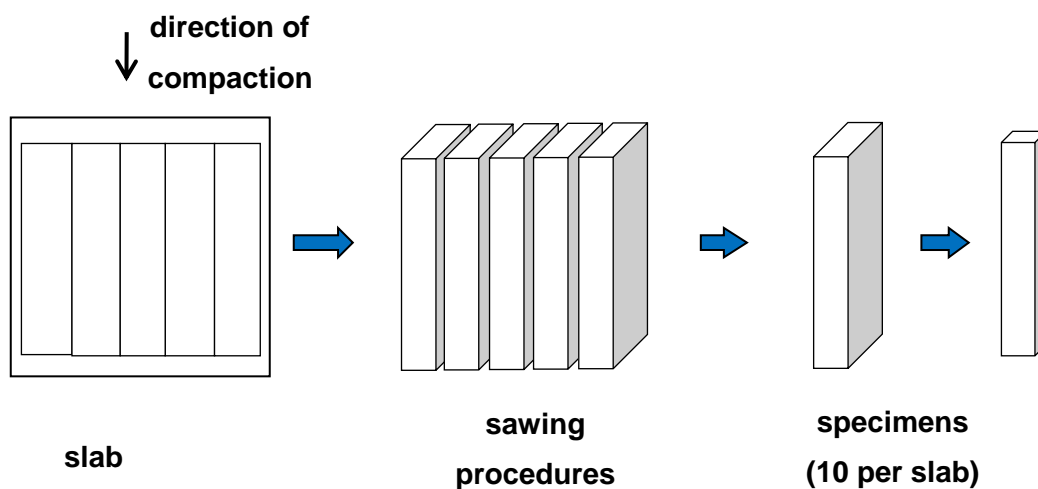


**Figure 80** 4PB Coring and trimming procedure

Regarding the dimensions of the prismatic specimen, both the AASHTO T 321 and ASTM D7460-10 require the beams to be  $380 \pm 6$  mm in length,  $50 \pm 2$  mm in height, and  $63 \pm 2$  mm in width. The length of 380 mm traditionally depends on the chosen span (distance between the clamps) that it is typically 118.5 mm ( $118.5 \times 3 = 355.5$  mm plus the width of the outer clamps; that's why it is 380 mm for most machines).

The BS EN 12697-24:2012 is more general. The standard suggests that the width (B) and height (H) of the specimen should be at least three times larger than the maximum aggregate size (D) of the mixture and, in order to ensure the slenderness of the beam, the effective length between the outer clamps (L) should be at least six times the maximum value for B and/or H.

After determining the maximum aggregate size, what really matters are both the height and the effective distance between the outer clamps' edges.

Depending on the height of the beams, different clamp sets are available. The 4PB at the University of Nottingham was designed to ensure that beams with different heights (within a certain range) can be tested with the same machine. In a bending test the specimen is clamped; the clamps allow both free horizontal translations and free rotations. Ideally the centre of the rotation must be the same as (or very close to) the centre of the beam (for example 25 mm from the bottom for a 50 mm high beam). So having the same machine, we use thicker (taller) clamp supports for smaller (thinner, less tall) beams and, conversely, smaller (less tall) clamp supports for higher beams. That's because the centre of rotation of the clamps is fixed in a certain position, so in a way by using different clamp supports for different beam's sizes the centre of rotation of the clamps (fixed) is practically aligned with the centre of the beam (see Figure 81).

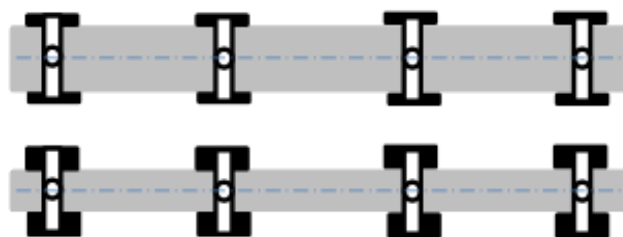


**Figure 81** Different beam heights for the 4PB

The dimensions chosen for a 10 mm size DBM, are reported in Figure 82 and Table 12.

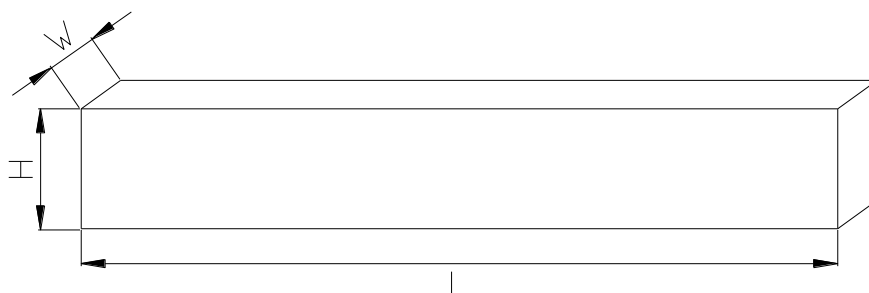


**Figure 82** Geometry of prismatic specimens: BS EN 12697-24: 2004.

**Table 12** Dimensions of the specimens: BS EN 12697-24: 2004.

Dimensions of the Specimens	Type of Mixture
	<i>10 mm DBM</i>
<i>L</i>	380
<i>W</i>	50
<i>H</i>	60

### 6.3 Calibration of the testing machine

4 PB testing machine was bought in September 2012. Before starting any tests, the new machine was checked and calibrated by means of an aluminium specimen where geometrical and mechanical properties were known. Table 13 shows the geometrical characteristics of the aluminium beam. Figure 83 and Figure 84 show the section and the longitudinal profile of the aluminium beam used for the calibration of testing machines.

**Table 13** Dimensions of aluminium specimens

Specimen Reference	Total length (mm)	Width (mm)	Height (mm)	Mass (g)	Stiffness Modulus (GPa)
<i>Dogbone</i>	470	10.23	49.92	1318.1	73573

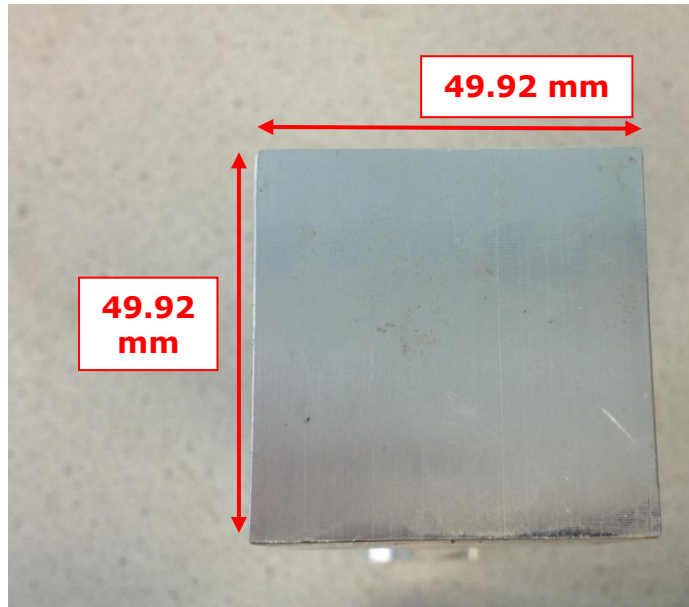


**Figure 83** Section of aluminium beam

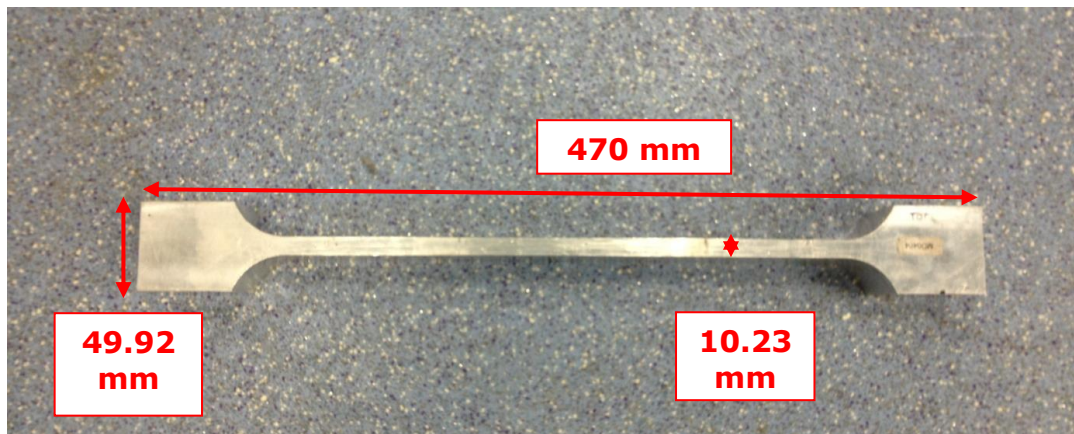


**Figure 84** Longitudinal profile of aluminium beams

Depending on the size of the specimen, three different clamping longitudinal position configurations could be used for testing as shown in Figure 85.

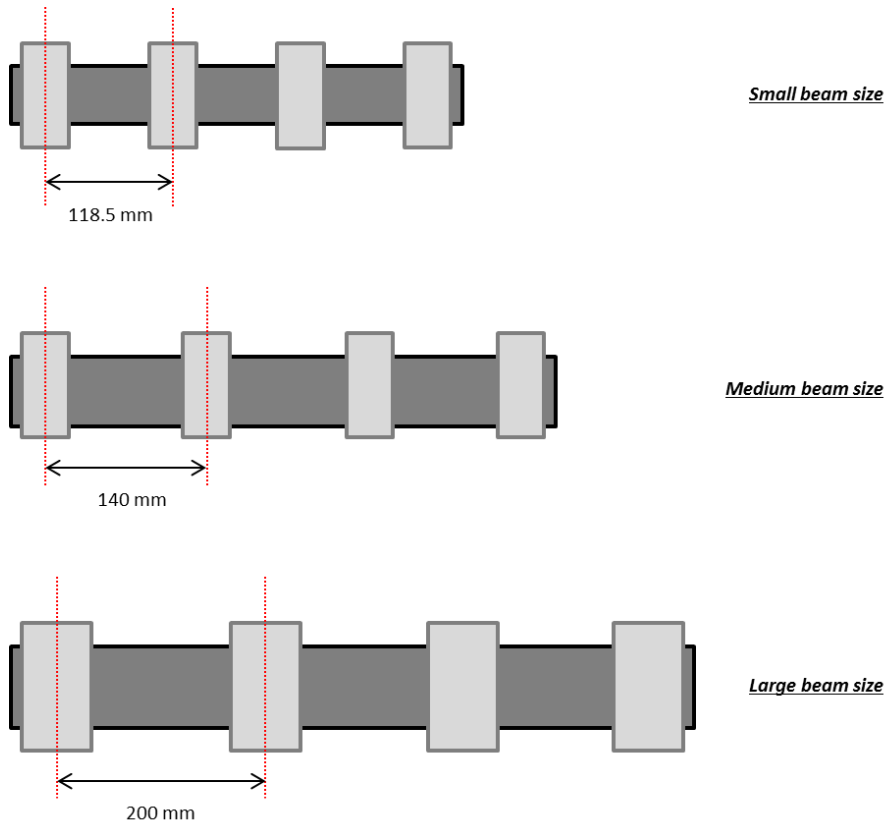


**Figure 85** Small, medium and large beam size configurations

The dogbone aluminium beam was tested in strain control at two different strain levels (50 and 100  $\mu\epsilon$ ) at 20°C at 12 different frequencies (from 1 to 60 Hz). Figure 86 and Figure 87 show the stiffness and phase angle evolution when frequency increases for the aluminium beam; stiffness and phase angle values become more unstable for frequency higher than 30-40 Hz.

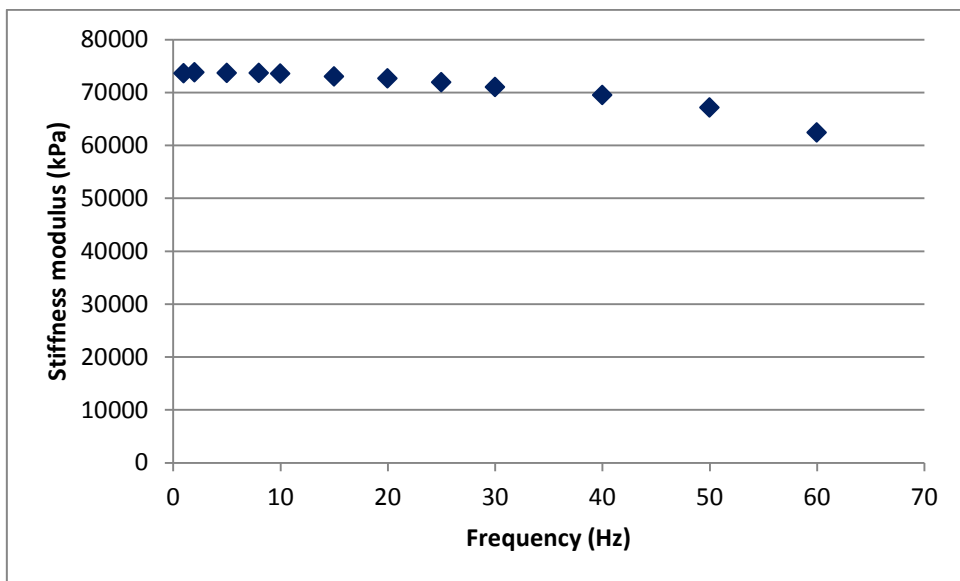


**Figure 86** Stiffness versus frequency. Aluminium beam

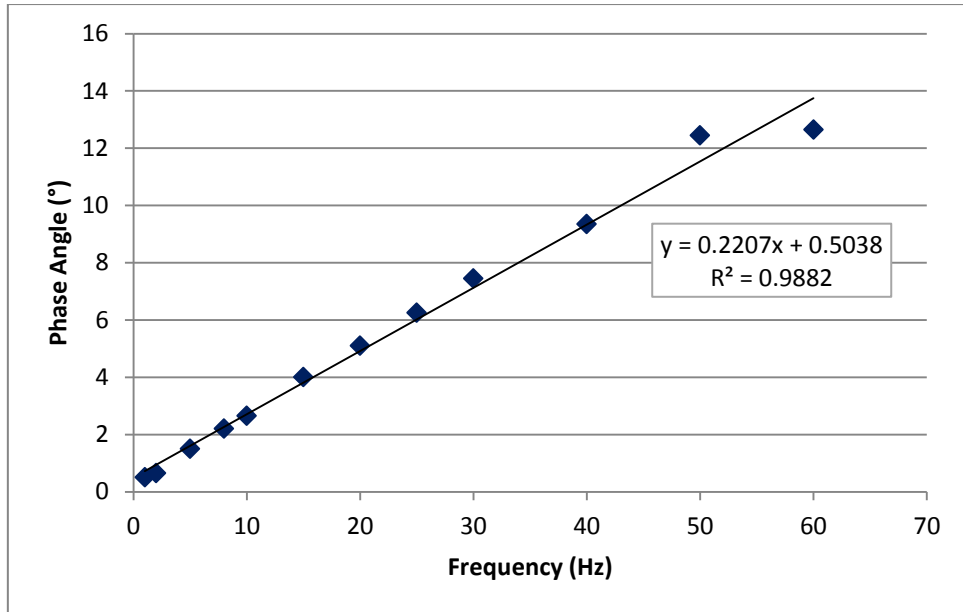


**Figure 87** Phase angle versus frequency. Aluminium beam

After testing the aluminium beam, correction factors were determined (see Table 14) and inserted into the software as shown in Appendix A.

After determining the phase correction values and inserting them into the software, a validation on asphalt beams was made at different frequencies (from 1 to 30 Hz). Figure 88, Figure 89, Figure 90 and Figure 91 show the improvement obtained after the calibration in stiffness and phase angle results obtained for the aluminium beam. Figure 92 and Figure 93 show the behaviour of asphalt material before and after the determination of phase angle compensation.

**Table 14** Phase compensation

Phase Angle (°) - Compensation Factors			
Frequency (Hz)	First Test	Second Test	Average Value
1	0.4	0.6	0.5
2	0.5	0.7	0.6
5	1.6	1.4	1.5
8	2.0	2.2	2.1
10	2.9	2.7	2.8
15	4.1	4.0	4.0
20	5.1	5.1	5.1
25	6.4	6.1	6.3
30	7.2	7.2	7.2
40	9.7	9.4	9.5
50	12.0	12.2	12.1
60	12.9	12.7	12.8

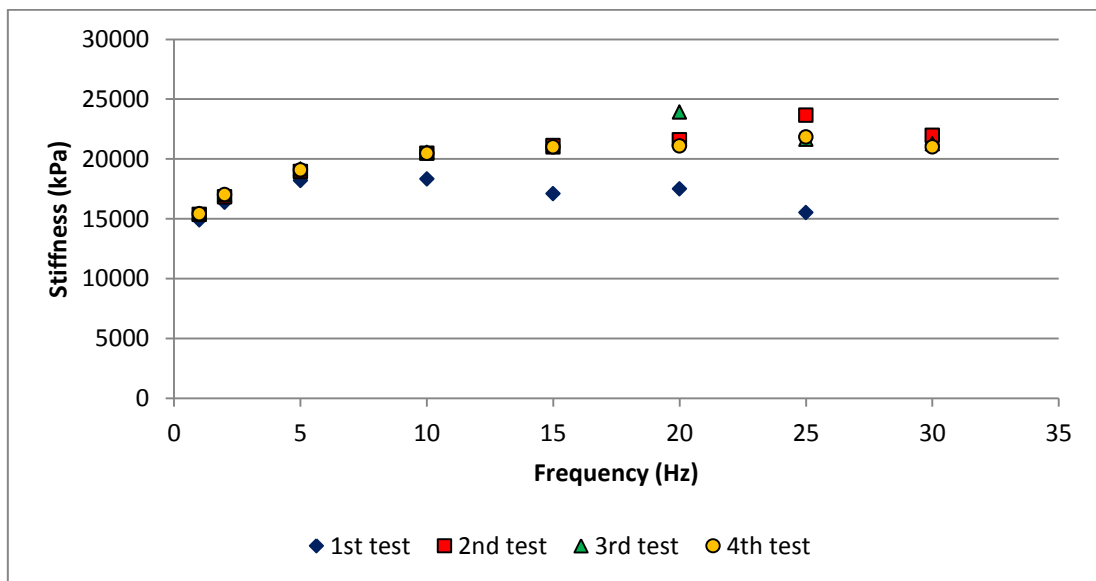


**Figure 88** Stiffness versus frequency before calibration (20mm DBM)

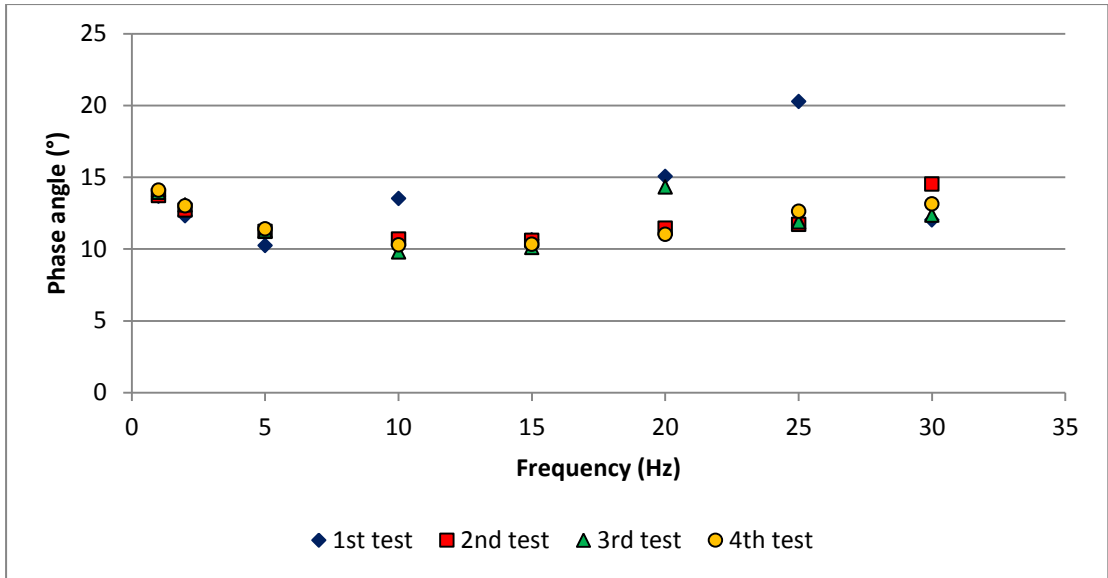


**Figure 89** Phase angle versus frequency before calibration (20mm DBM)

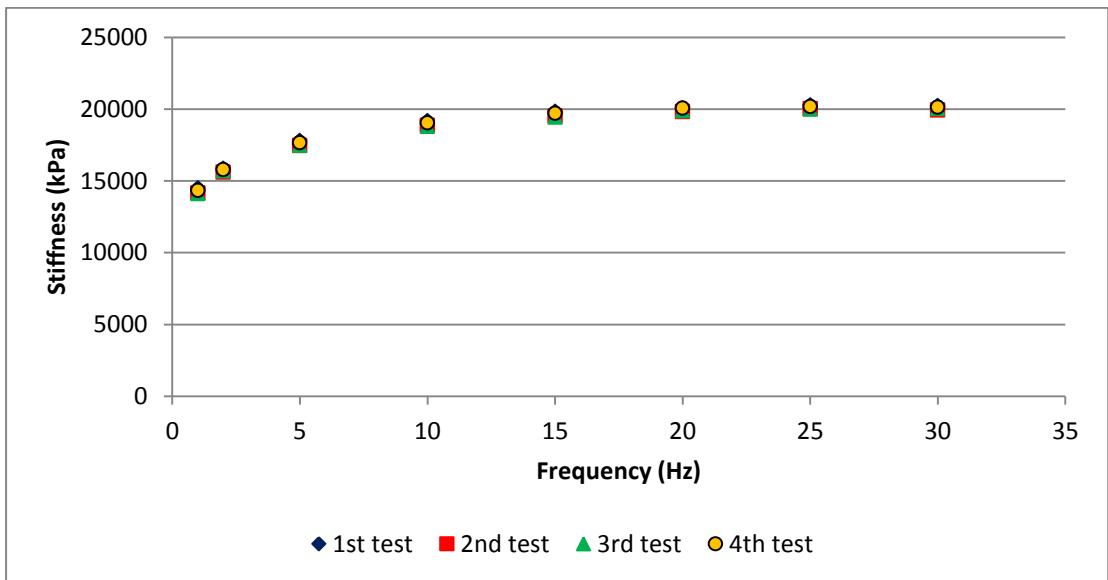


**Figure 90** Stiffness versus frequency after calibration (20mm DBM)

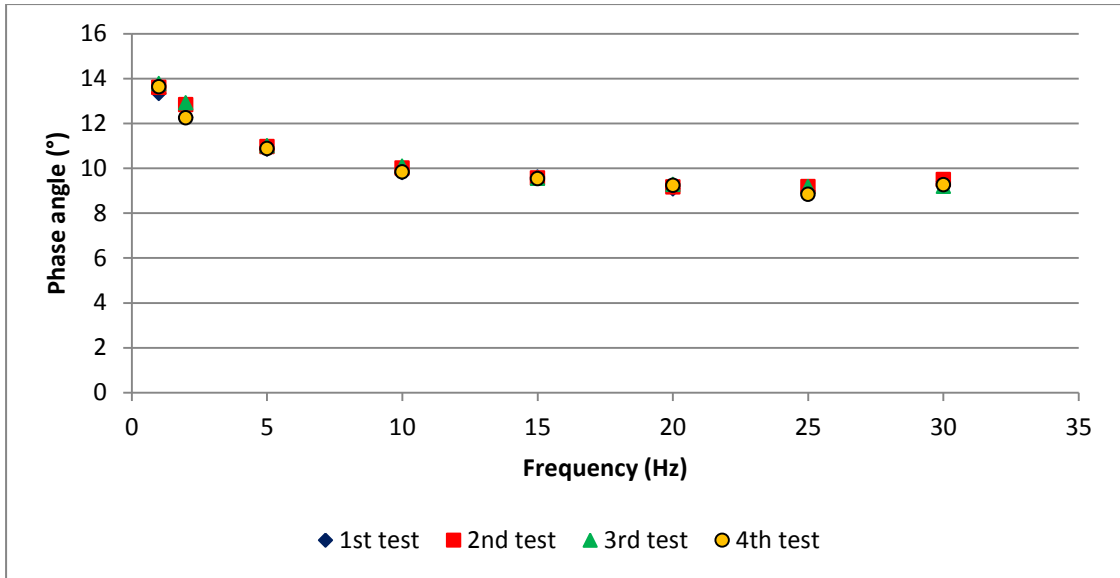


**Figure 91** Phase angle versus frequency after calibration (20mm DBM)

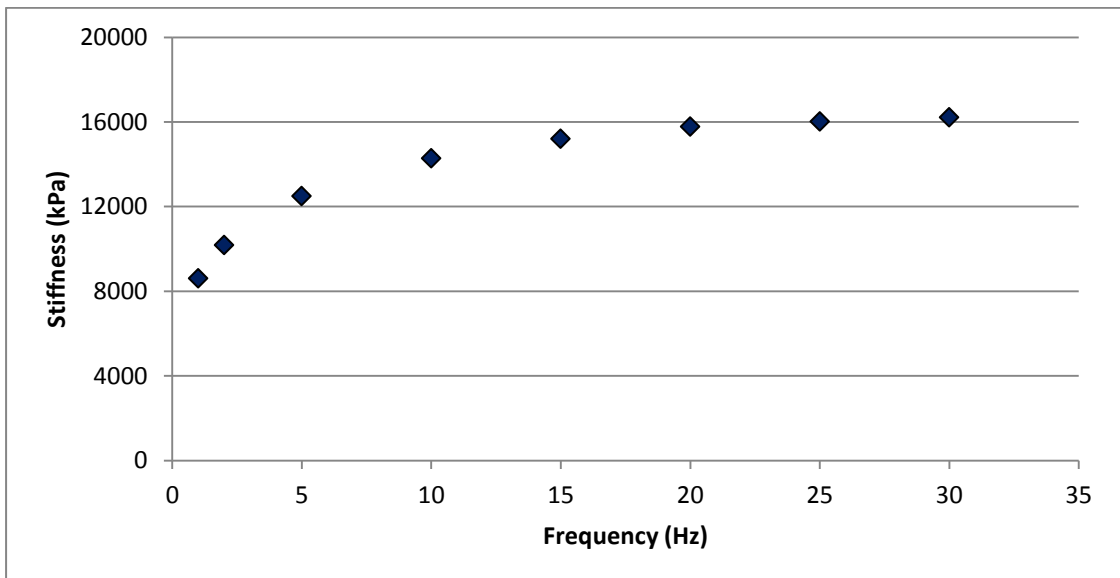


**Figure 92** Stiffness versus frequency after calibration (10mm DBM)

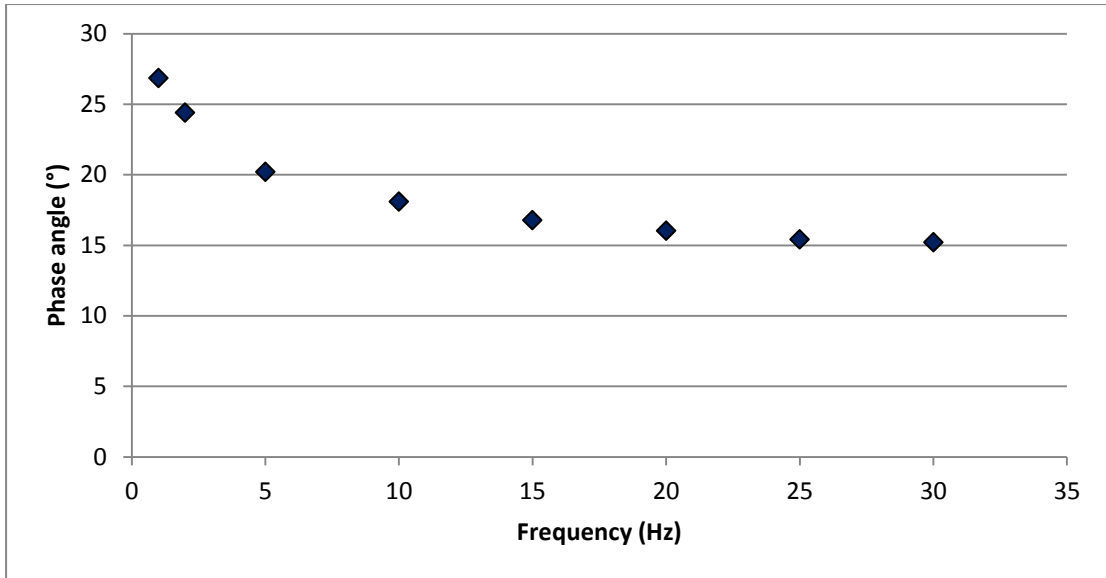


**Figure 93** Phase angle versus frequency after calibration (10mm DBM)

## 6.4 Test results

### 6.4.1 10mm DBM

#### Stiffness modulus

According to the standards BS EN 12697:26:2004, the form ( $\gamma$ ) and the mass factor ( $\mu$ ) for a prismatic specimen are expressed as:

$$\gamma = \frac{L^2 A}{bh^3} \left( \frac{3}{4} - \frac{A^2}{L^2} \right) \quad \text{Equation 101}$$

$$\mu = R(X) \left( \frac{M}{4} + \frac{m}{12(A)} \right) \quad \text{Equation 102}$$

Where:

$$R(X) = \frac{12L}{A} \times \left[ \frac{1}{3X/L - 2X^2/L^2 - A^2/L^2} \right] \quad \text{Equation 103}$$

$$\bullet \quad A = \frac{L-l}{2} \quad \text{Equation 104}$$

- $X$  is the coordinate at which the deflection is measured;
- $L$  is the span length between outer supports in the bending tests;
- $h$  is the mean thickness of the specimen;
- $M$  is the mass of the specimen;

- $m$  is mass of the movable parts;
- $b$  is the length of the prismatic specimen.

Stiffness and phase angle values are obtained at 10°C and 25 Hz; it was not possible to obtain isothermal curves or master curves due to lack of time (the machine was reliable only after calibrating it at the end of the project).

If the stiffness values obtained by means of the 4PB are compared with the values obtained by means of the 2PB, it can be noticed the difference between the two machines is bigger at lower frequency; stiffness obtained with the 4PB is higher than that one with 2PB (see Figure 94).

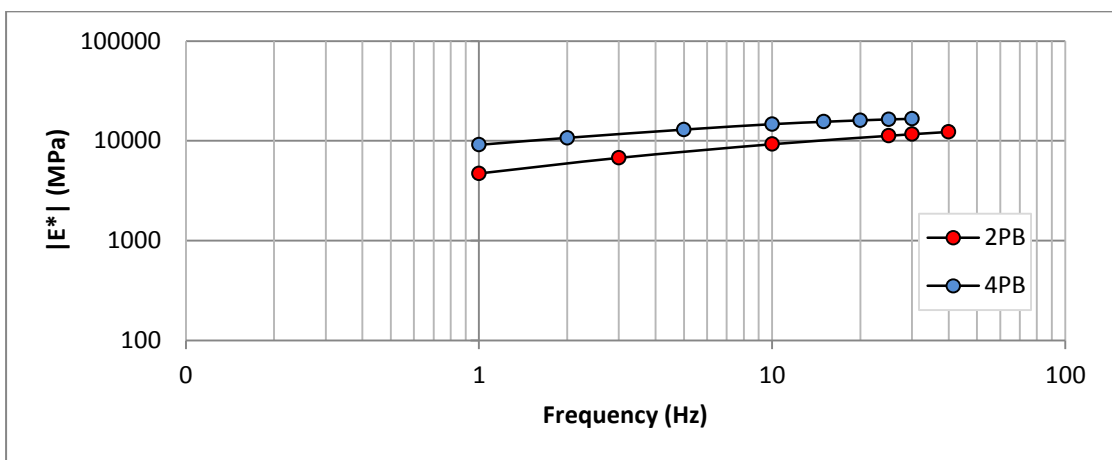


**Figure 94** Isotherm curve at 10°C (2PB and 4PB data)

If the phase angle values obtained by means of the 4PB are compared with the values obtained by means of the 2PB, it can be noticed the difference between the two machines is bigger at lower frequency; phase angle values obtained with the 4PB are lower than that one with 2PB (see Figure 95).

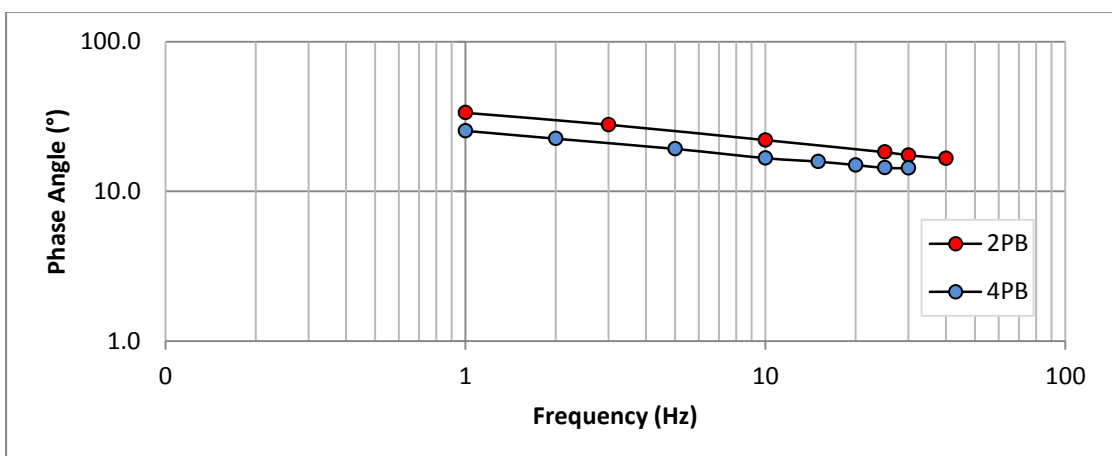


**Figure 95** Phase angle at 10°C (2PB and 4PB data)

Considering the 2PB results, phase angle values increase more than 4PB values at higher temperature; also stiffness values are slightly different. As said previously, higher values of phase angle indicate a tendency towards more viscous behaviour, whilst lower values indicate more elastic response, thus it seems that 2PB stiffness tests at high temperature underline more the viscous behaviour of the materials compared with the 4PB stiffness tests.

### **Fatigue**

Fatigue tests were carried out at 10 °C and 25 Hz in strain control mode for the 10mm DBM; strain levels applied vary from 100 to 220  $\mu\epsilon$ . Healing was also involved considering different loading and resting time periods; the fatigue test at 160  $\mu\epsilon$  was taken as a reference test to compare healing effects. Results obtained according the phenomenological approach (Nf,50) are shown in Figure 96.

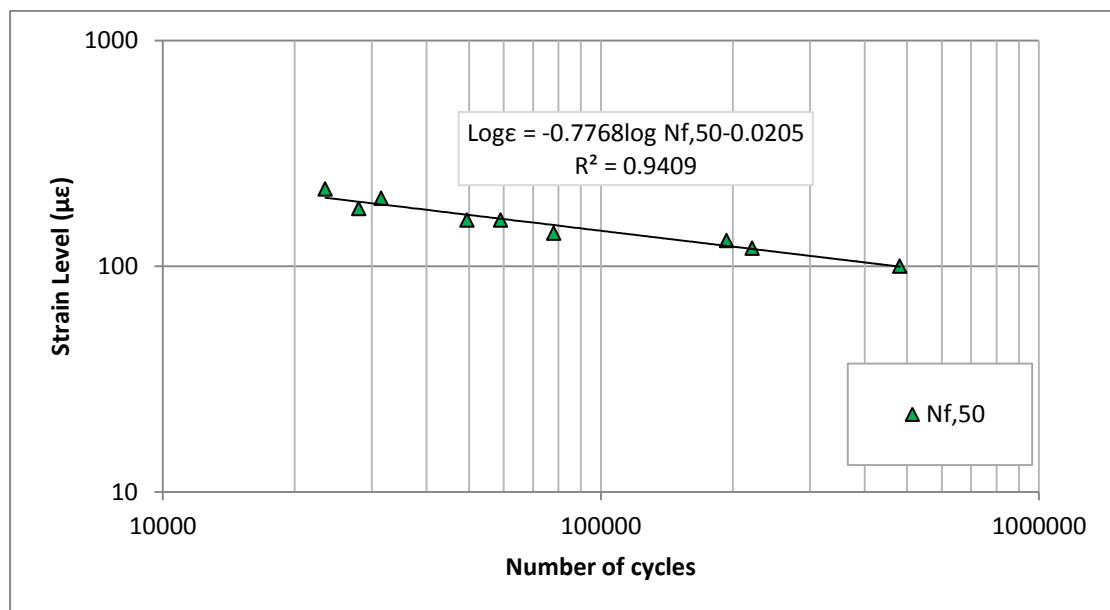
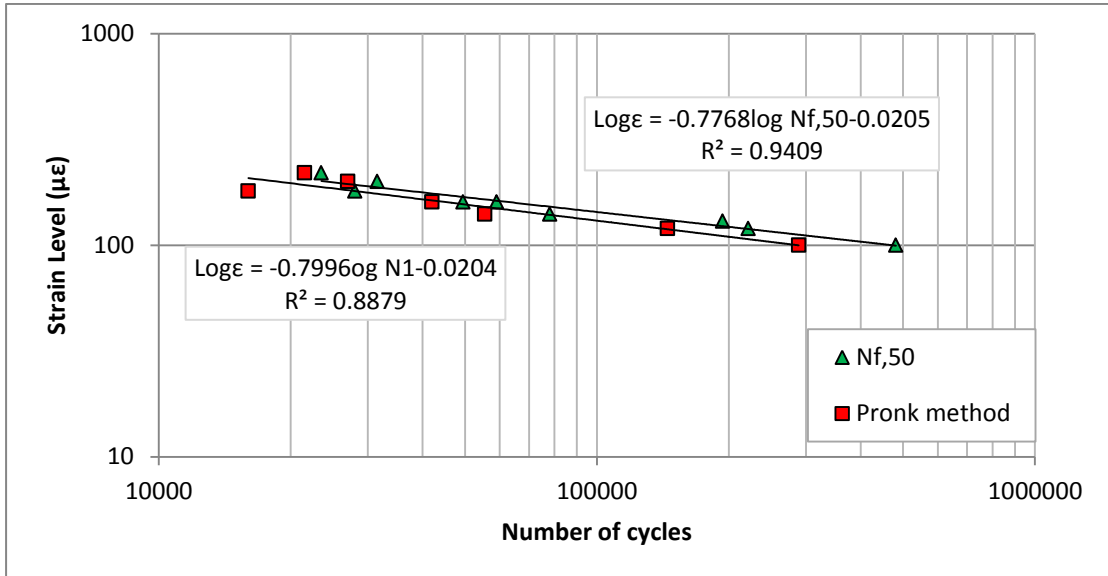


**Figure 96** Fatigue life at 10°C and 25 Hz in strain control mode (10 mm DBM)

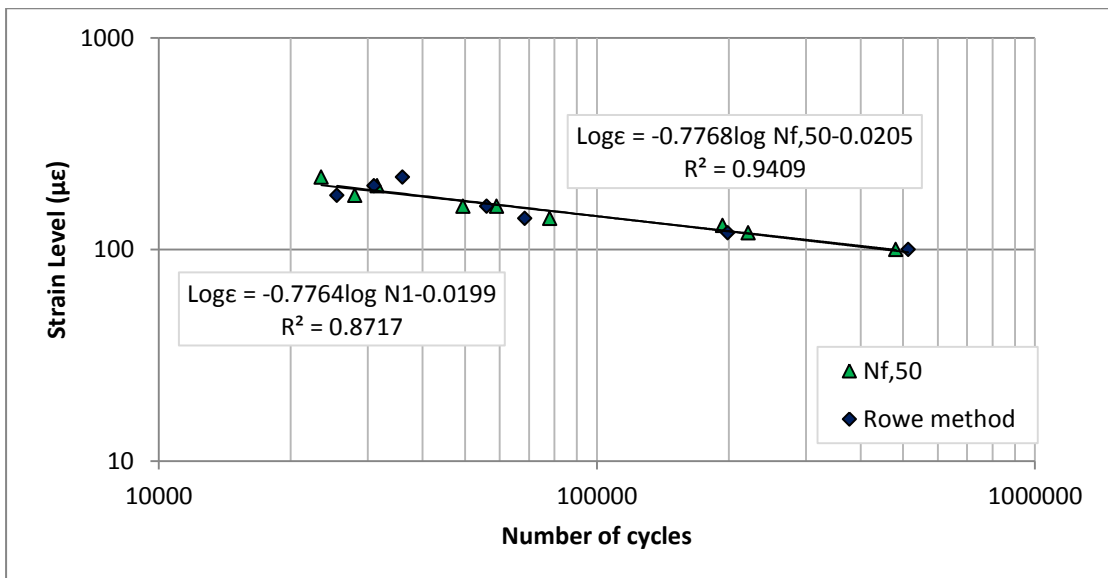
Different dissipated energy methods were considered and comparisons with the traditional approach were made; in particular the criteria chosen were: traditional method (Nf,50), Dissipated Energy Ratio (N1 Pronk), Energy Ratio (N1 Rowe) and RDEC method (PV).

Figure 97, Figure 98 and Figure 99 show the fatigue lives obtained from the different dissipated energy methods at 10°C and 25 Hz. The Energy Ratio method by Pronk generates fatigue life values smaller than the traditional

method. The same method reviewed by Rowe generates fatigue lives very similar to Nf,50 values; the two trend lines coincide. The last method considered was Shen's method (Nfm); graphically, Nf,50 values are smaller than Nfm.



**Figure 97** Fatigue lives obtained by means of Dissipated Energy Ratio (Pronk) and traditional methods



**Figure 98** Fatigue lives obtained by means of Energy Ratio (Rowe) and traditional methods

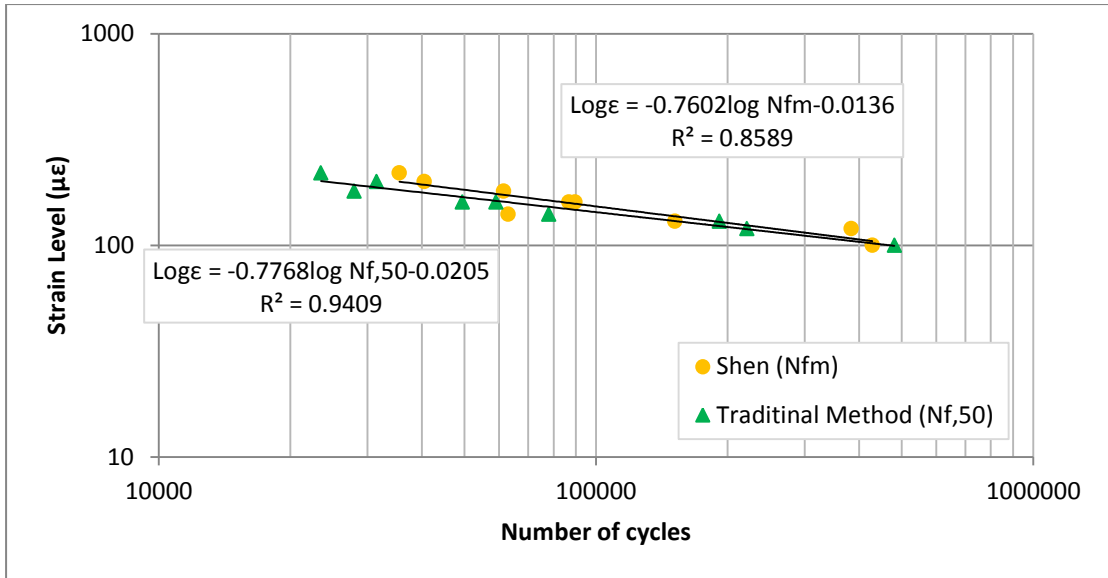


**Figure 99** Fatigue lives obtained by means of RDEC (Shen) and traditional methods. Regression lines were calculated for each case and then compared by using the appropriate statistical method. Statistically, first the hypothesis of equality between elevations of different regressions was tested with the analysis of covariance (ANCOVA); the hypothesis is  $H_0: \beta_1 = \beta_2 = \dots = \beta_k$  was not rejected for both significance level of 0.05. Therefore, Dunnett's test was necessary to compare the regressions; results show that the regression lines obtained by the different DE methods are not different from the traditional method (Nf,50).

**Table 15** DE method comparison by using Fisher test

Case	Slope	Elevation	Results
Nf,50 - DER - ER - Nfm	$F=0.85 < F_{0.05(1),3,28}=2.95$	$F=10.3 > F_{0.05(1),3,28}=2.95$	Regressions are not the same for a significance level $\alpha=0.05$
Nf,50 - ER	$q'=0.91 < q'_{0.05(1),28,3}=2.0$	$q'=0.9 < q'_{0.05(1),28,3}=2.0$	Regressions are the same for a significance level $\alpha=0.05$
Nf,50 - DER	$q'=0.02 < q'_{0.05(1),28,3}=2.0$	$q'=0.01 < q'_{0.05(1),28,3}=2.0$	Regressions are the same for a significance level $\alpha=0.05$
Nf,50 - Nfm	$q'=0.7 < q'_{0.05(1),28,3}=2.5$	$q'=0.81 < q'_{0.05(1),28,3}=2.0$	Regressions are the same for a significance level $\alpha=0.05$

The third method used for this set of data was RDEC; PV was calculated and the relationship between PV and Nf,50 was experimentally calculated. 4PB fatigue data were compared with 2PB fatigue data at 10°C and 25 Hz. Regression lines were compared using the *t test*. As shown in Table 16, and seen in Figure 100, the two regression lines are not the same. In this case it is

not possible to consider a unique regression line for both sets of data; fatigue data are not independent of the test used.

**Table 16** RDEC: 2PB-4PB comparison at 10°C and 25 Hz

Cases	Slope	Elevation	Result
2PB – 4PB	$t=2.27 > t_{0.05(2),19}=2.093$		Regressions are different

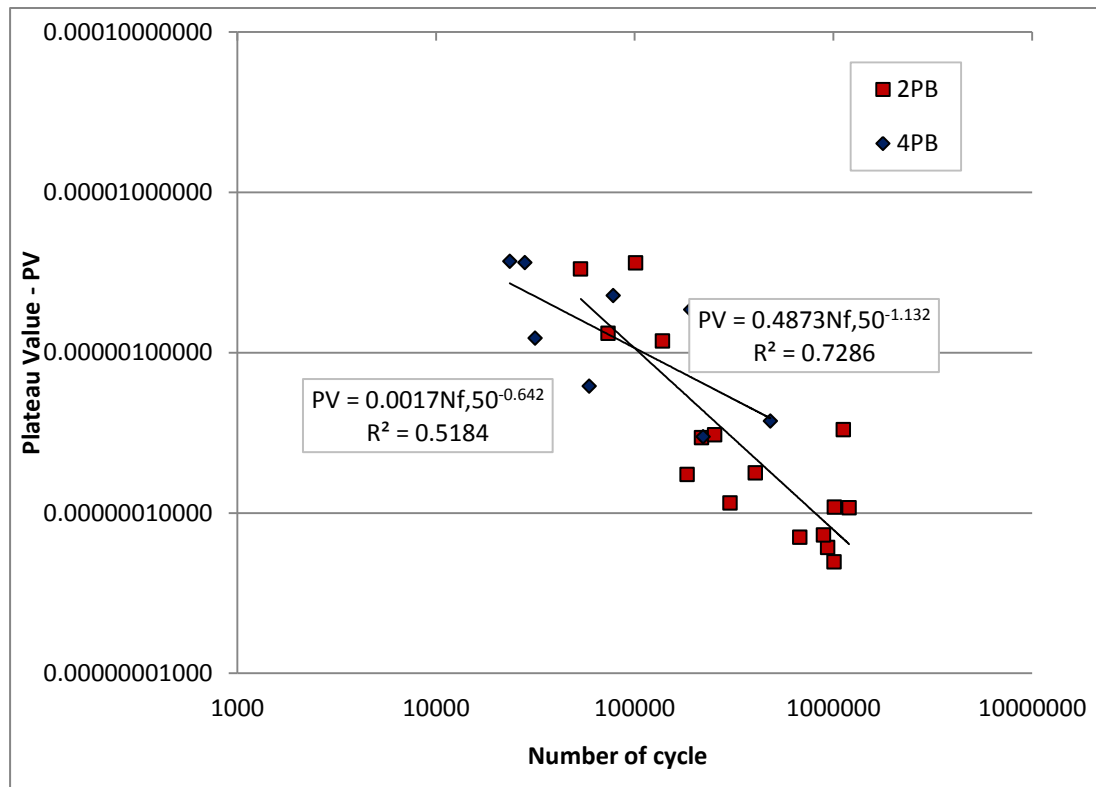


**Figure 100** PV- Nf, 50 relationship obtained by 4PB and 2PB

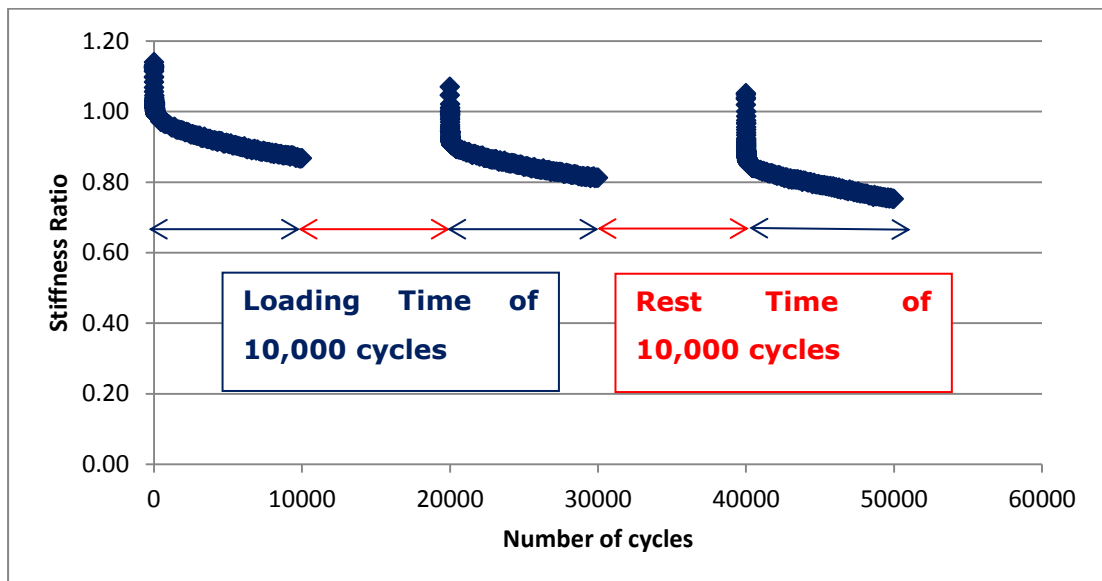
## Healing

Healing was involved in this study. Healing tests were undertaken at 10°C, 25 Hz; the applied strain was  $160\mu\epsilon$  for each test and five different rest times and four different loading times were considered. Table 17 shows the eight combinations of loading time and rest time chosen for the healing tests.

**Table 17** Loading times and rest times (in number of cycles)

Number of cycles	
Loading time	Rest time
1,000	10,000
10,000	10,000
	30,000
	50,000
	75,000
	100,000
20,000	10,000
30,000	10,000

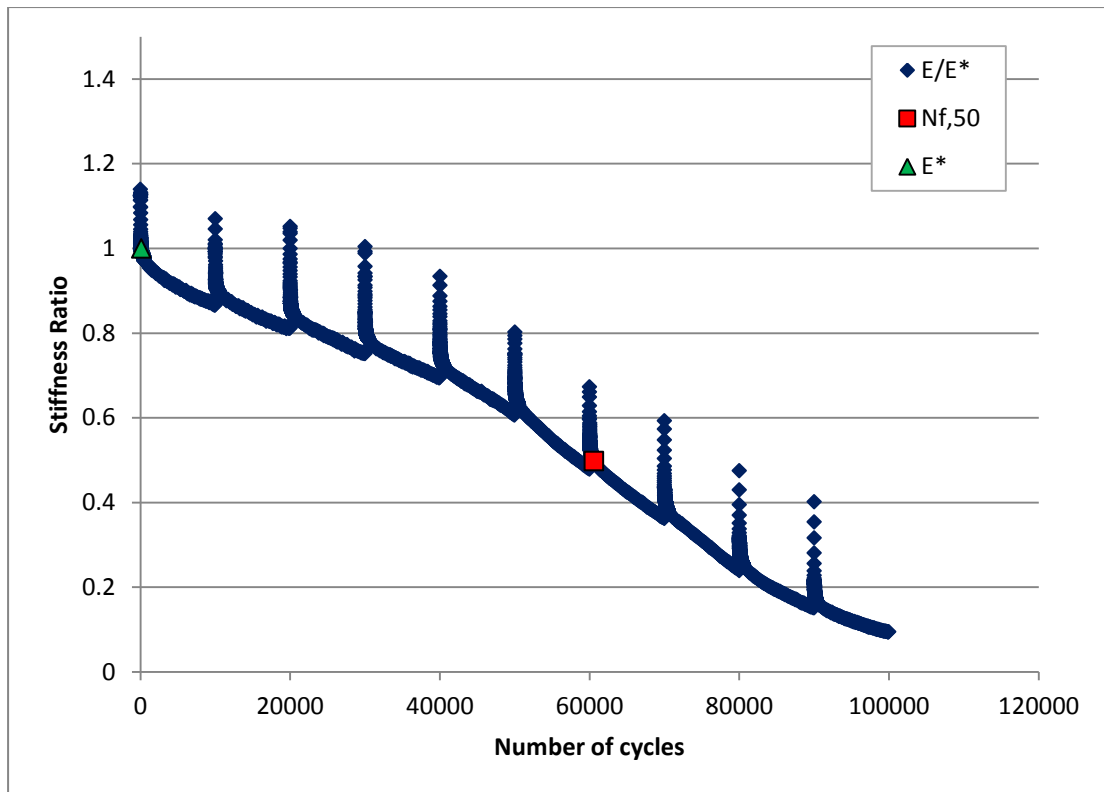
A fatigue test usually is divided in several stages of loading times and rest times. During the loading time,  $160 \mu\epsilon$  is applied on the specimen; during the rest time, the specimen is unloaded ( $0 \mu\epsilon$ ) as shown in Figure 101.



**Figure 101** Healing test: 10,000 cycles for each loading time stage and 10,000 cycles for each rest time stage

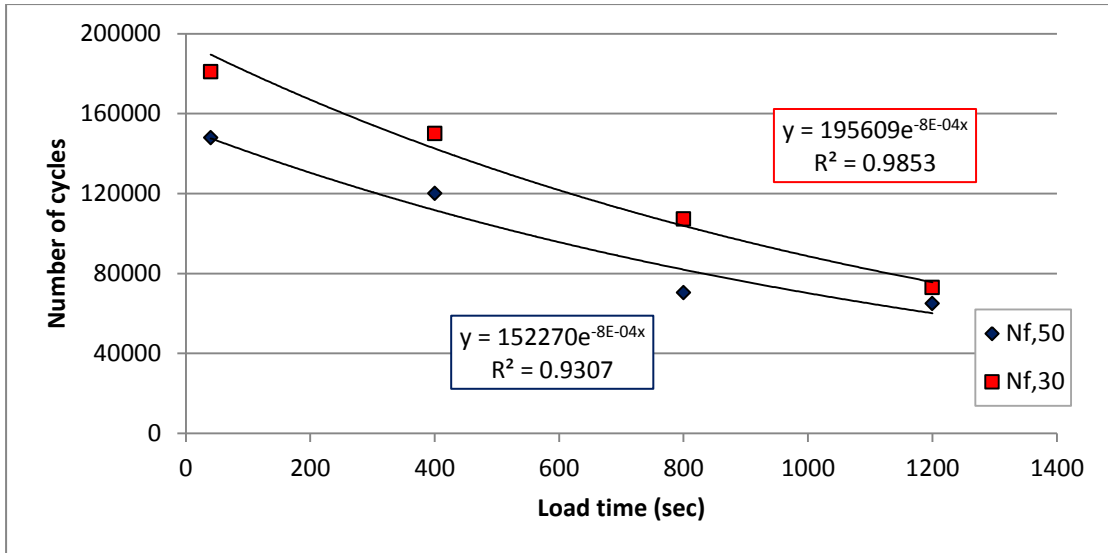
At the end of the test, all data of each stage is registered and analysed.

Figure 102 shows the behaviour of asphalt material during a fatigue test when healing is included in the test. In this particular case, the fatigue test was undertaken at  $160 \mu\epsilon$  at  $10^\circ\text{C}$  and 25 Hz; the specimen was loaded for 10,000 cycle (400 seconds) and it was left to rest for other 10,000 cycles (400 seconds).

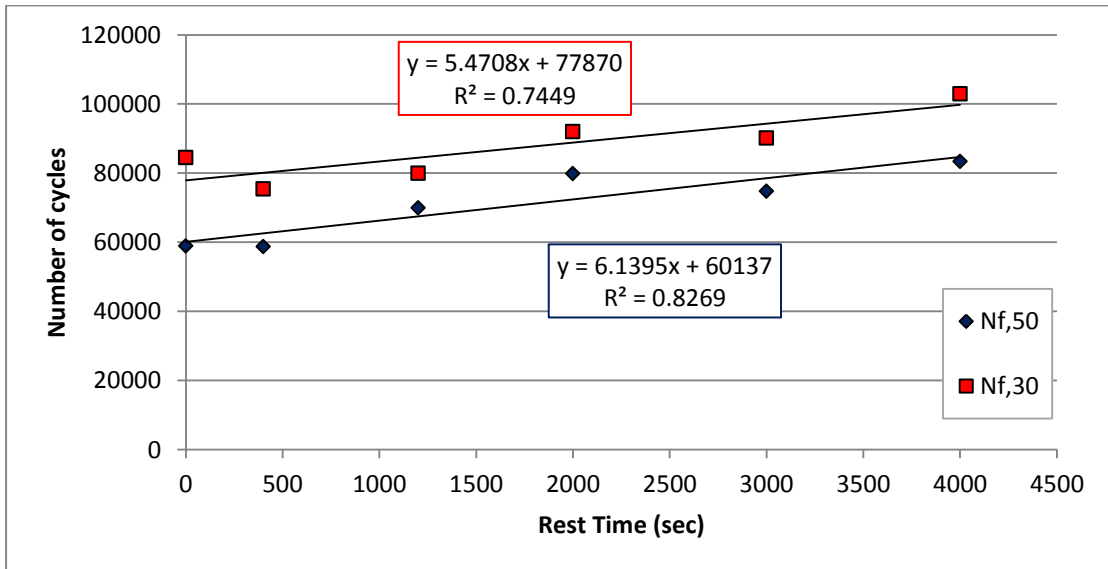


**Figure 102** Example of healing test (10,000 cycles of loading time and 10,000 cycles of rest time)

Figure 103 shows the number of cycle of failure ( $N_f,50$  and  $N_f,30$ ) for different loading times when rest time is constant (10,000 cycles that corresponds to 400 seconds). Figure 104 shows the number of cycles to failure ( $N_f,50$  and  $N_f,30$ ) for different rest time periods when loading time is constant (10,000 cycles that corresponds to 400 seconds). Fatigue life decreases when loading time period decreases; it increases when rest time period increases. The behaviour of asphalt material in tests with longer loading time periods is closer to a fatigue test without rest periods; that is because the first rest time period may happen after fatigue phenomena have started in the specimen already. The behaviour of asphalt material in tests with shorter rest time periods is closer to a fatigue test without rest periods because the material does not have enough time to heal (to recover the stiffness).



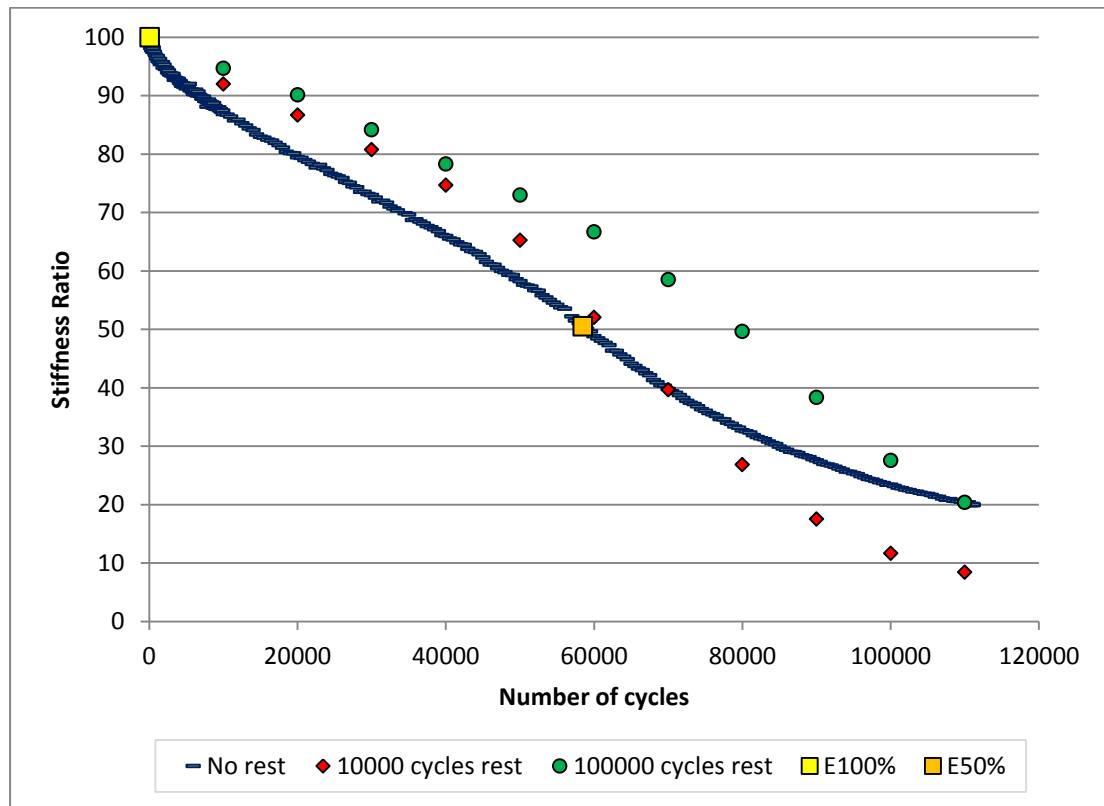
**Figure 103** Number of cycles (Nf,50 and Nf,30) for different loading times (constant rest time)



**Figure 104** Number of cycles (Nf,50 and Nf,30) for different resting times (constant loading time)

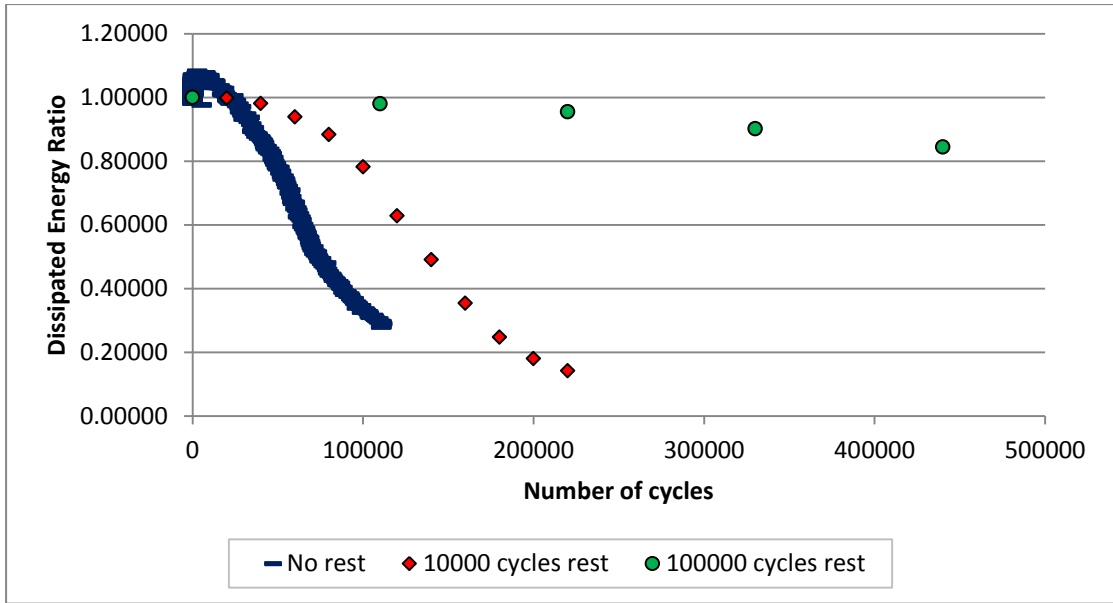
Figure 105, Figure 106 and Figure 107 show a comparison between a traditional fatigue test (at  $160 \mu\epsilon$  at  $10^\circ\text{C}$  and  $25 \text{ Hz}$ ) and two healing tests characterised by the same loading time period (10,000 cycles) and two different rest time periods (10,000 and 100,000 cycles of rest time). In terms of fatigue, both healing tests show a bigger (and similar) stiffness ratio for the first half of the test. Once the stiffness ratio has reached the 50% ( $E_{50\%}$ ) of its initial value ( $E_0$ ), the first healing test (10,000 cycle of rest time period) seems to have a very similar behaviour to the traditional fatigue test; the second

healing test (100,000 cycles of rest time period) has a different behaviour: stiffness ratio has a bigger value, thus the number of cycles to failure (50% reduction in stiffness) is bigger.



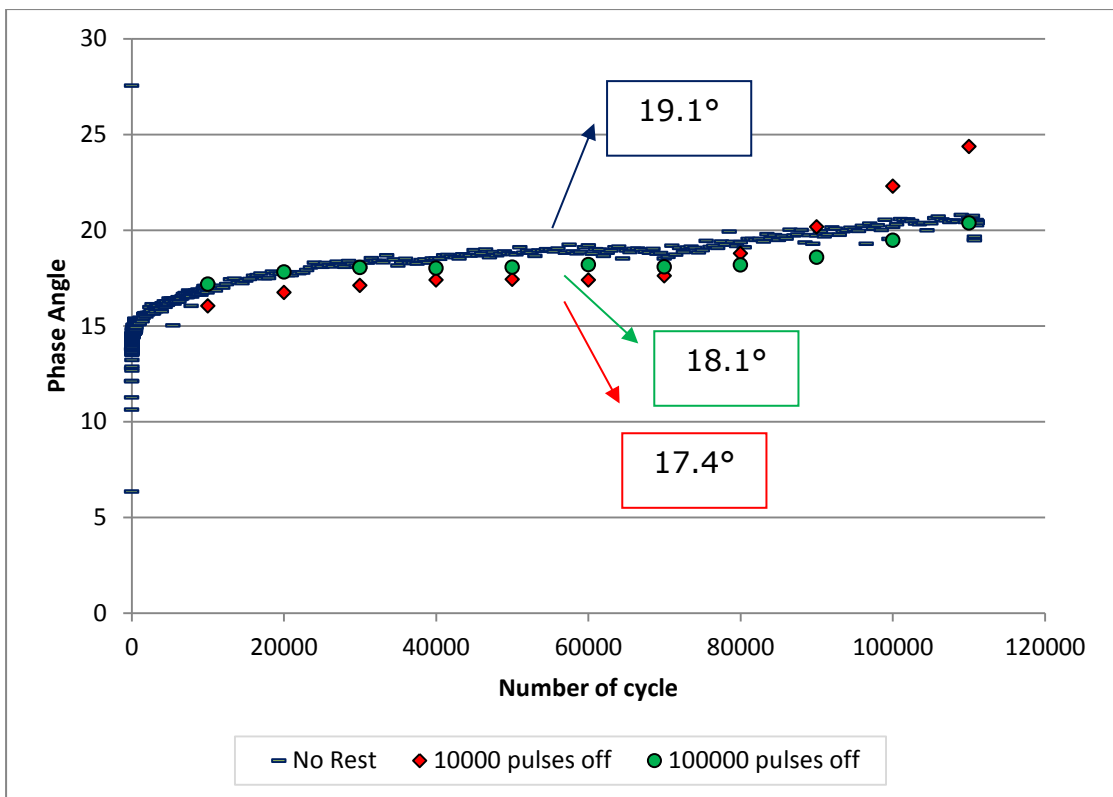
**Figure 105** Variation in stiffness at different rest time periods (fixed loading time = 10,000 pulses)

In terms of dissipated energy, the dissipated energy ratio was used. It is the ratio between the dissipated energy per cycle divided by the initial dissipated energy (obtained at 50<sup>th</sup> cycle). A clear healing effect is observed in the three tests; although energy is dissipated more slowly in the test with the highest rest time, there is a lower dissipated energy change (see Figure 106).



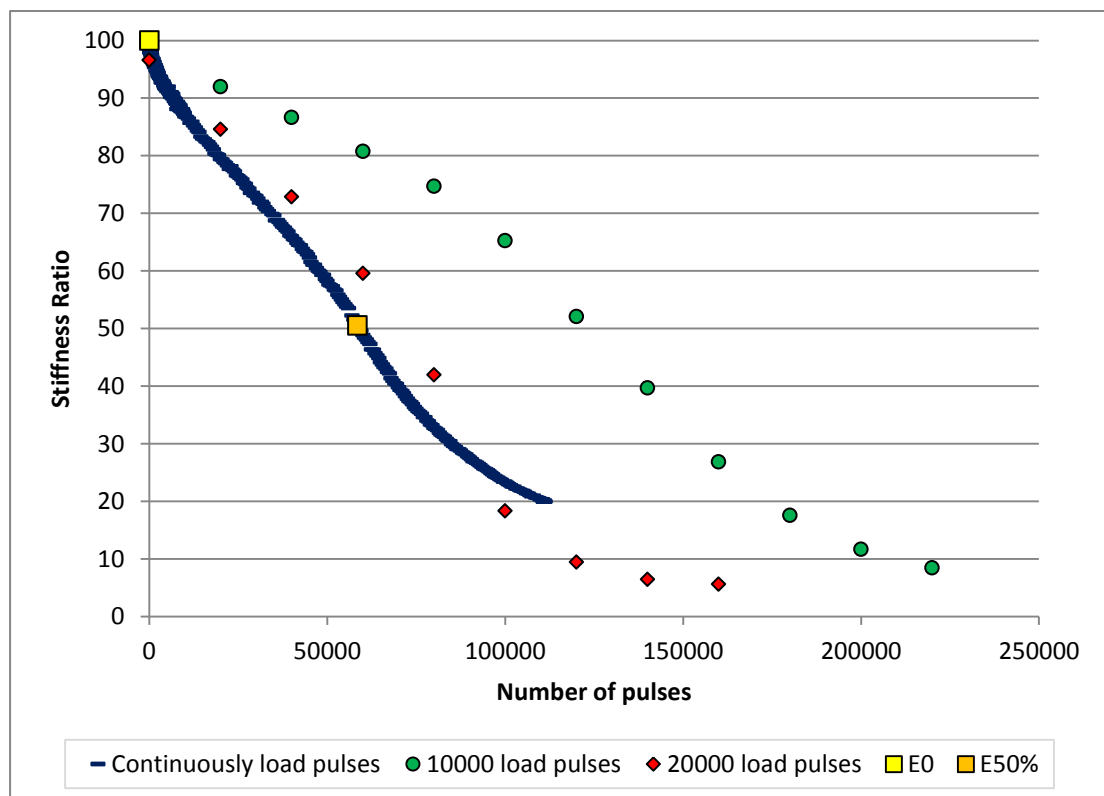
**Figure 106** Variation in dissipated energy at different rest time periods (fixed load time = 10,000 pulses)

In terms of phase angle, small differences can be noticed for the three tests; although those differences are not that big: phase angle varies by 2° (see Figure 107).



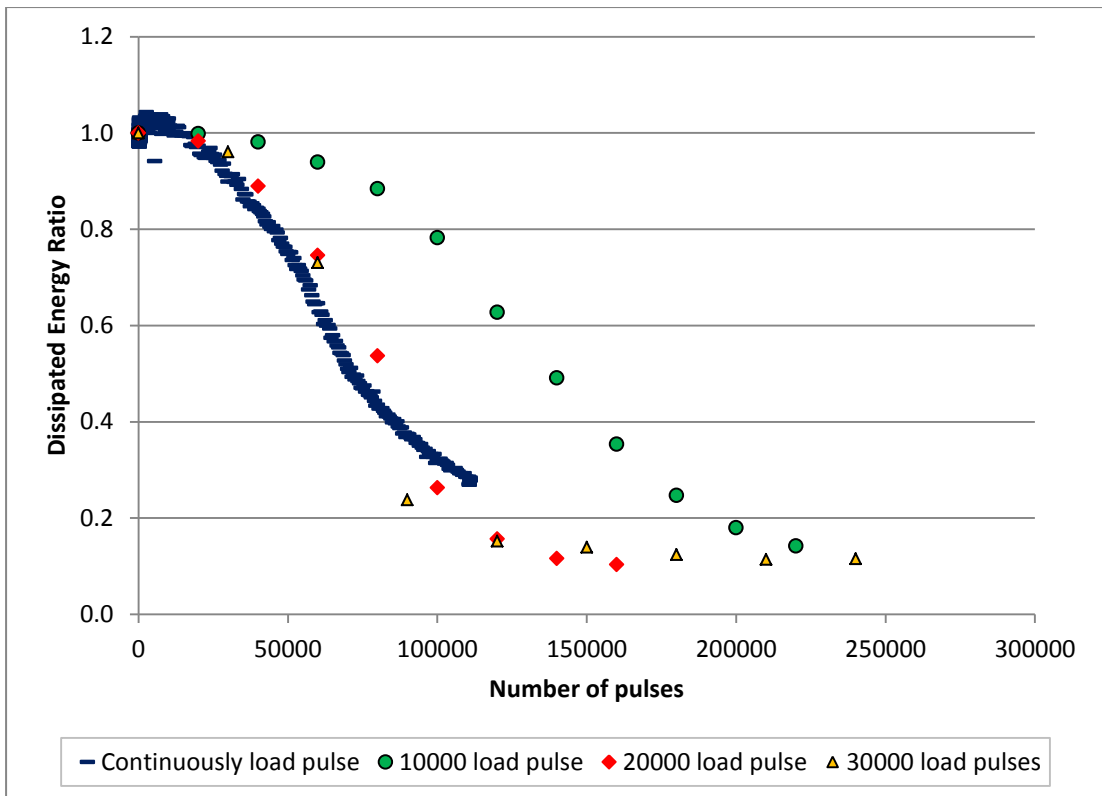
**Figure 107** Variation in phase angle at different rest time periods (fixed load time = 10,000 pulses)

Figure 108, Figure 109 and Figure 110 show a comparison between a traditional fatigue test (at  $160 \mu\epsilon$  at  $10^\circ\text{C}$  and  $25 \text{ Hz}$ ) and two healing tests characterised by the same rest time periods (10,000 cycles) and different loading time period (10,000 and 20,000 cycles). In terms of fatigue, in both healing tests there is an improvement in terms of stiffness: in particular, stiffness improves by 10% when the loading time period is 10,000 cycles; it improves by 30% when the loading time period is 20,000 cycles. Therefore in both cases, the number of cycles to failure is bigger than the traditional fatigue test continuously loaded (see Figure 108).



**Figure 108** Variation in stiffness at different load time periods (fixed rest time = 10,000 pulses)

In terms of dissipated energy, when loading time period increases the behaviour of the material tends to be similar to the behaviour of the material during a traditional fatigue test (when a rest period is not included) as shown in Figure 109. This was confirmed by a final test undertaken at the same loading conditions, characterised by 30,000 cycles of loading time period and 10,000 cycle of rest time period.



**Figure 109** Variation in dissipated energy at different load time periods (fixed rest time = 10,000 pulses)

Also in this case, in terms of phase angle, small differences can be noticed for the three tests; although those differences are not that big, phase angle varies by  $2^\circ$  (see Figure 107).

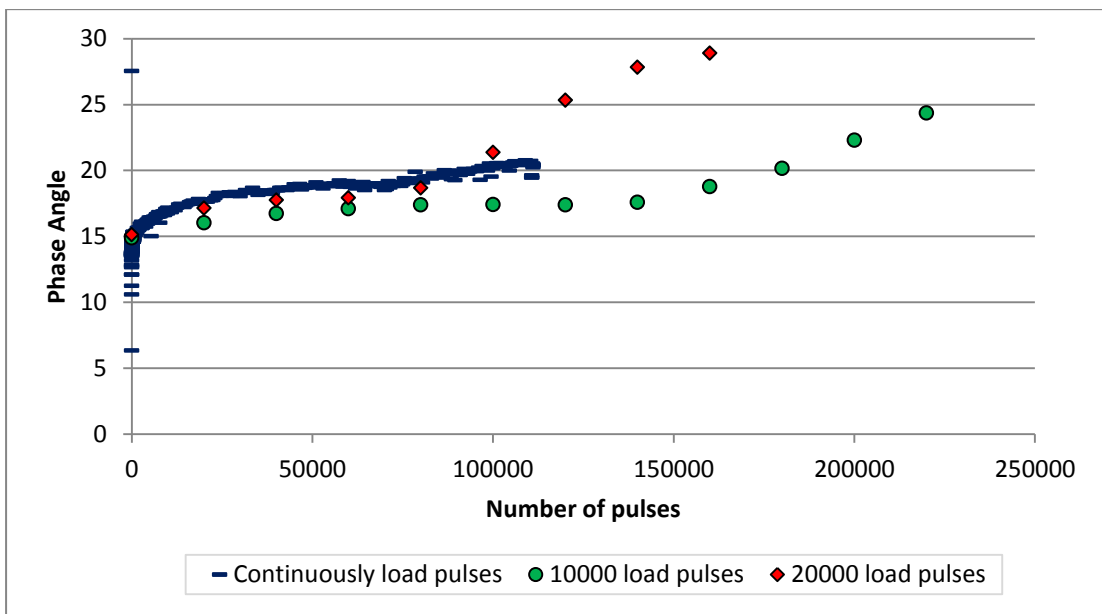


**Figure 110** Variation in phase angle at different load time periods (fixed rest time = 10,000 pulses)

A Healing Ratio was determined with the following equation to be able to represent the healing test results:

$$HR = \frac{N_h}{N} \quad \text{Equation 105}$$

Where  $N_h$  is the number of cycles when rest periods are included in a fatigue test;  $N$  is the number of cycles during a fatigue test when rest periods are not included. The two values are compared at the same Stiffness Ratio value. Results are shown in Figure 111 and Figure 112.

For different loading time periods, when the loading time period increases, the healing test is similar to a traditional fatigue test; the specimen is already partially damaged after a longer loading time period (as 30,000 cycles).

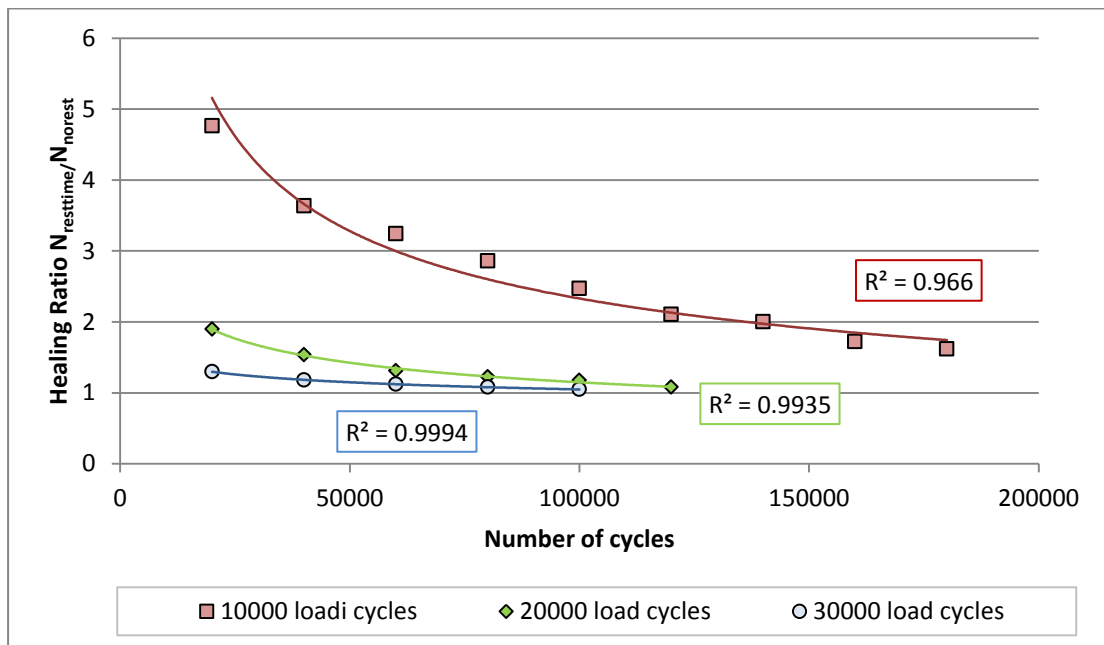


**Figure 111** Healing Ratio for different load time periods (fixed rest time = 10,000 cycles)

For different rest time periods, when the rest time period decreases, the healing test is similar to a traditional fatigue test. In both scenarios healing effects are bigger at the first stage of the test. The effects are similar if rest time (or load time) varies after a certain amount of cycles; increasing rest time does not make a huge difference for rest time values bigger than 50,000 cycles (see Figure 112).

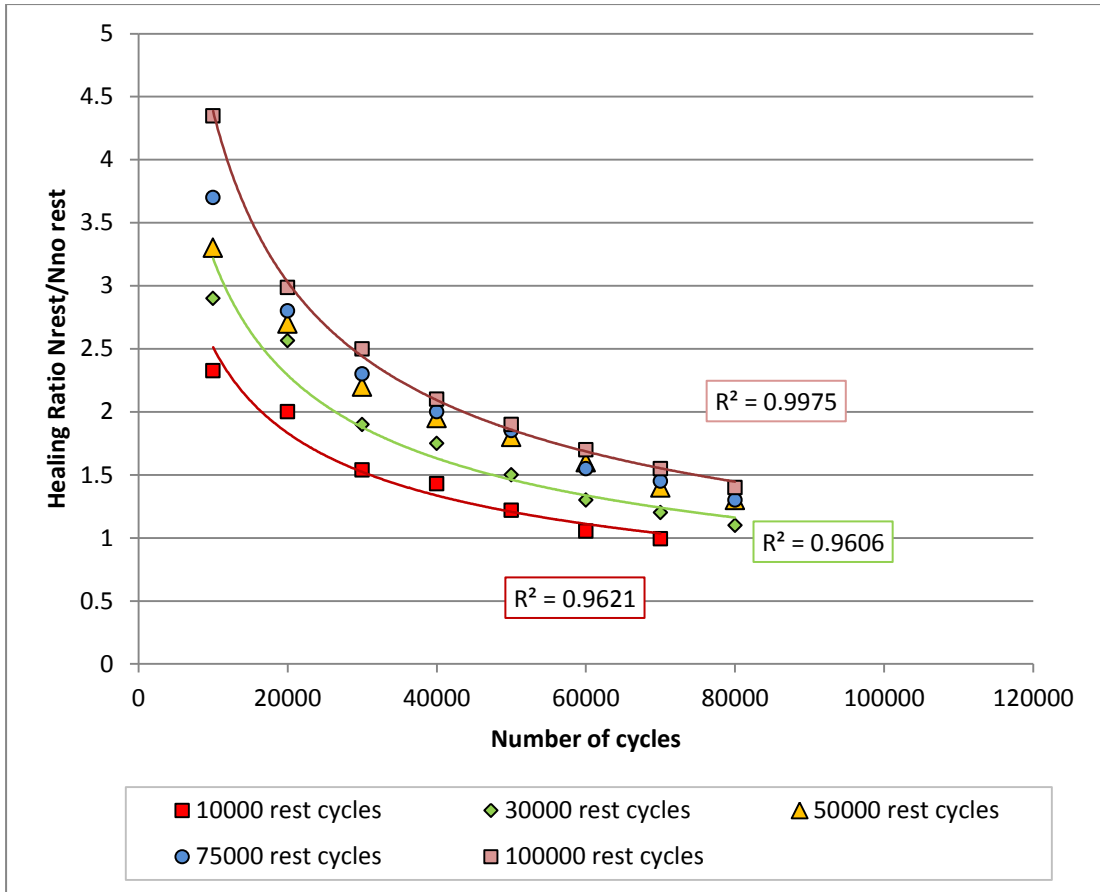


**Figure 112** Healing Ratio for different rest time periods (fixed load time = 10,000 cycles)

Another phenomenon to be taken in consideration is that healing effects are influenced by the amount of heat produced inside the specimen during a test. The main assumption was that loading and environmental conditions are homogenous in the specimen during the test. This research did not take into consideration the heating phenomenon due to experimental limits; however Pronk has previously shown that the decrease in stiffness due to internal heating is small compared to the decrease in stiffness due to damage (Pronk, 2000).

## 6.5 Summary

A detailed description of the 4PB test, the production of prismatic specimens and configuration of the machine are presented. The following conclusions can be drawn for this chapter:

- A comparison with 2PB tests was made and results show that stiffness values obtained by 2PB are smaller than values obtained by 4PB; phase

angle values obtained by 2PB are bigger than values obtained by 4PB. Higher values of phase angle indicate a tendency towards more viscous behaviour, whilst lower values indicate more elastic response, thus it seems that 2PB stiffness tests at 10°C underline more the viscous behaviour of the materials compared with the 4PB stiffness tests.

- In terms of fatigue, the hypothesis of equality between elevations of different regressions (obtained by using different DE methods) was not rejected for a significance level of 0.05. Therefore, Dunnett's test was necessary to compare the regressions; results show that the regression lines obtained by the different DE methods are not different from the traditional method (Nf,50).
- 4PB fatigue data were compared with 2PB fatigue data considering the RDEC method. The two regression lines are not the same. In this case it is not possible to consider a unique regression line for both sets of data; therefore RDEC is dependent on the test used.
- In terms of healing, results show that the number of cycles to failure decreases if loading time increases; it increases if resting time period increases. In terms of DE, it was found that the specimen dissipates energy very slowly when a rest time is included during a fatigue test: small changing in DE was noted when a rest time is included in a fatigue test. Thus, DE might not be a very good parameter to include the effect of healing in the evaluation of fatigue behaviour.

## CHAPTER 7

# Indirect Tensile Fatigue Test

### 7.1 Introduction

The Indirect Tension Fatigue Test (ITFT) is a simple fatigue test with widespread use in the United Kingdom due to the fact that it is a simple test, easily suitable for cylindrical specimens manufactured in the laboratory or cored from a flexible pavement. A disadvantage of this testing arrangement is the accumulation of permanent deformation which tends to hide the real fatigue damage; thus the ITFT does not measure fatigue behaviour directly, especially at high temperatures where the viscoelastic behaviour is more dominant (Cocurullo et al., 2008, Read, 1996, Hartman, 2001).

Among the advantages, it is important to stress that the test is simple to conduct and suitable to characterise the stiffness and fatigue properties of asphalt materials particularly for construction sites.

The ITFT configuration was used to determine the stiffness modulus and the fatigue behaviour of the asphalt mixture in both stress and strain controlled modes. ITFT is usually undertaken in load controlled mode: a repeated compressive load with a haversine signal is applied through the vertical diameter plane of the cylindrical specimen. In this project, the ITFT in deformation controlled mode was developed: repeated deformation amplitude with a haversine signal is applied through the vertical diameter plane on the cylindrical specimen.

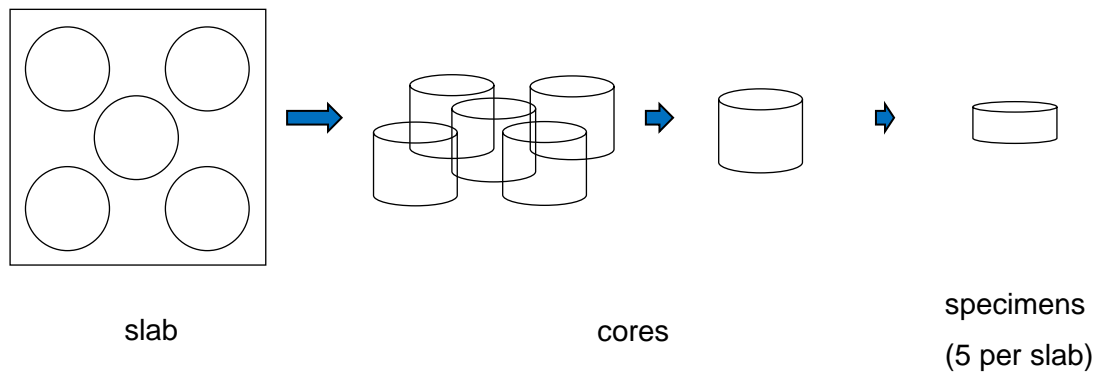
### 7.2 Cylindrical specimens

To obtain specimens for the indirect tensile test configuration, five cores (100 mm in diameter) are taken from each slab (305 x 305 mm and 60 mm high), uniformly mixed and compacted according to EN 12697-35:2002 and EN 12697-33:2003. Cylindrical specimens, 100 mm in diameter and 40 mm high, are then obtained by trimming the top and the bottom of each core using a

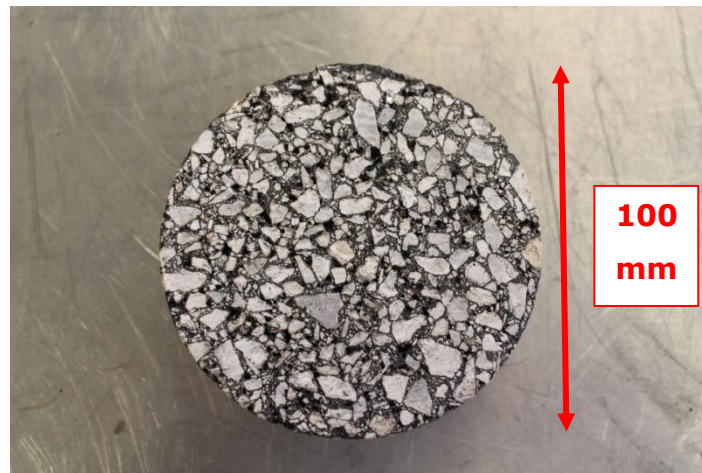
masonry saw (see Figure 114). This is done in order to eliminate the parts that usually contain higher air void contents.

Figure 113 shows a schematic representation of the coring and cutting procedure.

The cylindrical specimens were used for the Indirect Tension to CYlindrical specimen (IT-CY) and Indirect Tensile Fatigue test (ITFT).



**Figure 113** Coring and trimming procedure



**Figure 114** Cylindrical specimen (10mm DBM)

### **7.3 Indirect tension to cylindrical specimen - IT-CY**

#### **Equipment**

In order to understand this type of test, a brief description of the equipment is given. As shown in Figure 115 the equipment is composed of several parts: a steel load frame holds the specimen and the pulsating load/deformation is applied by means of a pneumatic actuator. The specimen is located in a central position between two loading platens (upper and lower); two LVDTs

are mounted in a frame and they, being directly in contact with the specimen along the width, record the horizontal deformation when the vertical force is applied (see Figure 116).

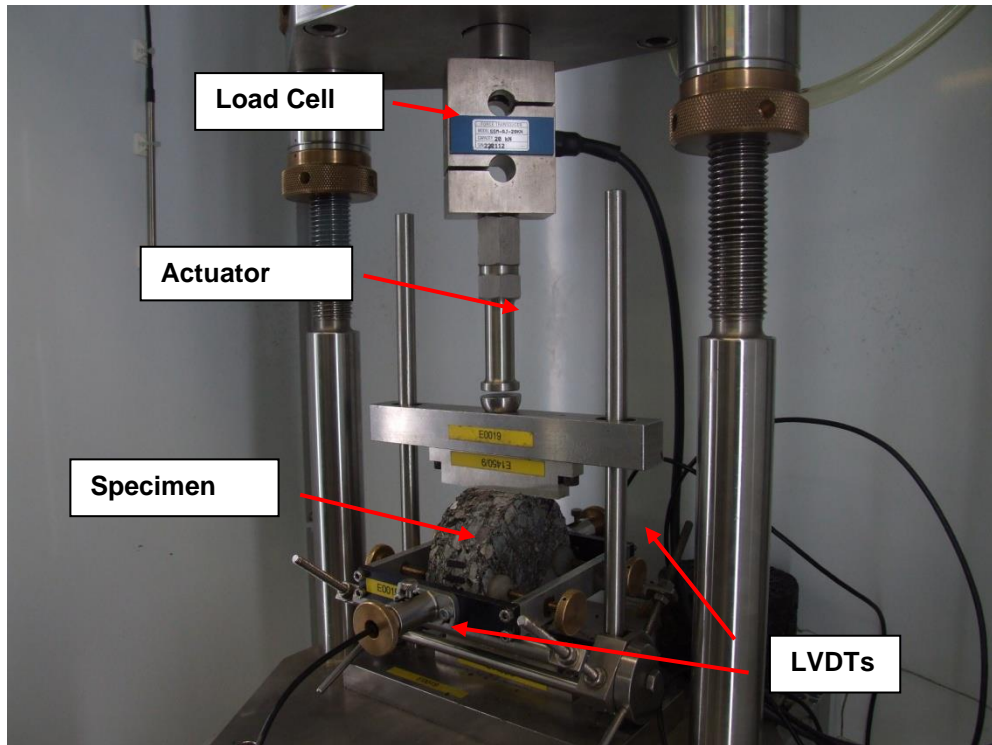


Figure 115 IT-CY Stiffness Modulus test.

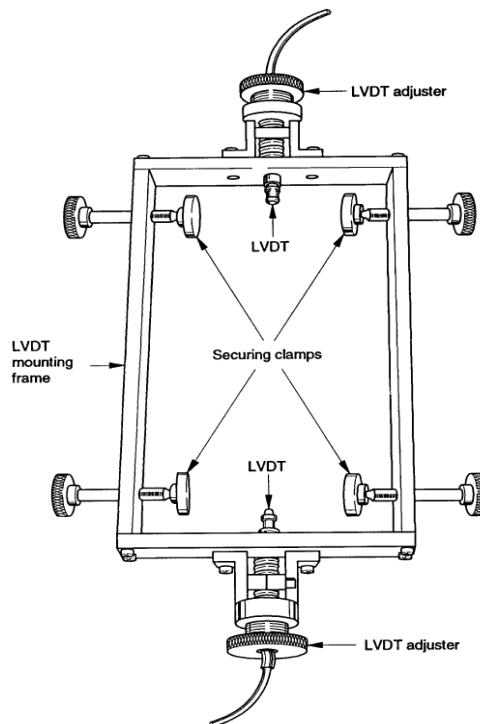
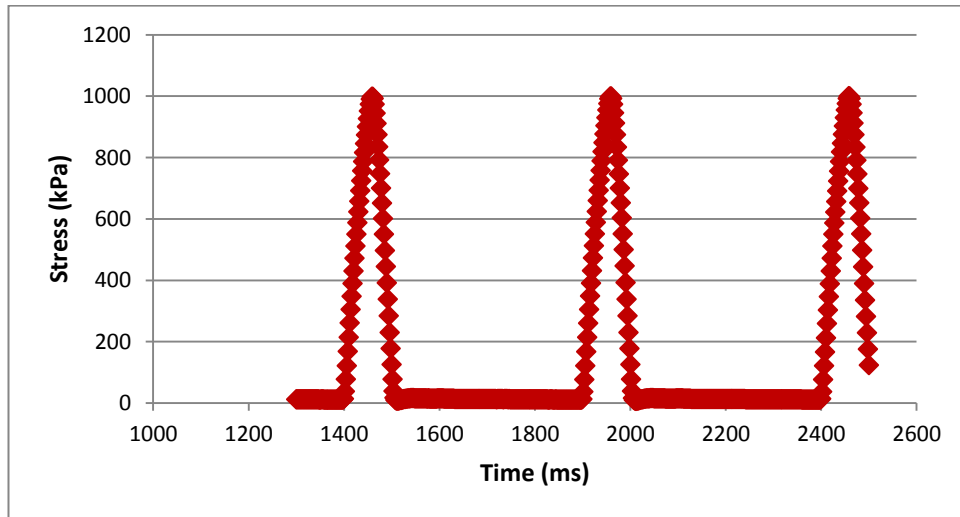
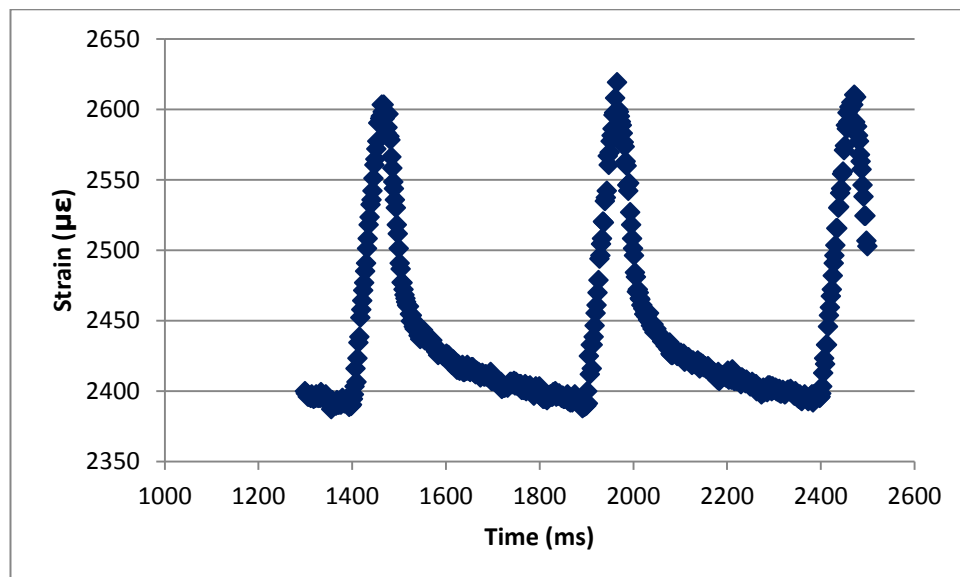


Figure 116 Frame for measuring horizontal diametral deformation

To evaluate stiffness modulus of the mixture, repeated load pulses with rest periods are applied along the vertical diameter of the specimen. The load waveform is haversine and the rise-time is  $124 \pm 4$  ms according to EN 12697-26:2004 (see Figure 117). The peak deformation is measured along the horizontal diameter using linear variable displacement transducers (LVDT) (see Figure 118); experience indicates  $5 \pm 2 \mu\epsilon$  as suitable values for a 100 mm diameter specimen.



**Figure 117** Stress pulse applied.



**Figure 118** Strain waveform recorded.

Usually 10 preloading pulses are applied before applying 5 load pulses for the determination of stiffness. After that, the specimen is rotated through  $90^\circ$  in order to repeat the same procedure. Stiffness modulus is obtained from the average values recorded at those two tests. In order to achieve a correct

stiffness modulus mean value the second test should be within +10% and -20% of the mean value recorded for the first test.

The test parameters for the stiffness modulus tests are:

- Two test temperatures: 10 and 20 °C;
- Poisson's ratio: 0.35
- Loading rise-time:  $124 \pm 4$  ms;
- Pulse repetitions:  $3 \pm 0.1$  sec;
- Number of load pulses: 10 (preloading time) + 5 (recording time)
- Peak horizontal deformation:  $5 \pm 2$   $\mu\epsilon$ .

The measured stiffness modulus  $S_m$  is calculated using the following formula:

$$S_m = \frac{F \times (\nu + 0.27)}{(z \times h)} \quad \text{Equation 106}$$

Where F is the peak value of the applied vertical load (N); z is the amplitude of the horizontal deformation obtained during the load cycle (mm); h is the mean thickness of the cylindrical specimen (mm);  $\nu$  is the Poisson's ratio (0.35).

### **Stiffness results**

IT-CY tests were conducted mainly at 10 and 20 °C on the 10mm DBM, because a fatigue analysis was conducted at the same temperatures. Specimens with either low (<3.5%) or high (>5.0%) air void content were not included in the specimen set for fatigue analysis. The rejected specimens were used to calibrate and develop the new test machine (ITFT in strain control mode). Variations in air void content between 3% and 5% do not result in big variation of stiffness modulus as shown Figure 119.

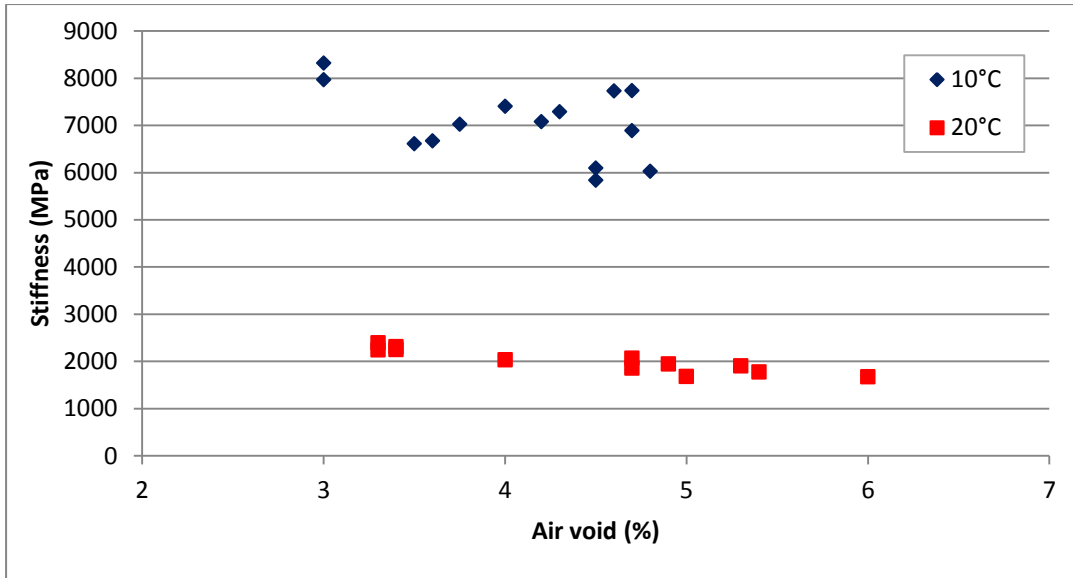


**Figure 119** Stiffness versus air void content (10mm DBM)

A few tests were conducted at 5°C in order to evaluate the viscoelastic behaviour of the material at different temperatures. Figure 120 shows the relationship between the temperature and stiffness values. Stiffness values strongly decrease when temperature increases for this material (10mm DBM mixture with 100 pen bitumen is highly dependent on the temperature).

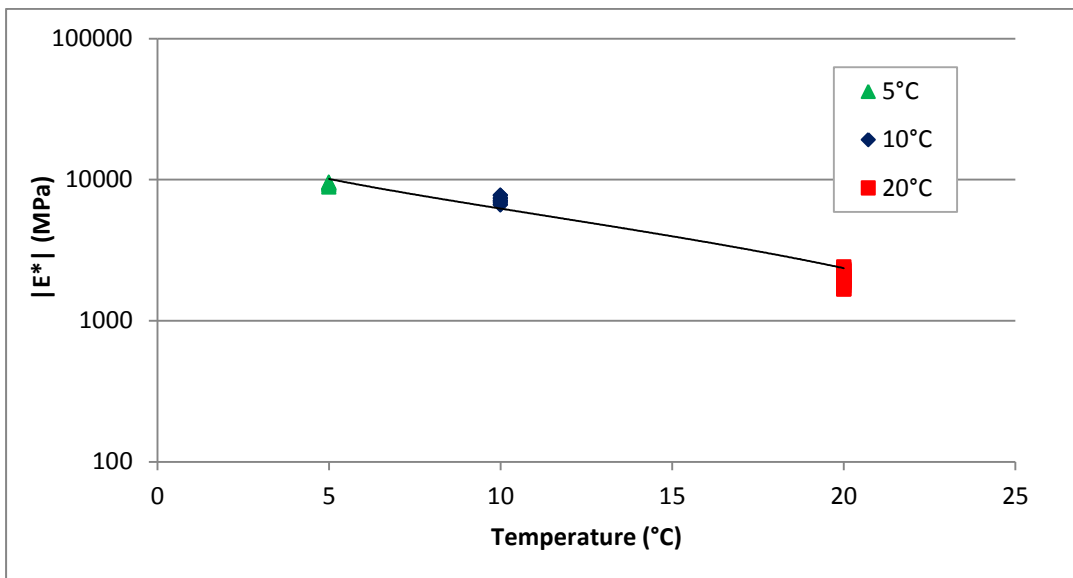


**Figure 120** Stiffness results for 10mm DBM mixture with 100 pen bitumen (10mm DBM)

## 7.4 Indirect Tension Fatigue Test (ITFT)

### Equipment

The specimen is located in a central position between two loading strips (upper and lower), characterised by a concave surface and rounded edges; two deformation strips are glued on opposite sides of the horizontal diameter plan using a position rig. Also the deformation strips have a concave surface and they hold two LVDTs located horizontally in order to record the variation of the horizontal diameter considering the variation of the distance between the two deformation strips (see Figure 121).

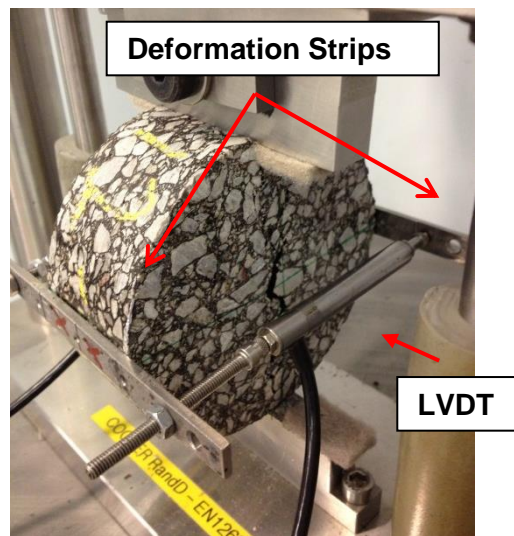


**Figure 121** ITFT apparatus.

Indirect tension fatigue tests (ITFT) in stress and strain controlled mode will be conducted to better understand the fatigue behaviour of the mixture; healing effects will also be included (see Figure 122).

The experimental test is analogous to the IT-CY but with some changes. In stress controlled mode a haversine compressive load is applied to the vertical diameter plane of the cylindrical specimen with 0.1 sec loading time and 0.4 sec rest time. This creates a uniform “indirect” tensile stress perpendicular to the direction of the applied load (along the horizontal diameter). Repeated applications of the vertical force will usually result in a crack along the vertical diameter; in stress control mode, failure corresponds with the fracture in two halves of the specimen (see Figure 123).

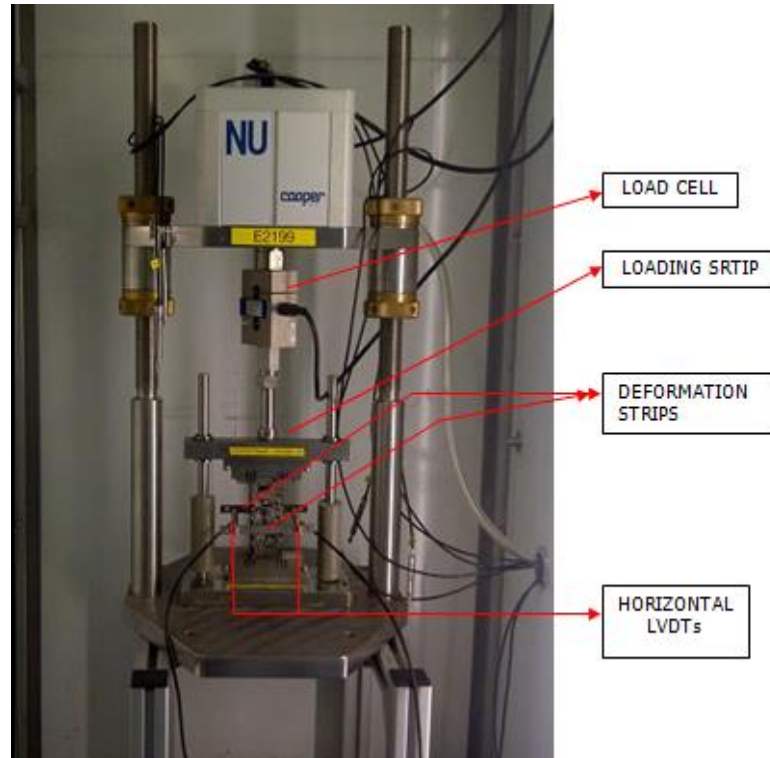


**Figure 122** Indirect Tension Fatigue Test

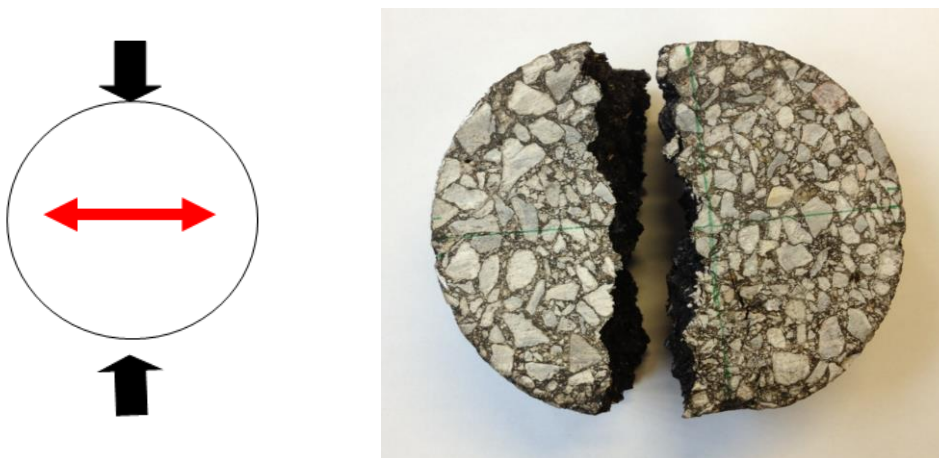


**Figure 123** Mechanism of failure in stress control mode

The rest time is usually fixed for the standards. Healing effects can be studied by varying the rest time after every loading pulse or by considering a rest time after a certain amount of pulses. The second option was chosen for this project (see Section 2.5.1).

Fatigue life is usually determined as the number of load applications that cause the complete fracture of the asphalt specimen.

The test parameters for the fatigue tests are:

- Two tests temperatures: 10 and 20 °C;
- Poisson's ratio: 0.35
- Loading time: 0.1 sec;
- Rest time: 0.4 sec;
- Failure indication: 9 mm vertical deformation.

The maximum tensile stress  $\sigma_{\max}$  (MPa) and the maximum tensile strain in the centre of the specimen  $\varepsilon_{\max}$  ( $\mu\varepsilon$ ) are:

$$\sigma_{\max} = \frac{2P}{\pi \times t \times \Omega} \quad \text{Equation 107}$$

$$\varepsilon_{\max} = \left( \frac{2\Delta H}{\Omega} \right) \cdot \left( \frac{1 + 3\nu}{4 + \pi \times \nu - \pi} \right) \quad \text{Equation 108}$$

Where P is the maximum load applied (N); t is the specimen thickness (40 mm);  $\Omega$  is the specimen diameter (100 mm);  $\nu$  is the Poisson's ratio (0.35);  $\Delta H$  is the horizontal deformation (mm).

For the 10mm DBM mixture, fatigue tests were conducted at 10 and 20°C at stress levels between 100 and 600 kPa (see Figure 124). Fatigue life at 20°C is represented only by a few specimens because the tests were hard to control due to the fact that the LVDTs went out of the range very often (thus many tests could not be included as reliable data). This can be explained by the fact that 10mm DBM (100 pen) is a soft material and the viscous behaviour is more evident at higher temperatures.

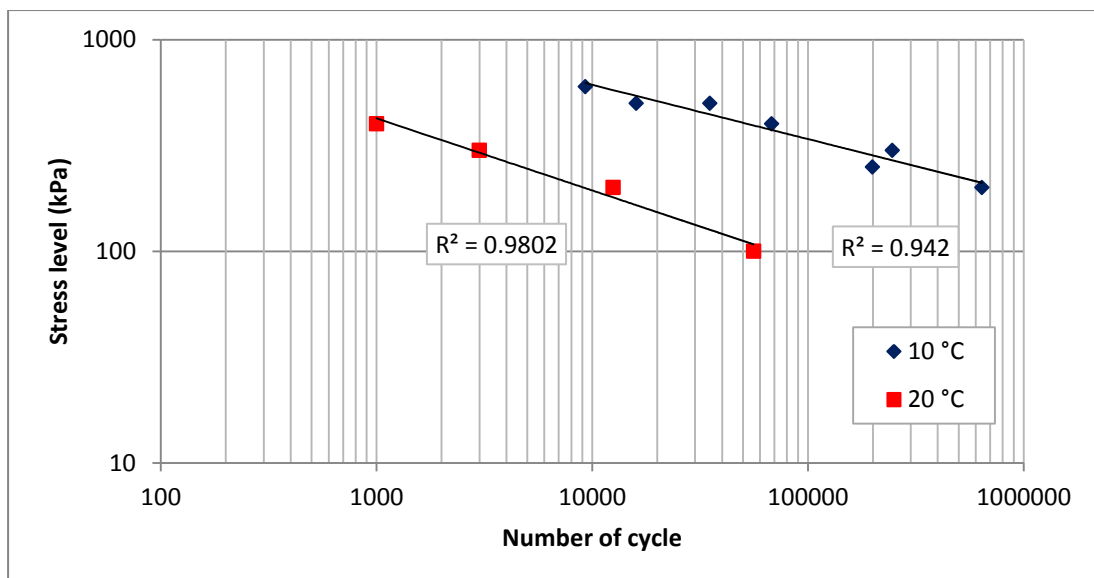


**Figure 124** Fatigue tests in stress control mode at 10 and 20°C (10mm DBM)

## 7.5 ITFT in strain control mode

In this research project, the ITFT was also developed to be undertaken in strain control mode.

The equipment and the specimen preparation in the new test is exactly the same as for the ITFT in stress control mode. The test consists of applying a constant deformation during the fatigue test; with the recoverable deformation being chosen as the constant parameter for the test (see Figure 125); it occurs during the unloading time of one pulse. Permanent deformation is the amount of deformation that is unrecoverable after one pulse and it is the total deformation minus the recoverable deformation. The main aim of the development of ITFT in strain control mode was to be able to compare stiffness and fatigue results with pure fatigue tests such as 2PB and 4PB. Pure fatigue tests are characterised by a sinusoidal loading waveform about zero stress point, thus no permanent deformation are involved. Therefore, recoverable deformation was chosen to not include permanent deformation when an ITFT test is undertaken.

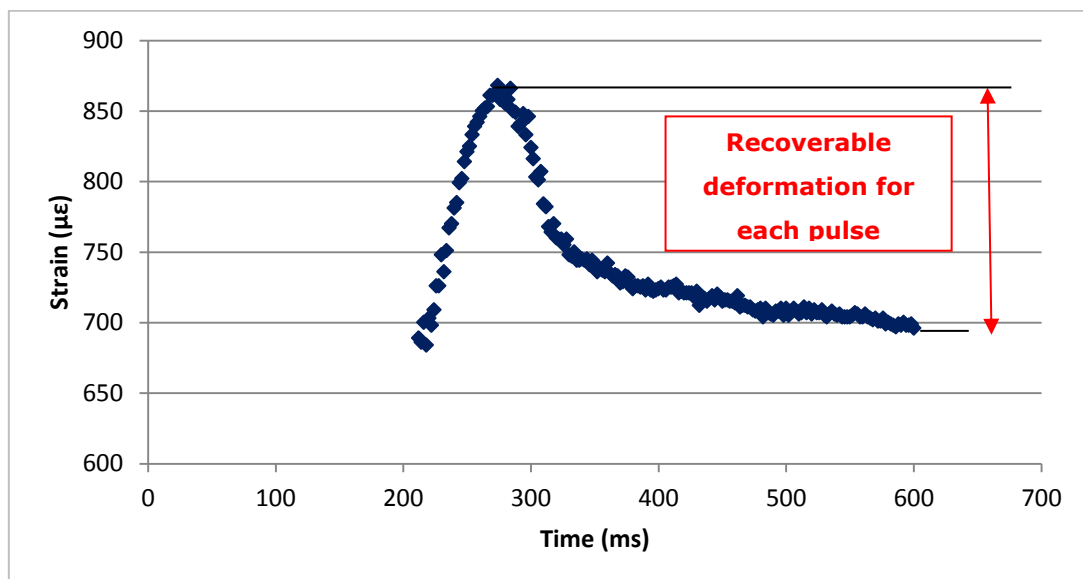


**Figure 125** Recoverable deformation (10 mm DBM)

In strain control mode, the specimen does not reach the complete fracture along the vertical diameter at failure as in the case of a stress control test; it is characterised by localised deformation at the edge of the loading strips with visible cracks observed along the vertical plane of the specimen as shown in Figure 126.

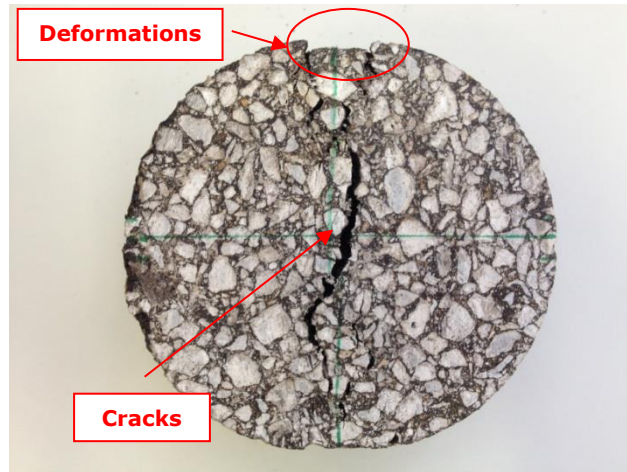


**Figure 126** Failure in strain control mode

Fatigue life is determined as the number of pulses that causes a 50% reduction of stiffness from its initial value.

For the 10mm DBM mixture, fatigue tests were carried out at 10°C at different strain levels between 80 and 180  $\mu\epsilon$  (see Figure 127).

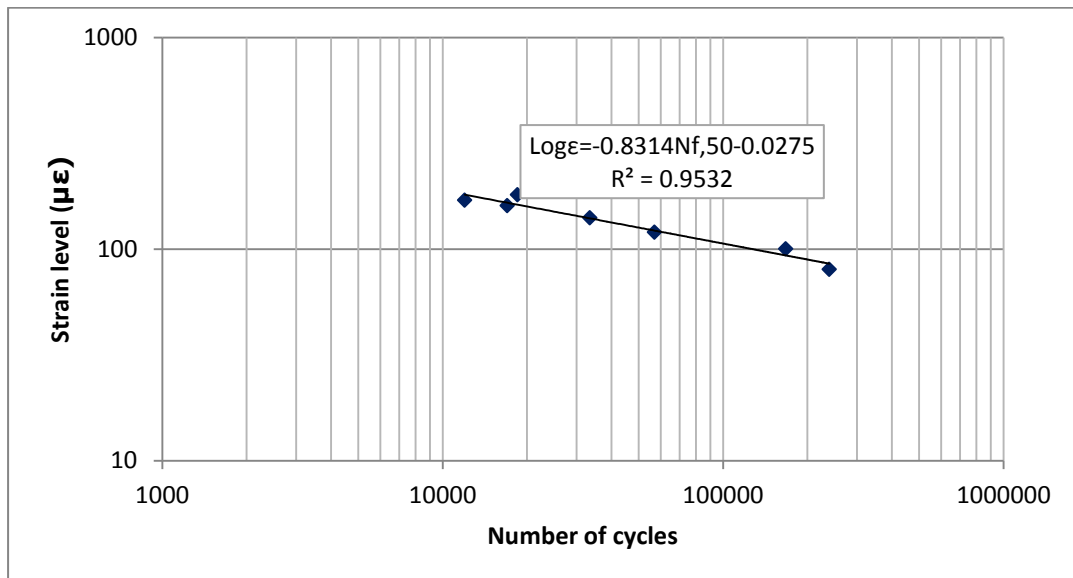


**Figure 127** Fatigue life in strain control mode at 10°C (10mm DBM)

Dissipated energy concepts were included during the development of the testing machine in the software. Dissipated energy is traditionally the hysteresis loop when stress (sinusoidal waveform) is plotted against strain (sinusoidal waveform) and its shape is elliptical. In the case of the ITFT, stress and strain are characterised by a haversine waveform, thus dissipated energy looks like half of a typical elliptical hysteresis loop; this is due to the rest time after every single pulse (see Figure 128 and Figure 129).

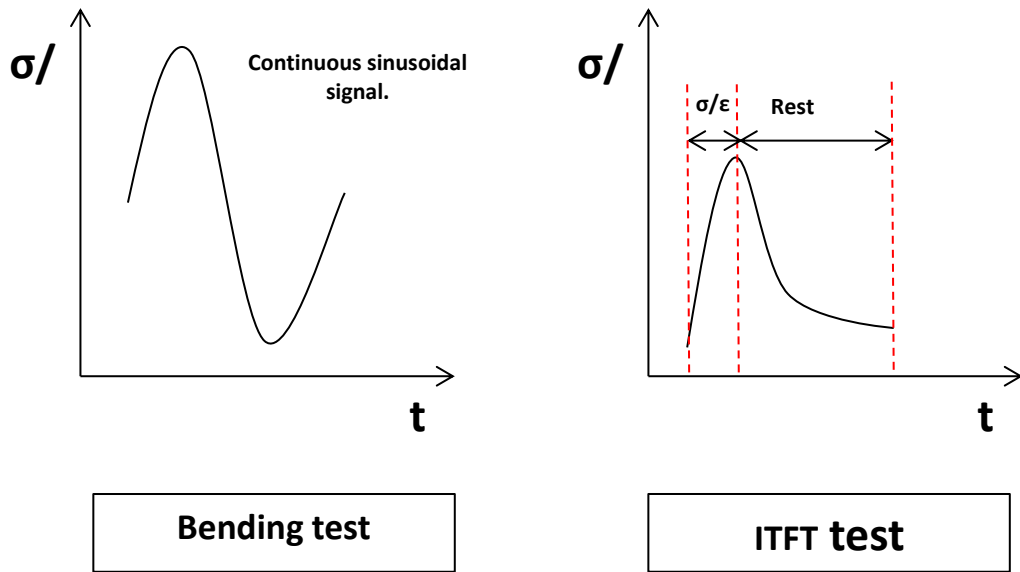


**Figure 128** Signals for a bending test and the ITFT

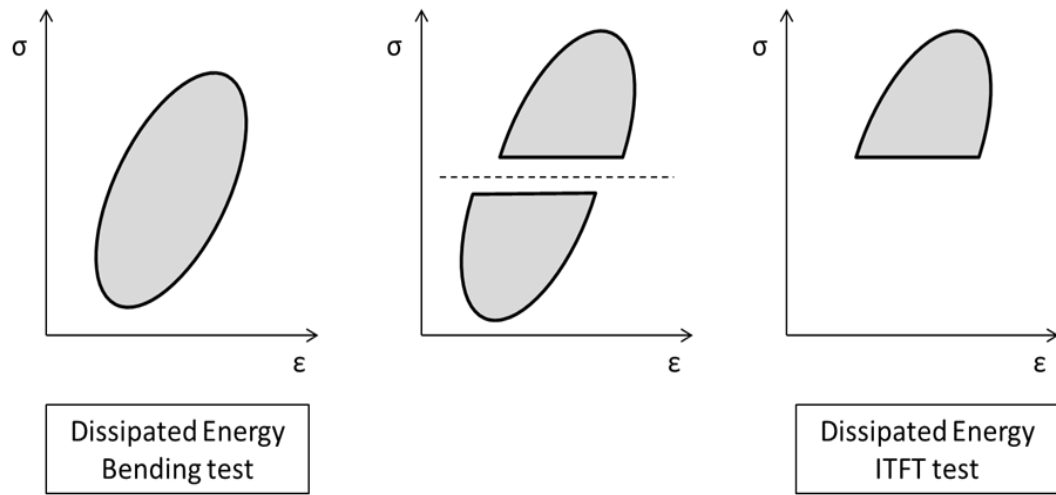


**Figure 129** Dissipated energy for a bending test and the ITFT

Figure 130 shows the real hysteresis loop when stress pulse (raw data) is plotted against strain pulse (raw data) during an ITFT test.

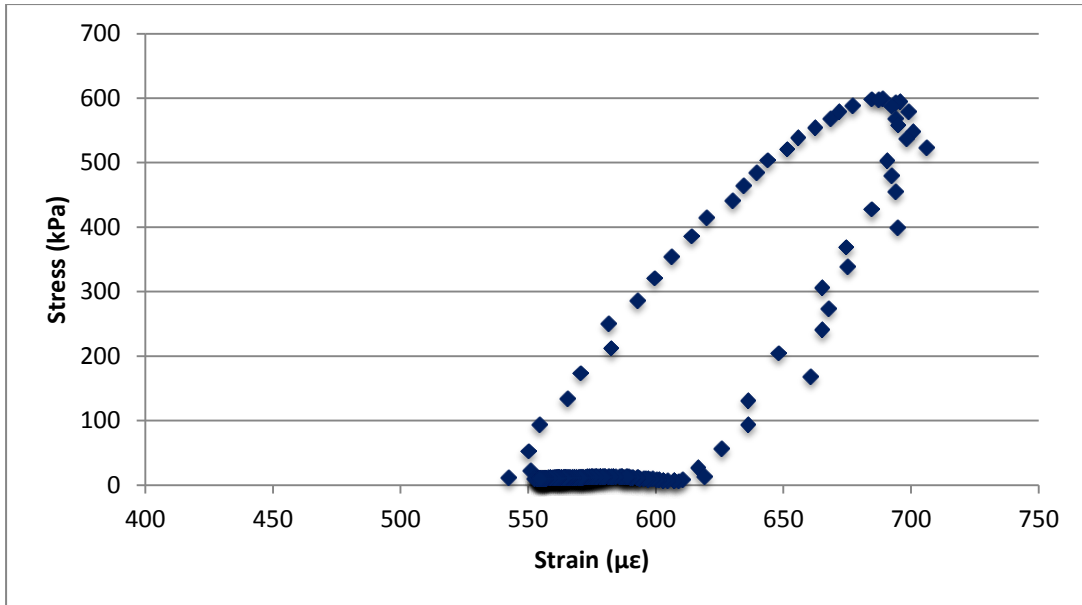


**Figure 130** Stress-strain hysteresis loop for a single pulse in ITFT (10mm DBM)

The software did not calculate dissipated energy before starting the project. Dissipated energy was calculated as the sum of small trapezoidal areas of two following experimental points as shown in Figure 131. In terms of equations the infinitesimal dissipated energy (trapezoidal area) is calculated by the following equation:

$$DE_1 = \frac{(\sigma_1 + \sigma_2) \cdot (\varepsilon_2 - \varepsilon_1)}{2} \quad \text{Equation 109}$$

The total dissipated energy (the area of the hysteresis loop) is the sum of each infinitesimal area as follows:

$$DE = \sum_{i=1}^N DE_i \quad \text{Equation 110}$$

Where N is the total number of points recorded by the software.

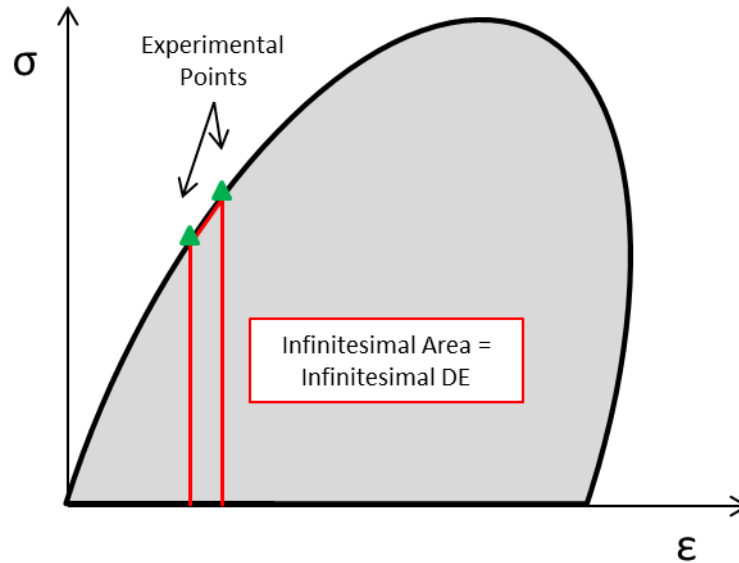


**Figure 131** Calculation of Dissipated Energy

The software records the dissipated energy for each cycle and the cumulative dissipated energy during a fatigue test.

## 7.6 Test results

### 7.6.1 Fatigue life: initial strain calculation

Three different ways to calculate the initial strain value for each fatigue test in stress control mode were considered:

- EN 12697-24: 2004. Resistance to fatigue
- EN 12697-26: 2004. Stiffness
- EN 12697-24:2012. Resistance to fatigue

According to EN 12697-24:2004, the maximum tensile stress ( $\sigma_0$  in MPa) and strain ( $\varepsilon_0$  in  $\mu\varepsilon$ ) at the centre of the specimen shall be calculated using the following equations:

$$\sigma_0 = \frac{2P}{\pi \times t \times \Omega} \quad \text{Equation 111}$$

$$\varepsilon_0 = \frac{2H}{\Omega} \times \frac{1+3\nu}{4+\pi \times \nu - \pi} \quad \text{Equation 112}$$

If  $\nu=0.35$ , then:

$$\varepsilon_0 = 2.1 \times \frac{H}{\Omega} \quad \text{Equation 113}$$

Where:

- P is the applied load (in Newton),
- t is the specimen thickness (in mm),
- $\Omega$  is the specimen diameter (in mm),
- $\Delta H$  is the horizontal deformation (in mm).

The initial strain value is then calculated from the difference between the average of the total deformation of 5 load applications from 98<sup>th</sup> to 102<sup>nd</sup> cycle and the average of the minimum horizontal deformations of 5 load applications from 60<sup>th</sup> to 64<sup>th</sup> as shown in Figure 132.

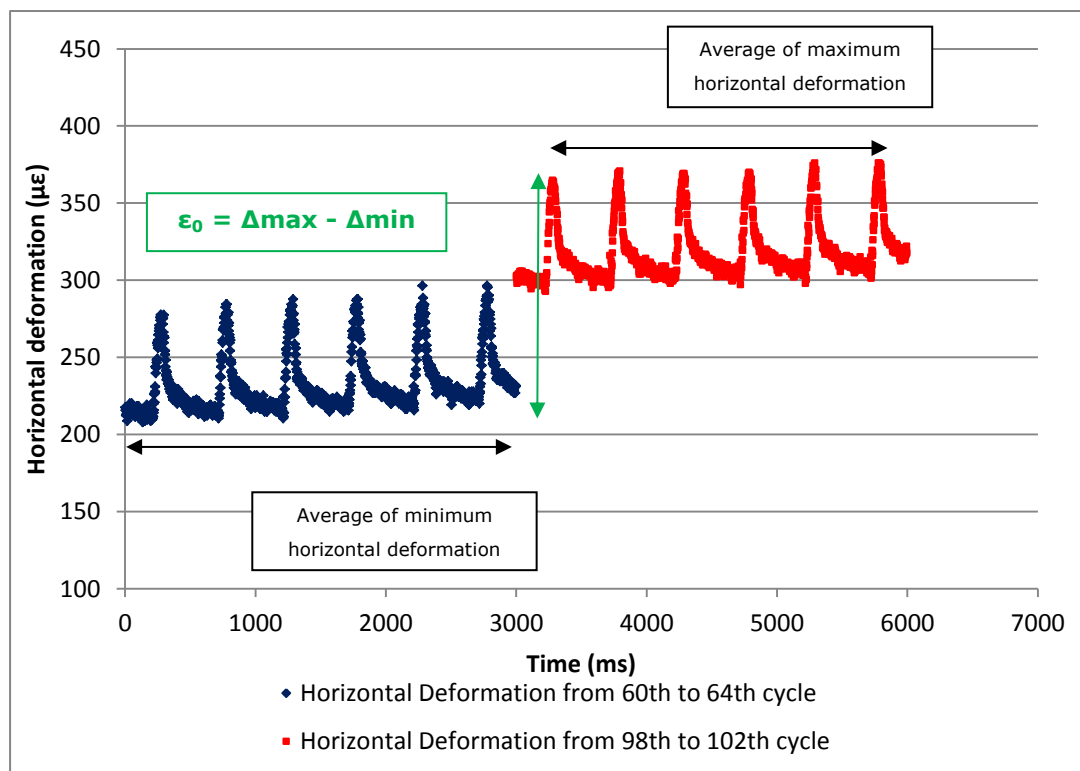


**Figure 132** Initial strain amplitude EN 12697-24:2004

According to EN 12697-26:2004, the horizontal deformation ( $\epsilon_0$  in  $\mu\epsilon$ ) is the distance between the segment that links the maximum values of horizontal deformation of two consecutive cycles and the segment that links the minimum values of horizontal deformation of two consecutive cycles (see Figure 133).

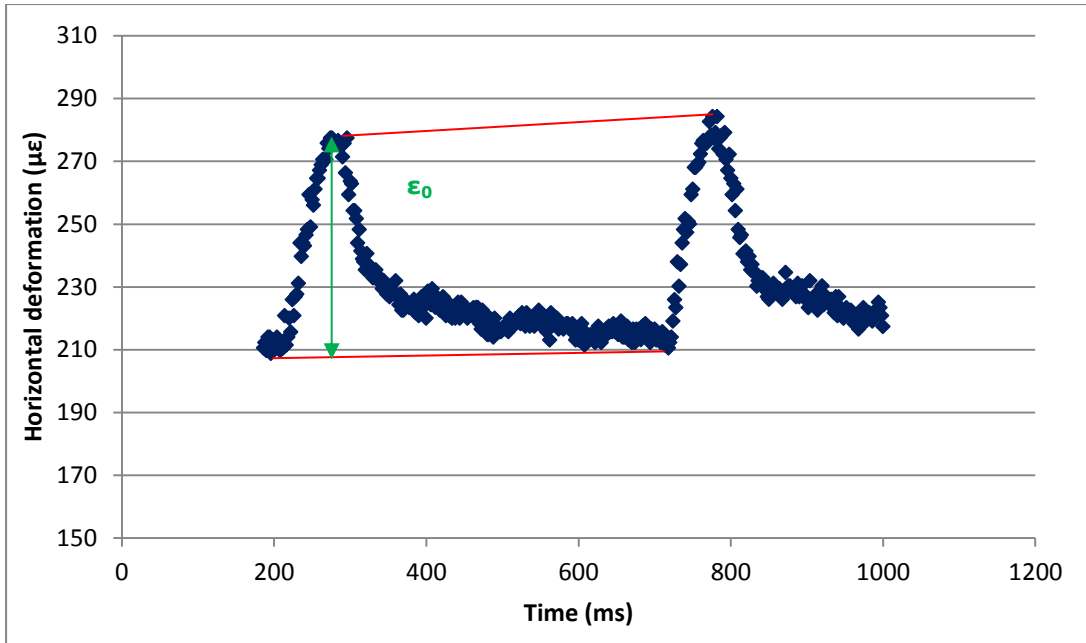


**Figure 133** Initial strain amplitude EN 12697-26:2004

According to EN 12697-24:2012, the tensile stress ( $\sigma_0$  in MPa) and strain ( $\epsilon_0$  in  $\mu\epsilon$ ) at the centre of the specimen shall be calculated using Equation 111, Equation 112 and Equation 113. The new standard introduces the resilient (or recoverable) strain value ( $\epsilon_{0,in}$  in  $\mu\epsilon$ ) : this is the total horizontal deformation at the 100<sup>th</sup> load pulse minus the plastic deformation ( $\epsilon_{pl,in}$  in  $\mu\epsilon$ ). See Figure 134.

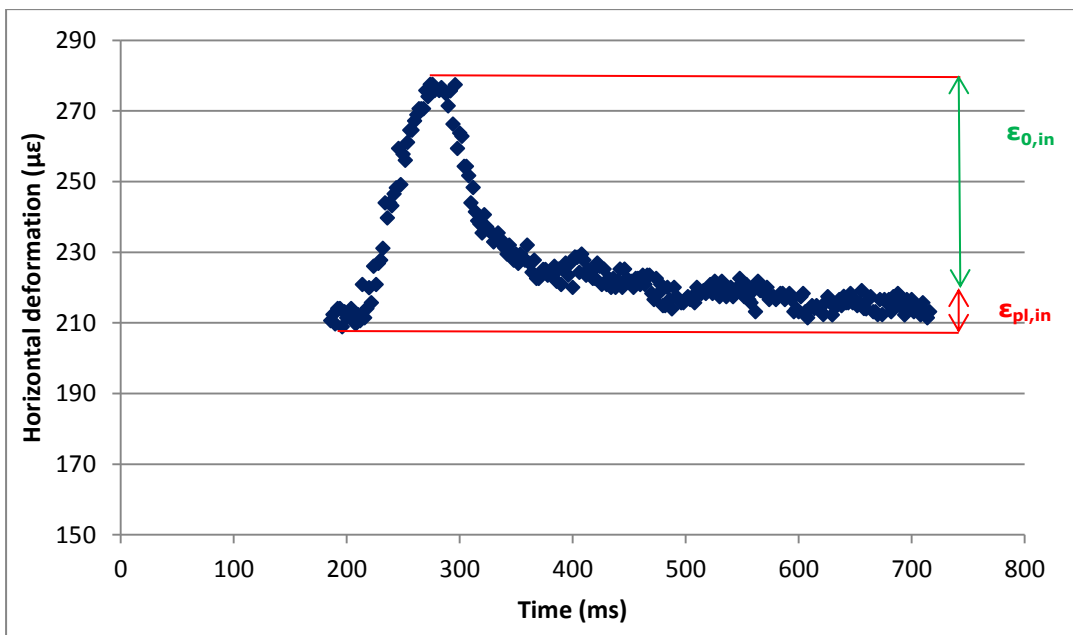


**Figure 134** Initial resilient strain amplitude EN 12697-24:2012

The ITFT in strain control mode was developed initially considering the strain according to EN 12697-24:2004. The first material to be tested was the 20mm DBM at 10°C at different strain levels between 125 and 220  $\mu\epsilon$  (see Figure 135). Subsequently, the ITFT in strain control mode was developed considering the resilient strain value ( $\epsilon_{0,in}$  in  $\mu\epsilon$ ) constant during the fatigue test, according to the new standard EN 12697-24:2012; the tested material was the 10mm DBM (see Figure 136). In both cases (for both materials: 10mm DBM and 20mm DBM), fatigue tests were undertaken also in stress control mode.

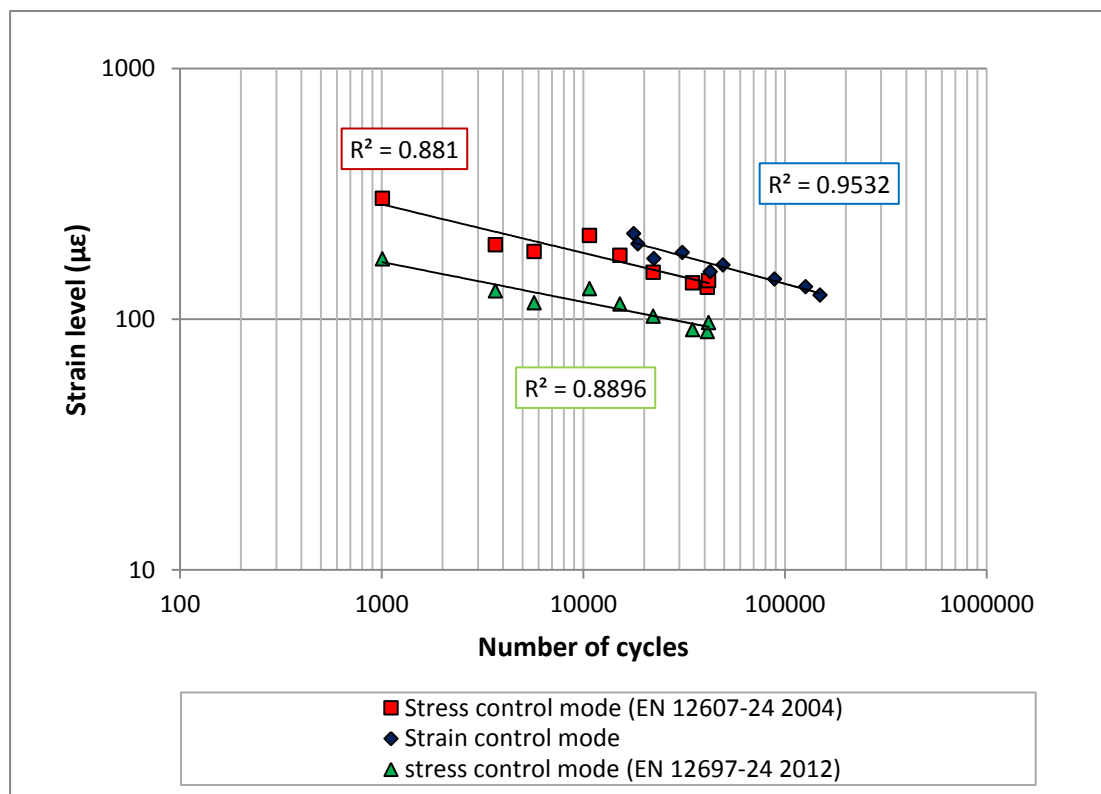


**Figure 135** Fatigue life obtained in stress and strain control modes (20mm DBM)

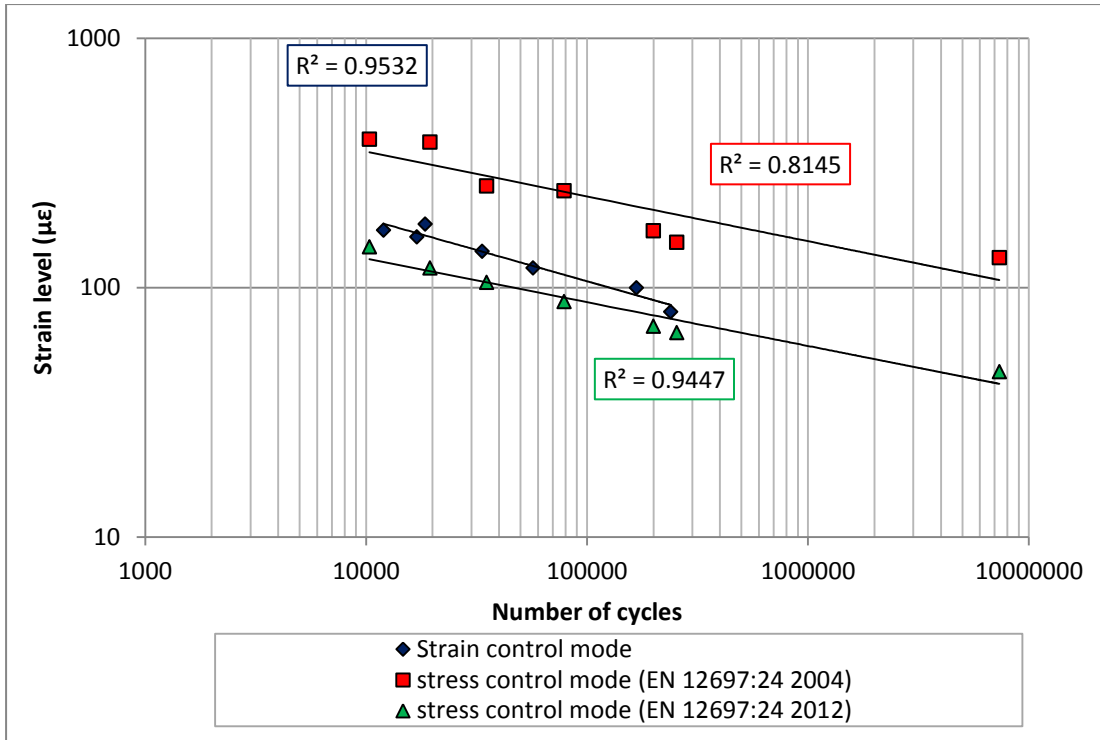


**Figure 136** Fatigue life obtained in stress and strain control modes (10mm DBM)

Fatigue life strongly depends on the definition of initial strain; as it can be noticed there is a big different between fatigue lines. The resilient strain was chosen as the strain to apply during a fatigue test because permanent deformation is not included (EN 12697-24:2012); therefore strain amplitude in the oldest standard (EN 12697-24:2004) is bigger than in the new standard. This allows a more reasonable comparison between ITFT (in strain control mode) and other fatigue tests such as 4PB and 2PB.

Statistically, a comparison between the three regression lines was made for the 10mm DBM. In this case, the t test was used to better evaluate the difference between the stress control fatigue lines (strain levels were calculated considering EN 12697-24:2004 and 2012). Results show that strain control and stress control fatigue (2012) lines have similar regression lines; strain control and stress control (2004) fatigue lines are different for the 10mm DBM after the new calibration (see Table 18). The aim of the calibration was to allow researchers to make a more reasonable comparison between ITFT and bending tests, avoiding including permanent deformation in the calculation of the strain.

**Table 18** Strain control fatigue life vs stress control fatigue life – 10mm DBM

10mm DBM			
Case	Slope	Elevation	Results
Strain vs Stress (2004)	$t=2.414 > t_{0.05(2),10}=2.228$	-	Regressions are not the same for a significance level $\alpha=0.05$
Strain vs Stress (2012)	$t=0.64 < t_{0.05(2),10}=2.228$	$t=0.3 < t_{0.05(2),10}=2.228$	Regressions have same slopes and elevations

### 7.6.2 Fatigue life: dissipated energy

As discussed previously, the development of the ITFT in strain control mode also included the development of dissipated energy concepts during a fatigue test. Thus different dissipated energy methods were considered and comparisons with the traditional approach were made for ITFT undertaken on 10mm DBM. The criteria chosen were: traditional method (Nf,50), Dissipated Energy Ratio (N1, Pronk), Energy Ratio (N1, Rowe) and RDEC method (PV). Figure 137, Figure 138 and Figure 139 show the fatigue lives obtained from the different dissipated energy methods at 10°C in strain control mode. As for the 2PB and 4PB, the Energy Ratio method by Pronk generates fatigue life values smaller than the traditional method (the two trend lines almost coincide though). The same method reviewed by Rowe generates fatigue life values bigger than the Nf,50 values. Nfm generates fatigue lives slightly bigger than Nf,50.

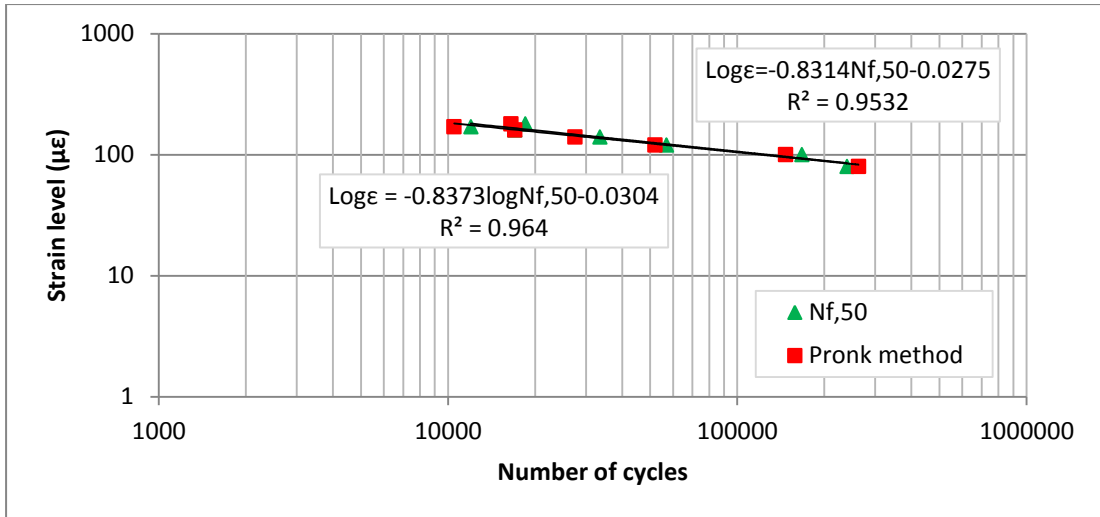


**Figure 137** Fatigue lives obtained by means of Dissipated Energy Ratio (Pronk) and traditional methods

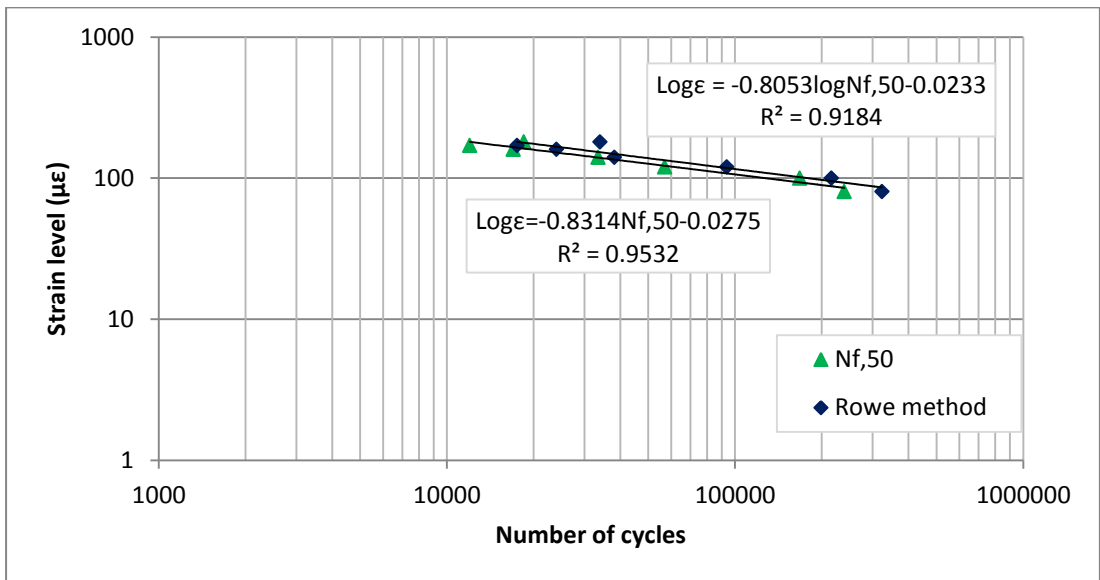


**Figure 138** Fatigue lives obtained by means of Energy Ratio (Rowe) and traditional methods

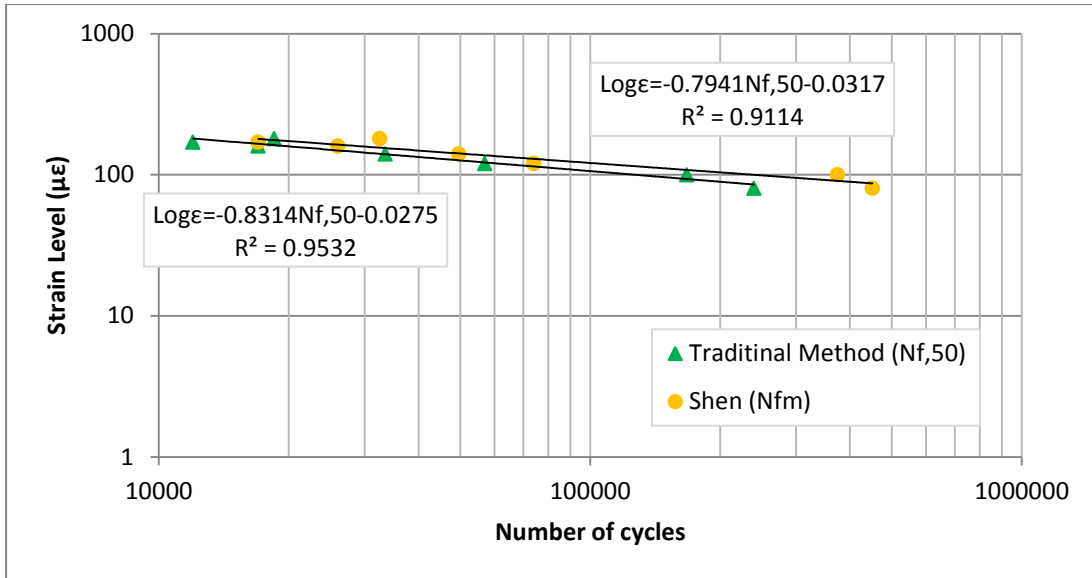


**Figure 139** Fatigue lives obtained by means of RDEC (Shen) and traditional methods

Regression lines were calculated for each case and then compared by using the appropriate statistical method. Statistically, first the hypothesis of equality between slopes of different regressions was tested with the analysis of covariance (ANCOVA); the hypothesis is  $H_0: \beta_1 = \beta_2 = \dots = \beta_k$ ; the hypothesis was confirmed by the Fisher test; Therefore, regression lines obtained from different dissipated energy methods statistically have the same slopes and elevations. Results are shown in Table 19.

**Table 19** DE method comparison by using Dunnett's test

Case	Slope	Elevation	Results
Nf,50 - DER - ER - Nfm	$F=0.61 < F_{0.05(1),3,20}=3.1$	$F=2.59 < F_{0.05(1),3,20}=3.1$	Regressions have same slope and elevation for a significance level $\alpha=0.05$

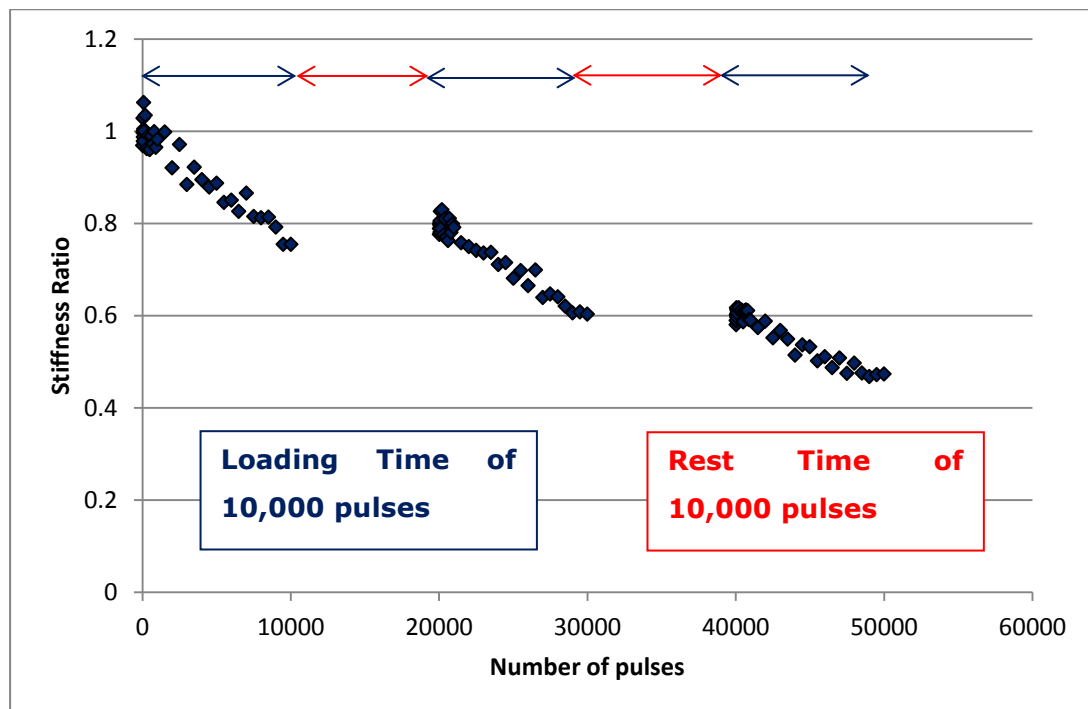
### 7.6.3 Fatigue life: healing

Healing was involved in this study (only the 10mm DBM was tested for the healing analysis). Healing tests were undertaken at 10°C; the applied strain was 160µε for each test and four different rest time periods and three different loading time periods were considered. Table 20 shows the nine combinations of loading time and rest time chosen for the healing tests.

**Table 20** Loading times and rest times (in number of pulses)

Number of pulses	
Loading time	Rest time
5,000	1,000
	5,000
	10,000
	15,000
10,000	5,000
	10,000
15,000	5,000
	10,000
	15,000

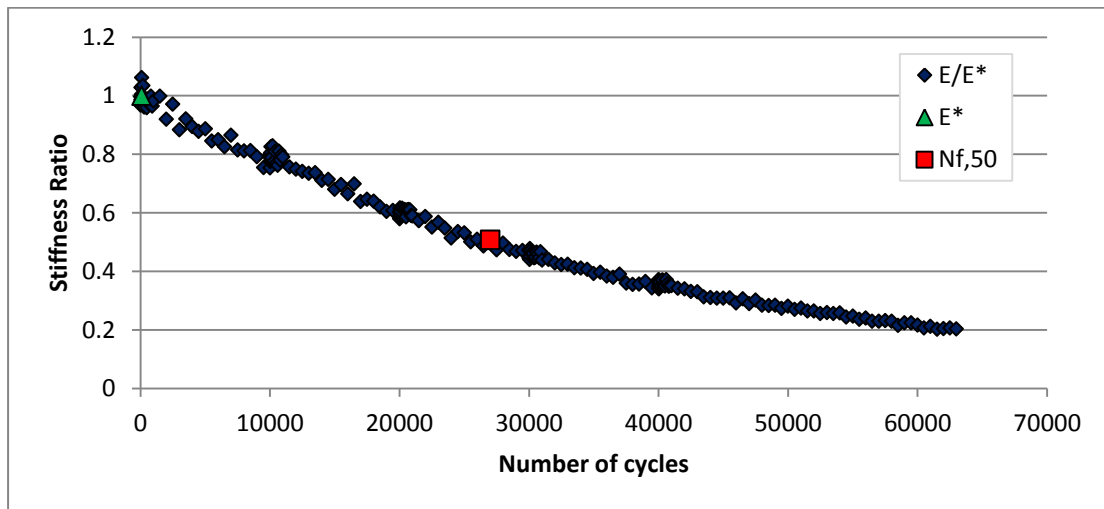
A fatigue test usually is divided in several stages of loading times and rest times. During the loading time,  $160 \mu\epsilon$  is applied on the specimen; during the rest time, the specimen is unloaded (no strain is applied in the specimen) as shown in Figure 140.



**Figure 140** Healing test: 10,000 pulse for each loading time stage and 10,000 pulse for each rest time stage

Figure 141 shows the behaviour of asphalt material during a fatigue test when healing is included in the test. In this particular case, the fatigue test was undertaken at  $160 \mu\epsilon$  at  $10^\circ\text{C}$ ; the specimen was loaded for 10,000 cycle (84 minutes) and it was left to rest for other 10,000 cycles (84 minutes). The

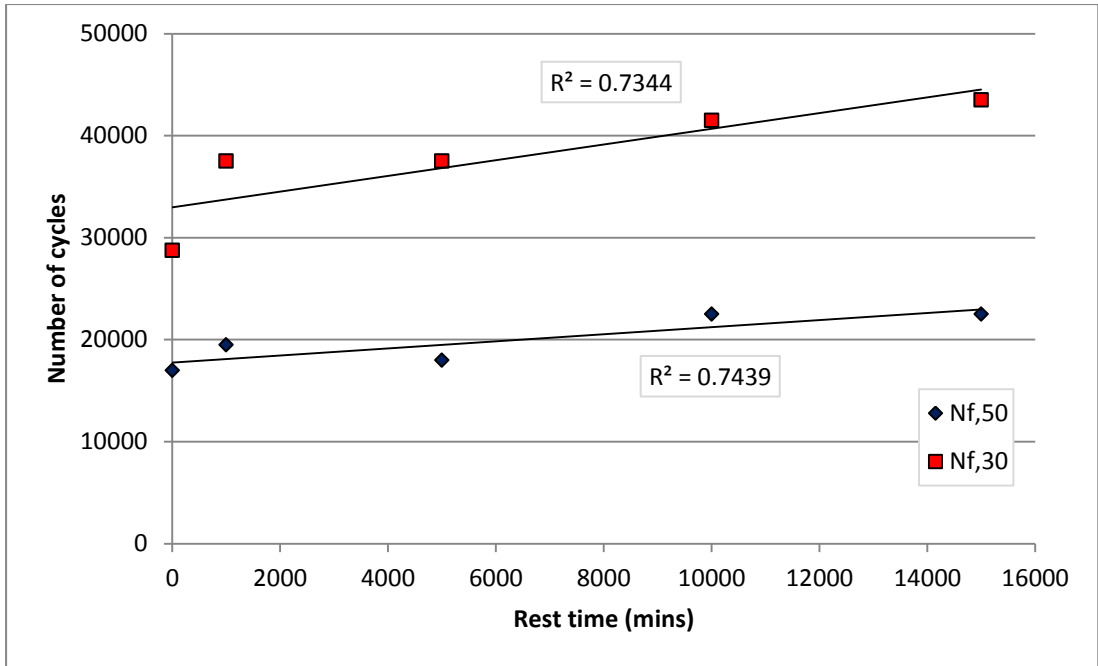
healing behaviour is less pronounced if ITFT data are compared with 4PB data; although fatigue life values are bigger when rest time is included in a fatigue test.



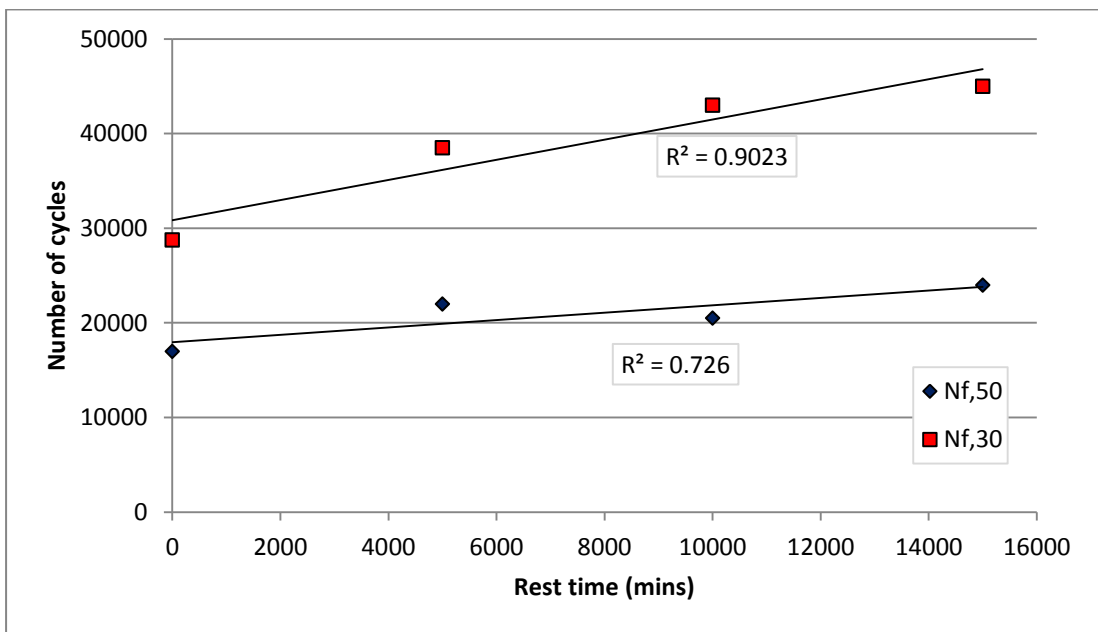
**Figure 141** Example of healing test (10,000 pulses of loading time and 10,000 pulses of rest time)

Figure 142 and Figure 143 show the number of cycles to failure ( $N_{f,50}$  and  $N_{f,30}$ ) for different rest time periods when loading time is constant (5,000 cycles corresponding to 42 minutes and 15,000 cycles corresponding to 126 minutes). Figure 144 and Figure 145 show the number of cycles to failure ( $N_{f,50}$  and  $N_{f,30}$ ) for different loading times when rest time is constant (10,000 pulses corresponding to 84 minutes and 15,000 pulses corresponding to 126 minutes). As for the 4PB, fatigue life decreases when loading time period decreases; it increases when rest time period increases.

As noted previously, the behaviour of asphalt material in tests with longer loading time periods is closer to a fatigue test without rest periods; that is because the first rest time period may happen after the fatigue phenomenon has already started in the specimen. The behaviour of asphalt material in tests with shorter rest time periods is closer to a fatigue test without rest period because the material does not have enough time to heal (to recover the stiffness).



**Figure 142** Number of cycles (Nf,50 and Nf,30) for different rest times (constant loading time = 5000 consecutive pulses)



**Figure 143** Number of cycles (Nf,50 and Nf,30) for different rest times (constant loading time = 15000 consecutive pulses)

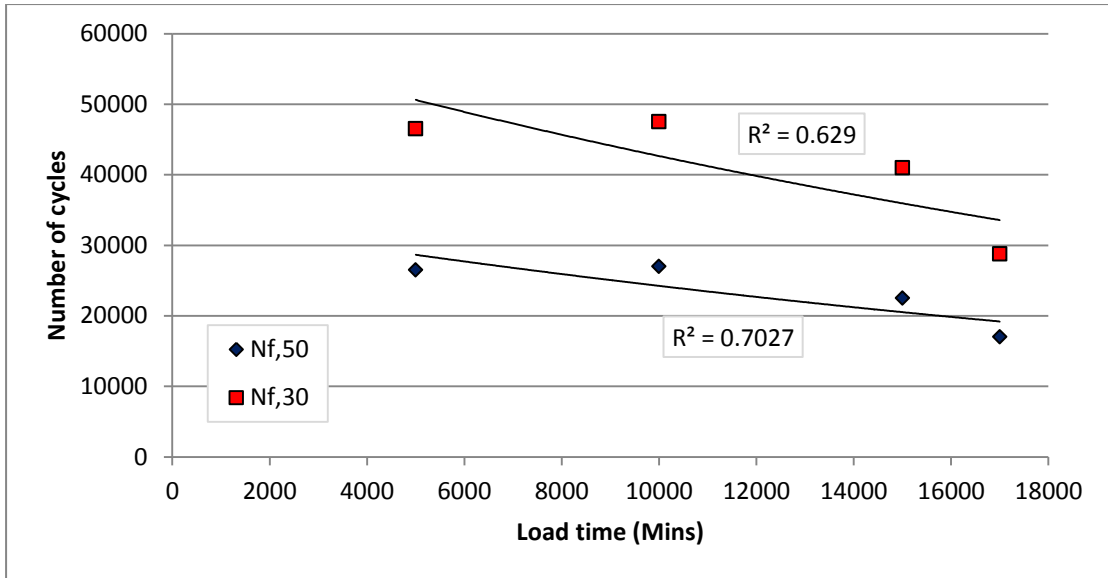


**Figure 144** Number of cycles (Nf,50 and Nf,30) for different loading times (constant rest time = 10,000 consecutive pulses)

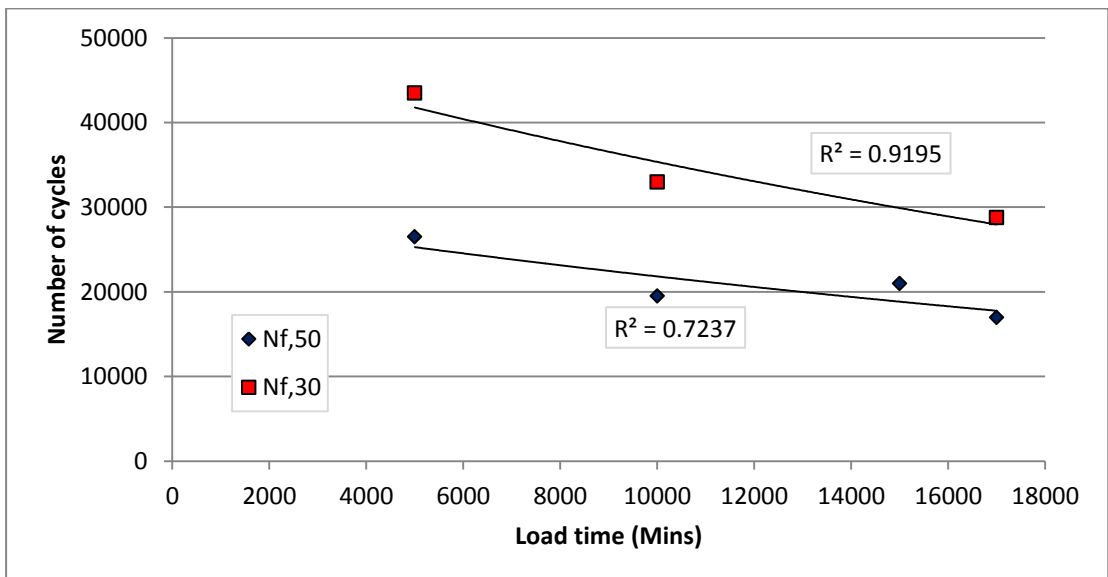
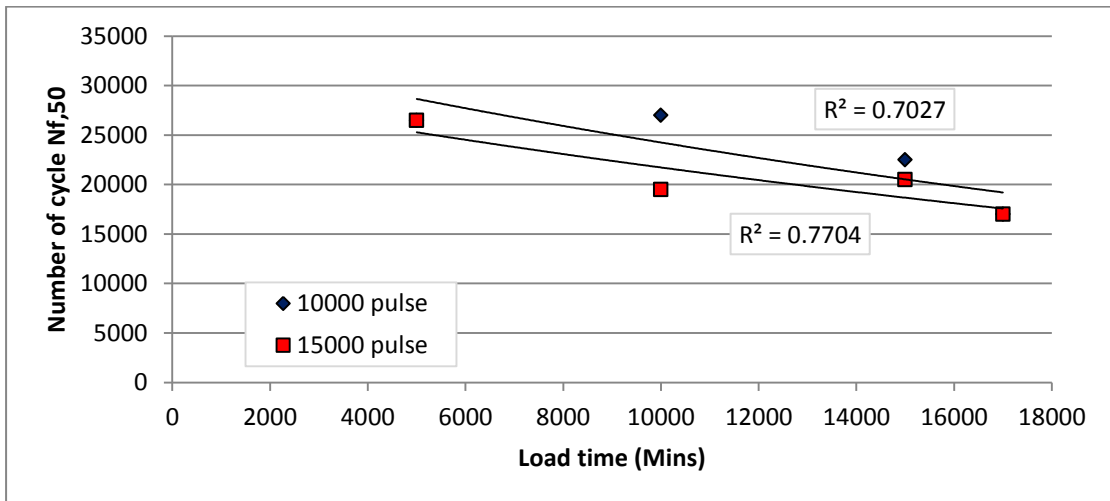


**Figure 145** Number of cycles (Nf,50 and Nf,30) for different loading times (constant rest time = 15,000 consecutive pulses)

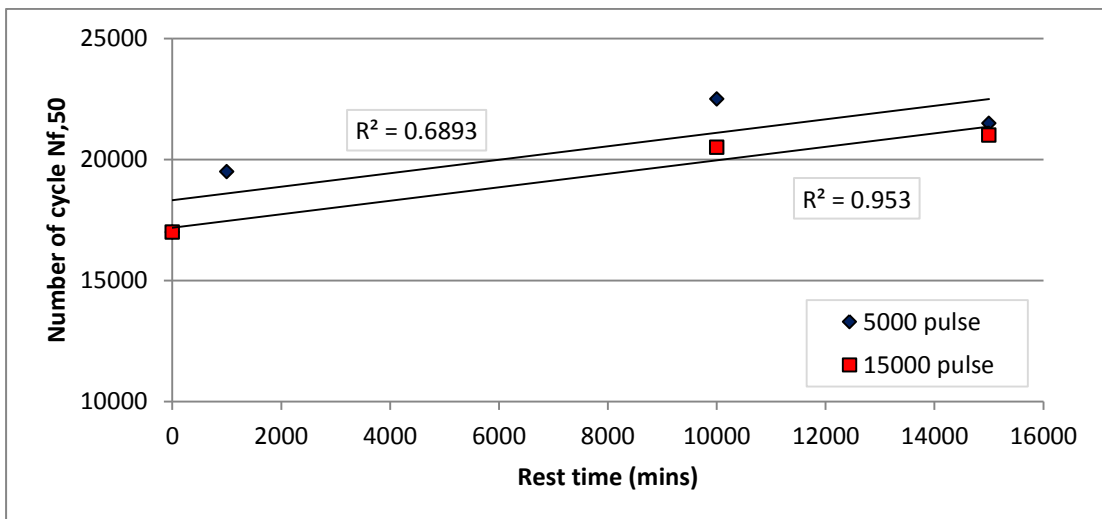
If fatigue tests at different constant rest times (10,000 and 15,000) are plotted for different loading times, it is noted that for a shorter rest time (10,000 pulses) fatigue lives are bigger than for a longer rest time (15,000 pulses). This is true for Nf,50 and Nf,30 values (see Figure 146).

Figure 147 shows instead Nf,50 plotted versus different rest times considering two constant loading times (5,000 and 15,000 pulses); also in this case, it was noted that fatigue life values are bigger when a loading time of 5,000 pulse is considered. This may be due to the accumulation of permanent deformation in

this kind of test. Permanent deformation is much more accumulated after 15,000 pulses than after 5,000 pulses, thus it is not easy to heal a bigger amount of accumulated permanent deformation for the asphalt material. Unfortunately only few healing data are used for this comparison (also only one material and one temperature condition was tested due to lack of time). Thus, further investigation should be carried out to verify if the results found are still valid for other asphalt mixtures and temperatures.



**Figure 146** Number of cycles (Nf,50) plotted vs different loading times considering two constant rest times (10,000 and 15,000 pulses)



**Figure 147** Number of cycles (Nf,50) plotted vs different rest times considering two constant load times (5,000 and 10,000 pulses)

Figure 148 and Figure 151 show the evolution of stiffness for different rest times and load time periods. Stiffness increases in every single case considered; although the maximum improvement in stiffness was obtained

when 10,000 pulses (84 minutes rest) was considered as either rest time or load time. Figure 149 and Figure 152 show the evolution of dissipated energy for different rest time and load time periods. Asphalt material dissipates more energy if a rest time is included due to the healing effects; the maximum amount of dissipated energy is registered when a rest time of 10,000 pulses is included. If load time changes, it seems to have an insignificant difference in terms of dissipated energy.

Total vertical deformation is shown in Figure 150 and in Figure 153. It is primarily an accumulation of small amounts of deformation happening at the end of each pulse. Asphalt material is characterised by two different stages: a zone of initial adjustment and a zone of stable condition where the behaviour of the total vertical deformation is linear. Some researchers (Kennedy, 1983) believe that a third stage exists, the failure zone; it corresponds to the complete failure of the specimen in which excessive vertical deformation develops; this stage was not recorded in the tests undertaken. In this study, it was found that the total vertical deformation is a function of the rest period (see Figure 150); it was not found to make a significant difference if the loading time changes in fatigue tests (see Figure 153). If the first stage is ignored, the experimental relationship between the total vertical deformation and the number of pulses for different rest times can be determined as shown in Figure 154.

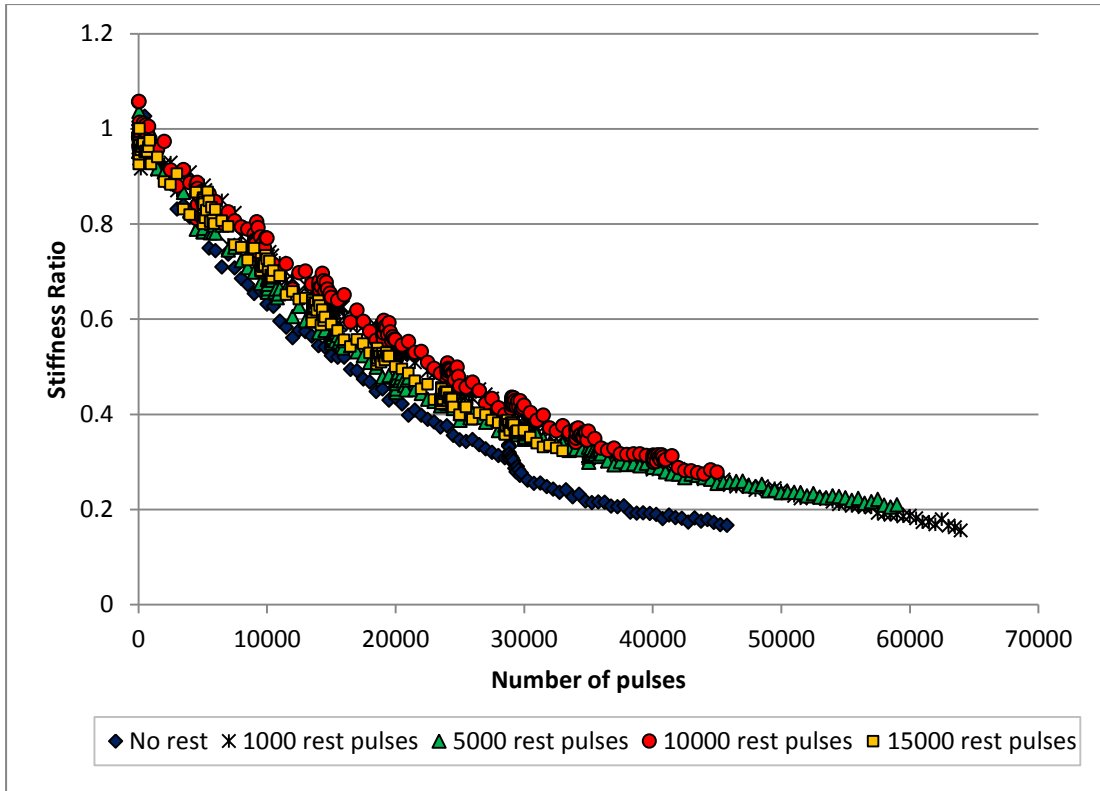


**Figure 148** Stiffness ratio for different rest times when load time is constant (5,000 pulses)

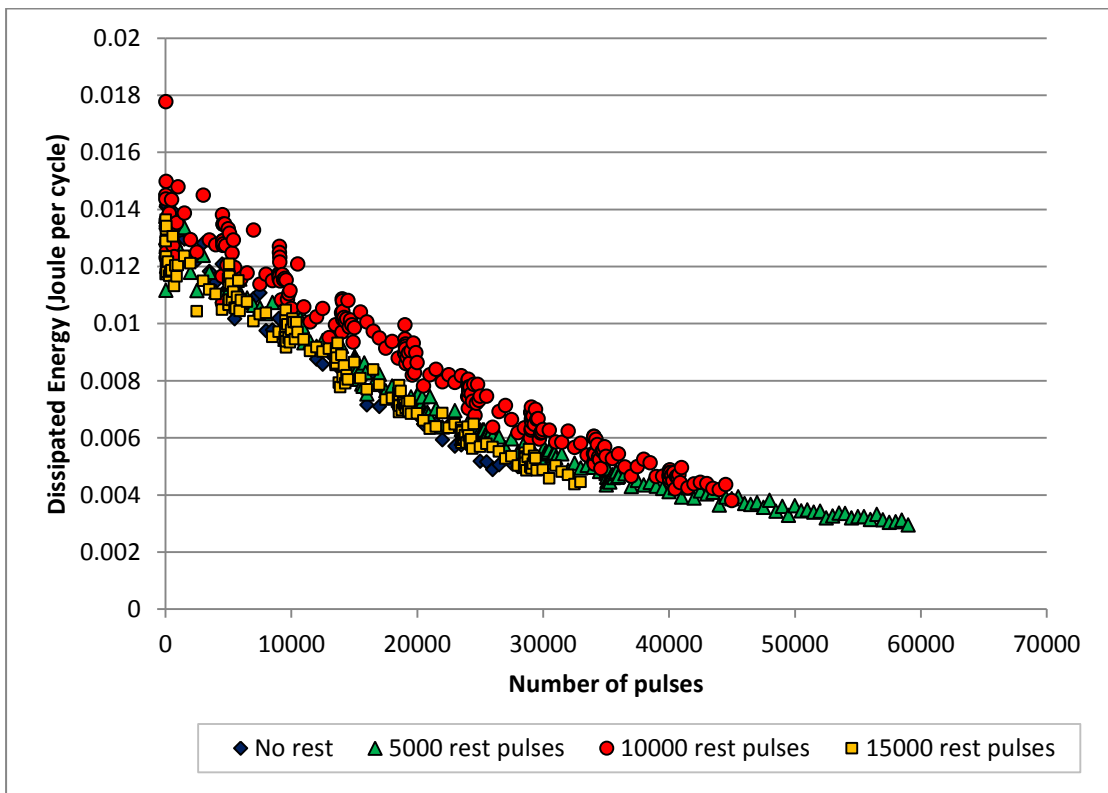


**Figure 149** Dissipated Energy for different rest times when load time is constant (5,000 pulses)

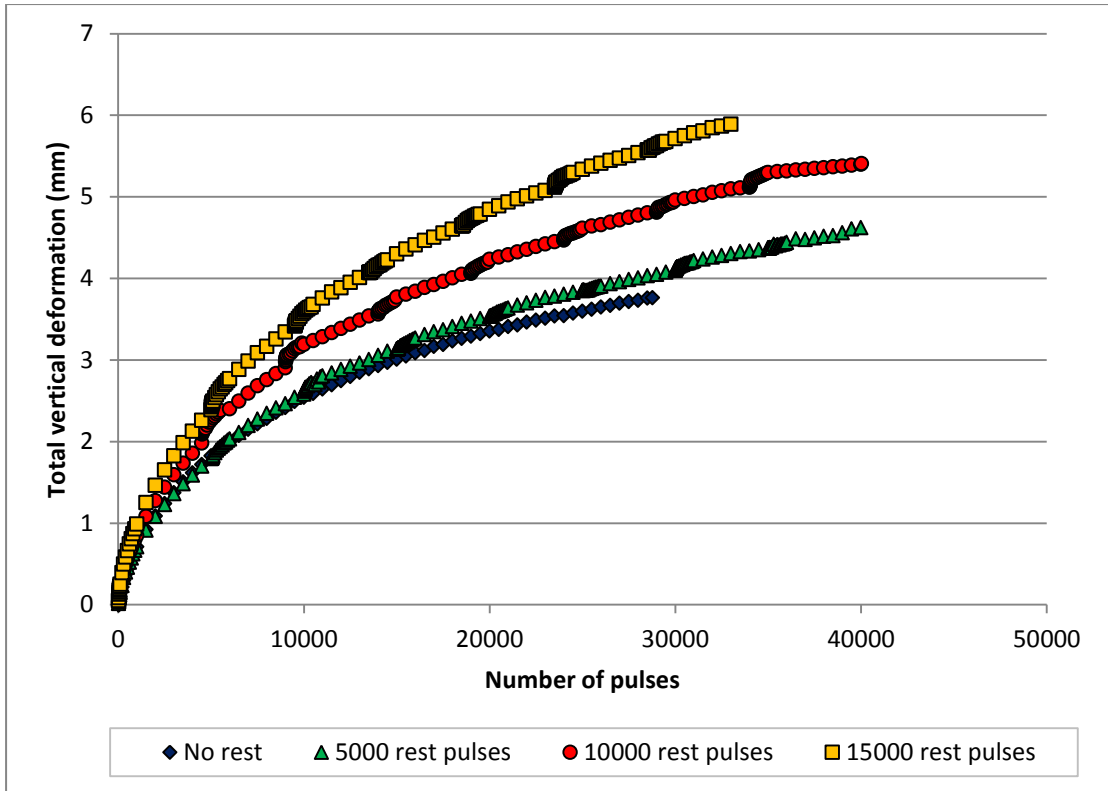


**Figure 150** Total vertical deformation for different rest times when load time is constant (5,000 pulses)

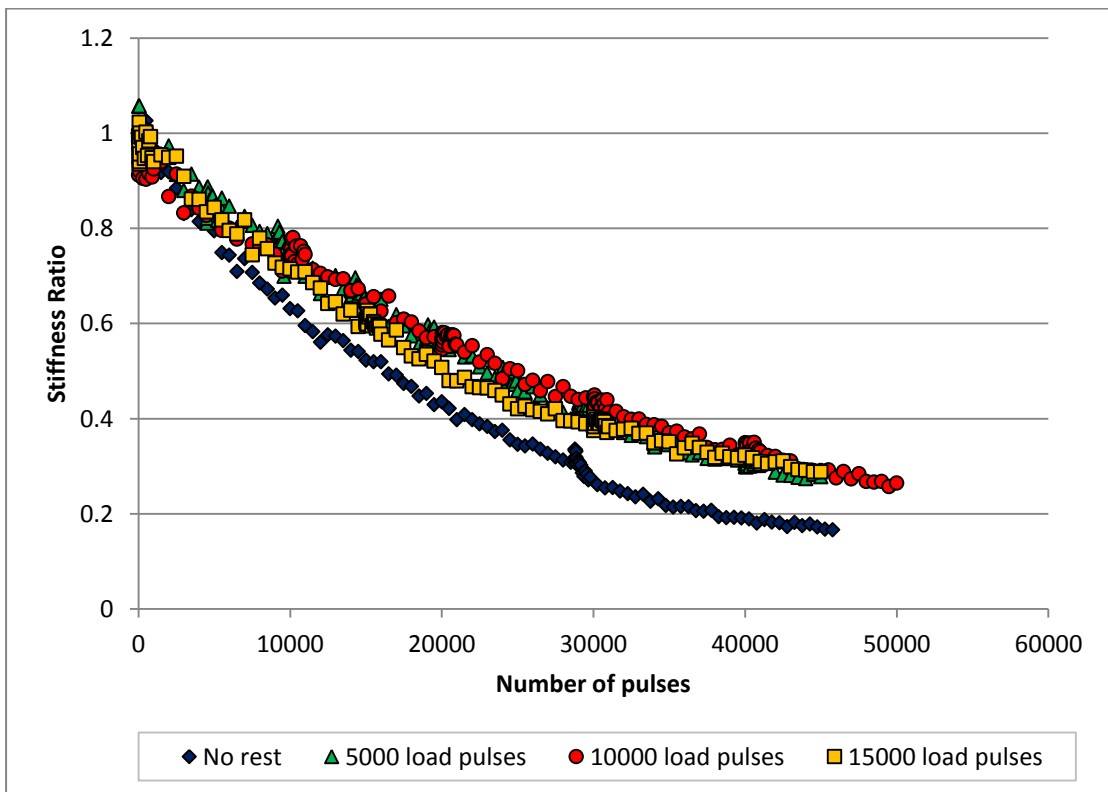


**Figure 151** Stiffness ratio for different load times when rest time is constant (10,000 pulses)

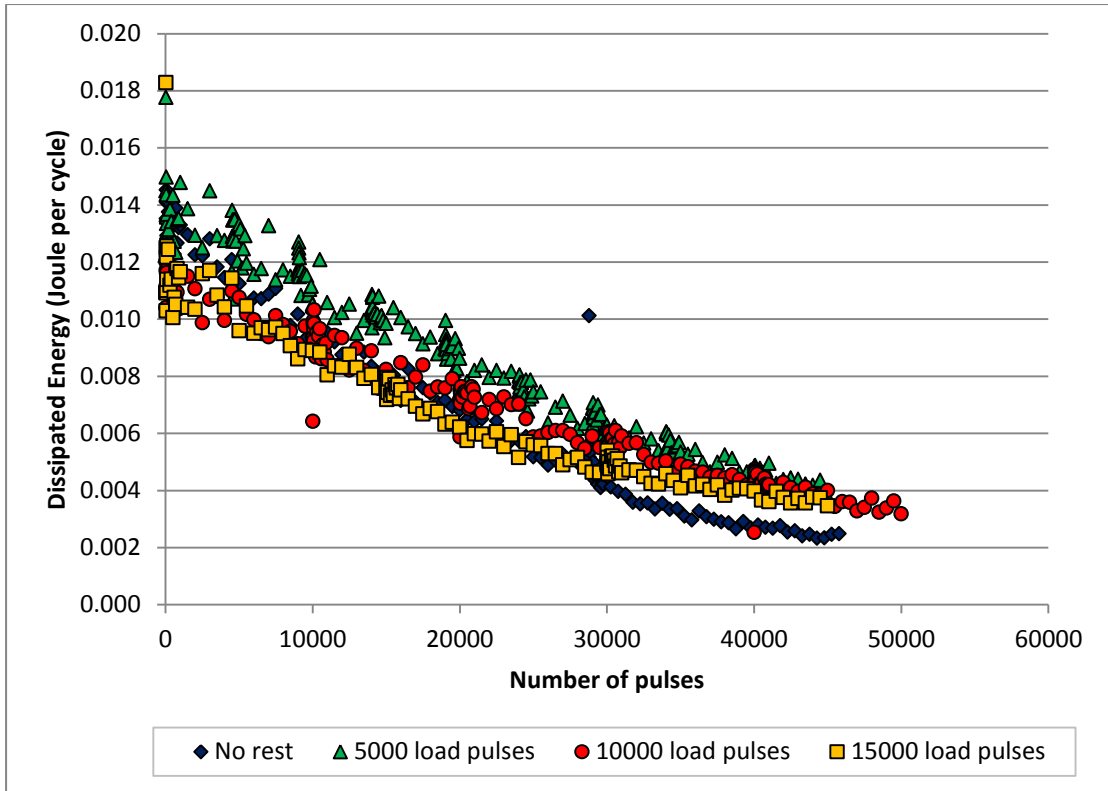


**Figure 152** Dissipated Energy for different load times when rest time is constant (10,000 pulses)

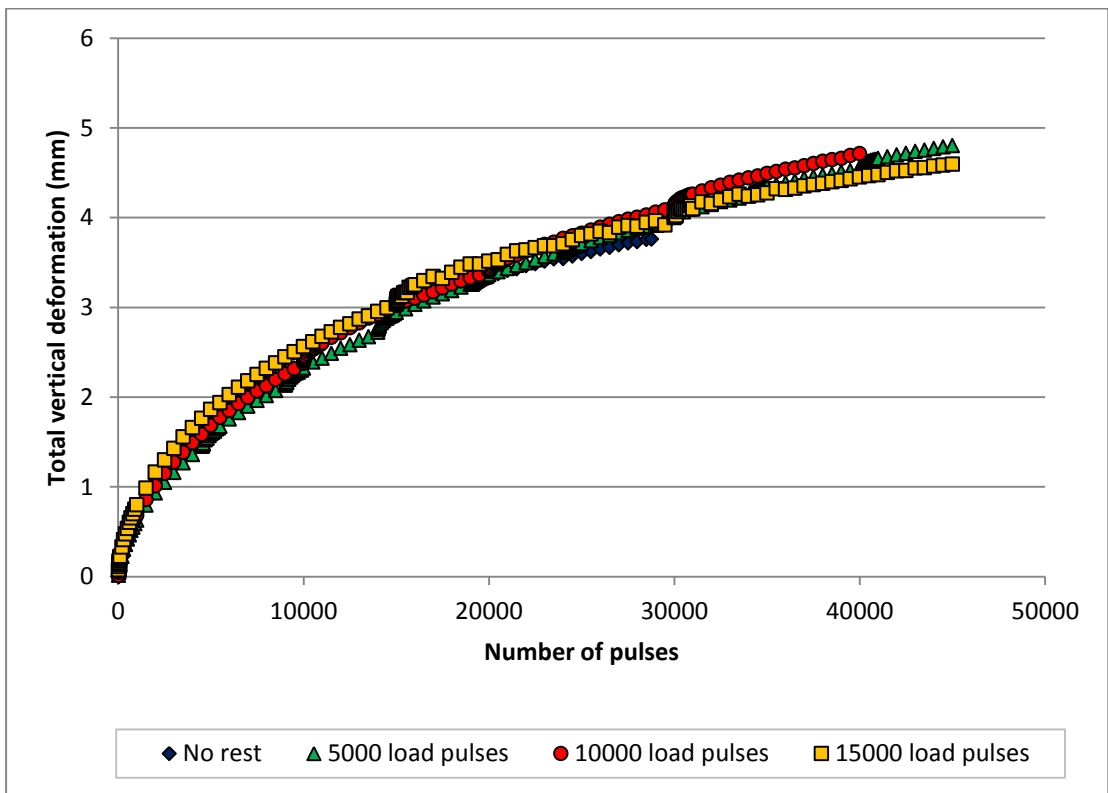


**Figure 153** Total vertical deformation for different load times when rest time is constant (10,000 pulses)

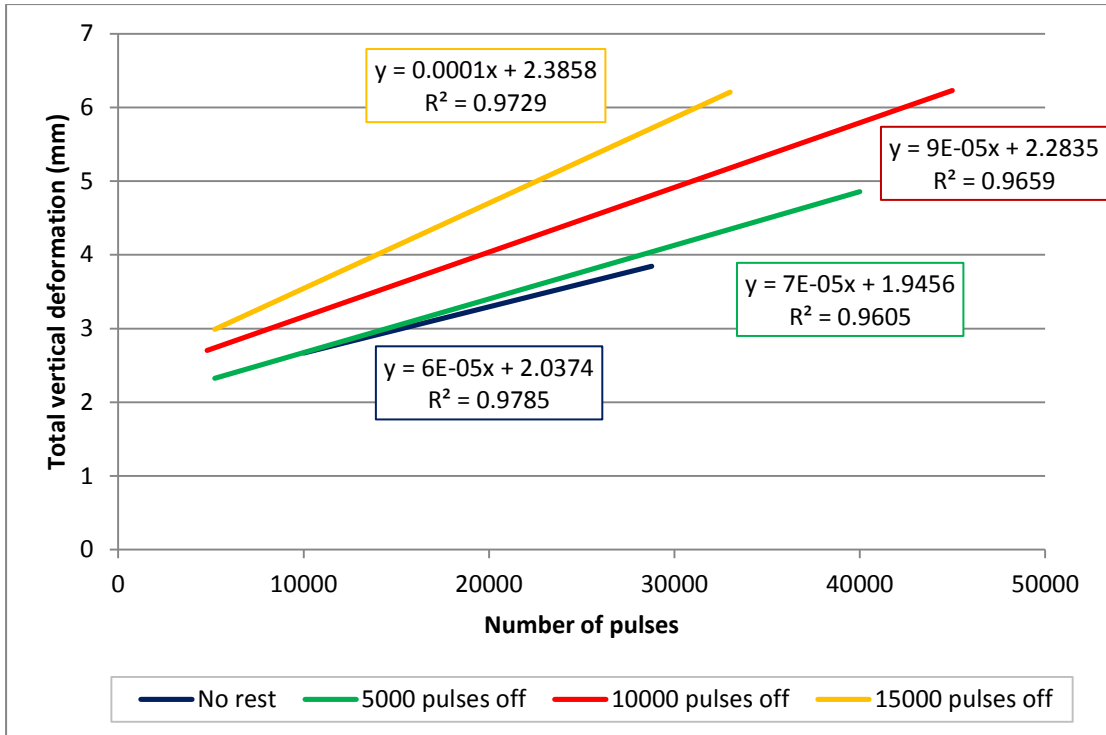


**Figure 154** Linear relationship between total vertical deformation and number of pulses for different rest times when load time is constant (5,000 pulses)

The Healing Ratio (HR) was determined with Equation 105. For different load time periods, when the loading time period increases, the healing ratio decreases; healing tests tend to have the same behaviour as a traditional fatigue test; this is because the specimen is already partially damaged after a longer loading time period and there is a higher amount of accumulated permanent deformation (see Figure 155).

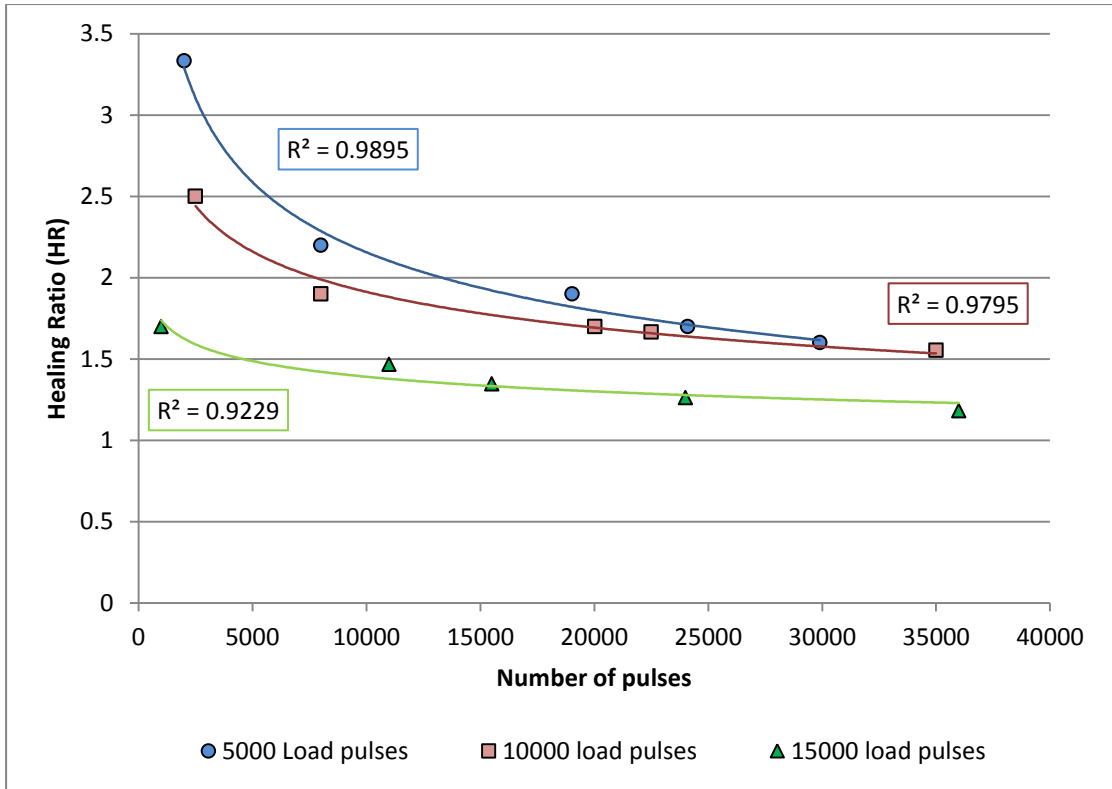


**Figure 155** Healing Ratio for different load time periods (fixed rest time = 10,000 pulses)

For different rest time periods, when the rest time period decreases, healing ratio decreases; healing test tends to have the same behaviour of a traditional fatigue test; shorter rest periods do not allow the specimens to heal deformations. If the rest time increases, HR increases up to a certain point; in the case of this project the maximum value of HR was reached for 10,000 pulses as the load time period (see Figure 156).

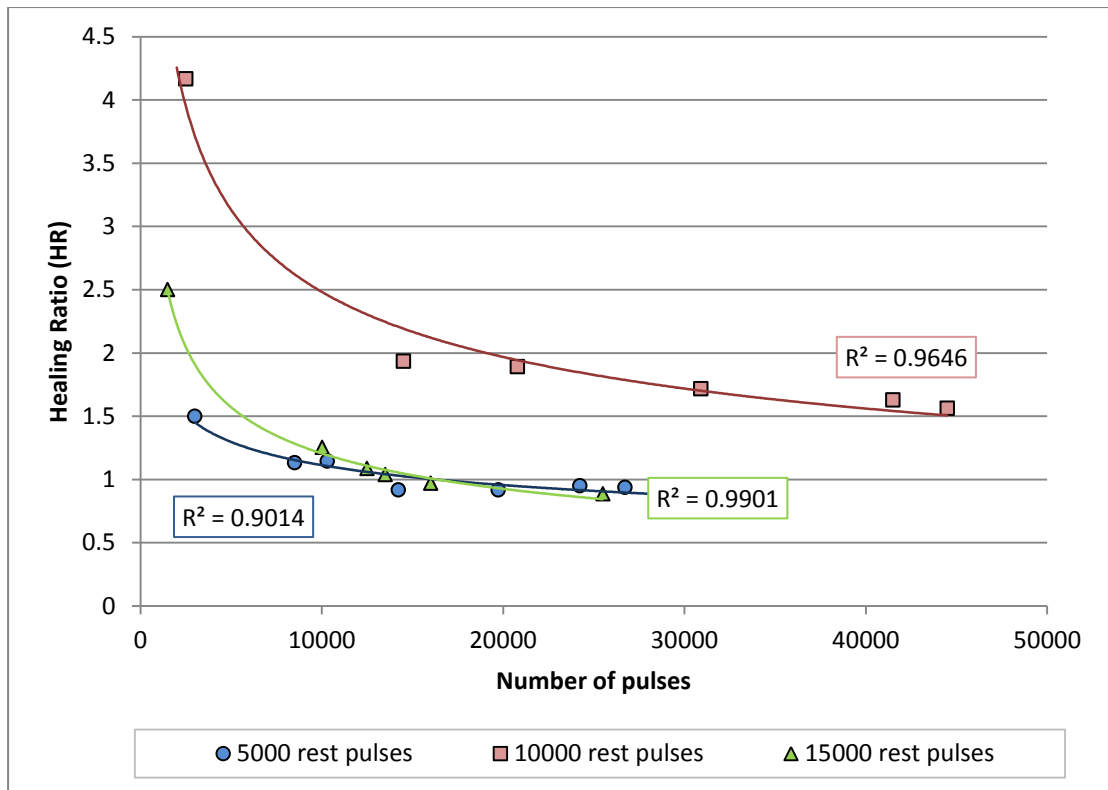


**Figure 156** Healing Ratio for different rest time periods (fixed load time = 10,000 pulses)

#### 7.6.4 Fatigue life: permanent deformation

Mode of loading was also compared in terms of permanent deformation for specimens tested at the same temperature (10°C) and same loading conditions (140µε in strain control mode and 600kPa=146µε in stress control mode). Permanent vertical deformation is shown in Figure 157 ; permanent horizontal deformation is shown in Figure 158.

In stress control mode, permanent deformation reaches higher values quicker (both horizontal and vertical) because strain increases during the test and it is characterised by three stages (as previously described): failure corresponds to the fracture in two halves of the specimen (see Figure 123); this is due to the increase of the strain level during a test. In strain control mode, the strain level is constant during the test and the evolution of permanent deformation is slower (both horizontal and vertical) and it is characterised by two stages: the specimen does not reach complete failure; as a consequence localised deformation at the edge of the loading strips is observed in the specimen (see Figure 126).

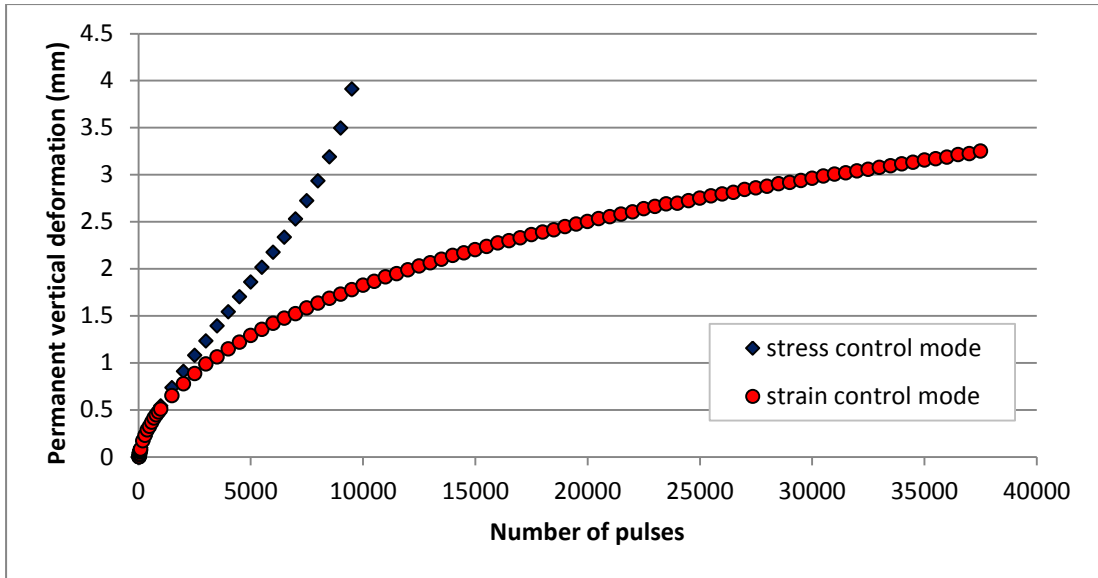


**Figure 157** Permanent vertical deformation depending on the mode of loading

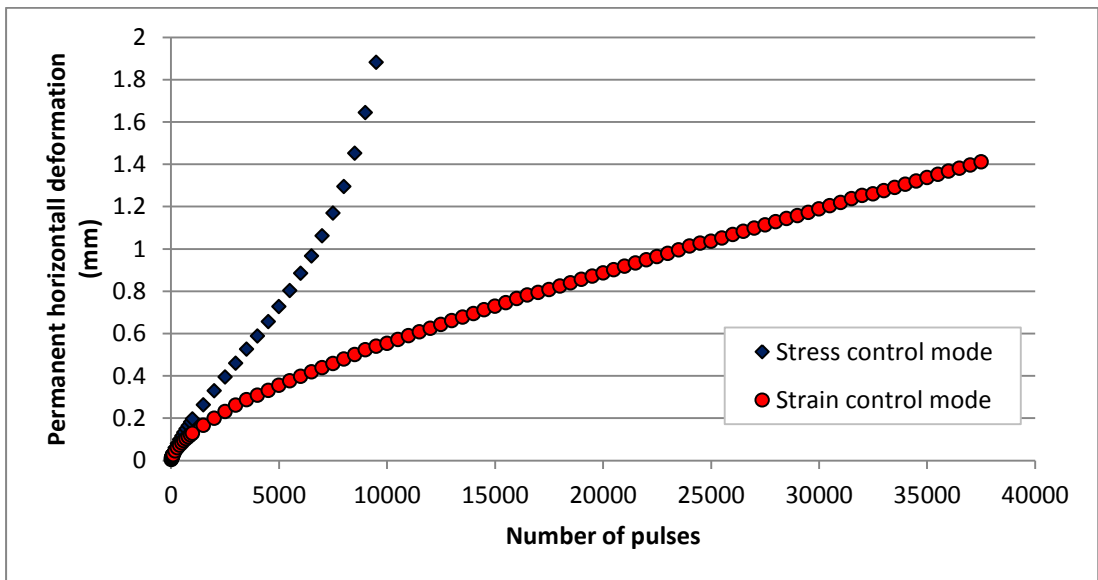


**Figure 158** Permanent horizontal deformation depending on the mode of loading

## 7.7 ITFT and other fatigue tests

As presented in Chapter 4, several fatigue tests have been undertaken by means of different testing machines, under different loading conditions. A summary is shown in Table 4 and

Table 5 (see Paragraph 4.7).

A final comparison was made for the three machines used in this project for the 10mm DBM; fatigue curves obtained by the traditional method (Nf,50) at 10°C in strain control mode is shown in Figure 159; comparisons in terms of dissipated energy (DER, ER and Nfm methods) are shown in Figure 160,

Figure 161 and Figure 162. Graphically, fatigue life depends on the test used. In all cases, fatigue curves obtained by ITFT are characterised by smaller value of fatigue life than 2PB and 4PB; this is due to the accumulation of permanent deformation during the test in addition to fatigue damage. In all cases, fatigue lives obtained by 2PB are smaller than values obtained by 4PB; this may be linked to the manufacture and shape of the specimen. Trapezoidal shape is not easy to obtain compared to the trapezoidal shape and the specimen may be affected by during the sawing time; also, stresses and strains in the specimen is not homogenous in the trapezoidal specimen as in the prismatic specimen (between inner clamps).

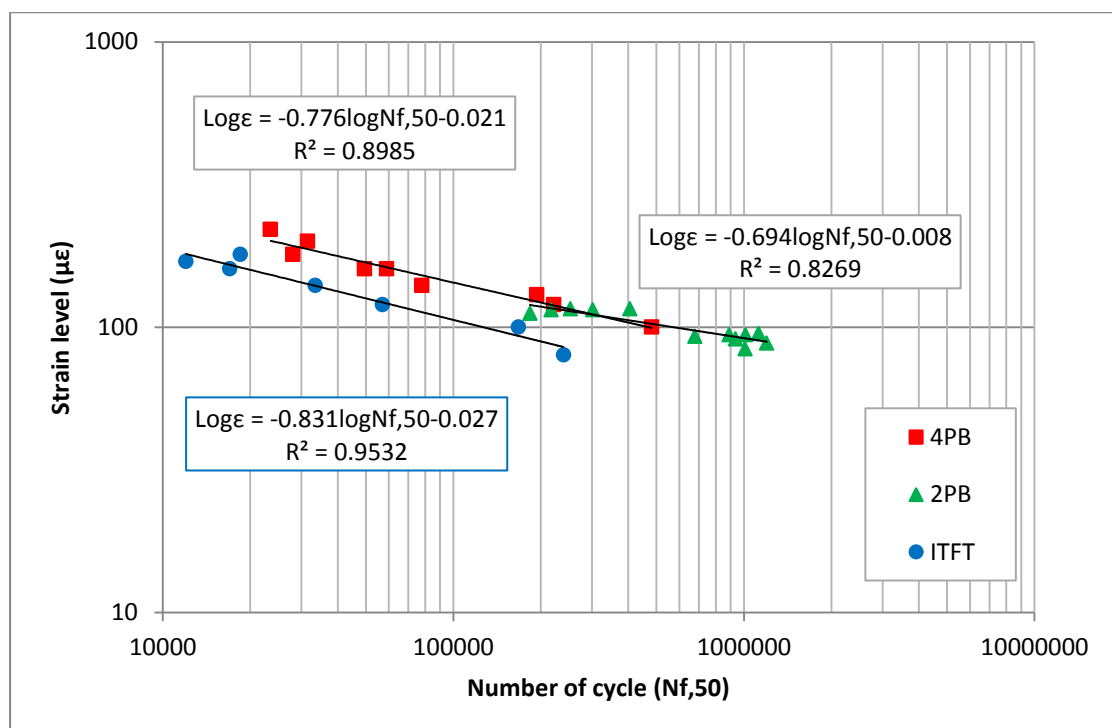


**Figure 159** Fatigue life obtained in strain control mode, at 10°C by means of 2PB, 4PB and ITFT according to the phenomenological method ( $N_{f,50}$ ) for the 10mm DBM

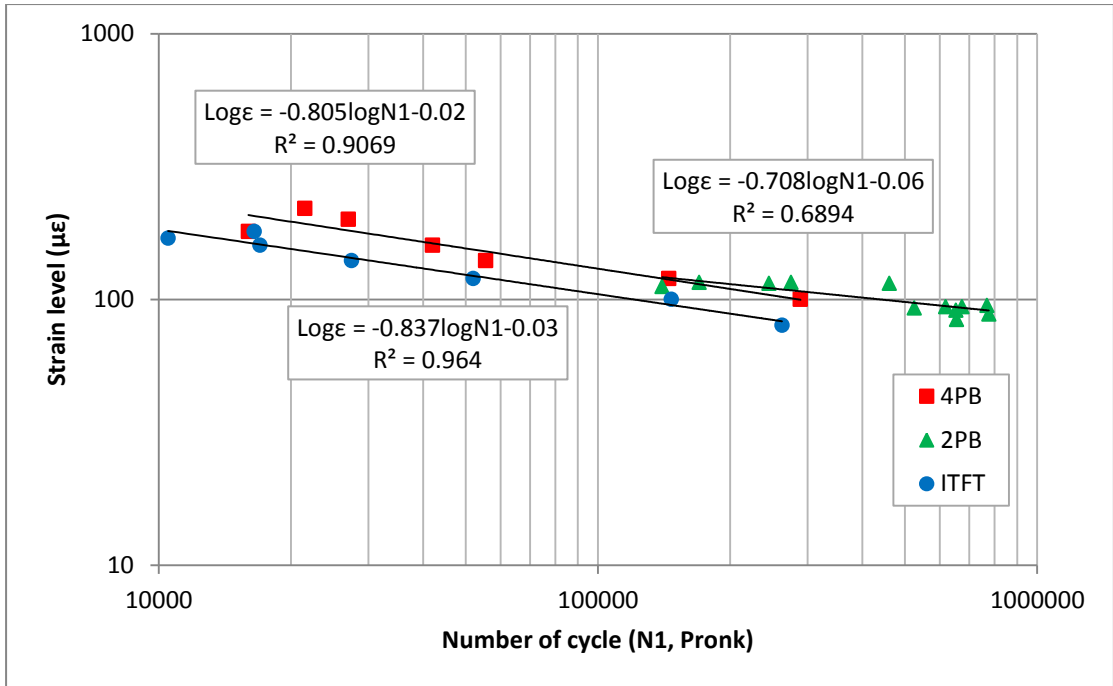


**Figure 160** Fatigue life obtained in strain control mode, at 10°C by means of 2PB, 4PB and ITFT according to the Dissipated Energy Ratio (Pronk) for the 10mm DBM

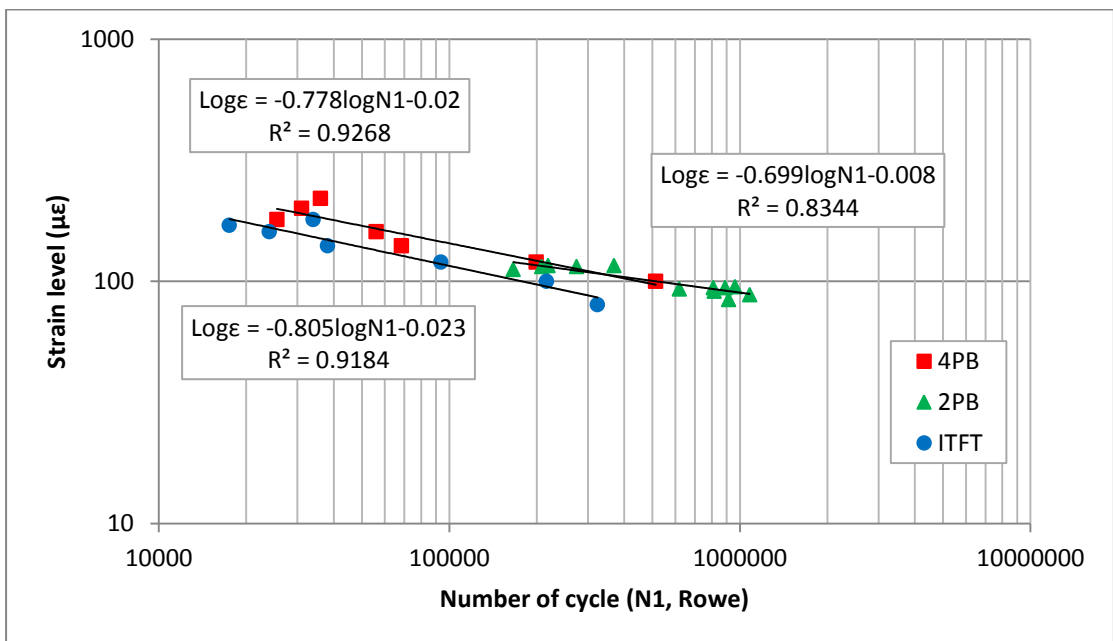


**Figure 161** Fatigue life obtained in strain control mode, at 10°C by means of 2PB, 4PB and ITFT according to the Energy Ratio (Rowe) for the 10mm DBM

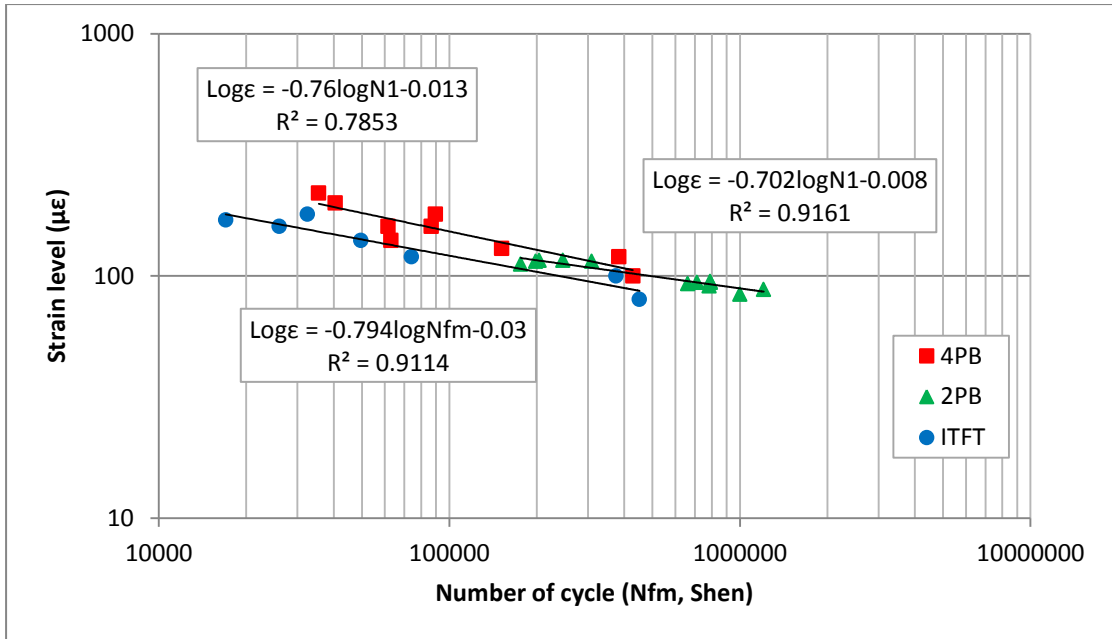


**Figure 162** Fatigue life obtained in strain control mode, at 10°C by means of 2PB, 4PB and ITFT according to the RDEC (Shen) for the 10mm DBM

Statistically, a comparison between the three regression lines was made in each scenario. First the hypothesis of equality between slopes of different regressions was tested with the analysis of covariance (ANCOVA); the hypothesis is  $H_0: \beta_1 = \beta_2 = \dots = \beta_k$  and it was rejected for a significance level of 0.05. In this case, Tukey's test was used to better evaluate the difference between each possible pairs of slopes in the group of the three regressions. Results show that fatigue regression lines obtained from ITFT and 4PB tests are characterised by similar regression lines (they have same slope but slightly different elevation in each case analysed); fatigue results may be independent of the fatigue testing machine but more fatigue tests are needed to confirm this finding. Opposite results are obtained if fatigue lives obtained by means of ITFT and 2PB are compared; the two regression line in all cases are different. Also 2PB and 4PB give similar fatigue results and this was noted previously when 2PB and 4Pb fatigue life values were compared with the *t* test (see Table 21, Table 22, Table 23 and Table 24).

**Table 21** ITFT, 2PB and 4PB – Phenomenological approach (Nf,50)– Tukey’s Test

Case	Slope	Elevation	Results
ITFT – 2PB – 4PB	$F=19.6 > F_{0.05(1),2,22}=3.44$	-	Regressions are not the same for a significance level $\alpha=0.05$
ITFT – 2PB	$q=8.26 > q_{0.05,22,3}=3.55$	-	Regressions are not the same
ITFT – 4PB	$q=2.96 < q_{0.05,22,3}=3.55$	$q=3.78 > q_{0.05,22,3}=3.55$	Regressions have same slope but not elevations
2PB – 4PB	$q=1.6 < q_{0.05,22,3}=3.55$	$q=1.79 < q_{0.05,22,3}=3.55$	Regressions have same slope and elevation

**Table 22** ITFT, 2PB and 4PB – DER approach – Tukey’s Test

Case	Slope	Elevation	Results
ITFT – 2PB – 4PB	$F=10.9 > F_{0.05(1),2,20}=3.49$	-	Regressions are not the same for a significance level $\alpha=0.05$
ITFT – 2PB	$q=7.64 > q_{0.05,22,3}=3.55$	-	Regressions are not the same
ITFT – 4PB	$q=1.62 < q_{0.05,22,3}=3.55$	$q=3.73 > q_{0.05,22,3}=3.55$	Regressions have same slope but not elevations
2PB – 4PB	$q=1.5 < q_{0.05,22,3}=3.55$	$q=1.02 < q_{0.05,22,3}=3.55$	Regressions have same slope and elevation

**Table 23** ITFT, 2PB and 4PB –ER approach – Tukey’s Test

Case	Slope	Elevation	Results
ITFT – 2PB – 4PB	$F=13.6 > F_{0.05(1),2,20}=3.49$	-	Regressions are not the same for a significance level $\alpha=0.05$
ITFT – 2PB	$q=6.65 > q_{0.05,22,3}=3.55$	-	Regressions are not the same
ITFT – 4PB	$q=1.41 < q_{0.05,22,3}=3.55$	$q=3.69 > q_{0.05,22,3}=3.55$	Regressions have same slope but not elevations
2PB – 4PB	$q=0.9 < q_{0.05,22,3}=3.55$	$q=0.94 < q_{0.05,22,3}=3.55$	Regressions have same slope and elevation

**Table 24** ITFT, 2PB and 4PB –RDEC approach – Tukey’s Test

Case	Slope	Elevation	Results
ITFT – 2PB – 4PB	$F=9.77 > F_{0.05(1),2,22}=3.44$		Regressions are not the same for a significance level $\alpha=0.05$
ITFT – 2PB	$q=5.83 > q_{0.05,22,3}=3.55$	-	Regressions are not the same
ITFT – 4PB	$q=1.95 < q_{0.05,22,3}=3.55$	$q=3.65 > q_{0.05,22,3}=3.55$	Regressions have same slope but not elevations
2PB – 4PB	$q=1.9 < q_{0.05,22,3}=3.55$	$q=3.23 < q_{0.05,22,3}=3.55$	Regressions have same slope and elevation

## 7.8 Summary

IT-CY and ITFT are presented in this chapter. A detailed description of the test in stress control mode, the production of specimens and configuration of the machine is presented. The main part of the chapter focused on the development of a new testing procedure: the ITFT in strain control mode.

The following conclusions can be drawn for this chapter:

- In terms of stiffness, three temperatures were considered to better understand the viscoelastic behaviour of the material. Stiffness values strongly decrease when temperature increases for this material (10mm DBM mixture with 100pen bitumen highly depends on the temperature). Ideally it is recommended to undertake stiffness test at 10°C to avoid that viscous effects influence the stiffness values of the material.
- In terms of fatigue, tests were undertaken in stress and strain control mode at different loading conditions. A comparison was made for the two modes of loading; it was necessary to calculate the initial strain for each fatigue test undertaken in stress control mode (to compare the modes of loading). Mainly two different standards (EN 12697-24:2012 and EN 12697-24:2004) were followed to calculate stress and strain. Test results show that EN 12697-24:2012 generates strain levels statistically not different to the strain levels applied during fatigue tests undertaken in strain control mode; this means that fatigue lines statistically do not have

significant difference when EN 12697-24:2012 is used to calculate initial strain levels. This finding allows a more reasonable comparison between ITFT and bending tests, avoiding including permanent deformation in the calculation of the strain.

- Dissipated energy methods were also used to determine fatigue life values; statistically no significance difference was found between them. This means that they are giving the same answer in term of fatigue life as the traditional method ( $N_f, 50$ ). The ITFT is consistent with the other tests used.
- In terms of healing, results show that HR decreases if loading time increases; it increases if resting time period increases up to certain limit. This is due to the accumulation of permanent deformation and shorter rest time periods do not allow the specimen to recover and heal properly. The optimum value was found to be 10,000 pulses loading; for higher values there is not a significant improvement in the fatigue life.
- ITFT is characterised by accumulation of permanent deformation during a test. In stress control mode, permanent deformation reaches higher values quicker (both horizontal and vertical) than in strain control mode. This is explained because strain increases during a fatigue test in stress control mode; it is constant in strain control mode, thus the evolution of the strain is characterised by a slower process, although localised deformation at the edge of the loading strips is observed in the specimen at the end of the test.
- Asphalt material dissipates more energy if a rest time is included due to the healing effects; the maximum amount of dissipated energy is registered when a rest time of 10,000 pulses is included. If load time changes, it was not found a significant difference in terms of dissipated energy.
- A comparison between ITFT in strain control mode and flexural fatigue tests such as 2PB and 4PB was done. Based on the plots, fatigue life depends on the test used. In all cases, fatigue lives obtained by 2PB and 4PB can be fitted by the same fatigue curve; therefore there is a good correlation between the two different sets of data. Fatigue curves obtained by ITFT are characterised by smaller value of fatigue life than 2PB and

4PB; this is due to the accumulation of permanent deformation during the test in addition to fatigue damage. Statistically, a comparison between the three regression lines was made in each scenario. Tukey's test was used to better evaluate the difference between each possible pairs of slopes in the group of the three regressions. Results show that fatigue regression lines obtained from ITFT and 4PB tests are characterised by similar regression lines (they have same slope but slightly different elevation in each case analysed); fatigue results may be independent of the fatigue testing machine but more fatigue tests are needed to confirm this finding. Opposite results are obtained if fatigue lives obtained by means of ITFT and 2PB are compared; the two regression lines in all cases are different.

## CHAPTER 8

# Conclusions and future work

### 8.1 Conclusions

This project is part of the Marie Curie Initial Training Network, TEAM - Training in European Asset Management, funded under the Seventh Framework Programme (FP7) by the European Commission that deals with Training in European Asset Management. TEAM is arranged in three different clusters: this project is in Pavement Service Life Optimization and its aim is to improve understanding of fatigue damage in asphalt mixtures.

More specifically, the main key points developed in this research project are:

- Critical review of fatigue phenomenon in asphalt materials by means of different research methods.
- Due to lack of statistical techniques in pavement engineering, statist was involved to collect, analyse and interpret fatigue data.
- Fatigue data were obtained by means of simple flexural (such as 2PB and 4PB) and diametral tests (such as Indirect Tensile Fatigue Test or ITFT).
- Development of a new fatigue method: ITFT in strain control mode. ITFT test is currently one of the few tests used in industry by pavement engineers for pavement assessment (HD29/08); therefore, ITFT represents a good link between research and industry.

The starting point in this project was a deep literature review about fatigue and healing phenomena in asphalt pavement; comparison and evaluation of the different approaches that characterise the fatigue and healing behaviour in asphalt mixtures, with particular attention to the dissipated energy approaches was considered because it takes into account the evolution of the material during a fatigue test (see Chapter 2).

The findings from the literature review showed a lack of statistical techniques in pavement engineering used to analyse and evaluate differences between

different sets of data; this was one of the main reasons to introduce knowledge of statist in pavement engineering (see Chapter 3).

Further research involved the use of different traditional fatigue tests, in particular simple flexural tests such as 2PB and 4PB (see Chapter 5 and 6) and diametral fatigue test, such as ITFT (see Chapter 7).

Currently, the ITFT characterises the behaviour of asphalt material only under repeated constant load; so no ITFT data obtained in strain control mode exist. To overcome this lack of data, the ITFT was developed in strain control mode; this allows comparing of results between simple flexural tests and diametral tests also in strain control mode (see Chapter 7).

Writing procedures to perform correctly 4PB, 2PB and, particular, the new ITFT test in strain control mode for future research (and researchers) was one of the goals of the project; the new procedures can be found in Appendix A. For each test, the procedure, the characteristics of the test and the manufacturing of specimens are described; stiffness, fatigue and healing tests have been performed by means of each test, in stress and in strain control mode.

The main conclusions that can be drawn from this research project are the following:

1. Several approaches are usually used in characterising fatigue behaviour in asphalt materials. This research project decided to focus more on energy-based approaches because asphalt is a viscoelastic material; it dissipates energy under the form of mechanical work, heating and damage. Dissipated energy is history dependent (the energy dissipated in a cycle depends on the energy dissipated in the previous cycle). In order to have damage in the material there should be a change in the hysteresis loop, and thus a change in dissipated energy. Since the dissipated energy is path dependent, it is a parameter well related to the damage accumulation in a specimen. Among several dissipated energy methods, three in particular have been chosen to analyse fatigue data: the Dissipated Energy Ratio (DER) by Pronk, the Energy Ratio (ER) by Rowe, and the Ratio of

Dissipated Energy Change (RDEC) by Carpenter and Shen. These were chosen because a strong correlation between the changing of dissipated energy and fatigue damage was previously found. Many dissipated energy methods do not distinguish the amount of DE due to damage rather than viscoelasticity or heating phenomena and they strongly depend on loading and environmental conditions. A comparison between the traditional fatigue method and the three dissipated energy methods chosen was made by using statistical analysis. Graphically, results shows that each DE method gives different fatigue life values from the phenomenological approach (traditional method or  $N_f,50$ ).

2. Due to lack of information in pavement engineering, statistics was involved in this study by presenting a wider range of techniques for the analysis of different data sets. Commonly, multiple comparisons are made by employing the *Student t test*; depending on the data and on the hypothesis there is a high chance to get a mistaken answer, and therefore a mistaken analysis and findings. This thesis presents several multiple comparison procedures (such as Fisher, Tukey and Dunnett theories) that properly suits comparison of several sets of fatigue data in different situations. The results of statistical analysis show that, statistically, different DE methods are giving a similar answer; the failure point obtained by each method does not lie far away from the transition point from micro to macro cracking determined with the traditional method ( $N_f,50$ ). Thus, the phenomenological failure criterion still represents an easy and quick way to determine the failure point.

Further investigations involved different test methodologies used to evaluate and understand fatigue in asphalt material in the laboratory. Three different fatigue tests were used: 2PB, 4PB and ITFT.

3. In terms of stiffness, results show that stiffness values obtained by 2PB are smaller and phase angle values obtained by 2PB are bigger than values obtained by 4PB. Higher values of phase angle indicate a tendency towards more viscous behaviour, whilst lower values indicate more elastic response, thus it seems that 2PB stiffness tests at lower temperature

reflect more the viscous behaviour of the materials compared with the 4PB stiffness tests. In terms of fatigue, fatigue lives obtained by 2PB are smaller than values obtained by 4PB; this may be linked to the manufacture and shape of the specimen. The trapezoidal shape is not easy to obtain compared to the prismatic shape and the specimen may be affected during the sawing time; also, stresses and strains in the specimen are not homogenous in the trapezoidal specimen as in the prismatic specimen (between inner clamps). RDEC was used to compare the two fatigue lines and results show that regression lines (compared using the *t test*) are not the same. In this case it is not possible to consider a unique regression line for both sets of data; fatigue data are not independent on the test used when RDEC is used.

A diametral fatigue test was also used in this project: the Indirect Tensile Fatigue Test (ITFT). Currently, the ITFT could only be performed in stress control mode; in this project, the ITFT in strain control mode was developed. Fatigue tests were performed in stress and strain control mode and the results were compared. Test results show that EN 12697-24:2012 generates strain levels statistically closer to the strain levels applied to the developed fatigue tests (fatigue lines statistically do not have significant difference when EN 12697-24:2012 is used to calculate initial strain levels). This allows researchers to make a more reasonable comparison between ITFT and bending tests, avoiding including permanent deformation in the calculation of the strain.

4. A comparison between ITFT in strain control mode and flexural fatigue tests such as 2PB and 4PB was done. Based on the plots, fatigue life depends on the test used. In all cases, fatigue lives obtained by 2PB and 4PB can be fitted by the same fatigue curve; therefore there is a good correlation between the two different sets of data. Fatigue curves obtained by ITFT are characterised by smaller value of fatigue life than 2PB and 4PB; this is due to the accumulation of permanent deformation during the test in addition to fatigue damage. Statistically, a comparison between the three regression lines was made in each scenario. Tukey's test was used to

better evaluate the difference between each possible pairs of slopes in the group of the three regressions. Results show that fatigue regression lines obtained from ITFT and 4PB tests are characterised by similar regression lines (they have same slope but slightly different elevation in each case analysed); fatigue results may be independent of the fatigue testing machine but more fatigue tests are needed to confirm this finding. Opposite results are obtained if fatigue lives obtained by means of ITFT and 2PB are compared; the two regression lines in all cases are different.

Those results show that fatigue life obtained by ITFT in strain control mode is not different from fatigue life obtained by 4PB. 4PB test simulates the pavement behaviour under traffic loading better than the 2PB. The main advantage of using the ITFT in strain control mode is related to the simplicity of performing the test and specimen's manufacture. ITFT cores can be easily extracted from a pavement, and can therefore provide original and real characteristics of pavements; traditional test methods would require bigger pieces of pavement. The ITFT in stress control mode is already part of the standards; ITFT in strain control mode is not. Therefore, this research allows overcoming of the lack in the standards and performing of fatigue tests also in strain control mode. Numerical quantification of the repeatability and reproducibility of the ITFT in strain control mode needs to be obtained in order for the test method to become a full national standard. Also, further testing of unusual and new mixtures is required to ensure that the ITFT can be applicable to all mixture types.

- Healing is one of the factors that greatly influence fatigue performance in asphalt materials. Healing is still a very complicated factor to evaluate, mostly because not many testing machines are suitable to set up a rest time after a load cycle. This was one of the most challenging issues in this project and the solution was to undertake healing tests considering a rest time period after a certain number of load cycles. It was not feasible to perform healing tests by means of the 2PB due to the test set up; thus, healing tests were undertaken by means of 4PB and ITFT in strain control mode. Related to the 4PB, it was found that the specimen dissipates

energy very slowly when a rest time is included during a fatigue test: small changing in DE was noted when a rest time is included in a fatigue test. Thus, DE might not be a very good parameter to include the effect of healing in the evaluation of fatigue behaviour. Related to the ITFT, it was found that the optimum value was found to be 10,000 pulses loading; for higher values there is not a significant improvement in the fatigue life; this is due to the accumulation of permanent deformation, shorter rest time periods do not allow the specimen to recover and heal properly.

To conclude, researchers usually tend to use strain control mode to evaluate mixes for thin pavements (thickness of asphalt layers less than 50 mm); stress control mode for thicker and relatively stiffer structures (thickness of asphalt layers greater than 150 mm). Currently, the Indirect Tensile Test characterises the behaviour of asphalt material under repeated constant load; so no ITFT data obtained in strain control mode exists. To overcome this lack, ITFT was developed in strain control mode; this allows comparing results between simple flexural tests and diametral tests also in strain control mode. Results show that in fact fatigue lives obtained by means of the ITFT are statistically not different from 4PB results.

It is true that pure fatigue does not really exist in real life; failure is a more complicated phenomenon. Thus, developing ITFT in strain control mode could allow reducing the gap between research in laboratory (where pure fatigue tests often are used) and in the field (where experience showed that quick and simple tests are preferred by civil engineers). As researchers, we should not forget that the first aim is always to describe and understand the reality and flexural fatigue is still one of the main failure modes in pavements. As pavement engineers, we should not forget that the first aim is to design a more efficient pavement and in order to do that we would need a laboratory machine that better describes reality; the ITFT is a very good link between research and reality.

## **8.2 Future work**

There are many areas where this research could be developed in the future. The following outlines the key topics which were observed through this study.

### Effect of specimen sizes

It has been observed that phenomena such as size effect experimentally exist and it affects the strength and the fracture toughness of structural materials such as cement concrete, composite materials, etc. Concerning asphalt mixtures in fatigue, the influence of the shape has been observed in the literature (SHRPA-404 1994; Benedetto et al., 2003) but only few researchers have evaluated the influence of specimen size (Bodin et al., 2006). Specifically, Bodin et al. showed that the stiffness decrease vs the number of cycles is faster when specimen size is bigger; the bigger the size, the shorter the fatigue life and the effect of the size seems to be more important with the increasing of the loading level; the fatigue slope of Wöhler curves does not seem to depend on the size, the value of  $\varepsilon_6$  (the loading level leading to a fatigue life of  $10^6$  cycles) appears to be a function of the specimen size and decreases when size increases.

All the fatigue testing machines involved in this research project (2PB, 4PB and ITFT) have different set-ups depending on the aggregate size of the mixture.

**Table 25** Specimen dimensions (EN 12697-24: 2004)

Fatigue Test	Size	Shape
2PB	Two different sizes depending on the aggregate size	Two different shapes: prismatic and trapezoidal
4PB	Nominal proportions and tolerance limits between length, width and height of the specimen	Prismatic
ITFT	Two different sizes depending on the aggregate size	Cylindrical

A better evaluation of the specimen size effects in terms of fatigue is recommended for all the machines. Using the same material and loading conditions could be helpful to evaluate the specimen size influence on fatigue by using 2PB, 4PB and ITFT. Note that for the new 4PB machines (at the University of Nottingham) there are three different setups: small, medium and large (see Chapter 6).

### Effect of temperature

Asphalt is a viscoelastic material, therefore its properties depend on temperature. Many researchers (SHRPA-404 1994; Baburamani, 1999, Ongel,

and Harvey, 2004) have studied the effect of temperature on asphalt materials. Results show that stiffness of a general asphalt layer seems to decrease by three times with a temperature increase of 10°C, thus temperature influences the fatigue behaviour of asphalt material.

Other researchers (Bodin et al. 2010) conducted a study of temperature effects on fatigue characteristics of asphaltic mixes for a wide range of temperatures (from 0° to 30 °C). Results showed that  $\epsilon_6$  (the loading level leading to a fatigue life of  $10^6$  cycles) is not constant and follows a parabolic like trend with a minimum at intermediate temperatures and the slope decreases with the increase of temperature.

One of the main assumptions in these cases is that the temperature is constant for the whole fatigue test, but after starting a fatigue test stiffness will decrease immediately at a high rate (Phase I). This can be explained by the fact that the dissipated energy is transformed into heat and will warm up the specimen. However, it is not known which part of the decrease is due to the increase of temperature (self-heating) or to damage. Pronk (2000) tried to answer this question by using the uniaxial push-pull (UPP) test. Results showed that the decrease in stiffness due to internal heating is small compared to the decrease in stiffness due to damage. Nevertheless only one temperature and one frequency were tested; a wider range of temperatures and frequencies by using other tests such as 2PB, 4PB and ITFT is recommended.

### **Loading time and rest time - ITFFT**

In this project fatigue and healing were evaluated without changing the pulse characteristics of the test. Specially, fatigue tests were conducted considering repetitive pulses (0.1 sec loading time + 0.4 sec resting time) and healing was evaluated considering several continuous pulses followed by a rest time in which the test was stopped (no pulses applied).

To better evaluate fatigue and healing future investigations could analyse the effect of changing the loading time and resting time; therefore changing the pulse shape. Some researchers (Beeson, 2012) have already changed the rest times for ITFT in stress control mode by means of Universal Software (see Figure 163).

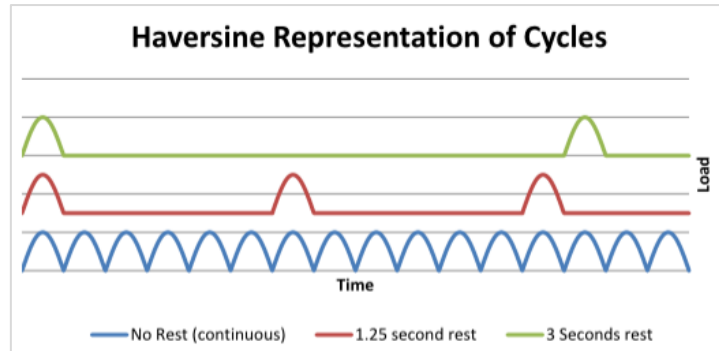


**Figure 163** Varying rest time in ITFT

Results showed that a longer rest period resulted in a greater fatigue life for the asphalt concrete specimens; this was due to a prolonged period of healing, as would be expected. Investigating the influence of varying rest time and, also, load time of the pulse during an ITFT in strain control mode could be interesting for future research.

Finding an answer to these key points would improve the knowledge about fatigue, healing and in particular would improve the new ITFT in strain control mode. A research project of this nature could only be successful if it was carried out with collaboration between researchers, technicians and engineers. Curiosity and passion about research is always the leading feature.

## References

- Airey, G. 2003. State of the Art Report on Ageing Test Methods for Bituminous Pavement Materials. International Journal of Pavement Engineering, 4, pp. 165-176. 2003
- Al-Khateen, G. and Shenoy, A. 2004. A distinctive fatigue failure. Journal of the Association of Asphalt Paving Technologists (AAPT), vol. 62, pp. 344-384.
- Al-Qadi, I. and Nassar, W.N. 2003. Fatigue shift factors to predict HMA performance. International Journal of Pavement Engineering, Volume 4, Number 2, pp 69-76. June 2003.
- Asphalt Institute 1982. Research and Development of The Asphalt Institute's Thickness Design Manual (MS-1). Ninth Edition. Research Report No. 82-2. The Asphalt Institute, Colelge Park, MD, August 1982.
- ASTM E739-10. Standard practice for statistical analysis of linear or linearized stress-life (S-N) and strain-life ( $\epsilon$ -N) fatigue data.
- Baburamani, P. 1999. Asphalt fatigue life prediction models:a literature review. Research Report ARR 334. ARRB TRansport Research Ltd., Vermont South, Victoria.
- Barenberg, E.J. and Thompson, M.R. 1992. Calibrated Mechanistic Structural Analysis Procedures for Pavements, NCHRP Project 1-26. Transport Research Board, National Research Council. Washington, D.C.
- Bazin, P., and Saunier, J. 1967. Deformability, fatigue and healing properties of asphalt mixes. Prooceding of the Second International Confonference on the Structural Design of Asphalt Pavements. Ann Arbor, Michiegan, USA.
- Beeson, J. 2012. Healing and fatigue characteristics of asphalt surface courses. Master Dissertation, submitted at the University of Nottingham. May 2012
- Bhasin, A., Narayan, A. and Little, D. N. 2009. Laboratory investigation of a novel method to accelerate healing in asphalt mixtures using thermal

treatment. Texas Transportation Institute. The Texas A&M University System College Station, Texas.

- Bodin, D., de La Roche, C. and Pijaudier-Cabot, G. 2006. Size effect regarding fatigue evaluation of asphalt mixtures – Laboratory cantilever bending tests. Road Materials and Pavement Design (EATA 2006), volume 7, pp 181-200. 2006
- Bodin, D., Terrier, J. P., Perroteau, C., Hornych, P. 2010. Effect of temperature on fatigue performances of asphalt mixes. Proceedings of 11th International Conference on Asphalt Pavement – ISAP 2010. Nagoya, Aichi, Japan, 1-6 August 2010
- Bonnaure, F., Gravos, A. and Udron, J. 1980. A new method for predicting the fatigue life of bituminous mixes. Proceedings of Associations of Asphalt Paving Technologist, volume 44, pp. 1-37, 1975. Associations of Asphalt Paving Technologist, Seattle.
- Bonnaure, F., Huibers, A. and Bonders, A. 1983. Etude en laboratoire de l'influence des temps de repos sur les caractéristiques de fatigue des enrobés bitumineux. Rev. Gén. Routes Aérodrom, 595, pp 74-82 (in French).
- British Standards Institution (1991), Guide to Statistical interpretation of data, BS 2846, 1991. London.
- British Standards Institution (2000), Methods of test for petroleum and its products, Bitumen and bituminous binders - Determination of needle penetration, BS EN 1426: 2000, London.
- British Standards Institution (2003), Bituminous mixtures – Test methods for hot mix asphalt – Part 33: Specimen prepared by roller compactor, BS EN 12697-33: 2003, London.
- British Standards Institution (2003), Bituminous mixtures – Test methods for hot mix asphalt – Part 6: Determination of bulk density of bituminous specimens, BS EN 12697-6: 2003, London.
- British Standards Institution (2003), Bituminous mixtures – Test methods for hot mix asphalt – Part 8: Determination of void characteristics of bituminous specimens, BS EN 12697-8: 2003, London.

- British Standards Institution (2003), Bituminous mixtures – Test methods for hot mix asphalt – Part 8: Determination of void characteristics of bituminous specimens, BS EN 12697-8: 2003, London.
- British Standards Institution (2003), Bituminous mixtures – Test methods for hot mix asphalt – Part 33: Specimen prepared by roller compactor, BS EN 12697-33: 2003, London.
- British Standards Institution (2004), Bituminous mixtures – Test methods for hot mix asphalt – Part 35: Laboratory mixing, BS EN 12697-35: 2004, London.
- British Standards Institution (2004), Bituminous mixtures – Test methods for hot mix asphalt – Part 24: Resistance to fatigue, BS EN 12697-24: 2004, London.
- British Standards Institution (2004), Bituminous mixtures – Test methods for hot mix asphalt – Part 26: Stiffness, BS EN 12697-26: 2004, London.
- British Standards Institution (2005), Coated Macadam (asphalt concrete) for roads and other paved areas – Part 1: Specification for constituent materials and for mixtures, BS EN 12697-33: 2003, London.
- British Standards Institution (2009), Bituminous mixtures – Test methods for hot mix asphalt – Part 5: Determination of the maximum density, BS EN 12697-5: 2009, London.
- Brunton, J.M., Brown, S. F. and Pell, P. S. 1987. Development of the analytic design method of asphalt pavements. Proceedings of the sixth International Conference on the Structural Design of Asphalt Pavements. Ann Arbor:University of Michigan.
- Carpenter, S.H. and Shen, S. 2005. Application of dissipated energy concepts in fatigue endurance limit testing. Journal of Transportation Research Record: No. 1929, Transportation Record Board, Washington, DC, 2005, pp. 165-173.
- Carpenter, S.H., Ghuzlan, K.A. and Shen, S. 2003. A fatigue endurance limit for highway and airport pavement. Journal of Transportation Research Record: No. 1832, Transportation Record Board, Washington, DC, 2003, pp. 131-138.

- Castro, M. and Sanchez, J.A. 2006. Fatigue and Healing of Asphalt Mixtures: Discriminate Analysis of Fatigue Curves. *Journal of Transportation Engineering*, 132 (2), pp 168-174. ASCE 2006
- Cocurullo, A, Airey, G. D., Collop, A. C. and Sangiorgi, C. 2008. Indirect Tensile versus Two Point Bending Fatigue Testing. *ICE Transport*, Vol.161, Issue TR4, pp. 207-220, 2008. ISSN 0965-092X.
- Colombier, G. 1997. Cracking in pavement: nature and origin of cracks. RILEM Report 18, Prevention of reflective cracking in pavements, edited by Vanelstaraete, A. and Francken, L. RILEM Publications, France.
- Daniel, J.S. and Kim, Y.R. 2001. Laboratory evaluation of fatigue damage and healing of asphalt mixtures. *Journal of Materials in Civil Engineering*, 13, pp. 434-440.
- De La Roche, C. and Riviere, N. 1997. Fatigue Behaviour of Asphalt Mixes: Influence of Laboratory Test Procedures on Fatigue Performance. *Proceeding of the Eight International Conference on Asphalt Pavements*, August 1997 Seattle, WA.
- Di Benedetto, H., De La Roche, C. and Francken, L. 1997. Fatigue of bituminous mixtures: different approaches and RILEM interlaboratory tests. *Mechanical tests for bituminous materials*. H. Di Benedetto and L. Francken, eds., Balkema, Rotterdam, The Netherlands, 15–26.
- Di Benedetto, H., de La Roche, C., Baaj, H., Pronk, A. and Lundstrom, R. 2003. Fatigue of bituminous mixtures: different approaches and Rilem group contribution. *Proceedings of the 6th International RILEM Symposium on Performance Testing and Evaluation of Bituminous Materials*. Zurich, Switzerland. 14-16 April 2003.
- Di Benedetto, H., Partl, M.n., Francken, L. and de La Roche, C. 2001. Stiffness testing for bituminous mixtures. *RILEM TC 182-PEB Performance testing and evaluation of bituminous materials*. *Materials and Structures*, Vol. 34, pp 66-70. March 2001
- Di Benedetto, H., Soltani, A.A. and Chaverot, P. 1996. Fatigue Damage for Bituminous Mixtures: A Pertinent Approach *Association of Asphalt Paving Technologist*, No. 65. 1996

- Dunnett, C.W. 1955. A multiple comparison procedure for comparing several treatments with a control. *Journal of the American Statistical Association*, Vol. 50, No. 272, pp. 1096-1121. December 1955.
- Dunnett, C.W. 1964. New table for multiple comparison with a control. *Biometrics*, Vol. 20, No. 3, pp. 482-491. International Biometrics Society. September 1964.
- Encyclopaedia Britannica, no date. Cross section of Roman road and John McAdam. Available at: <http://www.britannica.com/.html> (Accessed in December 2012)
- Finn, F.N., Saraf, C., Kulkarni, R., Smith, W. and Abdullah, A. 1977. The use of distress prediction subsystems for the design of pavement structures. *Proceedings of the 4<sup>th</sup> International Conference on the Structural Design of Asphalt Pavements*, volume 1. Ann Arbor: Michigan: The University of Michigan, 1977.
- Ghuzlan, K.A. and Carpenter, S.H., 2000. Energy-Derived, damage-based failure criterion for fatigue testing. *Transportation Research Record: Journal of the Transportation Research Board*, No. 1723, pp. 141-149, 2000.
- Ghuzlan, K.A. and Carpenter, S.H., 2001. Fatigue damage analysis in asphalt concrete mixtures using the dissipated energy approach. *Canadian Journal of Civil Engineering*, volume 33, No. 7, pp. 890-901. 2001
- Ghuzlan, K.A. and Carpenter, S.H. 2002. Traditional Fatigue Analysis of Asphalt Concrete Mixtures. Presented at the Transportation Research Board Annual Meeting, Washington D. C., January 2003.
- Hamed, F.K.M. 2010. Evaluation of Fatigue Resistance for Modified Asphalt Concrete Mixtures Based on Dissipated Energy Concept. PhD thesis at Technische Universität Darmstadt. Darmstadt, Germany.
- Hartman, A.M., Gilchrist, M.D. and Walsh, G. 2001. Effect of Mixture Compaction on Indirect Tensile Stiffness and Fatigue. *American Society Civil Engineers (ASCE), Journal of Transportation Engineering*, volume 125, issue 5, pp.370-378. October 2001.

- HD 29/08, Data for Pavement Assessment. DMRB – Design Manual for Road and Bridge, Volume 7, Section 3, Part 2. Highway Agency. London, UK
- Hopman, P.C., Kunst, P.A.J.C. and Pronk, A.C., 1989. A Renewed interpretation method for fatigue measurement, verification of Miner's rule. Fourth Eurobitumen Symposium, Madrid, Spain, October 4-6 1989, Vol.1, pp 557-561.
- HRB Special Report No 61E. 1962. The AASHO Road Test - Report 5, Pavement Research. Highway Research Board, National Research Council, Washington, D.C. 1962
- Hunter, R.N. 2000. Asphalts in roads construction (2000), London, Thomas Telford Publishing.
- Irwin, G.R. 1957. Analysis of stresses and strains near the end of a crack traversing a plate. Journal of Applied Mechanics, Transaction of ASME, Vol.24, 1957, pp 361-364
- Kennedy, T.W. 1983. Tensile characterization of highway pavement materials. Center for Transportation Research. The University of Texas at Austin. Austin, Texas. July 1983.
- Khattak, M. J., and Baladi G. Y., 2013. Analysis of Fatigue and Fracture of Hot Mix Asphalt Mixtures, Journal of Civil Engineering, International Society of Research Network, Volume 2013, pp 1-9, (Article ID 901652, DOI:10.1155/2013/901652). 2013.
- Kim, B. and Roque, R. 2006. Evaluation of Healing Property of Asphalt Mixtures. Transportation Research Record: Journal of the Transportation Research Board, 1970, pp. 84-91.
- Kim, R., Little, D. and Benson, F. 1990. Chemical and mechanical evaluation on healing mechanism of asphalt concrete. Association of Asphalt Paving Technologists (AAPT), 59, pp 240-275.
- Kim, Y.R., Little, D.N. and Burghardt, R.C. 1991. SEM Analysis on fracture and healing of sand-asphalt mixtures. Journal of Materials in Civil Engineering, 3, 140-153.

- Kim, Y.R., Little, D.N. and Lytton, R.L. 2003. Fatigue and Healing Characterization of Asphalt Mixtures. *Journal of Materials in Civil Engineering*, No. 15, pp. 75-83.
- Lay, M.G. 2009. *Handbook of road technology*, (2009) 4<sup>th</sup> Edition, Spon Press London and New York.
- Little, D. and Bhasin, A. 2008. Exploring mechanism of healing in asphalt mixtures and quantifying its impact. In: ZWAAG, S. (ed.) *Self Healing Materials*. Springer Netherlands.
- Little, D.N., Lytton, R.L., Williams, D. and Chen W.C. 2001. *Microdamage Healing in Asphalt and Asphalt Concrete, Volume I: Microdamage and Microdamage Healing*, Project Summary Report. Texas Transportation Institute The Texas A&M University System College Station, Texas.
- Little, R.E. 1975. *Manual on statistical planning and analysis*. American society for testing and materials. ASTM special technical publication 588. November 1975.
- Lytton, R., Uzan, J., Fernando, E.G., Roque, R. and Hiltunen, D.R. 1993. Development and validation of performance prediction models and specifications for asphalt binders and paving mixes. SHRP-A-357 ISBN 0-309-05617-9 Contract A-005 Product No. 1012. Strategic Highway Research Program National Academy of Sciences. Washington, DC.
- Lytton, R.L., Chen C.W. and Little, D.N. 2001b. *Microdamage healing in asphalt and asphalt concrete, Volume IV : a viscoelastic continuum damage fatigue model of asphalt concrete with microdamage healing*. Texas Transportation Institute. The Texas A&M University System College Station.
- Maggiore, C., Di Mino, G., Di Liberto, C.M., Airey, G., Collop, A. and Grenfell, J. 2012. Mechanical characterization of dry asphalt rubber concrete for base layers by means of the four bending points tests. *Proceeding of the third workshop on four point bending beam*. Pavement Research Center of the University of California at Davis. 17-18 September 2012. Davis, California.
- Majidzadeh, K., Kaufmann, E. M., and Ramsamooj, D. V. 1971. *Application of Fracture Mechanics in the Analysis of Pavement Fatigue*.

Journal of the Association of Asphalt Paving Technology, Vol.40, pp.227-246.

- Mallick R. and El-Korchi T. 2009. Pavement Engineering: Principle and Practise, CRC Press – Taylor and Francis Group, 2009.
- Mamlouk, M. and Mobasher, B. 2004. Cracking Resistance of Asphalt Rubber Mix Versus Hot-Mix Asphalt. International Journal of Road Materials and Pavement Design, Volume 5, No. 4, pp. 435-452. 2004.
- Masad, E., Branco, V., Little, D. N. and Lytton, R. L. 2008. A unified method for the analysis of controlled-strain and controlled stress fatigue testing. Interntional journal of Pavement Engineering, Volume 9, No. 4, pp. 233-246
- Miner, M.A. 1945. Cumulative Damage in Fatigue. Journal of Applied Mechanics, Transactions of ASME, Volume 67, p. 159. 1945.
- Molenaar, A.A.A. 1983. Structural performance and design of flexible pavements and asphalt concrete overlays. PhD thesis at the Delft University of Technology. The Netherladns, 1983.
- Monismith, C.L., Epps, J.A. and Finn, F.N. 1985. Improved asphalt mix design. Journal of the Association of Asphalt Paving Technologist, Volume 54, pp. 347-406.
- Ongel, A. and Harvey, J. 2004. Analysis of 30 Years of Pavement Temperatures using the Enhanced Integrated Climate Model (EICM). Report for California Department of Transportation, University of California, Davis. August 2004.
- Pais, J.C., Fontes, L., Pereira, P.A.A., Minhoto, M.J.C., Kumar, D.S.N.V.A. and Silva, B.T.A. 2009. Analysis of the variation in the fatigue life through four-point bending tests. Prooceding of the second workshop on four point bending beam. University of Minho. 24-25 September 2009. Guimaraes, Portugal.
- Paris, P. C. and Erdogan, F. 1963. A critical analysis of crack propagation laws. J. Basic Eng., Trans. ASME., 85, pp. 528–533.
- Pavement Interactive, no date. Rigid and Flexible Pavement Load Distribution. Available at: <http://www.pavementinteractive.org/.html>. (Accessed in December 2012).

- Pell, P.S. 1967. Fatigue of Asphalt Pavement Mixes. Proceedings of the Second International Conference on the Structural Design of Asphalt Pavements, 1967. Ann Arbor: Michigan, USA.
- Pell, P.S. and Cooper, K.E. 1975. The Fatigue of Testing and Mix Variable on the Fatigue Performance of Bituminous Materials. Journal of the Association of Asphalt Paving Technologists, Volume 44, pp. 1-37. 1975.
- Pell, P.S. 1987. Pavement Materials. Proceeding of the 6<sup>th</sup> International Conference on the Structural Design of Asphalt Pavement, 1987. Ann Arbor: Michigan, USA.
- Pronk, A.C. and Hopman, P.C., 1990. Energy dissipation: the leading factor of fatigue. Highway research: "shearing the benefits", Proceedings of the conference of the United States strategic highway research program. London, England, Telford. October 1990, pp 225-267.
- Pronk, A.C. 1995. Evaluation of the dissipated energy concept for the interpretation of fatigue measurement in the crack initiation phase. The Road and Hydraulic Engineering Division (DWW), Netherlands, P-DWW-95-001, 1995.
- Pronk, A.C. 1996. Temperature increase in an asphalt beam during fatigue – Theory and practice. Paper presented at the Wegbouwkundige werkdagen (Road research workshop) by C.R.O.W.; the Netherlands, Ede, 1996.
- Pronk, A.C. 1999. Harmonization of fatigue tests – Possible or not?. Proceeding of the seventh conference on asphalt pavements for southern africa. Victoria Falls, August-September 1999.
- Pronk, A. 2000. Determination of temperature increase in UPP tests. RILEM PEB – TG3. May 2000
- Quedeville, A. 1971. Enrobes bitumineux, fatigue du film de liant. Revue Generale des Routes et des Aerodromes. No. 461. January 1971.
- Raad, L., Saboundjian, S. and Minassian, G., 2001. Field aging effects on the fatigue of asphalt concrete and asphalt rubber concrete. Transportation Research Record, No. 1767, pp. 126-134. Transportation Research Board, Washington, D.C.

- Raithby, K.D. and Sterling, A.B. 1972. Some effects of loading history on the fatigue performance of rolled asphalt. Transport and Road Research Laboratory, Report No. LR 496, Crowthorne, U.K.
- Rao Tangella, S.C.S., Craus, J., Deacon, J.A. and Monismith, C.L., 1990. Summary Report on fatigue response of asphalt mixtures. Prepared for Strategic Highway Research Program A-003-A. National Research Council
- Read, J. M. 1996. Fatigue Cracking of Bituminous Paving Mixtures. PhD Thesis at the University of Nottingham. Nottingham Transportation Engineering Centre (NTEC). Nottingham, UK. 1996.
- Rowe, G. M. 1993. Performance of Asphalt Mixtures in the Trapezoidal Fatigue Test. Proceedings of the Association of Asphalt Paving Technologists, Volume 62, pp. 344-384. Austin, TX.
- Rowe, G.M. 1996. Application of the dissipated energy concepts to fatigue cracking in asphalt pavements. PhD Thesis at the University of Nottingham. Nottingham Transportation Engineering Centre (NTEC). Nottingham, UK. 1996.
- Shell, 1978. Shell Pavement Design Manual, Asphalt Pavement and Overlay for Road Traffic. Shell International Petroleum Company Limited, London.
- Shen, S. 2007. Dissipated energy concepts for HMA performance: fatigue and healing. PhD Thesis at the University of Illinois at Urbana-Champaign. USA.
- Shen, S. and Carpenter, S. 2007. Development of an Asphalt Fatigue Model based on Energy Principles. Journal of the Association of Asphalt Paving Technologists, Volume 76, pp. 525-574.
- SHRPA-404 1994. Fatigue Response of Asphalt-Aggregate Mixes. Washington, DC: Asphalt Research Program Institute of Transportation Studies University of California, Berkeley. Strategic Highway Research Program National Research Council.
- Si, Z., Little, D. and Lytton, R. 2002a. Evaluation of Fatigue Healing Effect of Asphalt Concrete by Pseudostiffness. Transportation Research Record: Journal of the Transportation Research Board, Volume 1789, pp. 73-79.

- Si, Z., Little, D.N. and Lytton, R. 2002b. Characterization of microdamage and healing of asphalt concrete mixtures. *Journal of Materials in Civil Engineering*, 14 (6), pp. 461-470.
- Sutharsan, T. 2010. Quantification of cohesive healing of asphalt binder based on dissipated energy analysis. Master dissertation at Washington State University, Department of Civil and Environmental Engineering. May 2010
- Tayebaldi, A.A., Deacon, J.A., Coplantz, J.S. and Monismith, C.L. 1993. Modeling Fatigue response of Asphalt-aggregate mixtures. *Proceedings of Associations of Asphalt Paving Technologist*, Volume 62, pp. 385–421, 1993. Austin, TX.
- Thom, N. 2008. *Principles of Pavement Engineering*. Thomas Telford Limited 2008 Technology and Engineering.
- Van Dijk, W. 1975. Practical Fatigue Characterization of Bituminous Mixes. *Proceedings of the Association of Asphalt Paving Technologist*, Volume 44, pp. 38-72. Seattle.
- Van Dijk, W. and Visser, W. 1977. The Energy Approach to Fatigue for Pavement Design. *Proceedings of the Association of Asphalt Paving Technologist*, Volume 46, pp. 1-41. Seattle.
- Zar, J.H. 2010. *Statistical analysis*. Fifth Edition. Prentice Hall, Upper Saddle River, NJ. ISBN: 0130845426, 9780130845429.

# **Appendix A**

## Fatigue Test Protocols

## Testing protocol for

### **Measurement of resistance to fatigue using Two Point bending test (2PB) in strain controlled mode.**

#### **1. Scope**

This procedure outlines the steps to be taken for characterising the fatigue behaviour and stiffness modulus of bituminous mixtures by 2 Point Bending (2PB) test in strain controlled mode.

#### **2. Equipment**

The main equipment includes:

- a rigid frame made from welded steel section;
- a three phase electric motor to received its supply from an inverter which is powered by a single phase, 230 V supply;
- an adjustable eccentric fitted to the drive shaft of the electric motor;
- a Proxister is mounted beneath the eccentric to provide a means of counting cycles and determining motor speed;
- a lever arm assembly hinged on leaf springs that gives a 1:5 reduction in horizontal movements;
- two horizontal mounted loading arms that transmit the reduced movement from the lever arm through force transducers to the tops of two trapezoidal test specimens;
- a rigidly mounted LVDT displacement transducer measures the horizontal movement of the loading arm assembly;
- a temperature cabinet;
- test software.

#### **3. Conditioning and test temperature**

The specimens shall be placed in the thermostatic chamber and exposed to the specified test temperature for at least 4 hours prior to testing.

#### **4. Sample Preparation**

See Section 5.2.

## 5. Geometric measurement of trapezoidal specimens

- Take eight measurements of thickness ( $e$ ) around the trapezoidal as shown in Figure A1, using the calliper with the fine point fittings measure to 0.1 mm. All readings shall be taken approximately 5 mm in from the edge. Record all measurements and calculate the mean of the eight thickness readings ( $e$ ) and record to 0.1 mm.
- Take two readings of the top width ( $b$ ) of the specimen as shown in . These readings need to be taken as close to the top of the specimen as is physically possible. Calculate the mean of the top width ( $b$ ) and record to 0.1 mm.
- Take two readings of the base width ( $B$ ) of the specimen as shown in Figure A1. These readings need to be taken as close to the bottom of the specimen as is physically possible. Calculate the mean of the base width ( $B$ ) and record to 0.1 mm.
- Take two readings of the height ( $h$ ) of the specimen as shown in Figure A1. These readings need to be taken with the steel rule against the specimen as the calliper does not expand enough). Calculate the mean of the height ( $h$ ) and record to 0.1 mm.
- Take the reading of the weight ( $W$ ) of the specimen

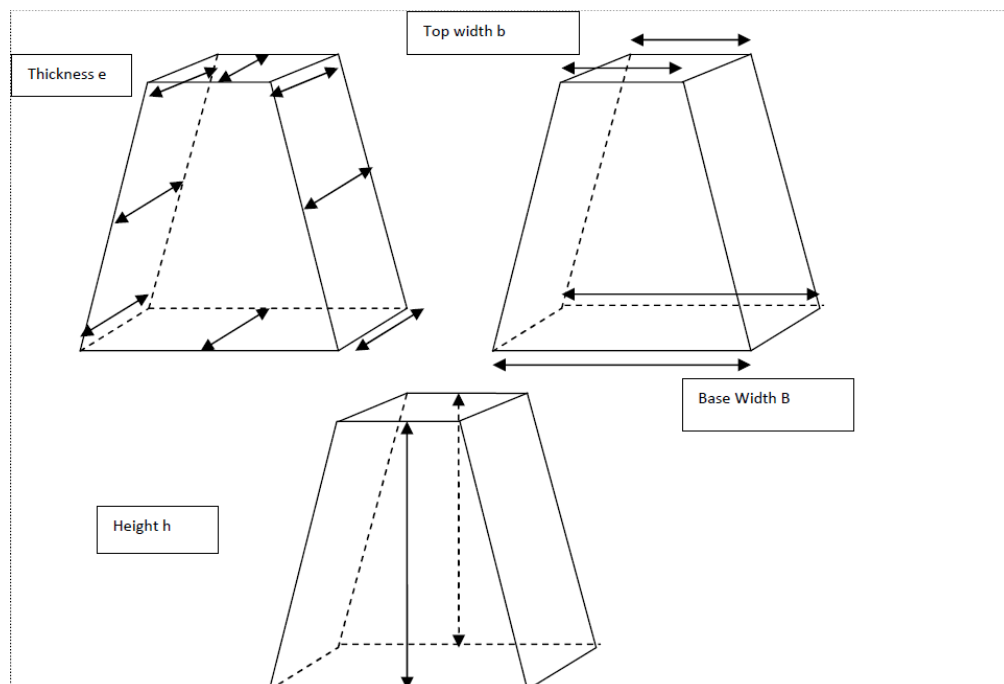


**Figure A1** Measurement of trapezoidal specimen

## 6. Procedure for evaluating resistance to fatigue in strain controlled mode

- Turn on the equipment (power bottom) and the computer system. Then, set up the test temperature (see Figure A2). **Note:** RESET bottom is on at this stage of the test.



Figure A2 2PB system

- Open the *2PB Bending 2.21.0* software by double clicking the software icon, shown in Figure A3 and Figure A4.



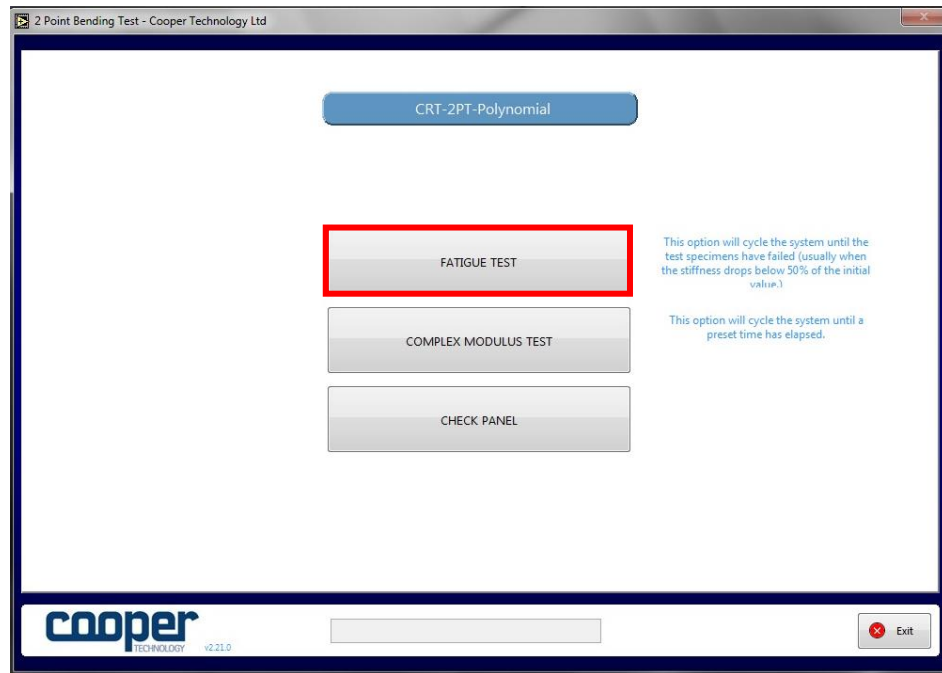
Figure A3 2PB strain controlled mode icon



Figure A4 2Pt Bending v 2.21.0 Software

- By means of the 2 Point bending test, it is possible either run a stiffness test or a fatigue test (see Figure A5). This procedure outlines

the steps to be taken for a fatigue test, thus the referent standard is the EN 12697 Part 24: Resistance to fatigue (see Figure A6).



**Figure A5** 2 Point Bending Fatigue Test (in strain controlled)

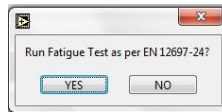


**Figure A6** EN 12697-24: Resistance to fatigue

- After clicking on *fatigue test*, the software requires data entry: the specimen dimensions (previously measured for both specimen A and B) and the test parameters (temperature, frequency, failure criterion and displacement amplitude) as shown in Figure A7.

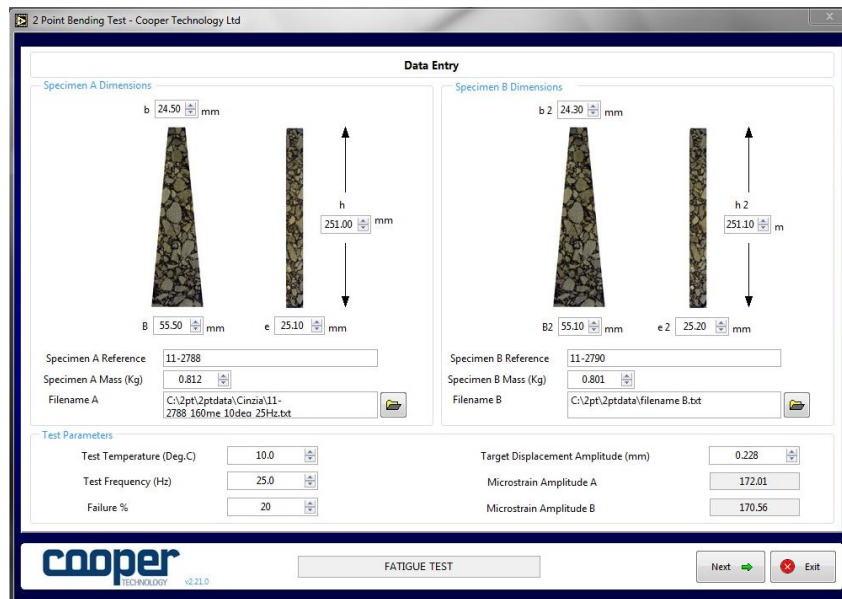


**Figure A7** Data Entry

- Once the tab *next* is clicked, the specimens could be inserted in the cabinet and the bottom plates could be fixed. Note: it is very important not to screw the top plates to the machine (see Figure A8).

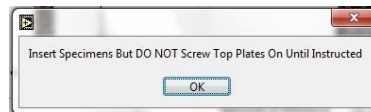


**Figure A8** Insert the specimen in the cabinet

- After clicking *ok*, the software shows the *system setup* screen. The main purpose at this point is to adjust the eccentricity of the system and set up the displacement chosen for the fatigue test. The system setup window shows three different amplitude (Figure A9):
  1. *Detected displacement amplitude*: it is the displacement (in mm) that the machine record after adjusting the eccentricity.
  2. *Microstrain amplitude*: it is the value (in microstrain) that corresponds to the detected displacement amplitude.
  3. *Required displacement amplitude*: it is the target displacement amplitude (in mm) setup in the previous tab (it is the desired strain level for the fatigue test).

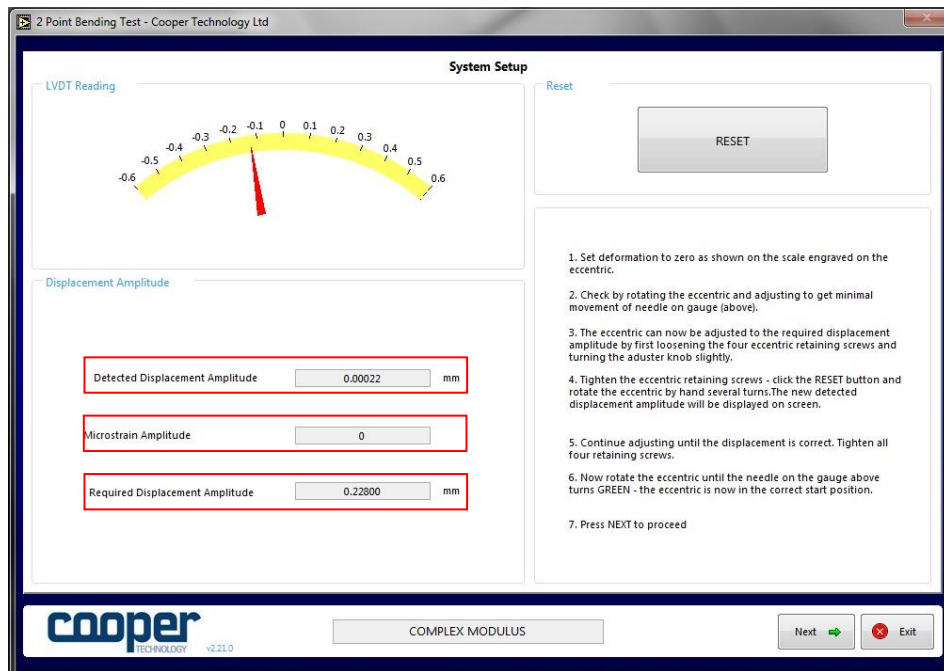


**Figure A9** LVDT reading and displacement amplitude

To adjust the eccentric, loosen the four clamping screw until the eccentric adjustment knob behind can be turned. Note: do not completely loosen all the clamping screw otherwise, when manually turning the drive, the eccentric will try to return towards the zero position.

In order to set up the right displacement the following steps are recommended:

1. Set the deformation to zero as shown on the scale engraved on the eccentric (see Figure A10). Note: the specimen is in position but without the top screw in place (so the top cap can slide to and fro on the specimen top plate).

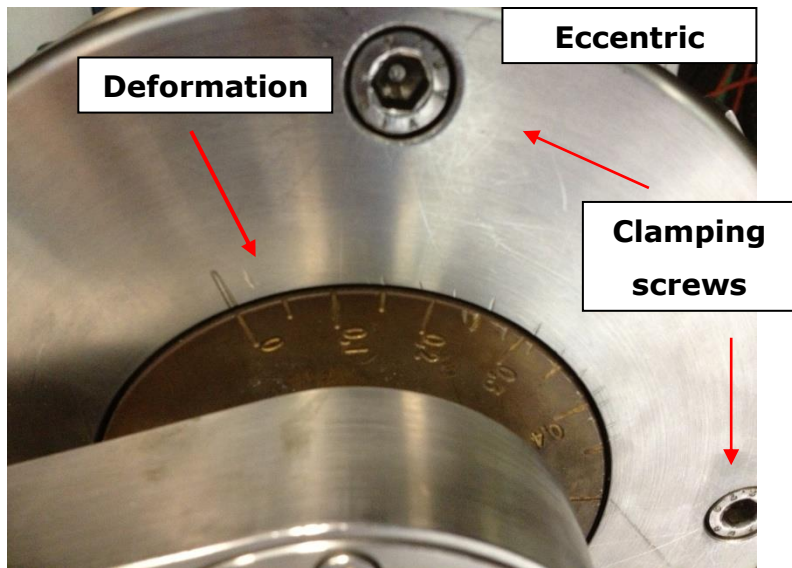


**Figure A10** Deformation = 0 mm in the eccentric.

2. Check by rotating the eccentric and adjust to get minimal movement of needle on gauge (see Figure A11).

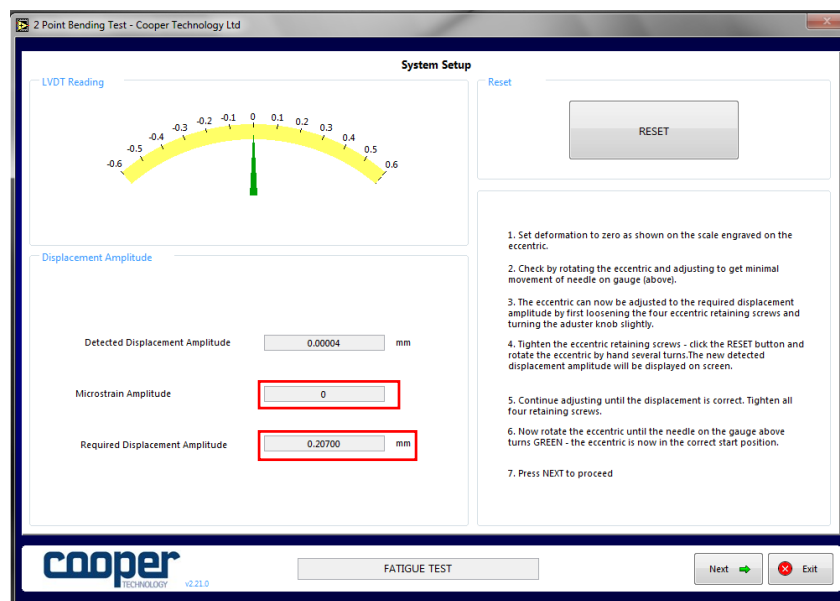


**Figure A11** Eccentricity: zero value

3. Tighten the eccentric retaining screws. Click RESET button and rotate the eccentric by hands several turns. The new detected displacement amplitude will be displayed on screen. Figure A12 is an example how to set the required displacement; specifically in this case the target displacement is 0.228 mm. Figure A13 shows how to compare the detected displacement amplitude with the required amplitude in order to be more précised.

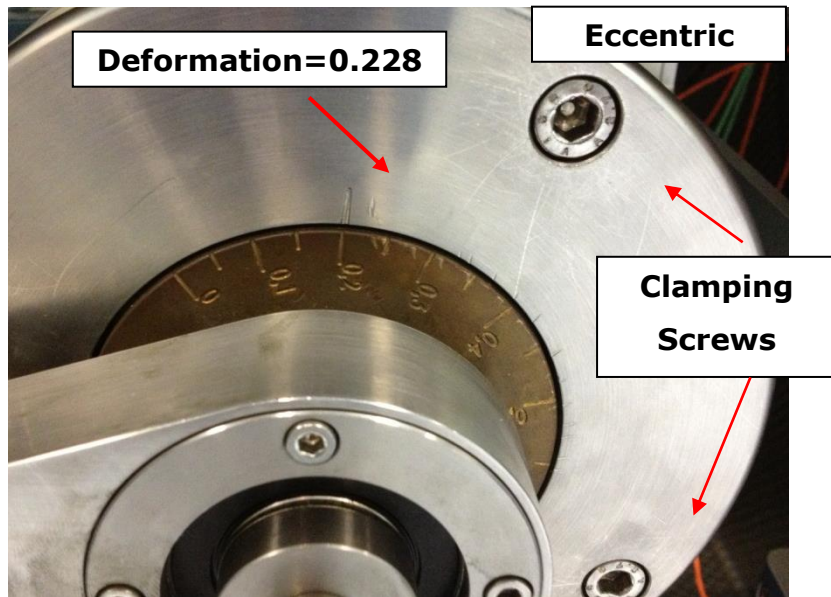


**Figure A12** Deformation = 0.228 mm in the eccentric.

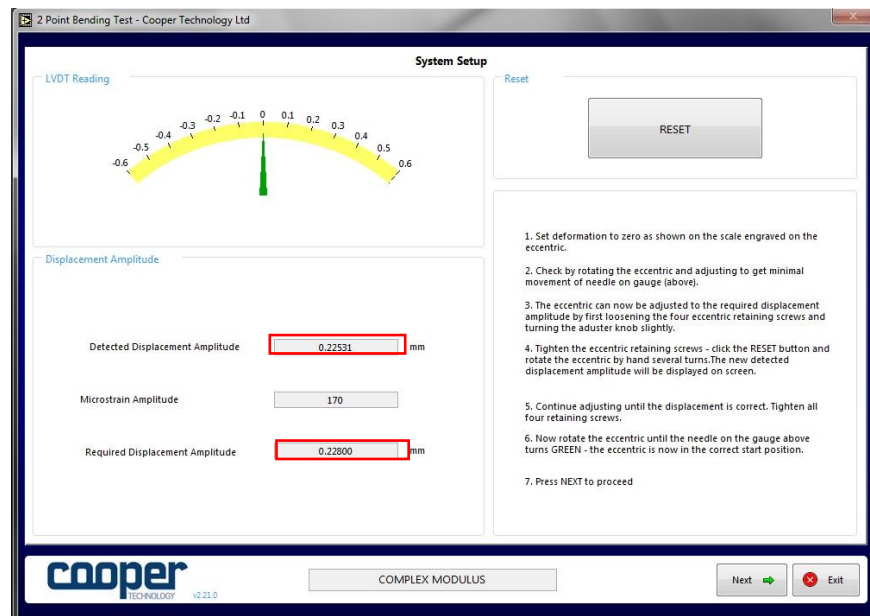


**Figure A13** Eccentricity: detected displacement amplitude=required displacement amplitude

4. Once the detected displacement is close enough to the required displacement, tighten all four clamping screws (see Figure A14).

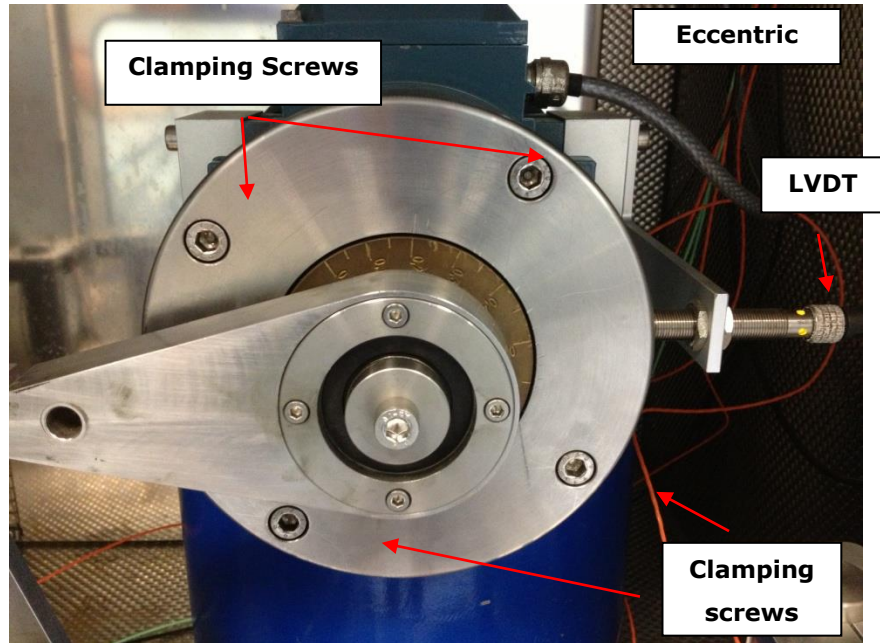


Figure A14 Set up displacement amplitude.

5. Rotate the eccentric until the needle on the gauge above turns green, in order to put the eccentric in the correct position before screwing the top plates of the specimens (see Figure A15).

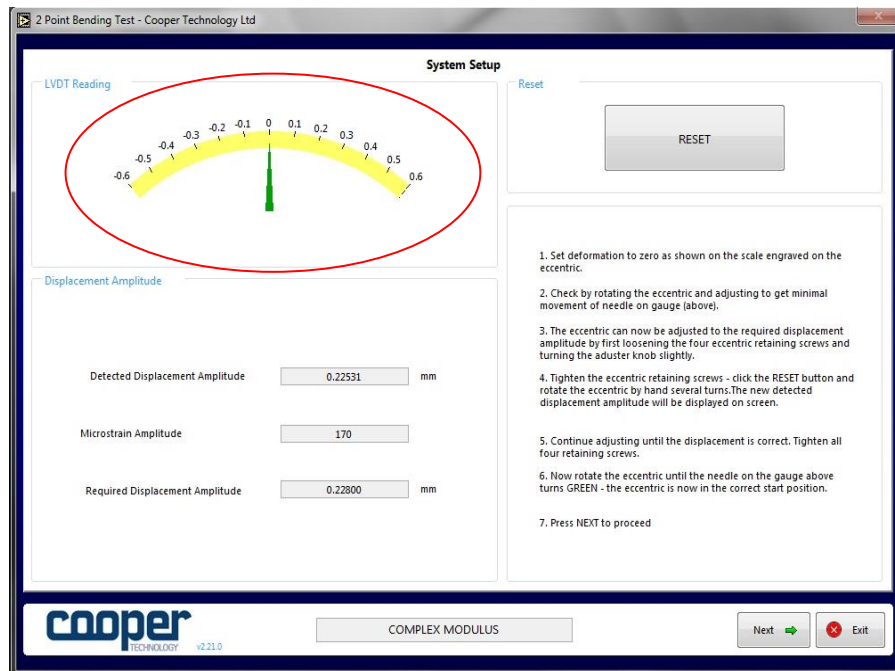


Figure A15 Correct start position.

**Note:** after adjusting the eccentric in order to reach the correct start position, close the temperature cabinet and wait few minutes before clicking next. The main reason is that the LVDTs are very temperature sensitive; they may slightly change

positions during to the temperature changing inside the cabinet. If they reach a new position and the needle become red again, the operator should adjust the needle again until it turns green again.

6. Once the needle is in the right start position (and it is green), click *next*.
- Once *next* is clicked, tight the top cap screws of both specimens; close the temperature cabinet and click on *RESET* (see Figure A16 and Figure A17). **Note:** if the operator does not press *RESET*, the test will not start after the conditioning stage.

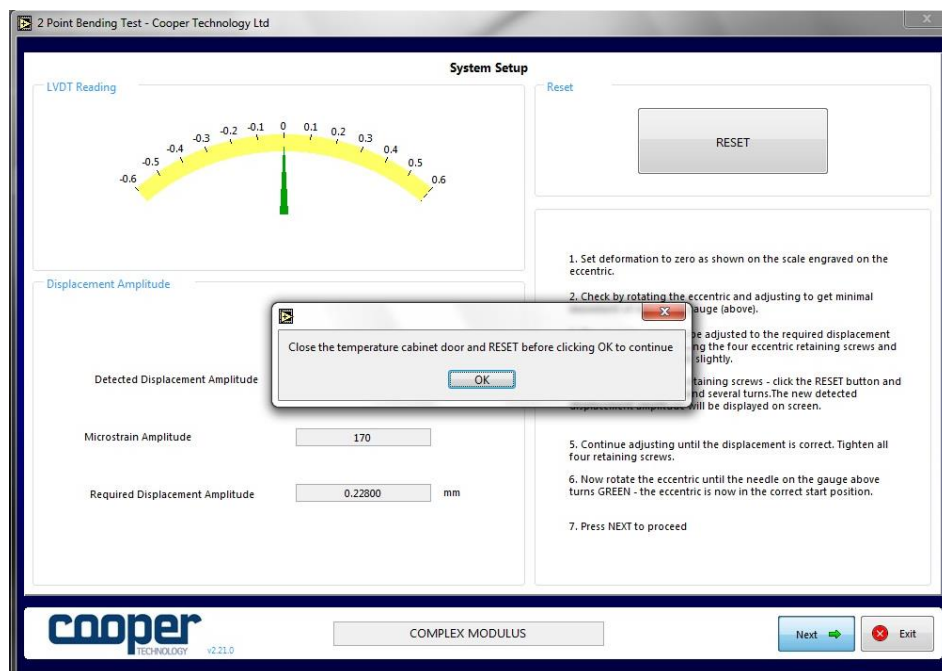


Figure A16 Close temperature cabinet and press *RESET*

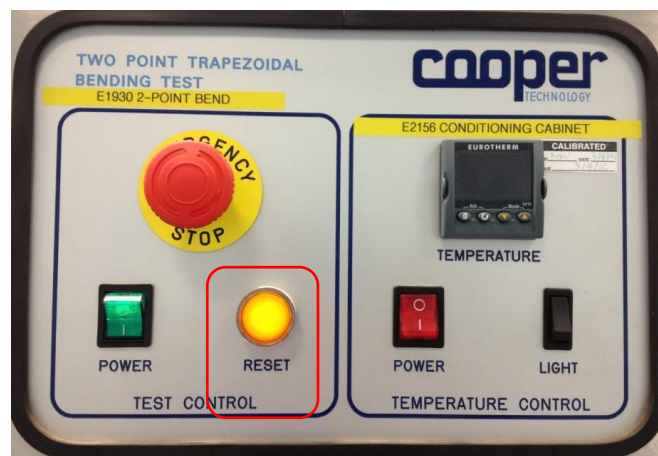
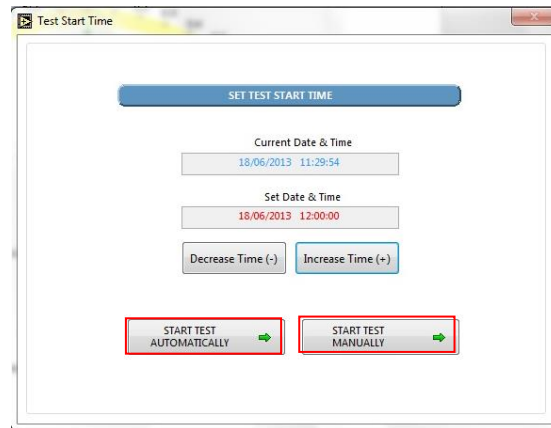
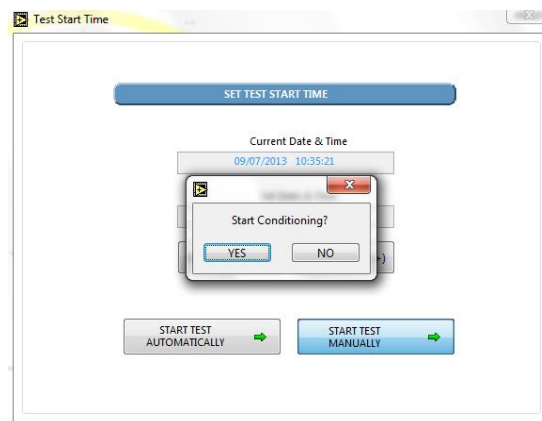


Figure A17 *RESET* button

- Once *ok* is clicked, the user can chose to start a fatigue test in two different ways before the condition stage (see Figure A18 and Figure A19)
  1. Start test automatically:
  2. Start test manually:



**Figure A18** Start testing



**Figure A19** Start conditioning

- Figure A20 shows the temperature conditioning window. As said before, it is recommended to condition the trapezoidal specimens for at least four hours before testing them.

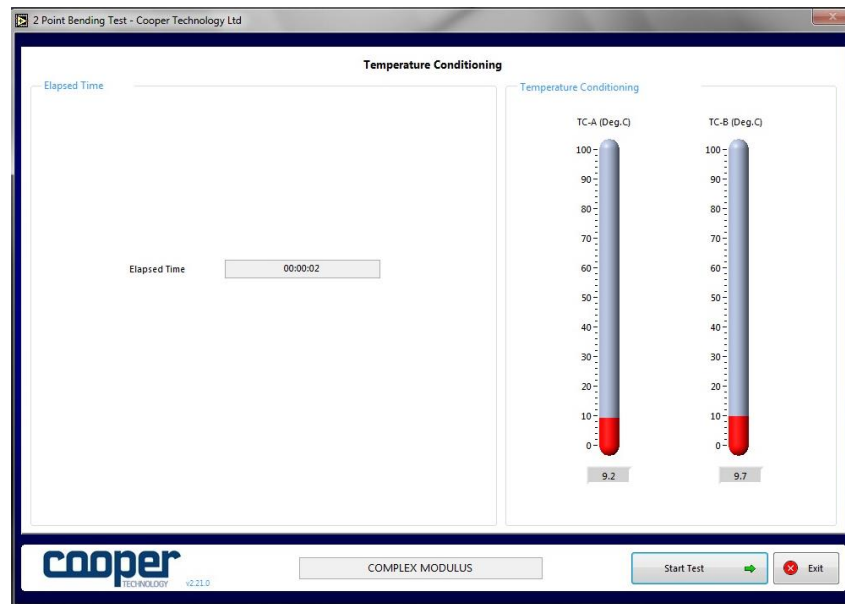


**Figure A20** Conditioning stage

- Once the specimens are conditioned, the fatigue test can start. For each of the two specimens regularly updated plots and text boxes are shown providing information on elapsed cycles, stress, strain, deformation, load, phase angle, stiffness (real part, imaginary part and complex modulus), frequency and temperatures. The test will end once both specimens have reached the failure point (failure criterion decided a priori during the data entry stage).
- At the end of the tests, the software shows the cycle at which both specimens have reached the failure point (see Figure A21).



**Figure A21** Failure cycles: end of the fatigue test

- At this point, the user can remove the failed specimens from the cabinet and install the next pair and re-adjust the eccentric if required.
- The test data is recorded every 100 cycles.

## 7. Measurement of stiffness

In order to run a stiffness test (see Figure A22), the procedure is the same as showed for a fatigue test; in this case the referent standard is the EN 12697 Part 26: Stiffness (see Figure A23).

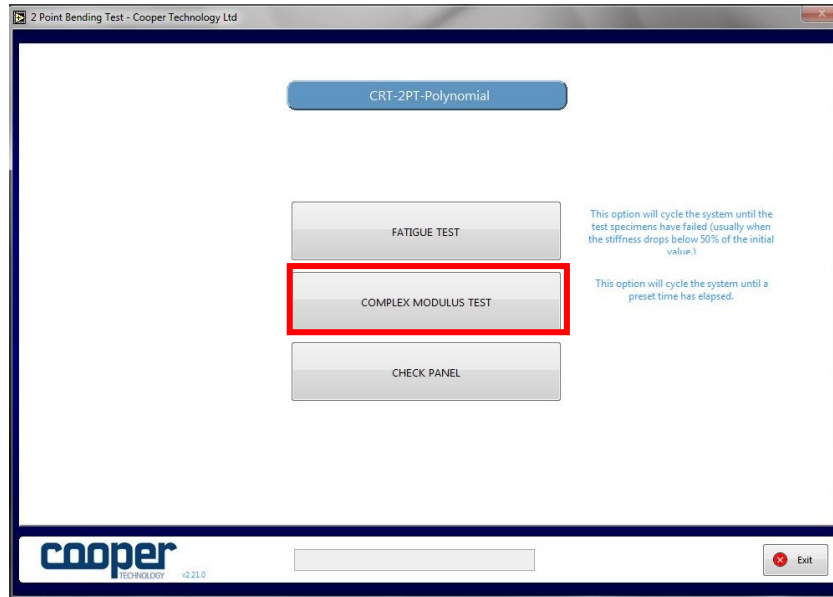


**Figure A22** 2 Point Bending Stiffness Test

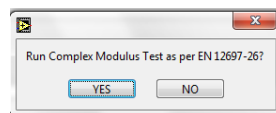


**Figure A23** EN 12697-26: Stiffness

The procedure is exactly the same as for a fatigue test. The test specimen is cycled for a pre-defined time (usually 2 minutes), with data being acquired over the last 10 seconds of the test and the mean of these value being recorded to file at the end of test. Thus, the test will end when the test time has elapsed.

## 8. Check Panel

By means of the check panel is possible to control the LVDTs readings (see Figure A24 and Figure A25).

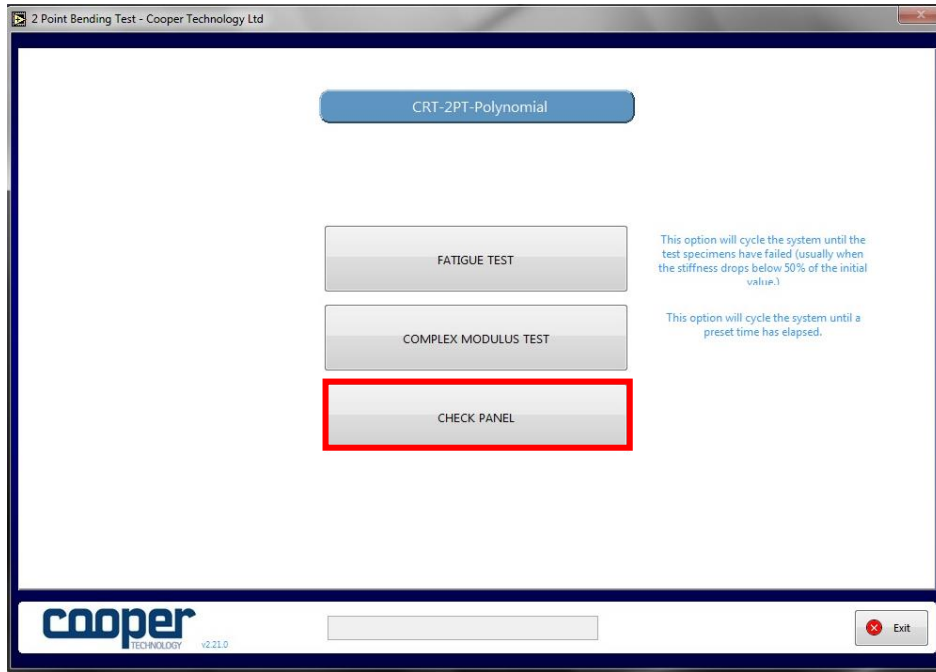


Figure A24 2 Point Bending Check Panel

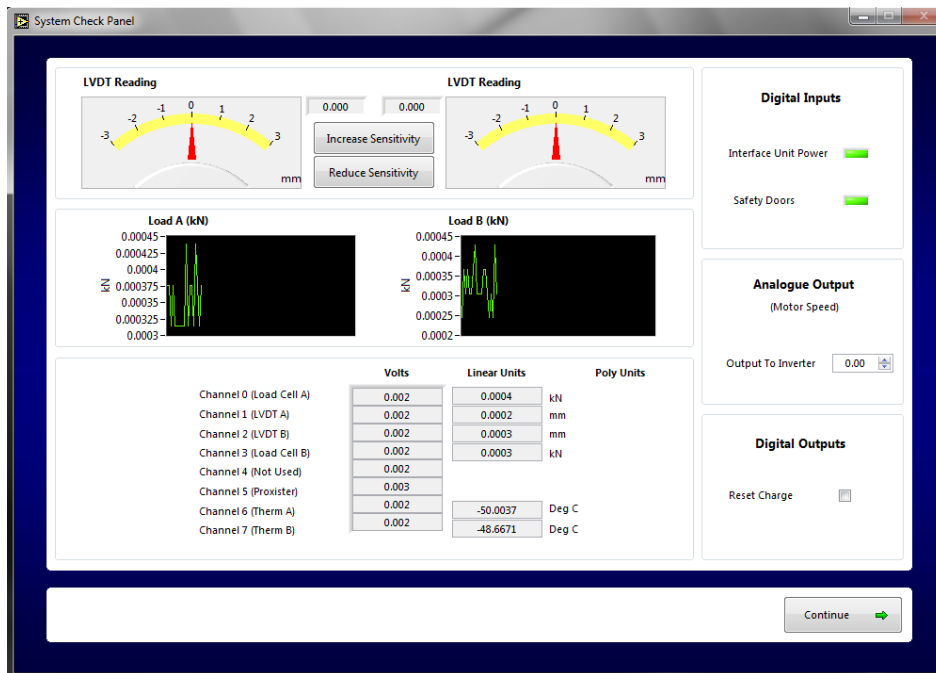


Figure A25 System check panel

## Testing protocol for

### **Measurement of resistance to fatigue using Four Point bending test (4PB) in strain controlled mode.**

#### **1. Scope**

The 4PB is a test widely used to determine the stiffness modulus and the fatigue resistance of the asphalt mixture. The four point bending tests are included in CEN (European Committee for Standardization), AASHTO (American Association of State Highway and Transportation Officials) and Chinese test specifications. The specimen is a prismatic beam which is subjected to sinusoidal loading in either the controlled strain or controlled stress modes

#### **2. Equipment**

The main equipment includes:

- Load cell;
- Main hydraulic actuator;
- Alignment plate;
- 4 clamps;
- Three LVDTs;
- Air inlet manifold;
- Servo valve;
- Actuator LVDT;
- Thermostatic chamber.

#### **3. Conditioning and test temperature**

The specimen is placed in the thermostatic chamber and exposed to the specified test temperature for at least 4 h prior to testing.

#### **4. Sample Preparation**

See Section 6.2.

#### **5. Measurement of resistance to fatigue**

- Turn on the equipment (on/off button and start button) and the computer system. Also, set up the temperature manually (see Figure A26).

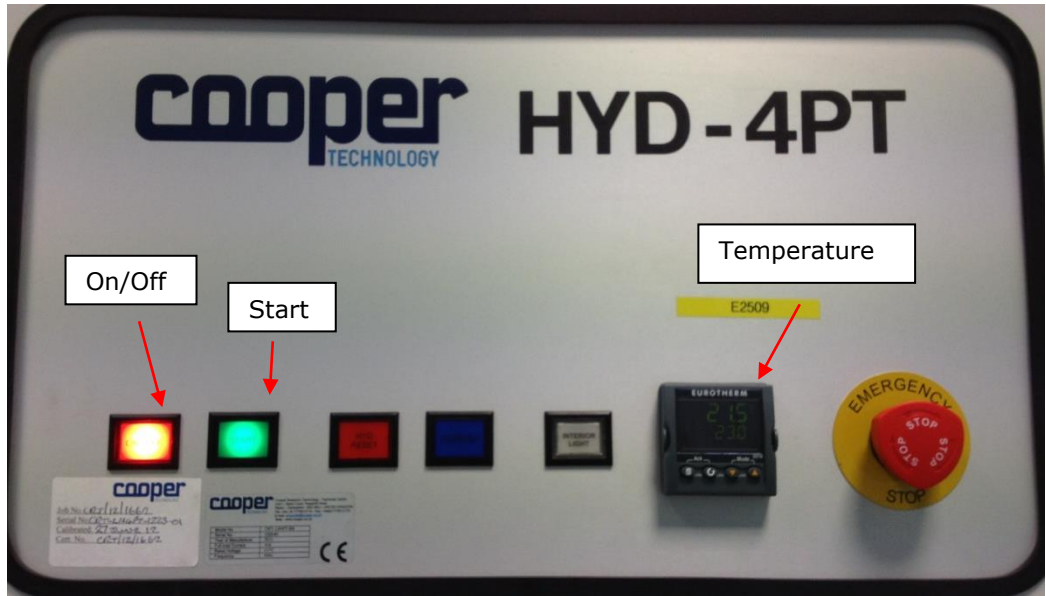


**Figure A26** 4PB system

Open the *4PB Bending 4.2.0* software by double clicking the software icon, shown in Figure A27 and Figure A27. Note: ensure that all operators are clear of the beam fatigue rig. Once the software is opened, the machine will rise up automatically (as red arrows show in Figure A28).

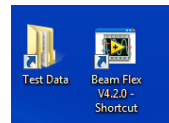


**Figure A26** 4PB icon



**Figure A27** 4 CRT Beam Flex Software

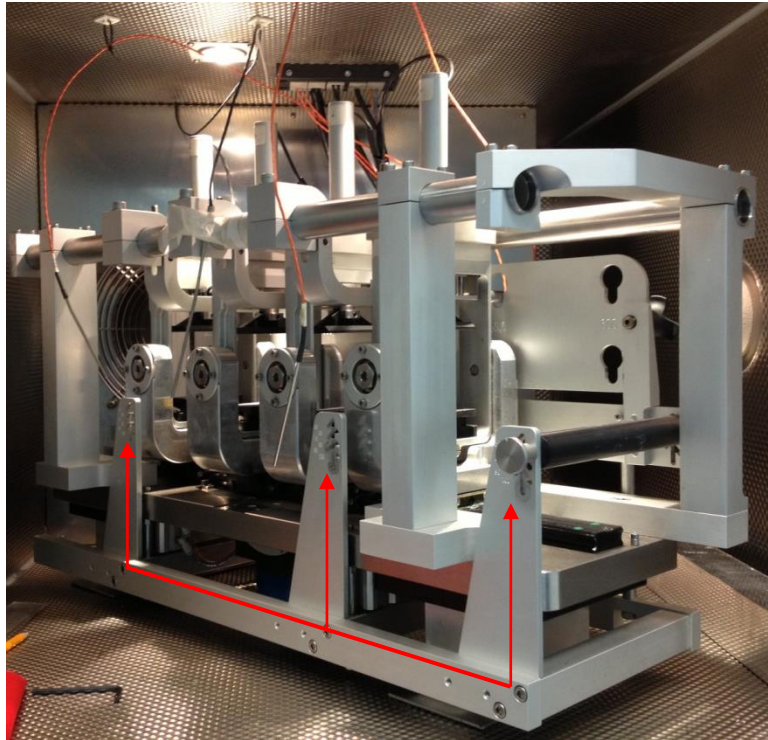


**Figure A28** 4 Point bending testing machine

By means of the 4 Point bending test, is possible either run a stiffness test or a fatigue test (see Figure A29). The following procedure outlines the steps to perform a fatigue test in strain control mode, thus the referent standard is the EN 12697-24: Resistance to fatigue (see Figure A30).



**Figure A29** 4 Point Bending Fatigue Test

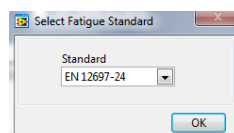


**Figure A30** EN 12697-24: Resistance to fatigue

**Note:** three different standards could be considered for a fatigue test in the software (see Figure A31). The three standards are:

1. EN 12697-24. The European Standard was approved by CEN (European Committee for Standardization) in 2004, a new version of the standard was recently released in 2012. The main aim is to characterise the fatigue of bituminous mixtures by different tests such as bending tests and direct and indirect tensile tests. This standard is used to rank bituminous mixtures on the basis of resistance to fatigue and as guide to evaluate the performance of road pavements in Europe.
2. AASHTO T321-07. The American standard is the standard method of test for determining the fatigue life of compacted hot-mix asphalt (HMA) subjected to repeat flexural bending until failure in United States. The standard was developed by AASHTO the American Association of State Highway and Transportation Officials.
3. T0739-2011. This is the Four-point Bending Fatigue Life Test of Bituminous Mixtures standard and it is part of the Chinese standards JTG E20-2011 Standard Test Methods of Bitumen and Bituminous Mixtures for Highway.

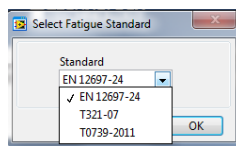


**Figure A31** Three different standards to run a fatigue test

- After selecting the appropriate standard, select the project where all the files will be collected; the operator can choose the project depending on the mode of loading (see Figure A32).

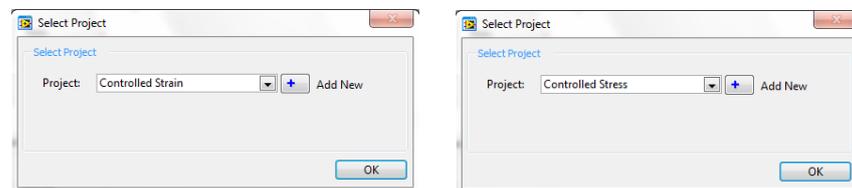


**Figure A32** Select project: stress and strain controlled

**Note:** the operator has the possibility to create a new project. In this case, click on *add new* and enter a project name as shown in Figure A33.

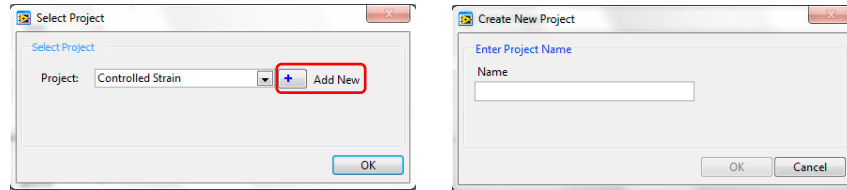


**Figure A33** Select project: new project

- After clicking on *fatigue test*, the software will require the data entry, that is: the measurement details, the specimen details (dimensions and weight of each specimen previously measured) and the test conditions (mode of loading, temperature, frequency, failure criterion and strain level).

As shown in Figure A34, measurement details refer to the beam size. Three different beam sizes are possible, thus three different configurations:

1. Small size: effective length 355.5 mm and middle span length 118.5 mm. Mass of clamp 16384.0 g (see Figure A35);
2. Medium size: effective length 420 mm and middle span length 140 mm. Mass of clamp 16798.0 g (see Figure A36);
3. Large size: effective length 600 mm and middle span length 200 mm. Mass of clamp 17474.0 g (see Figure A37).

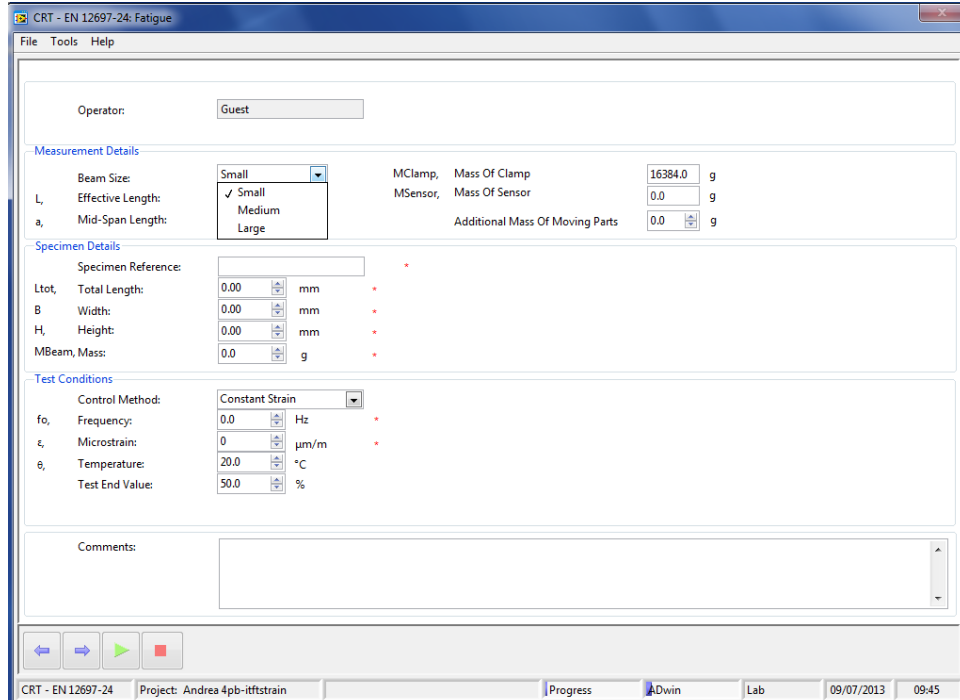


**Figure A34** Measurement details

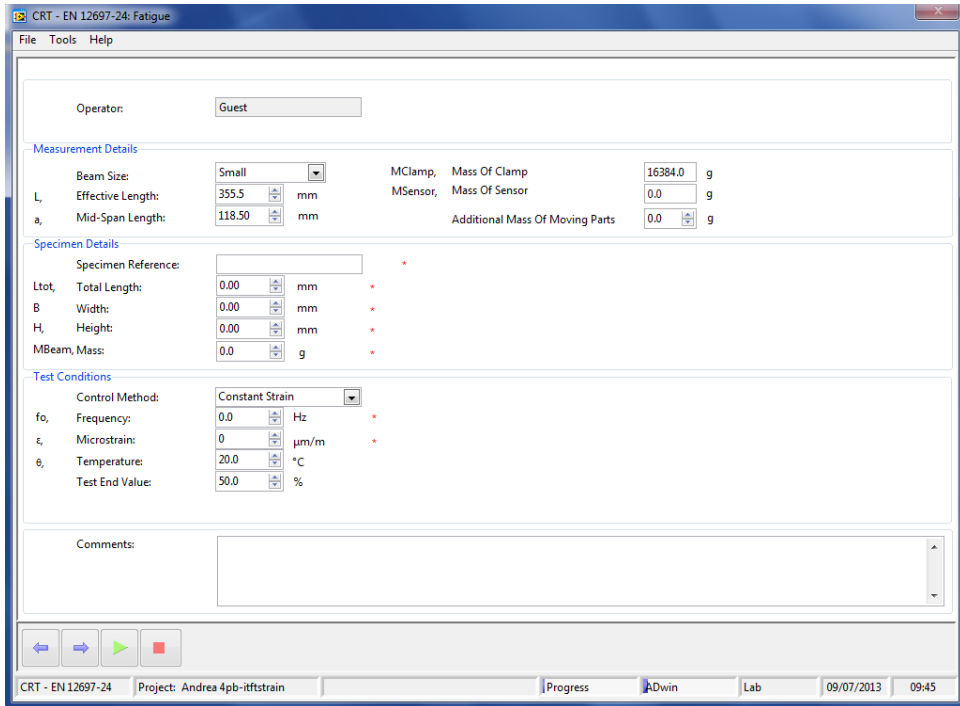


Figure A35 Small beam size

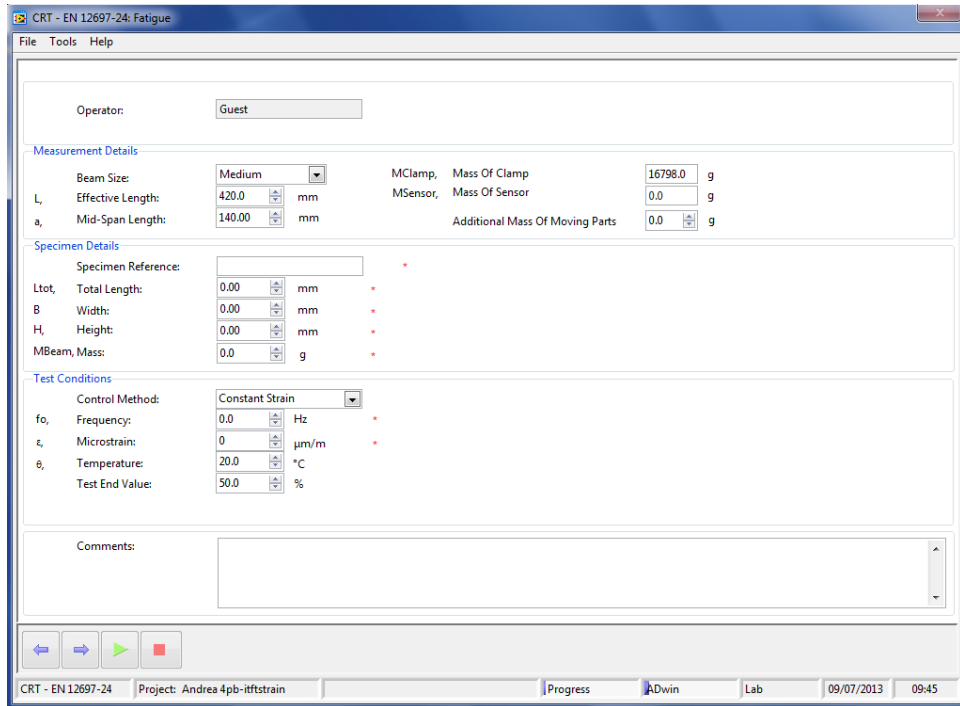
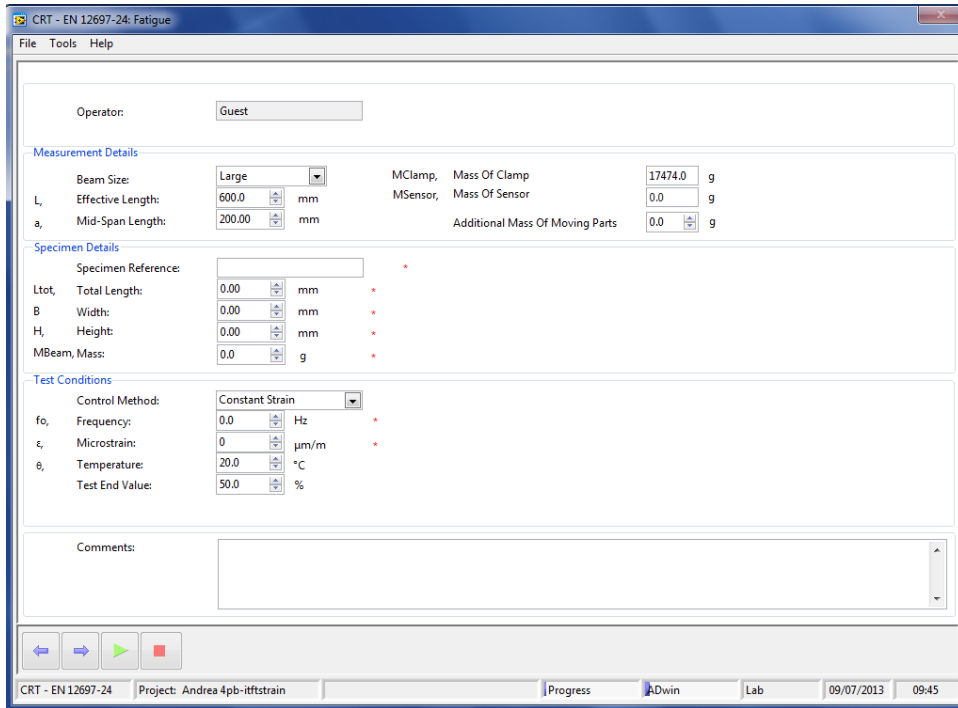
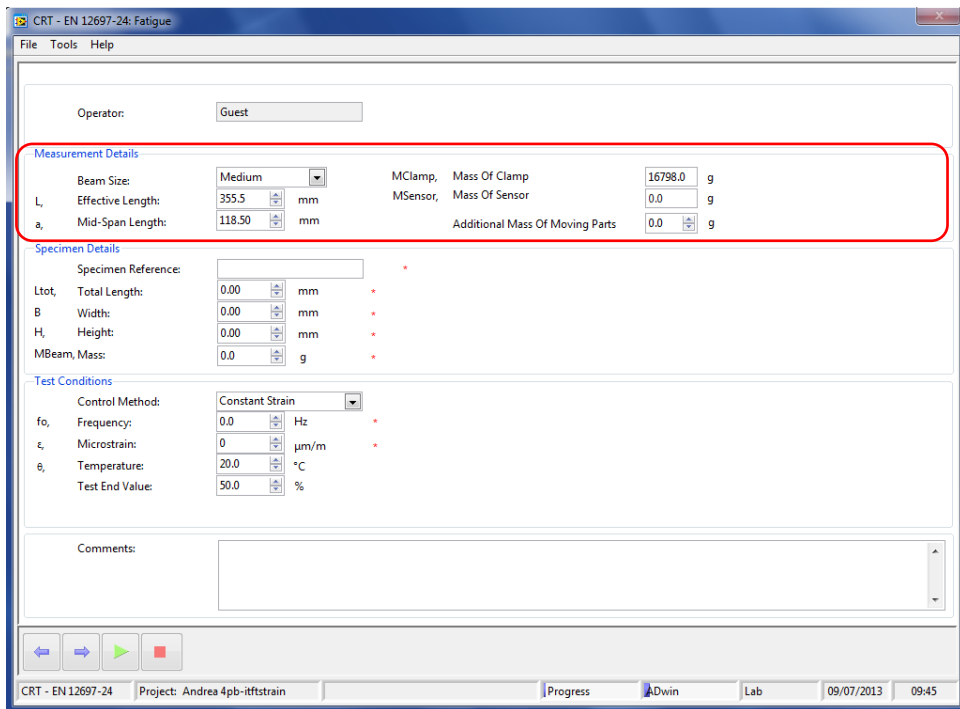


Figure A36 Medium beam size



**Figure A37** Large beam size

**Note:** the beam size used for this project is small (that is: effective length 355.5 mm and middle span length 118.5 mm). However, the specimens used in this project are slightly wider and higher thus a medium size clamping configuration was used (medium clamps size); in order to consider the mass of clamps correctly, the medium beam size configuration was chosen and then the effective length and middle span length was modified manually (see A38). Mass of clamps' value includes both sensors and moving parts, so the operator should not consider *mass of sensor* and *additional mass of moving parts* (values = zero).



**Figure A38** Medium clamping configuration for small specimens

- For each specimen, the total length (in millimetres), the width (in millimetres), the height (in millimetres) and the mass (in grams) have to be measured previously. It is recommended to measure four values for each face of the prismatic specimen (eight values of width and eight values of height in total) and four values of total length. After measuring and determined the average values, it is possible to complete the specimen details tabs as shown in Figure A39.

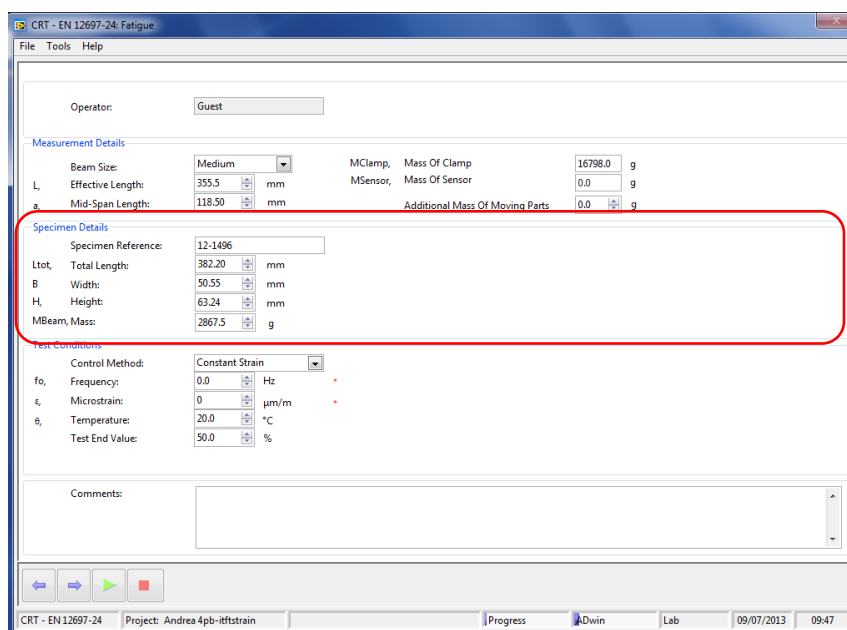


**Figure A39** Specimen details

- Choose the test conditions either for stress or strain controlled fatigue test (see Figure A40).

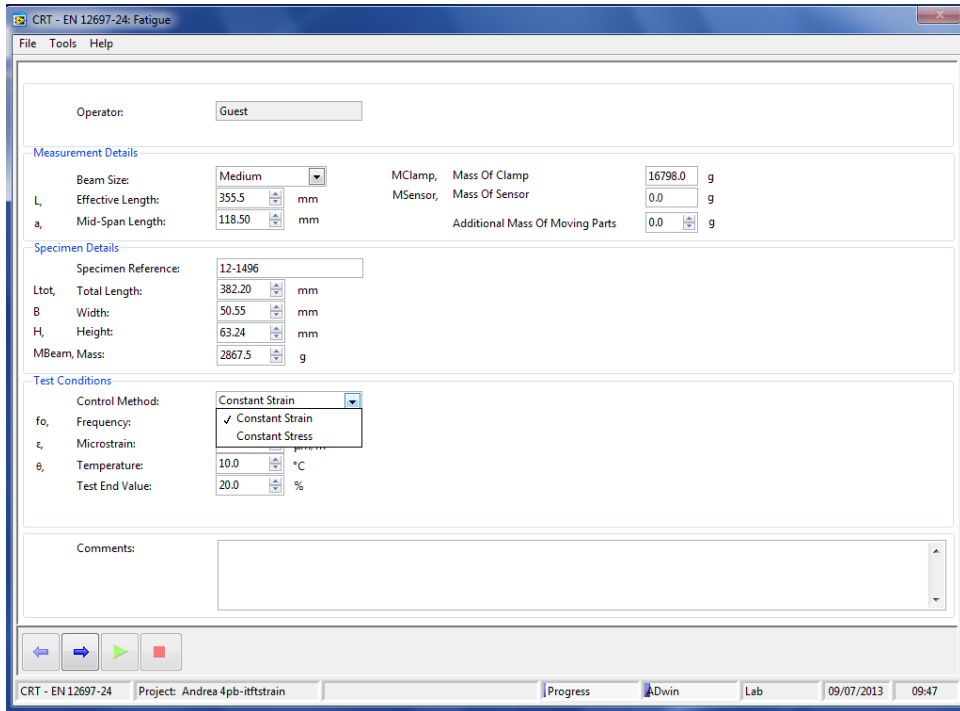
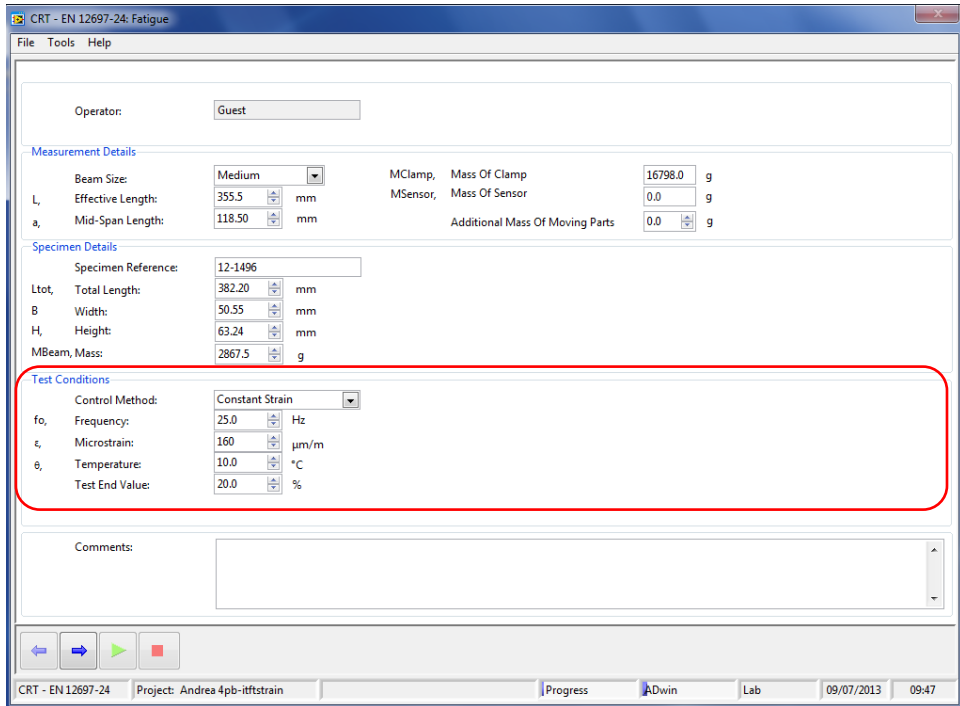


**Figure A40** Stress and strain controlled fatigue test

For a strain controlled fatigue test, frequency (in Hertz), temperature (in Celsius degree), test end value: failure criterion (for example, if the operator has chosen 20% as test end value, the test will stop when the stiffness values reaches the 20% of its initial value and strain level (in microstrain) are the parameters to choose for each test (see Figure A41).



**FigureA41** Strain controlled test conditions

For a stress controlled fatigue test, frequency (in Hertz), temperature (in Celsius degree), failure criterion (as percentage of initial stiffness value reduction) and stress level (in Kilo Pascal) are the parameters to choose for each test (see Figure A42).

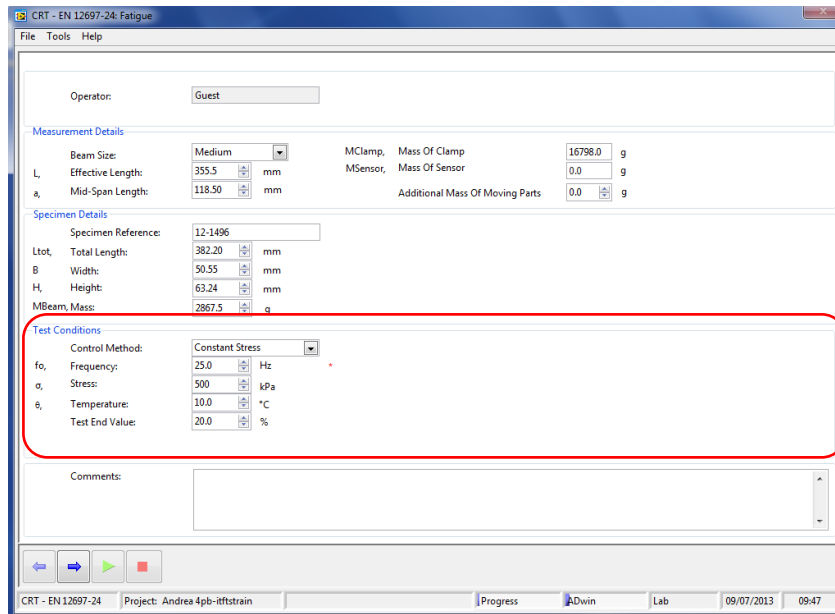


**Figure A42** Stress controlled test conditions

- After completing measurement and specimen details, and after choosing test conditions, press the blue arrow for the next tab: *save the test file*.

Identify a file name for the test (see Figure A43). Usually, the file name is chosen considering the ID number of the specimen and the test conditions (frequency, loading level and temperature).

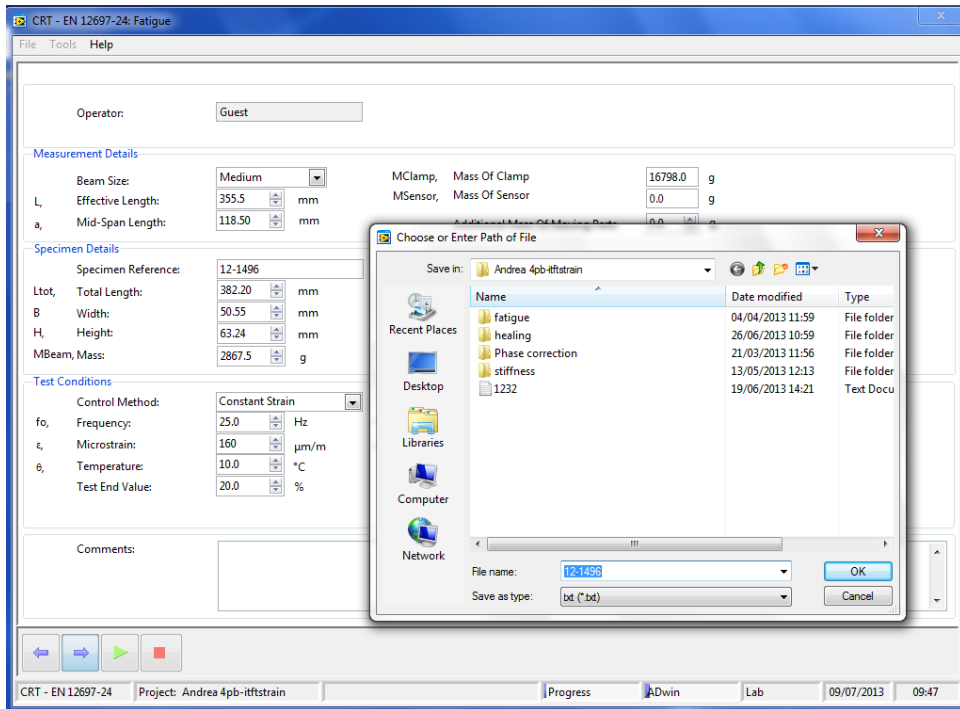


**Figure A43** Save test file

- Insert a specimen in the cabinet is the next step (see Figure A44).

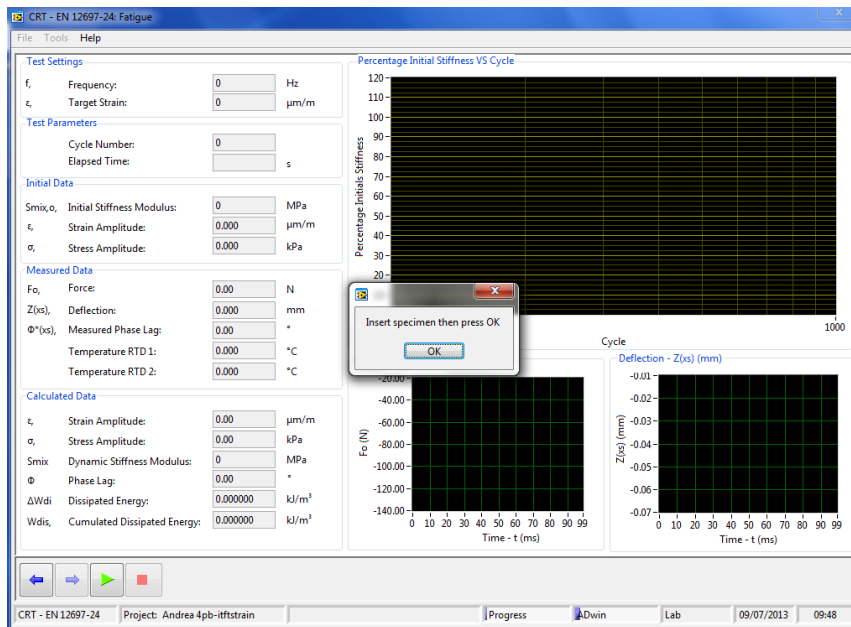


**Figure A44** Insert a specimen in the cabinet

**Note:** the specimen should be placed in a symmetric position with respect to the outer and inner clamps (see Figure A45). Also, the inner clamps are free

to translate along the longitudinal side and rotate; in order to place them in the right position, the inner clamps should be aligned at this stage as shown in Figure A46 (two arrows have been marked on the base. A ruler should be placed vertically against the clamp's support. The clamps' package should be moved (rotated) until the bottom edge of the ruler is aligned to the arrow drawn on the base plate).



**Figure A45** Specimen ready for clamping phase

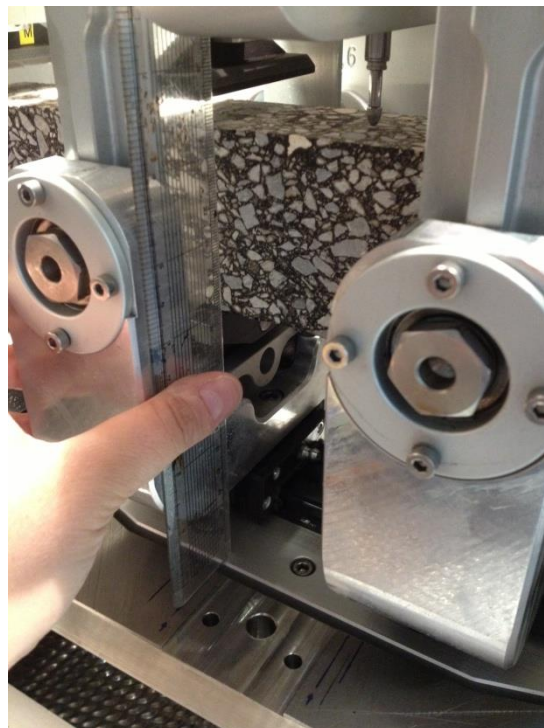


**Figure A46** Alignment of the inner clamps

- Clamping stage. After inserting a specimen (and press previously *OK*), the clamping phase starts (see Figure A47). Note: press continue when this phase is completed, that means the specimen is fully clamped (see Figure A48).

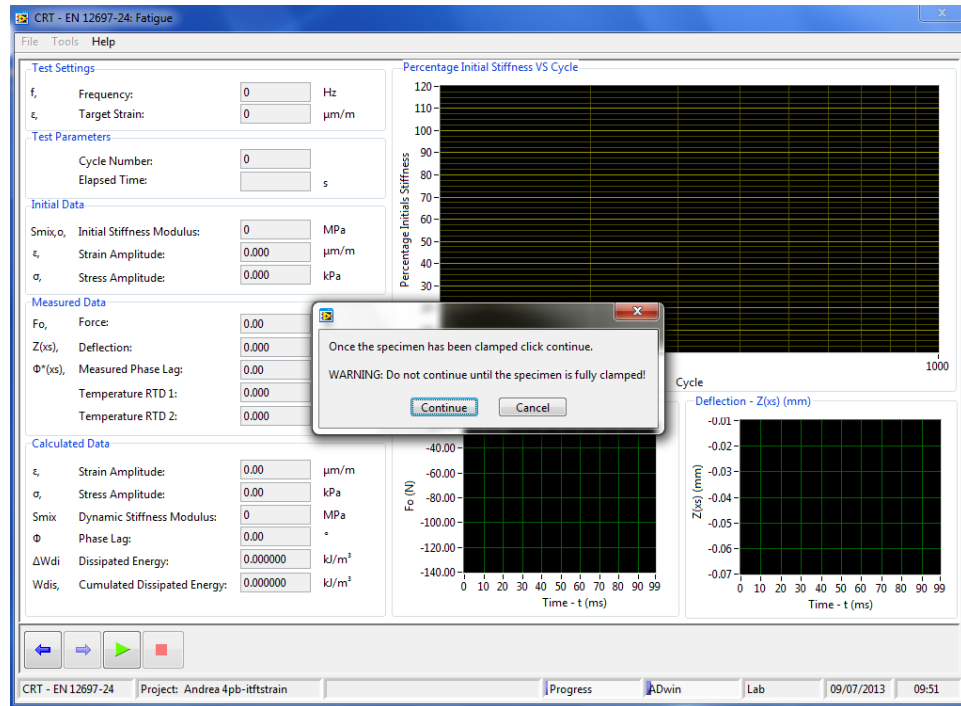


**Figure A47** Clamping phase



**Figure A48** Clamped specimen

- Figure A49 shows the following window that appears after pressing *continue*.

Adjust the three specimen LVDTs on the prismatic beam until each LVDT is in range (see Figure A49); in order to ensure that, the red cross should turn to green thick (see Figure A50 and Figure A51). Make sure the lvdts' supports are tightened appropriately.

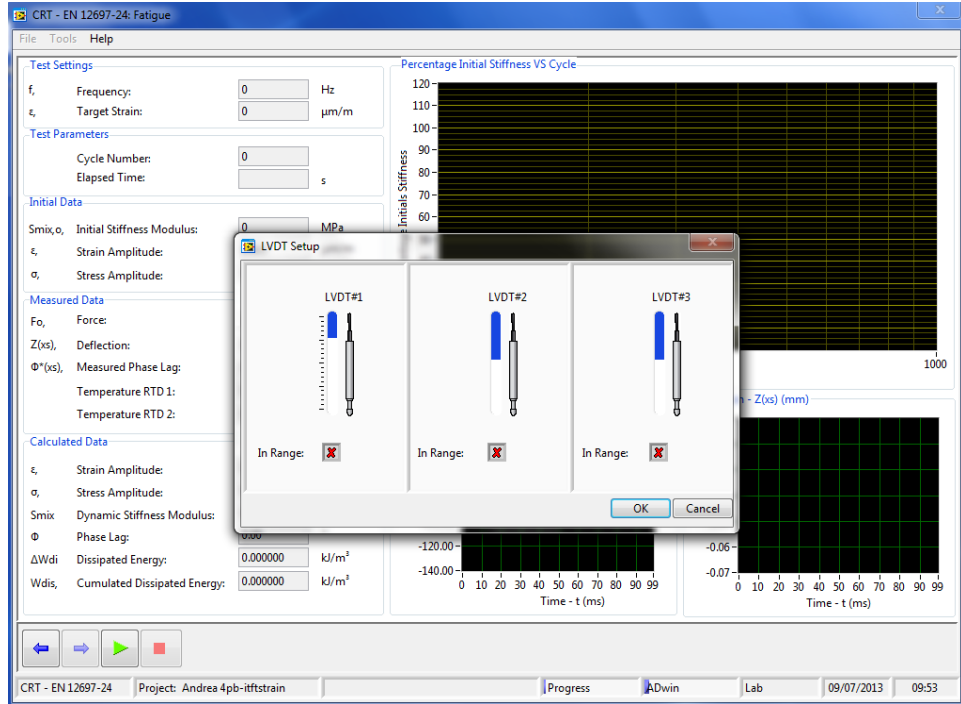


Figure A49 LVDTs Setup: not in range

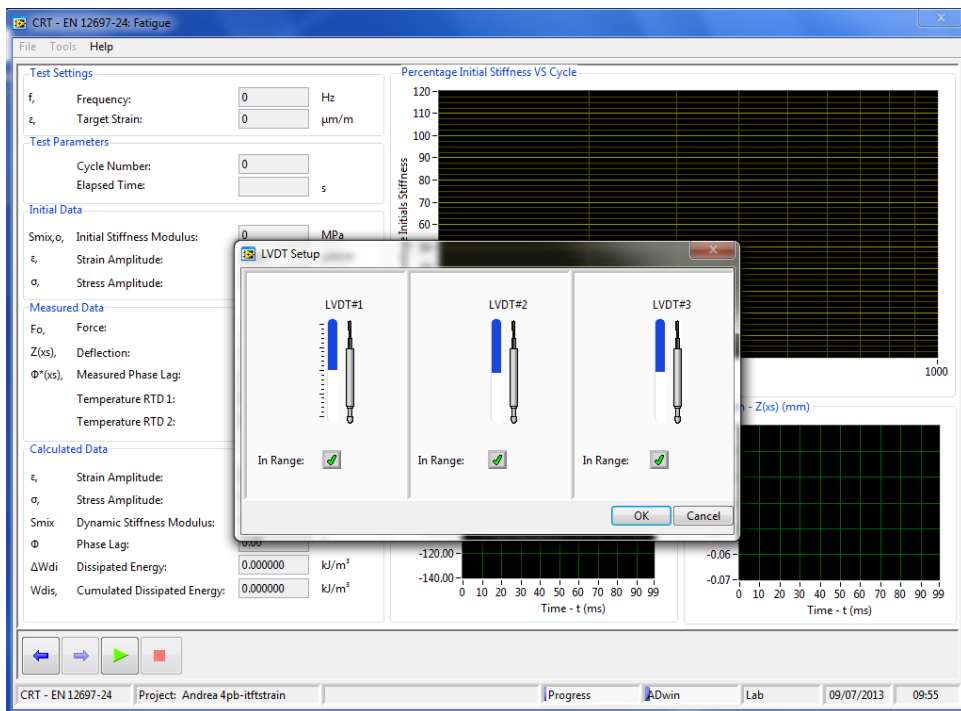
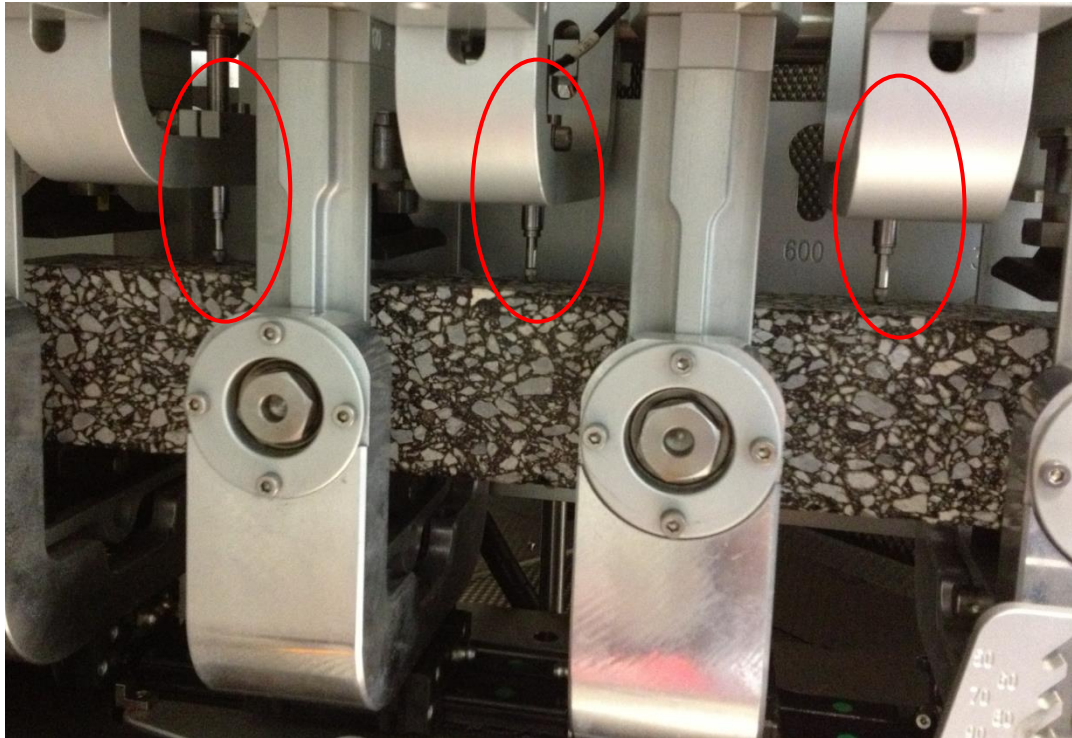
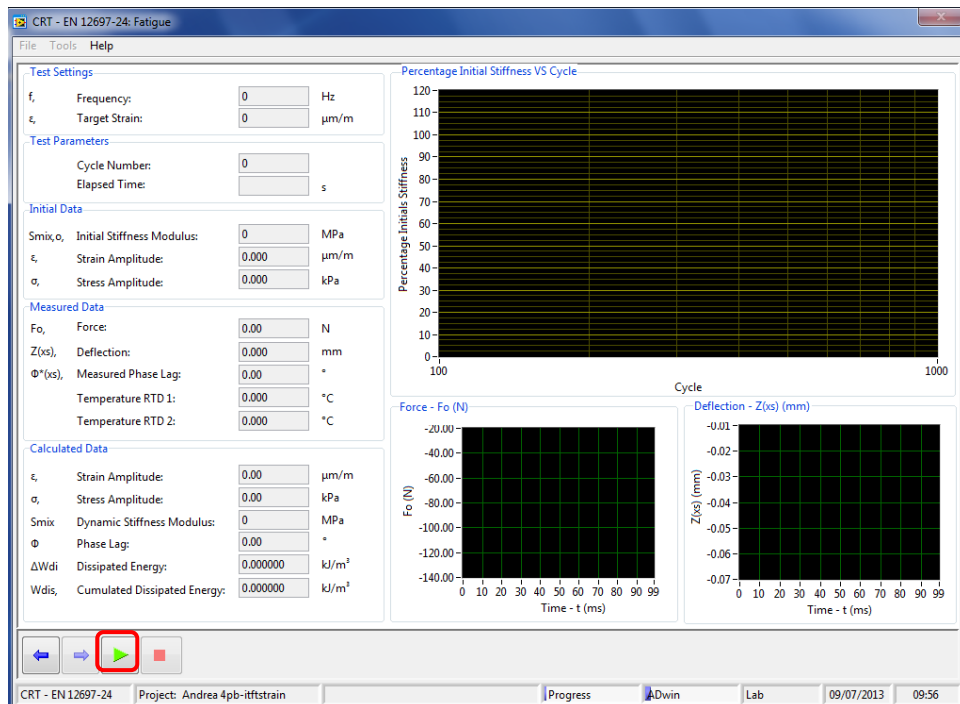


Figure A50 LVDTs Setup: in range.



**Figure A51** LVDTs in range.

- Once the LVDTs are set up, the conditioning stage can start. As said before, it is recommended to condition the prismatic beams for at least four hours before testing them. At this stage the software is waiting for the operator to press play and thus start the test (see Figure A52).



**Figure A52** Conditioning stage

- After the conditioning stage, the green button *play* will let the operator start the test. The main screen will show test settings (frequency and target strain/target stress), test parameters (current cycle number and time), initial data (initial stiffness modulus, initial strain and stress amplitude usually calculated at 100<sup>th</sup> cycle), measurement data (current force, deflection, and phase lag) and calculated data (current strain and stress amplitude, dynamic stiffness modulus, phase lag, dissipated energy and cumulative dissipated energy) as shown in Figure A53.

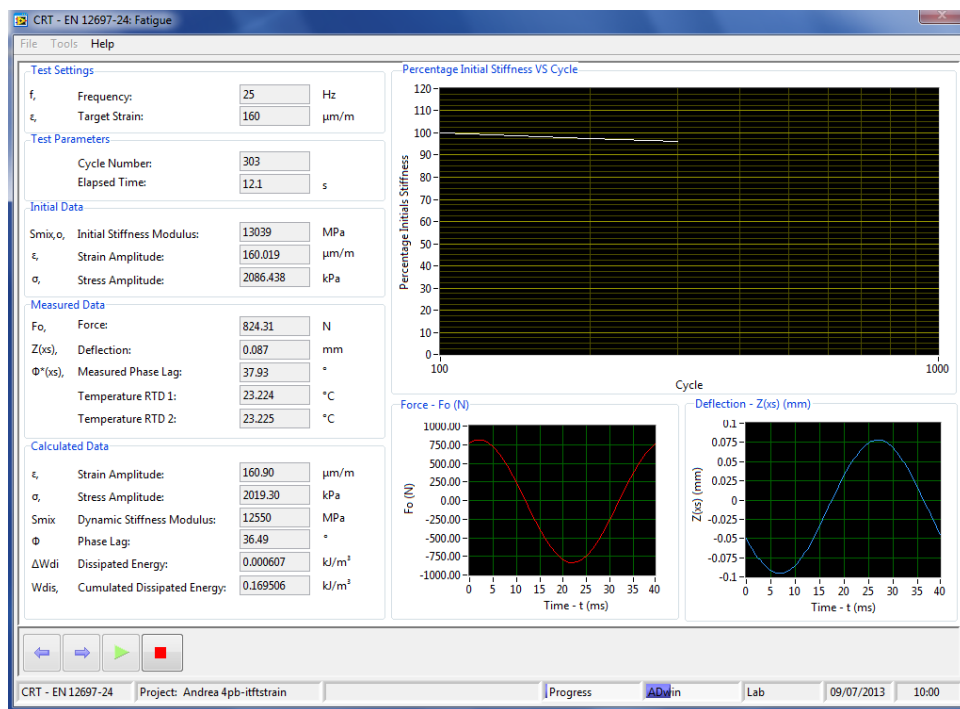


**Figure A53** Start test

- Once the specimen has failed, the test is finished and it is possible to remove the specimen from the machine (see Figure A54 and Figure A55). Failure corresponds to the complete failure of the specimen in stress controlled mode; fracture usually happens in the middle of the specimen where the bending moment is maximum (see Figure A56). In strain controlled mode, the specimen fails when the stiffness value has decrease of 50% from its initial value (determine at 100<sup>th</sup> cycle). Figure A57 shows the typical evolution of stiffness during a fatigue test in strain controlled mode; two different criteria are shown: 50% and 30% stiffness reduction from its initial value ( $E_0$ ).

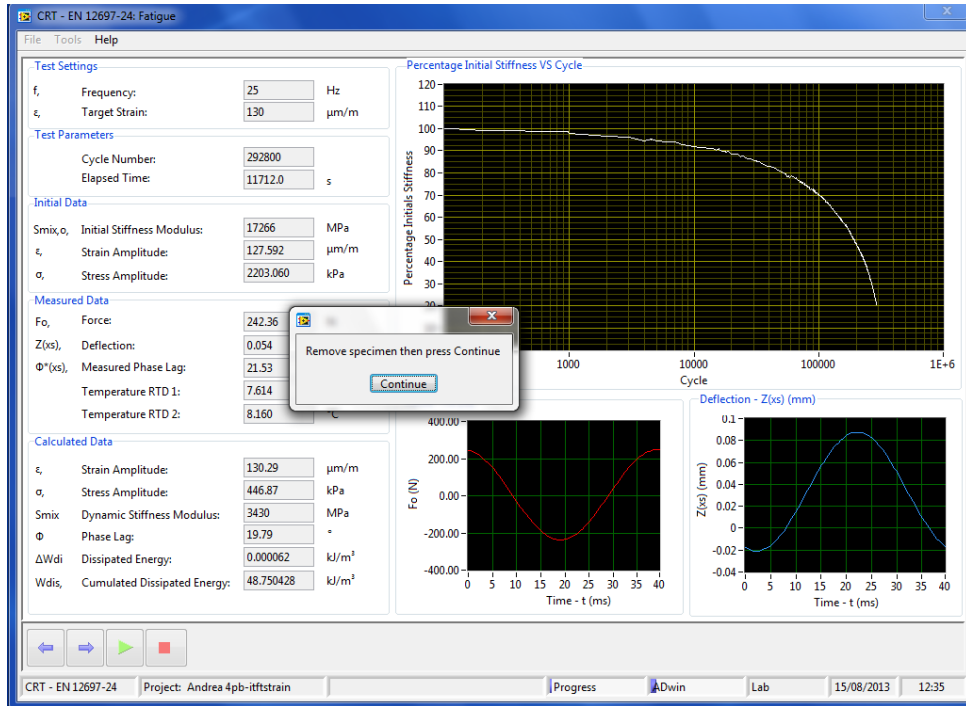


Figure A54 End test

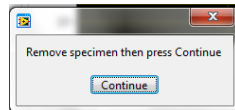
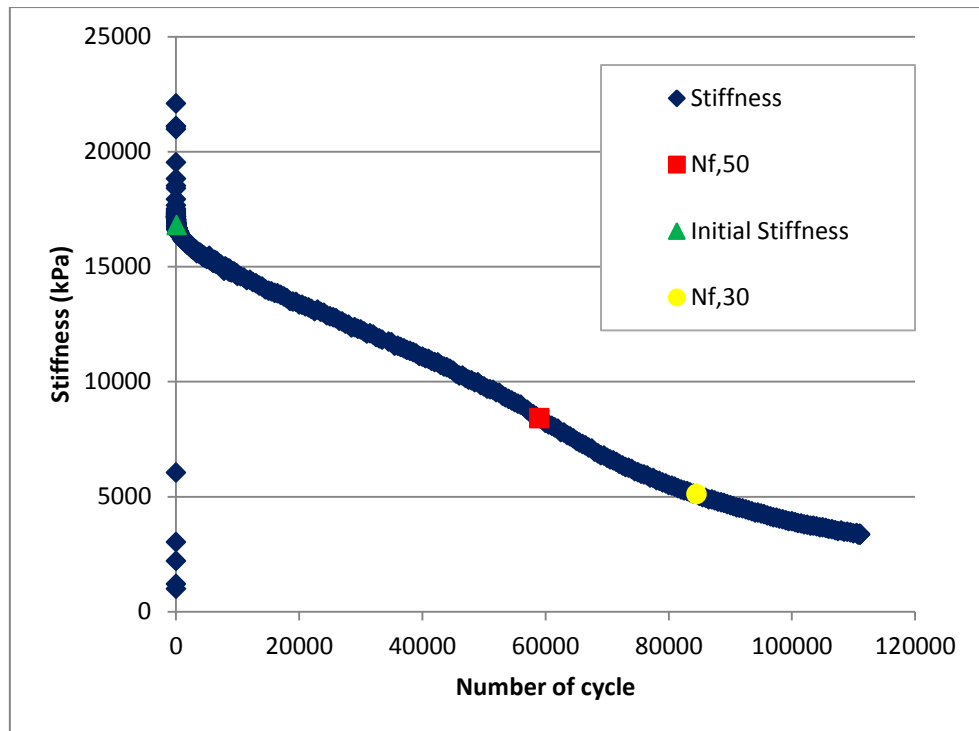


Figure A55 Message: remove specimen



Figure A56 Fracture in the middle of the specimen in stress controlled fatigue test



**Figure A57** Evolution of stiffness during a fatigue test in strain controlled mode

- At this point, the user can remove the failed specimens from the cabinet and place the next one and set a new test up.
- The test data is recorded every cycle for the first 500 cycles, every 100 cycles until the end of the test.

## 6. Measurement of stiffness

This procedure is for a stiffness test, thus the reference standard is the EN 12697-26: stiffness (see Figure A58).



**Figure A58** 4 Point Bending Stiffness Test

- After clicking on *stiffness test*, the software will require the data entry: the measurement details, the specimen details (such as dimensions and weight, previously measured) and the test conditions (mode of loading,

temperature, frequency, failure criterion and strain level). Figure A59 shows measurement and typical specimen details refer to the beam size for a stiffness test. See the previous section related to fatigue test.

The screenshot displays the 'CRT - EN 12697-26: Stiffness' software interface. The window title is 'CRT - EN 12697-26: Stiffness'. The menu bar includes 'File', 'Tools', and 'Help'. The interface is divided into several sections:

- Operator:** A text field containing 'Guest'.
- Measurement Details:**
  - Beam Size:** A dropdown menu set to 'Medium'.
  - Effective Length (L):** A numeric input field with '355.5' and 'mm'.
  - Mid-Span Length (a):** A numeric input field with '118.50' and 'mm'.
  - MClamp, Mass Of Moving Parts:** A numeric input field with '16798.0' and 'g'.
  - Additional Mass Of Moving Parts:** A numeric input field with '0.0' and 'g'.
- Specimen Details:**
  - Specimen Reference:** A text field containing '12-1496'.
  - Total Length (Ltot):** A numeric input field with '382.20' and 'mm'.
  - Width (B):** A numeric input field with '50.55' and 'mm'.
  - Height (H):** A numeric input field with '63.24' and 'mm'.
  - MBeam, Mass:** A numeric input field with '2867.5' and 'g'.
- Test Conditions:**
  - Control Method:** A dropdown menu set to 'Constant Strain'.
  - Test Temperature (θ):** A numeric input field with '20' and '°C'.
- Comments:** A large empty text area for notes.

At the bottom of the window, there is a toolbar with four icons: a left arrow, a right arrow, a green play button, and a red stop button. The status bar at the very bottom shows 'CRT - EN 12697-26', 'Project: Andrea 4pb-iftstrain', 'Progress', 'ADwin CPU', 'Lab', '09/07/2013', and '10:04'.

**Figure A59** Measurement and specimen details

Regarding the test conditions, choose to run the stiffness test either in controlled strain or stress (see Figure A60). The reference standard (EN 12697-26) describes the method to measure stiffness in strain control mode.

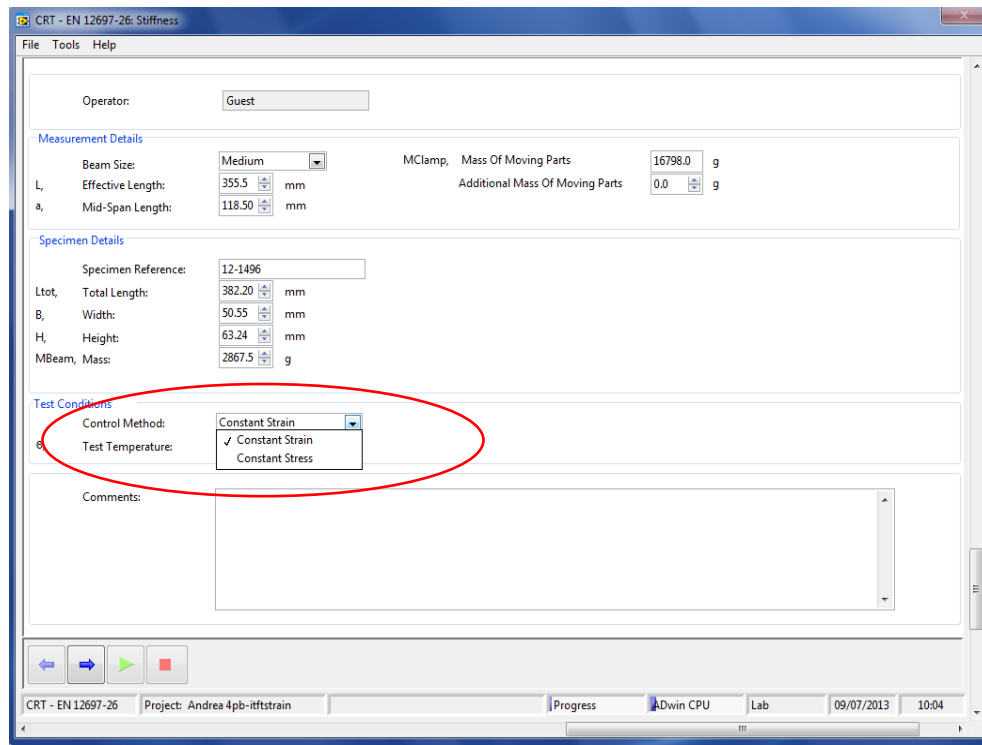


**Figure A60** Stiffness test either in strain or stress controlled mode

- Next stage is running a stiffness test. The operator has the chance to personalise the test depending on the frequencies and strain/stress levels desired. The amplitude of the load shall be such that no damage can be generated during the time needed to perform the measurements (usually  $50 \mu\epsilon$  is a typical value). The range of frequencies is device dependent. A typical set of frequencies could be 1 Hz, 2 Hz, 5 Hz, 10 Hz, 15 Hz, 20 Hz, 25 Hz and 30 Hz and again the starting frequency of 1 Hz. This last measurement is to check that the specimen has not been damaged during the loading with various frequencies. If the difference between stiffness of the specimen at the first and last measurements at identical frequency and at the same temperature is greater than 3%, it can be concluded that the specimen is damaged and, therefore, cannot be used for further testing

Two different options are available in the software (see Figure A61):

1. Create a new file test. Press *Add Stage* and choose frequency, strain level and number of cycles (see Figure A62). Repeat the same things as many as the number of frequency (and/or strain levels) it needs to be checked.
2. Open an existing test profile (previously built and saved) as shown in Figure A63.

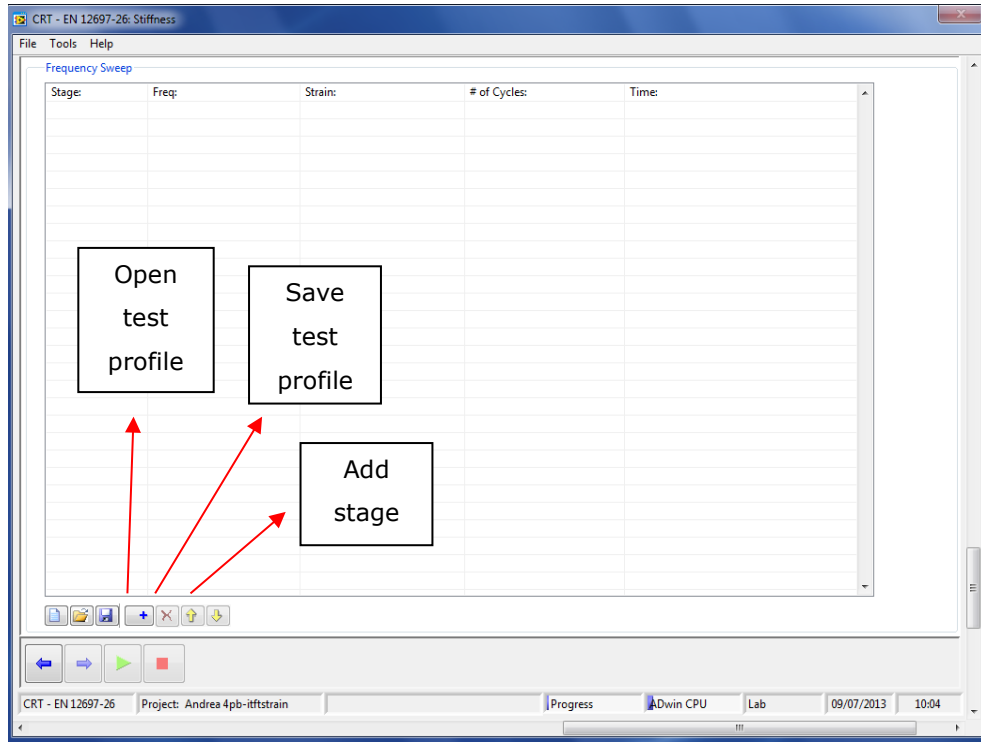


**Figure A61 Stiffness test**

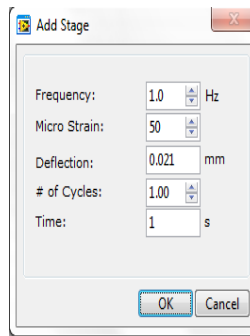


**Figure A62 Add stage**

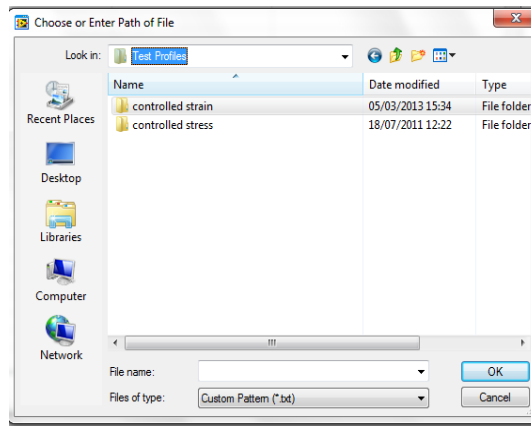


**Figure A63 Test profile**

A typical stiffness test profile is shown in Figure A64 where frequency varies from 1 to 30 Hertz and a strain level is 50  $\mu\epsilon$ . Each stage lasts 60 seconds,

thus the number of cycles depends on the frequency selected. The user is free to change the time and thus the number of cycles for each stage.

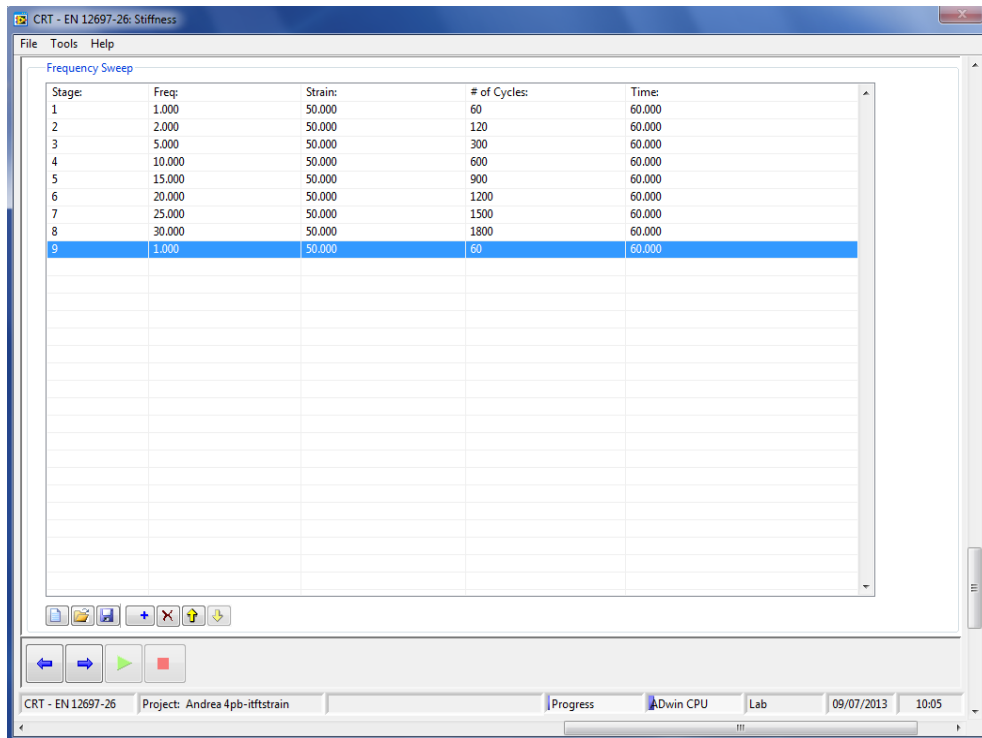


**Figure A64** Stiffness Test profile

- Identify a file name for the test (see Figure A65). The file name is, usually, chosen considering the ID number of the specimen and the test conditions (loading level and temperature).

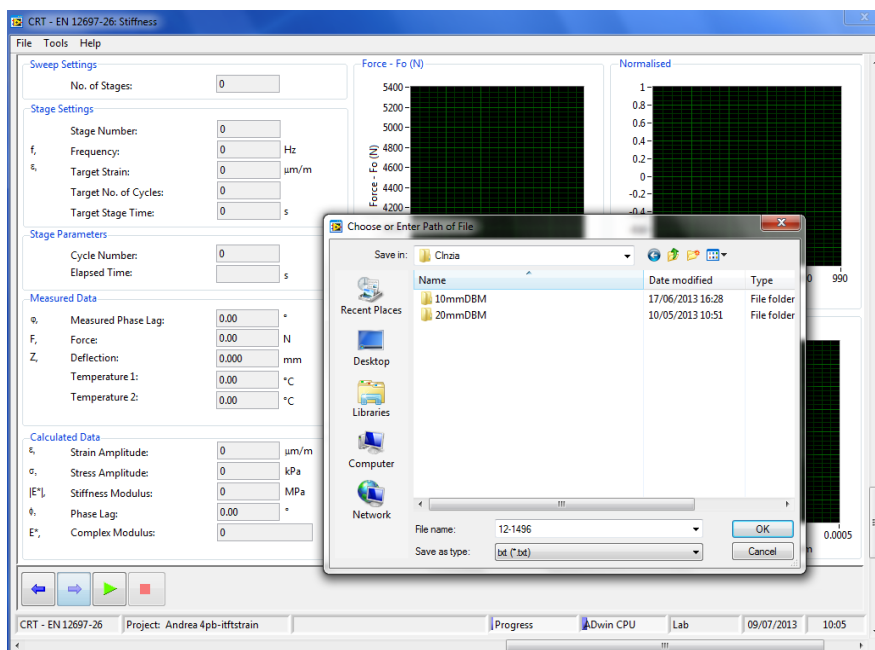


**Figure A65** Stiffness test: file name

- Insert a specimen in the cabinet is the next step (see Figure A66). See the section related to the fatigue test for the set-up of the specimen.

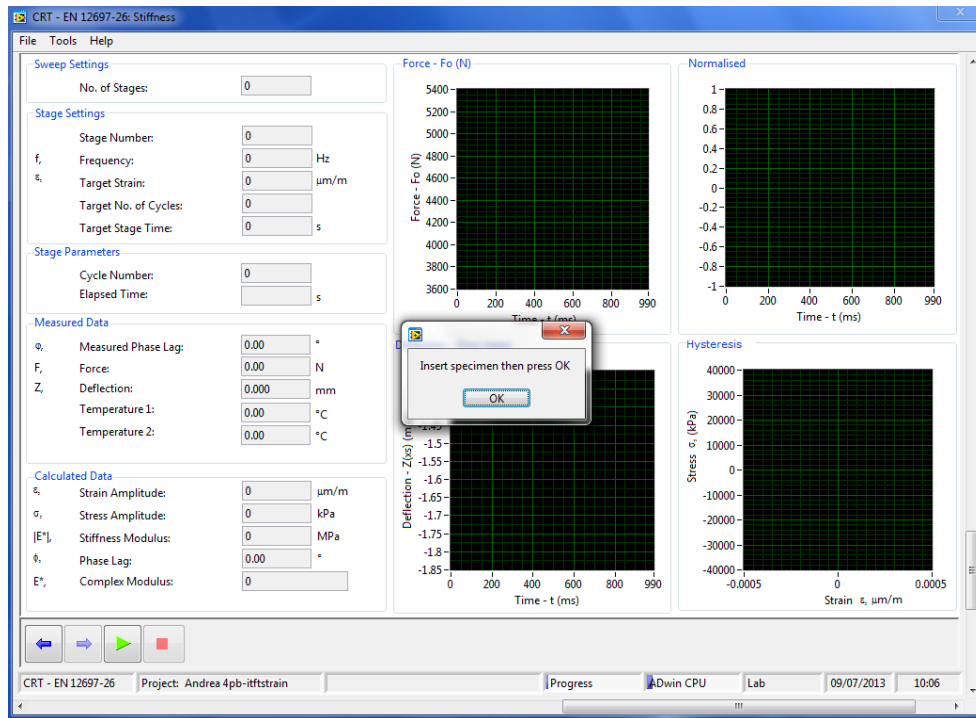


**Figure A66** Stiffness test: Insert the specimen

- Clamping stage. After inserting a specimen (and press previously OK), the clamping phase starts (see Figure A67). Note: press continue when this phase is completed, that means specimen fully clamped.

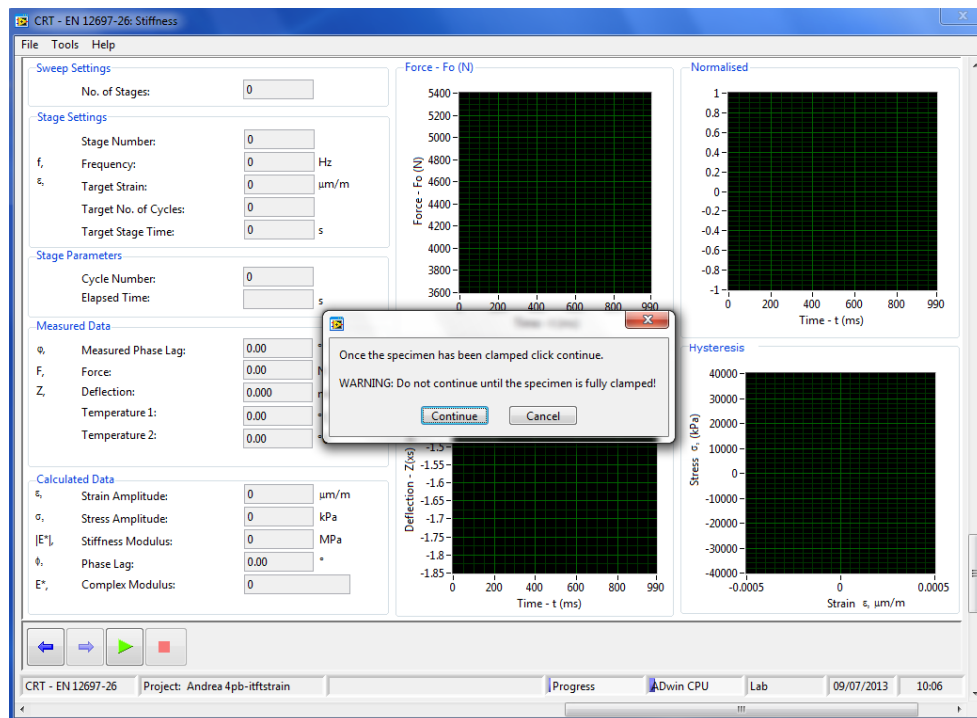


**Figure A67** Stiffness test: clamping phase

- As for the fatigue test, the operator needs to adjust the three specimen LVDTs on the prismatic beam until each LVDT is in range; in order to ensure that, the red cross should turn to green thick.
- Once the LVDTs are set up, the conditioning stage can start. As said before, it is recommended to condition the prismatic beams for at least four hours before testing them. At this stage the software is waiting for the operator to press play (see Figure A68).

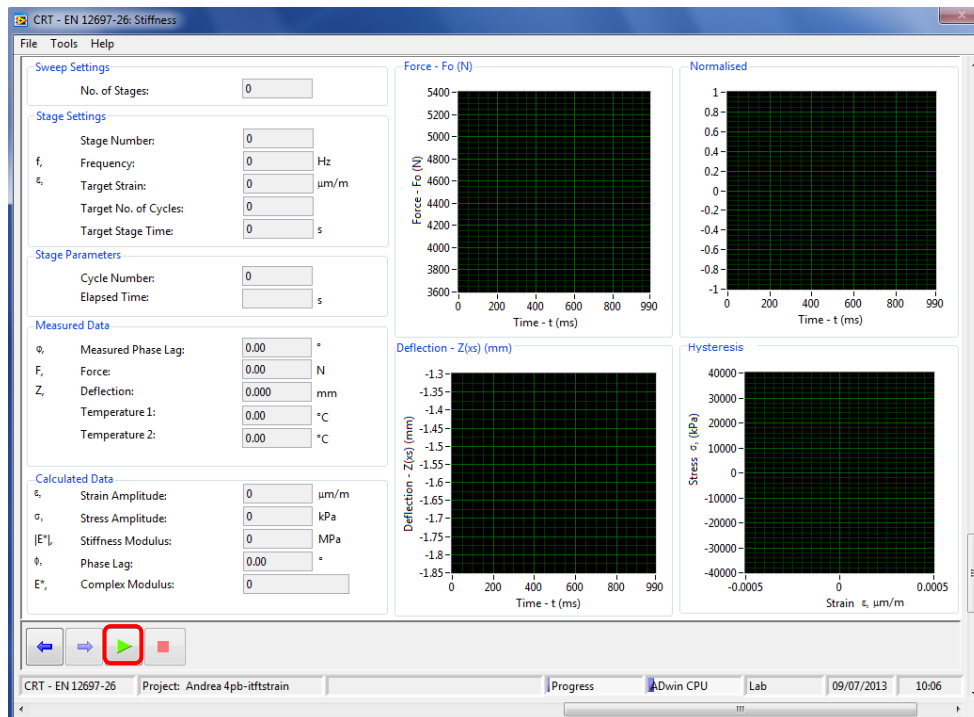


**Figure A68** Stiffness test: start

- After the conditioning stage, the green button will let the operator start the test. The main screen will show the stage settings (stage number, frequency and target strain/target stress, target number of cycle and time), stage parameters (current cycle number and time), measured data (phase lag, force, deflection and both temperatures) and calculated data (current strain and stress amplitude, stiffness modulus, phase lag and complex modulus) as shown in Figure A69.

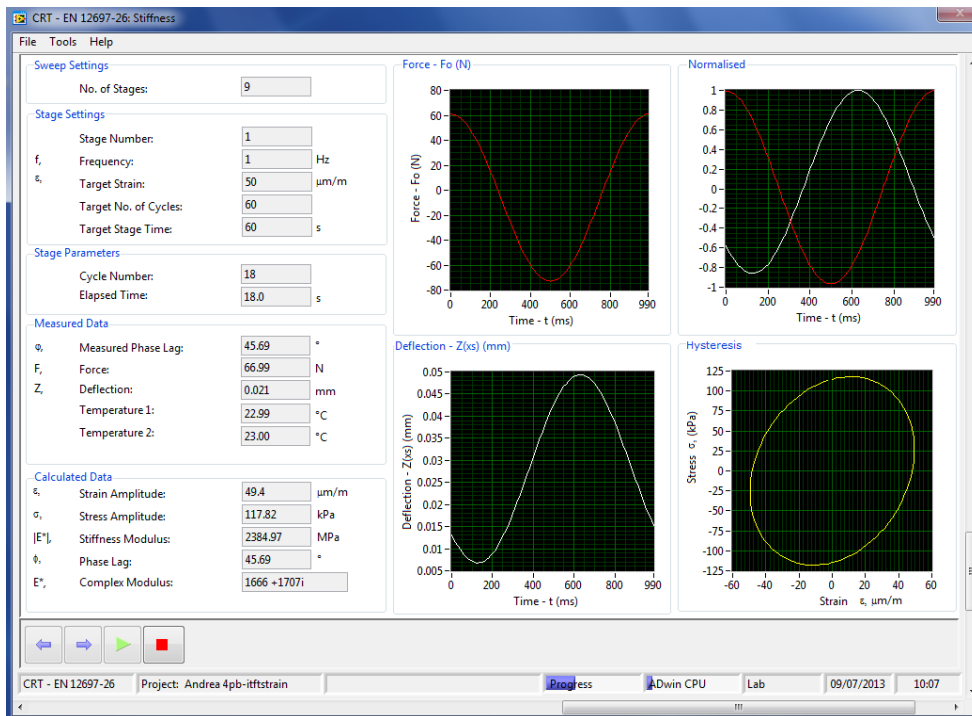


**Figure A69** Stiffness test

- Once the test is finished and it is possible to remove the specimen from the machine (see Figure A70).

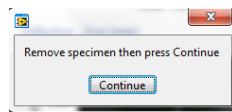


**Figure A70** Stiffness test: end

- The test data is recorded every cycle for the first 500 cycles, every 100 cycles until the end of each stage.

## 7. Advanced Software features

Advanced features of the software are restricted to selected users. There are three security levels:

- Lab Technician
- Technical Users
- CRT Engineer

To access restricted functions users are required to sign in. To sign in select sign in from the tools menu. Select the user name from the operator list and then enter the operator password.

## Phase compensation

The new machine was checked and calibrated by means of a dogbone aluminium specimen which geometrical and mechanical properties were known. A dogbone aluminum beam was tested in strain controlled at two different strain levels (50 and 100  $\mu\epsilon$ ) at 20°C at 12 different frequencies (from 1 to 60 Hz). After testing the aluminium beam, correction factors were determined (see Table A1).

**Table A1** Phase compensation

Phase Angle (°) - Compensation Factors			
Frequency (Hz)	First Test	Second Test	Average Value
1	0.4	0.6	0.5
2	0.5	0.7	0.6
5	1.6	1.4	1.5
8	2.0	2.2	2.1
10	2.9	2.7	2.8
15	4.1	4.0	4.0
20	5.1	5.1	5.1
25	6.4	6.1	6.3
30	7.2	7.2	7.2
40	9.7	9.4	9.5
50	12.0	12.2	12.1
60	12.9	12.7	12.8

The compensation values were inserted in the software and the following calibration procedure was followed:

- Click on phase correction after opening the tools menu (see Figure A71).

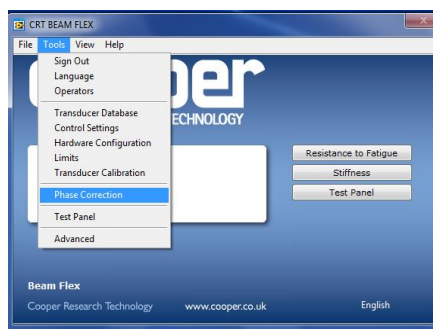


**Figure A71**Tools menu: Phase Correction

- After clicking on *phase correction* tab, the phase correction table will show the values set up previously. In order to correct the phase angle values, press *edit* (see Figure A72).

The image shows a dialog box titled "Phase Correction Table". Inside, there is a table with two columns: "Freq. (Hz)" and "Phase (°)". The table contains the following data:

Freq. (Hz)	Phase (°)
1.00	0.50
2.00	0.60
5.00	1.50
8.00	2.10
10.00	2.80
15.00	4.00
20.00	5.10
25.00	6.30
30.00	7.20
40.00	9.50
50.00	12.10
60.00	12.80

At the bottom of the dialog box, there are three buttons: "Edit..." (highlighted with a red box), "OK", and "Cancel".

**Figure A72** Phase Correction Table

- Enter the compensation value depending on the frequency tested (see Figure A73). Then press *ok*. Repeat the same thing for every frequency tested.

The image shows a dialog box titled "Enter Compensation Values". It contains two input fields: "Frequency (Hz)" with the value "1" and "Phase (°)" with the value "0.5". Both fields have up and down arrow buttons next to them. At the bottom, there are "OK" and "Cancel" buttons.

**Figure A73** Enter compensation value

### **Control Setting**

Among the software features, *controller gain settings* was used to set the stress and strain input in terms of waveforms.

Four different parameters have to be considered for tuning the machine:

- $K_o$  is the main system gain which affects the responsiveness of the system overall; a higher value will make the system more responsive at the risk of overshooting the target amplitude.
- $K_f$  is an additional term in the control algorithm; a higher value will actually have less effect (a lower value will have a greater effect). If the operator finds that the control performance is good at low frequencies (for example up to 5 Hz) but becomes progressive more unstable as frequency increases then increase  $K_f$  could be a solution.
- $K_{spstrain}$  affects both strain and stress control tests, a higher value will increase stability
- $K_{spstress}$  does not affect the test.

**Note:** changing the controller gain settings might affect the performance of the SA4PT-BB. Contact CRT before making any adjustments.

A sensible level of stability and minimal overshoot was found with the values reported in the Table A2.

**Table A2** Control parameters

Mode of loading	$K_0$	$K_{spStress}$	$K_{spStrain}$	$K_f$
Strain control mode	0.08	1000	1000	80
Stress control mode	0.3-0.4	1000	1000	80

**Note:**  $K_0 = 0.3$  was chosen for 10mm DBM;  $K_0 = 0.4$  was chosen for the 20mm DBM. In case of healing (in strain control mode) and stiffness test,  $K_0=0.8$  was found to be more suitable after the tuning of the machine.

In order to change the control parameters should be followed:

- Click on *Control Settings* after opening the tools menu (see Figure A74).

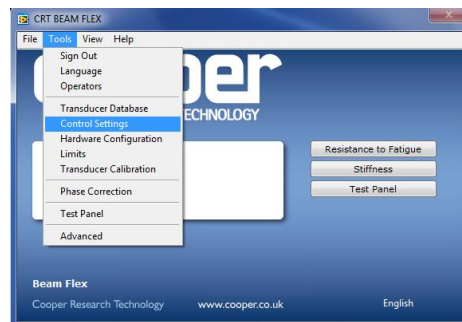


**Figure A74** Tools menu: Control Settings

- After clicking on *control settings* tab, the control factors table will show the values set up previously. Insert the correct load and deformation parameters and then press *OK* (see Figure A75).

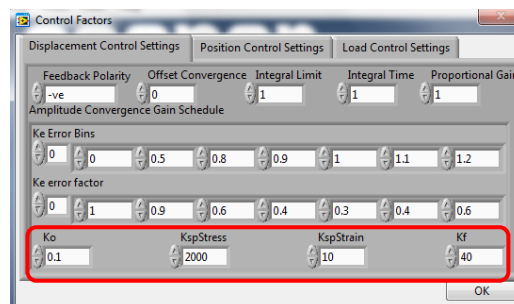


**Figure A75** Control factors

## Testing protocol for

### **Measurement of resistance to fatigue using Indirect Tensile Fatigue Test (ITFT) in strain controlled mode.**

#### **1. Scope**

This procedure outlines the steps to be taken for characterising the fatigue behaviour of bituminous mixtures by Indirect Tensile Fatigue Test (ITFT) in strain control mode.

#### **2. Equipment**

The main equipment includes:

- a steel loading frame;
- a load cell;
- two loading strips;
- two deformation strips (glued to the specimen);
- two LVDTs;
- a temperature cabinet;
- test software.

#### **3. Conditioning and test temperature**

The specimens shall be placed in the thermostatic chamber and exposed to the specified test temperature for at least 4 h prior to testing.

#### **4. Sample Preparation**

See section 7.2.

#### **5. Geometric measurement of cylindrical specimens**

- Take six measurements of diameters ( $d$ ) around the cylindrical specimen: two measures for each side of the specimen and two in the middle section as shown in Figure A76, using the calliper with the fine point fittings measure to 0.1 mm. Drawing the diameters could help in the measurements. Record all measurements and calculate the mean of the four diameters readings ( $d$ ) and record to 0.1 mm.

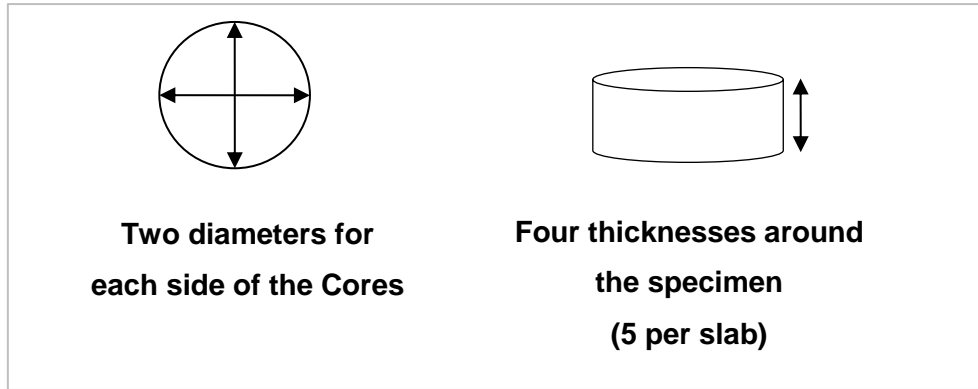


**Figure A76** Measurement of the cylindrical specimen

- Take four readings of the thickness ( $t$ ) of the specimen as shown in Figure A76. Calculate the mean of the top width ( $b$ ) and record to 0.1 mm.

#### 6. Measurement of resistance to fatigue in strain controlled mode

- Turn on the equipment (air compressor) and the control box (see Figure A77).

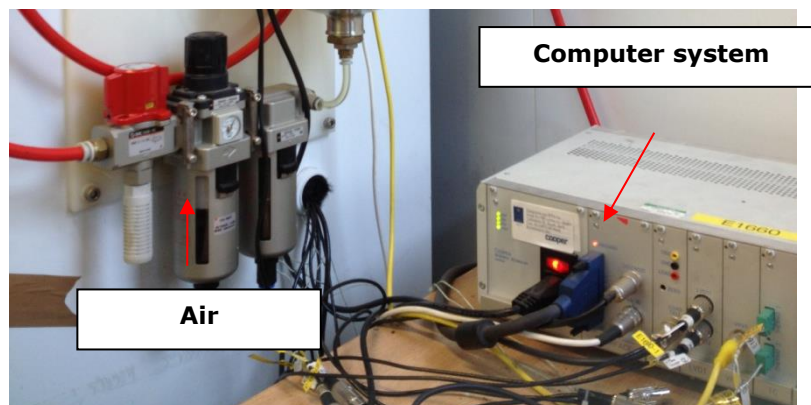


**Figure A77** Air compressor and computer system

- Open the *ITFT strain controlled* software by double clicking the software icon, shown in Figure A78.

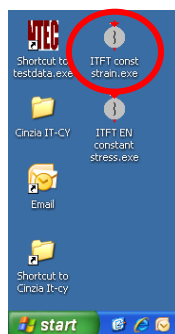


**Figure A78** ITFT strain controlled mode icon

- After opening the software, the first screen window shows the reference standards and gives a brief introduction of the fatigue test (see Figure A79).

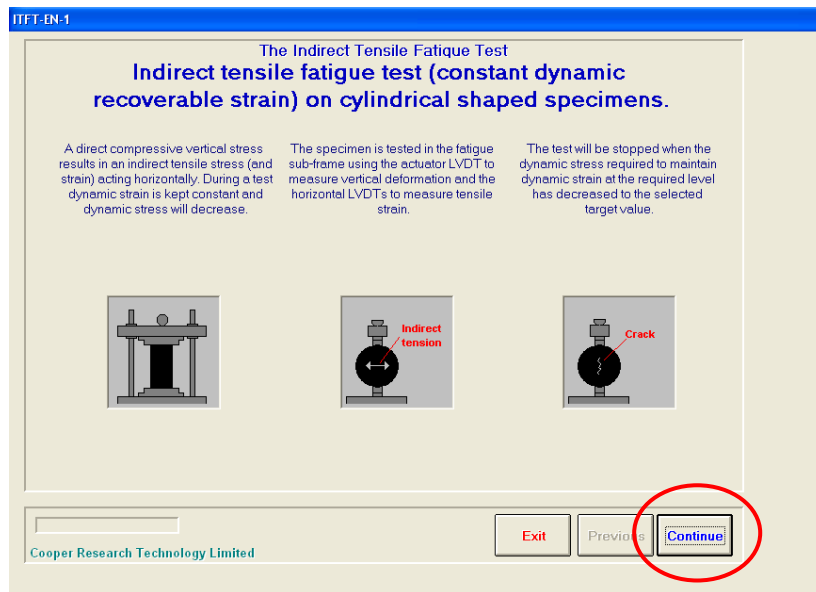


**Figure A79** The Indirect Tensile Fatigue Test (strain controlled)

- After pressing *continue*, the software automatically will ask for the name of the file in which the test data will be stored during the test. It is recommended to create a new folder first, and then choose a filename (example: specimen reference number\_strain level\_temperature). After that, click save.

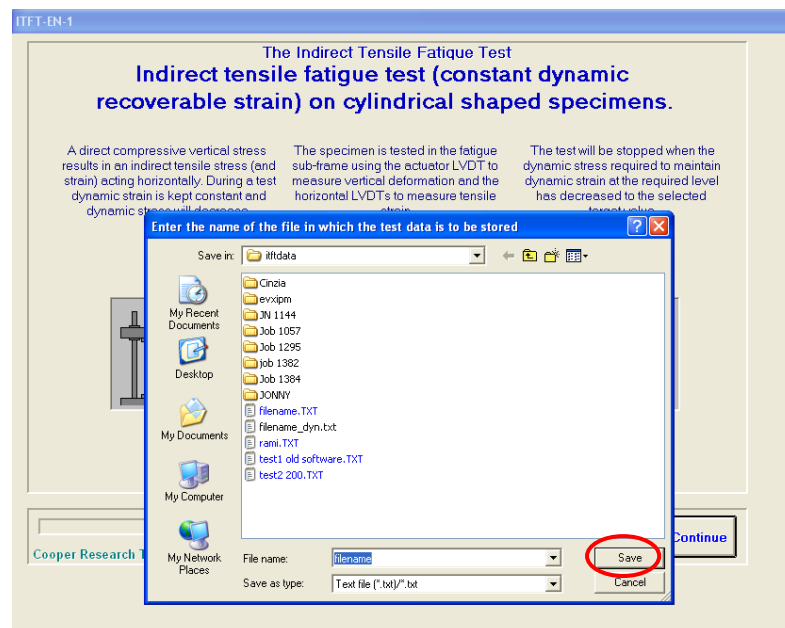


**Figure A80** Filename

- Before starting a test, it is necessary to choose the Operator (the user that will be in charge of the test). At this point, either add a new operator (by pressing *add*) or select a name on the list as shown in Figure A81. **Note:** it is recommended to know all the specimen's characteristics such as: thickness, diameter, specimen reference number, etc.

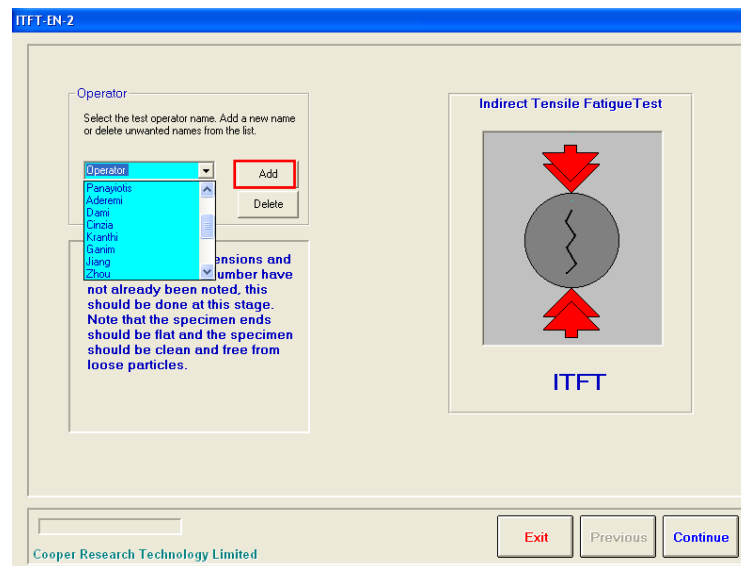


**Figure A81** Select or Add the operator

- Once *continue* is clicked, the software automatically will ask for the reference of the specimen (ID reference number) as shown in see Figure A82.

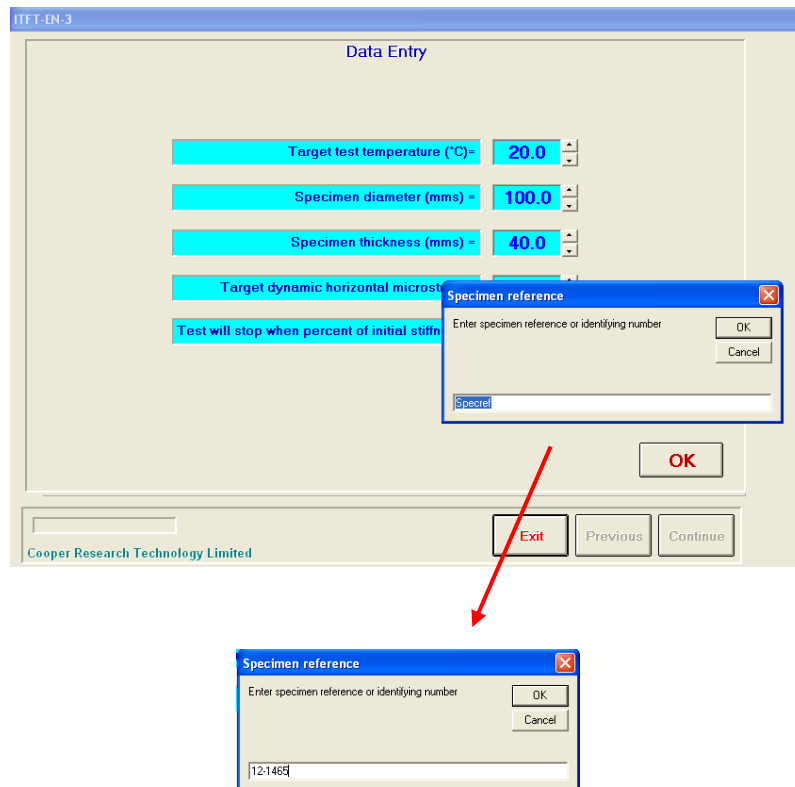


**Figure A82** Specimen reference number

- After clicking *OK*, a message box will ask if the test temperature is not significantly different from the previous test (see Figure A83). This is a new intuitive way to help the testing machine to reach the target strain level as fast as possible. Basically, if the test temperature is not significantly different from the previous test, the software knows the material stiffness and it will reach the target very quickly; if the test temperature is significantly different from the previous test and/or if the material is different from the previous test, the software will apply few initial pulses at very low strain level and slowly it will reach the target strain level; this was made in order to not over stress the specimen at the beginning of a fatigue test.

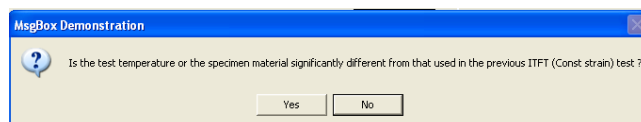


**Figure A83** Message Box: Temperature of the test

- *Data Entry* window is shown in Figure A84. The user has to set-up the target temperature, the diameter and the thickness of the specimen

(previously measured) and the strain level desired and the failure criterion. Press *ok* to go to the next tab.

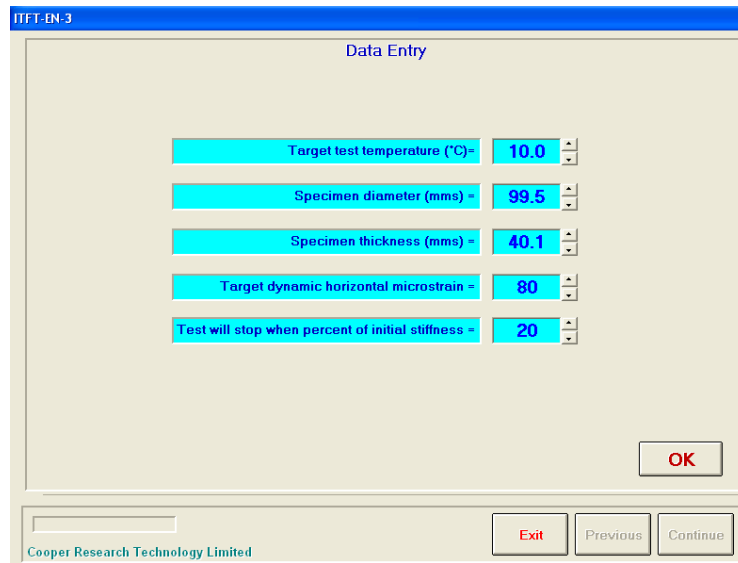


**Figure A84** Fatigue test set-up

- After clicking *ok*, the polynomial relationship between deformation in millimetres and binary bits is shown in the next window (see Figure A85).

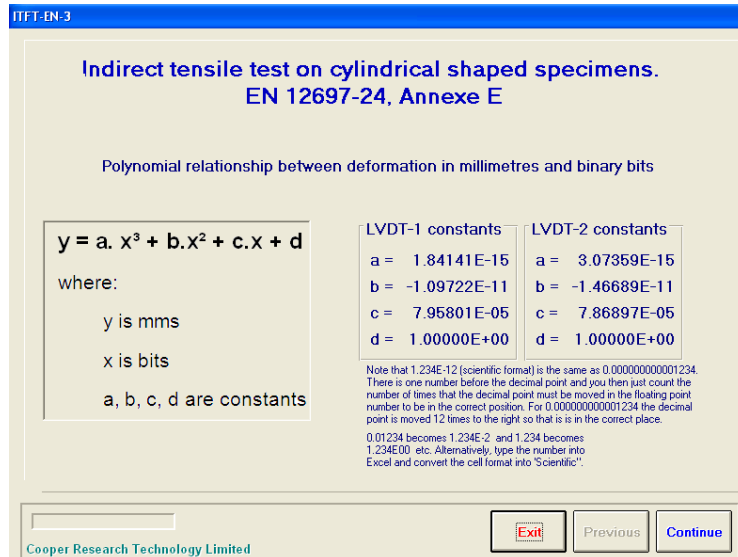


**Figure A85** Polynomial relationship between deformation in millimetres and binary bits

- After clicking *continue*, a new message box will appear (see Figure A86).

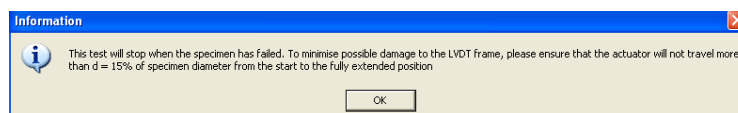


**Figure A86** Protection of the LVDT

The test will stop when the specimen fails (see Figure A87). In strain controlled mode, failure usually corresponds with the number of cycle at which stiffness values is 50% decreased from its initial value ( $E_0$ ). It is rare that the specimen breaks in two halves as in stress controlled mode, but it often shows a crack along the longitudinal diameter as shown in Figure A88.

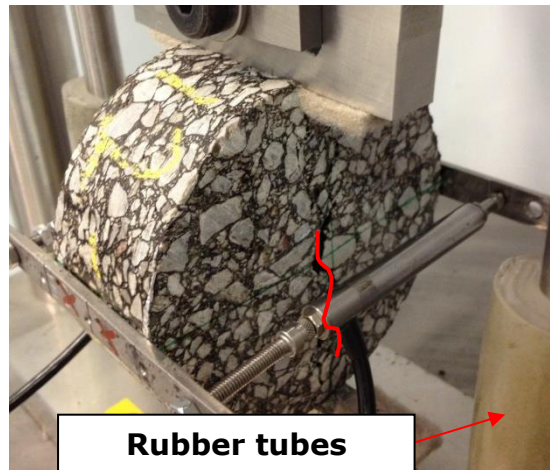


**Figure A87** Failure in strain controlled mode



**Figure A88** Cracked specimen after testing it

In order to minimise possible damage to the LVDT frame, it is necessary to ensure that the actuator will not travel more than the 15% of specimen diameter from the start to the fully end. Two pieces of rubber tube have been fitted in order to stop the upper loading strip

from falling down when the specimen splits. This way the LVDTs are protected.

- After ensuring that the crosshead nuts are tight and that the specimen is central on the lower loading strip, press *OK* (see Figure A89).



**Figure A89** Crosshead nuts should be tight and the specimen should be located centrally under the actuator

- Figure A90 shows how to adjust the range of the LVDTs by means of a spanner number 7. It is recommended not to set the LVDTs at the very end of their range.

**NOTE:** the end of LVDTs range corresponds to 0 mm on this case. So the LVDTs should be set-up at their maximum compression (0 mm) because the horizontal diameter will increase during the fatigue test (see Figure A91). The LVDTs should be adjusted so that they are almost fully retracted because the horizontal deformation increases during the test and the LVDTs need to be free to extend (see Figure A90). Make sure the LVDTs' reading is not too close to the end of travel to avoid damage. *Be aware that in stress control mode the maximum compression corresponds to 2.5 mm.* The LVDTs readings are different depending on the mode of loading.

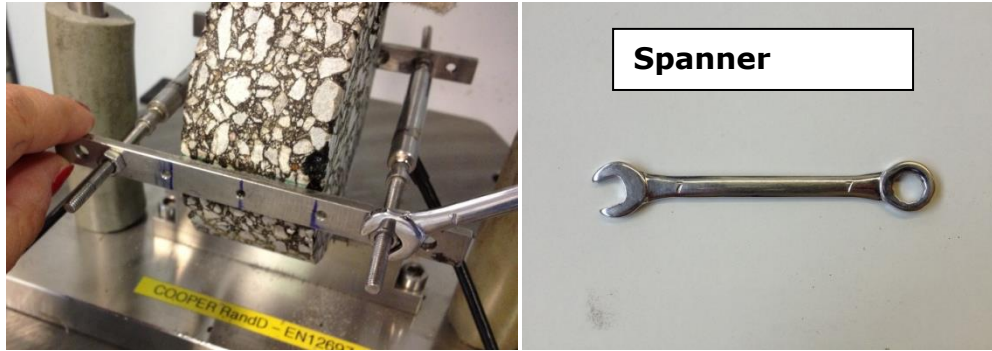


**Figure A90** Adjustment manually of the LVDTs.

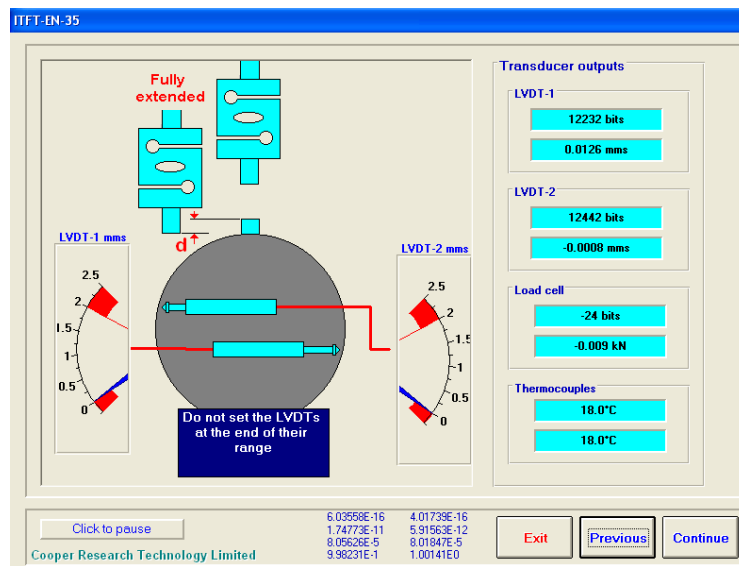


**Figure A91** Adjustment (software) of the LVDT: maximum compression

- Once the LVDTs are in the right position, after pressing *continue*, the software will remind the operator to place test assembly under the actuator when it has retracted (see Figure A92).

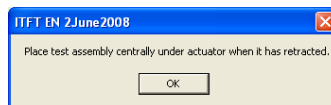


**Figure A92** Place test assembly under the actuator

- After pressing *OK* and placing the test assembly under the actuator, it is possible to start a fatigue test. NOTE: the actuator position should be at half of its range at this stage, which means around the zero value. See Figure A93.

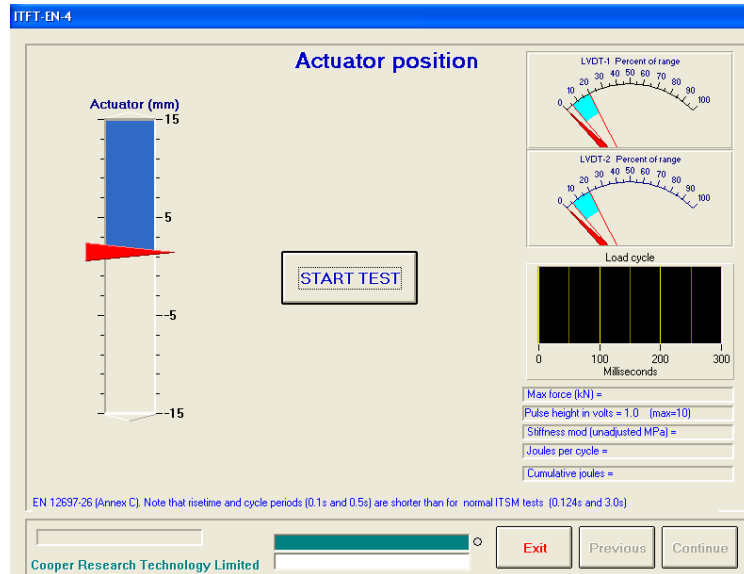


**Figure A93** Actuator position. Starting the fatigue test.

- During a fatigue test is possible to check the values of different measurements such as number of pulse, stiffness modulus, dissipated energy, cumulative dissipated energy, permanent horizontal and vertical deformations, etc. See Figure A94.

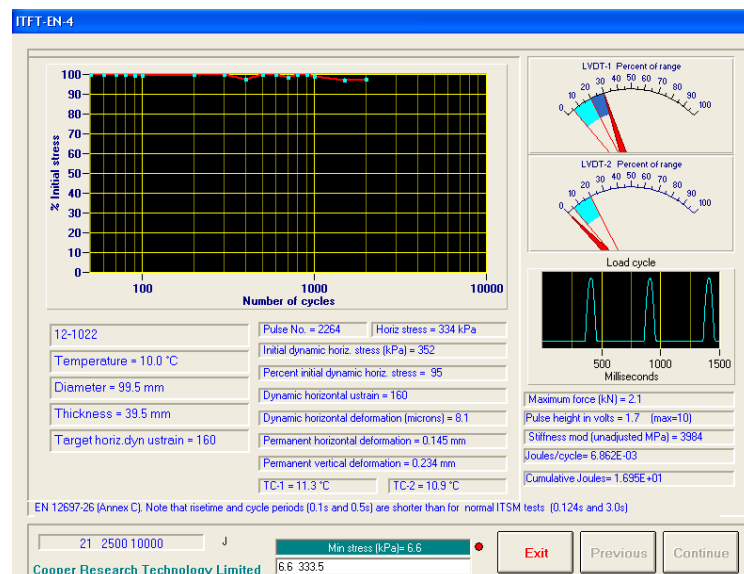


**Figure A94** Fatigue test

- During a test, it may happen that one of the LVDTs extends more than its calibrated range (see Figure A95). In this case, the operator needs to adjust them (see Figure A96) and press *resume test* when the LVDTs are in range again (see Figure A97).

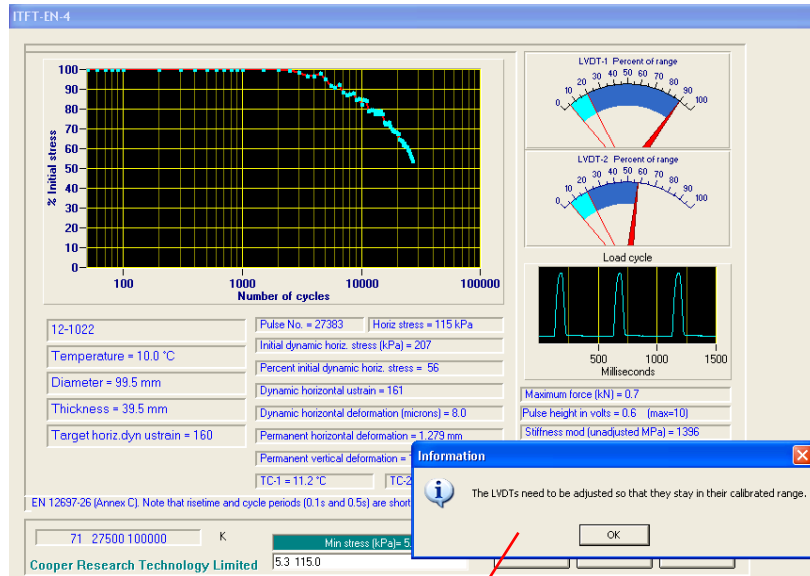


**Figure A95** LVDTs out of their calibrated range

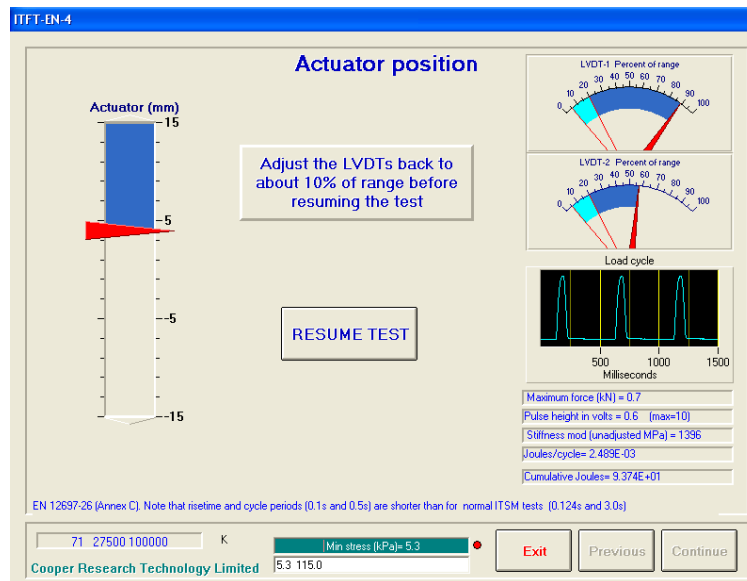


**Figure A96** Adjust LVDTs

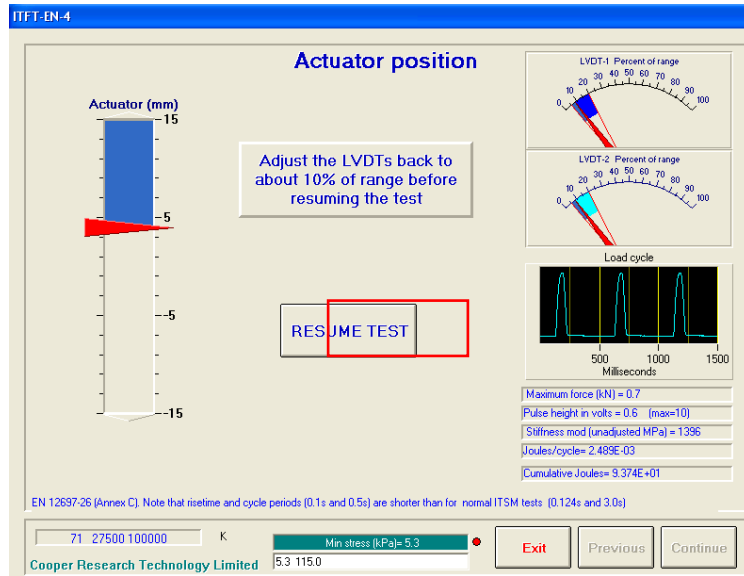


**Figure A97 Resume Test**

- When stiffness is at 50% of its initial value (see Figure A98), the test ends.

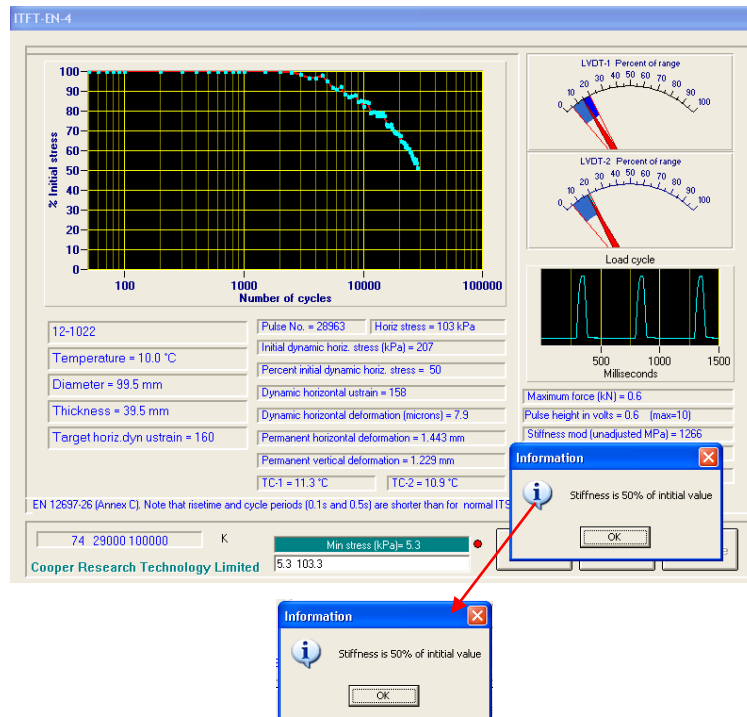


**Figure A98 End of test**

- At this point, the user can remove the failed specimen from the cabinet and install the next one and re-set up a new fatigue test.
- The test data is recorded every 10 cycles for the first 100 cycles; every 100 cycle for the first 1000 cycles; every 500 cycles until the end of the test.

# Appendix B

Data for 10mm DBM

**Table B1** Air Void and Dimensions of trapezoidal specimens (2PB)

Sample ID	Bulk Density (Kg/m <sup>3</sup> )	Maximum density (Kg/m <sup>3</sup> )	Air Void %	e (mm)	b (mm)	B (mm)	h (mm)
11-2801	2367	2479	4.5	24.9	23.9	54.5	250.2
11-2802	2320	2479	6.4	25.2	24	54	250.5
11-2803	2378	2479	4.1	25.1	24.7	54.5	250.5
11-2804	2368	2479	4.5	25.1	23.9	56	250.3
11-2805	2370	2479	4.4	25.3	23	55.3	251
11-2806	2346	2479	5.4	25.2	23.8	55.9	250.5
11-2807	2362	2479	4.7	25.1	23.3	54.9	250.5
11-2808	2347	2479	5.3	25.3	24.2	56	250.2
11-2809	2355	2479	5.0	25.3	23.9	56.1	250.3
11-2810	2317	2479	6.5	25.2	24.8	56.3	249.4
11-2811	2382	2479	3.9	25.2	24.2	55	249.9
11-2812	2353	2479	5.1	24.9	25.3	55.2	249.4
11-2813	2327	2479	6.1	25.1	24.8	55.6	249.4
11-2814	2367	2479	4.5	25.1	24	55.2	250
11-2815	2349	2479	5.2	24.3	24.5	54.5	249.7
11-2816	2350	2479	5.2	25.1	24.9	54.9	250
11-2817	2349	2479	5.2	25.2	24.5	54.9	249.7
11-2819	2327	2479	6.1	25.1	24.7	55.2	249.9
11-2821	2353	2479	5.1	24.7	24	54.7	249.5
11-2822	2342	2479	5.5	25.3	24.7	55.1	249.9
11-2823	2339	2479	5.6	24.9	25.1	54.8	250
11-2824	2356	2479	5.0	24.6	24	54.8	251.1
11-2825	2377	2479	4.1	25.2	24.4	54.6	251.6
11-2826	2345	2479	5.4	24.9	24.8	55.1	251.3
11-2827	2390	2479	3.6	25	24.4	54.4	251.2
11-2828	2361	2479	4.8	25	24.9	54.9	251.7
11-2829	2379	2479	4.0	24.8	24.5	54.8	251.1
11-2830	2363	2479	4.7	24.9	24.5	55	250.9
11-2831	2337	2479	5.7	24.8	24.1	55.5	250.6
11-2832	2337	2479	5.7	25.3	24.9	56.2	250.2
11-2833	2372	2479	4.3	24.3	23.8	54.3	251.4
11-2834	2321	2479	6.4	25.4	24.6	55	251.2
11-2835	2353	2479	5.1	25.1	24.9	55.5	252.3
11-2836	2362	2479	4.7	24.9	24.9	55.3	250
11-2837	2371	2479	4.4	25.2	24	54.3	250.5
11-2838	2382	2479	3.9	25.3	23.8	55	250.5
11-2839	2329	2479	6.1	25	24.5	56.1	249.9
11-2840	2368	2479	4.5	24.7	24	55	250
11-2841	2367	2479	4.5	24.8	25	55.4	250.4

11-2842	2384	2479	3.8	25	24.7	55.4	250.3
11-2843	2381	2479	4.0	25.2	24.7	55.4	250
11-2844	2355	2479	5.0	24.9	24.6	55.7	250.5
11-2845	2365	2479	4.6	25.1	24.3	55.2	250.5
11-2846	2358	2479	4.9	23.7	23.6	54.9	249.7
11-2847	2325	2479	6.2	24.9	24.9	56.3	249.8
11-2789	2332	2479	5.9	24.9	25	55.7	251.2
11-2799	2330	2479	6.0	25.1	24	56.4	250.4
11-2794	2329	2479	6.1	25.1	24	54.9	251.7
11-2795	2325	2479	6.2	25.3	24.7	55	251.4

**Table B2** Air Void of prismatic specimens (4PB)

Specimen ID	Bulk Density (Kg/m <sup>3</sup> )	Target density (Kg/m <sup>3</sup> )	Air void (%)	Length (mm)	Width (mm)	Height (mm)	Mass (g)
12-1489	2360	2344	5.3	381.7	51.28	64.82	2982.3
12-1490	2374	2344	4.8	381.4	51.38	62.73	2905
12-1491	2378	2344	4.6	381	50.45	63.36	2876.6
12-1492	2382	2344	4.5	380.5	50.11	63.33	2853.2
12-1493	2387	2344	4.3	380.87	50.34	63.15	2876.6
12-1494	2380	2344	4.5	380.37	50.8	64.18	2948.5
12-1495	2369	2344	5.0	381.5	50.77	64.09	2924
12-1496	2356	2344	5.5	382.2	50.55	63.24	2867.5
12-1497	2399	2344	3.8	381.5	53.06	67.32	3277.8
12-1498	2403	2344	3.6	380	52.23	64.48	3083.3
12-1499	2378	2344	4.6	383.25	53.17	65.75	3170.6
12-1500	2394	2344	4.0	380.1	52.38	64.21	3059
12-1501	2401	2344	3.7	380.3	52.55	64.26	3068.3
12-1502	2379	2344	4.6	383.25	52.14	62.90	2983.3
12-1503	2391	2344	4.1	382.5	52.59	64.08	3059.3
12-1505	2359	2344	5.4	380.6	50.9	63.5	2985
12-1506	2400	2344	3.7	380	50.19	64.20	2911
12-1507	2383	2344	4.4	380	50.03	64.51	2894.7
12-1508	2364	2344	5.2	380	49.7	63.65	2808.8
12-1509	2396	2344	3.9	380	50.03	64.64	2915.2
12-1510	2396	2344	3.9	380	49.80	63.37	2849.5
12-1511	2405	2344	3.5	380.1	49.9	63.5	2956.3
12-1512	2408	2344	3.4	379	49.85	63.75	2881.5

**Table B3** Air Void and Dimensions of cylindrical specimens (ITFT)

<b>Specimen ID</b>	<b>Bulk Density (Kg/m<sup>3</sup>)</b>	<b>Target Density (Kg/m<sup>3</sup>)</b>	<b>Air Void (%)</b>	<b>Diameter (mm)</b>	<b>Thickness (mm)</b>
12-159	2406	2367	2.90	99.6	40.2
12-160	2389	2367	3.60	99.1	39
12-161	2395	2367	3.40	99.1	41.7
12-162	2391	2367	3.50	99.3	40.9
12-163	2394	2367	3.40	99.2	41
12-164	2398	2367	3.30	99.4	40.6
12-165	2389	2367	3.60	99	40.5
12-166	2359	2367	4.80	99.2	41.2
12-167	2384	2367	3.80	99.1	37.9
12-168	2386	2367	3.80	99.1	40.4
12-169	2410	2367	2.80	99.1	40.8
12-170	2390	2367	3.60	99	40.7
12-171	2387	2367	3.70	99.2	40.4
12-172	2407	2367	2.90	99.1	40.6
12-173	2399	2367	3.20	99.2	39.4
12-174	2395	2367	3.40	99.2	40.2
12-175	2381	2367	4.00	99.1	40.5
12-176	2370	2367	4.40	99.1	38.7
12-177	2374	2367	4.20	99.2	39.8
12-178	2372	2367	4.30	99.2	39.9
12-1018	2403	2479	3.06	99.4	38.79
12-1019	2395	2479	3.4	99.4	39.3
12-1020	2362	2479	4.7	99.4	39.43
12-1021	2361	2479	4.7	99.41	40.15
12-1022	2378	2479	4	99.42	40.46
12-1023	2405	2479	3	99.38	39.83
12-1024	2375	2479	4.2	99.48	38.99
12-1025	2363	2479	4.7	99.47	39.86
12-1026	2380	2479	4	99.43	40.13
12-1027	2360	2479	4.8	99.52	39.55
12-1028	2397	2479	3.3	99.42	40.38
12-1029	2356	2479	4.9	99.44	39.64
12-1030	2343	2479	5.4	99.53	38.94
12-1031	2354	2479	5	99.48	38.8
12-1032	2362	2479	4.7	99.49	40.1
12-1033	2346	2479	5.3	99.45	39.21
12-1034	2367	2479	4.5	99.47	39.36
12-1035	2328	2479	6	99.52	40.51
12-1036	2386	2479	3.75	99.45	39.66
12-1037	2376	2479	4.13	99.41	40.23
12-1038	2364	2479	4.6	99.44	40.7

12-1039	2396	2479	3.35	99.41	39.01
12-1040	2392	2479	3.5	99.43	39.06
12-1041	2391	2479	3.4	99.45	40.15
12-1042	2396	2479	3.6	99.46	39.07

**Table B4** 2PB stiffness test (Nantes, France)

Temperature (°C)	Frequency (Hz)	E1	E2	Stiffness	Phase Angle (°)
		(MPa)	(MPa)	(MPa)	
-10	40	23820	1635	23877	3.9
-10	30	23531	1685	23592	4.1
-10	25	23349	1746	23415	4.3
-10	10	22271	1987	22360	5.1
-10	3	20633	2308	20762	6.4
-10	1	18948	2537	19117	7.7
0	40	18379	2728	18581	8.5
0	30	17900	2775	18115	8.8
0	25	17559	2847	17789	9.2
0	10	15802	3064	16096	11.0
0	3	13397	3295	13796	13.8
0	1	11045	3332	11536	16.8
10	40	11778	3504	12289	16.6
10	30	11118	3489	11653	17.4
10	25	10668	3524	11235	18.3
10	10	8584	3468	9258	22.0
10	3	5972	3157	6756	27.9
10	1	3932	2599	4714	33.5
15	40	8465	3530	9172	22.7
15	30	7806	3450	8534	23.9
15	25	7357	3430	8117	25.0
15	10	5389	3104	6219	30.0
15	3	3244	2445	4063	37.0
15	1	1856	1717	2529	42.8
20	40	5505	3195	6365	30.2
20	30	4932	3034	5790	31.6
20	25	4551	2957	5427	33.0
20	10	2979	2391	3820	38.8
20	3	1542	1588	2213	45.8
20	1	788	949	1234	50.3
30	40	1674	1762	2430	46.5
30	30	1403	1554	2093	47.9
30	25	1236	1435	1894	49.2
30	10	681	916	1141	53.4

30	3	321	463	564	55.3
30	1	175	229	288	52.8
40	40	408	636	756	57.3
40	30	339	531	630	57.5
40	25	298	476	561	57.9
40	10	179	268	322	56.2
40	3	110	126	167	48.8
40	1	74	62	97	40.4

**Table B5** 4PB stiffness test at 10 °C (University of Nottingham, UK)

Frequency (Hz)	Stiffness (MPa)	Phase Angle (°)
1	7957	26.4
2	9444	23.4
5	11523	20.2
10	13150	17.7
15	14048	16.2
20	14439	15.6
25	14648	15.1
30	14624	16.4
1	7670	27.2
1	8394	26.4
2	9947	23.7
5	12126	19.9
10	13810	17.5
15	14701	16.3
20	15275	15.7
25	15688	15.1
30	15974	15.0
1	8146	26.8
1	9119	25.4
2	10719	22.5
5	12962	19.2
10	14697	16.7
15	15522	12.0
20	16044	15.0
25	16397	14.4
30	16610	14.3
1	8749	25.6
1	9521	24.3
2	11155	21.8
5	13343	18.5
10	15030	16.0
15	15890	15.0

20	16385	14.4
25	16731	13.8
30	16921	13.7
1	9243	24.6
1	9459	24.2
2	11159	21.8
5	13416	18.4
10	15051	16.5
15	15908	15.1
20	16542	14.6
25	16931	14.4
30	17327	13.5
1	9244	24.9
1	9367	24.6
2	10994	22.1
5	13244	18.9
10	14948	16.5
15	15845	15.5
20	16269	15.1
25	16602	15.3
30	17325	17.5
1	9072	25.0
1	8603	26.8
2	10189	24.4
5	12492	20.2
10	14276	18.1
15	15206	16.8
20	15772	16.0
25	16020	15.4
30	16216	15.2
1	8303	27.5

**Table B6** IT-CY stiffness test (University of Nottingham, UK)

<b>Temperature (°C)</b>	<b>Stiffness (Mpa)</b>
5	8847
5	9428
5	9398
5	9589
5	9140
10	5284
10	5437
10	5058
10	5447
10	6491
10	8322
10	7736
10	7965
10	7077
10	7403
10	6028
10	6891
10	6092
10	7022
10	7286
10	7731
10	6609
10	6671
20	1516
20	1405
20	1648
20	1659
20	1763
20	2158
20	2241
20	2248
20	2069
20	2033
20	1858
20	2247
20	1942
20	1775
20	1681
20	1902
20	1674
20	2395
20	2314

**Table B7** 2PB Fatigue test at 20°C and 15Hz in strain control mode

Strain Level ( $\mu\epsilon$ )	Initial Stiffness $E_0$ (Mpa)	$N_{f_{50\%}}$
124	3756	953244
120	3759	681862
140	4095	595498
158	4332	399921
145	5917	303400
178	4051	172294
180	3428	195630

**Table B8** 2PB Fatigue test at 20°C and 25Hz in strain control mode

Strain Level ( $\mu\epsilon$ )	Initial Stiffness $E_0$ (Mpa)	$N_{f_{50\%}}$
142	4775	222437
142	5013	187850
160	4637	130307
157	4620	121058
185	4374	82147
180	4732	76547
187	4578	58497
190	4640	94470

**Table B9** 2PB Fatigue test at 10°C and 15Hz in strain control mode

Strain Level ( $\mu\epsilon$ )	Initial Stiffness $E_0$ (Mpa)	$N_{f_{50\%}}$
87	10069	1239150
90	10585	1127009
90	10358	848083
104	9947	561855
105	10688	602085
106	10734	640683
108	10463	557413
114	10025	351178
115	9987	343231
117	10830	177597
119	10189	132904
150	8950	47200
151	8941	124600
153	8281	39700
170	8599	75700
173	8587	32900

**Table B10** 2PB Fatigue test at 10°C and 25Hz in strain control mode

Strain Level ( $\mu\epsilon$ )	Initial Stiffness $E_0$ (Mpa)	$N_{f50\%}$
84	11888	1008972
88	11160	1198681
91	11862	935122
93	11788	678376
94	11967	1012494
94	11983	890526
95	11905	1123379
112	12107	183493
115	11791	302358
115	11163	216982
116	11873	405438
116	11456	252832

**Table B11** 4PB Fatigue test at 10°C and 25Hz in strain control mode

Strain Level ( $\mu\epsilon$ )	Initial Stiffness $E_0$ (Mpa)	$N_{f50\%}$
100	15880	481500
120	15501	221500
130	17266	191500
140	16359	78000
160	14450	49500
160	16805	59000
180	14766	28000
200	15827	31500
220	16016	23500

**Table B12** 4PB Healing test at 10°C and 25Hz in strain control mode

Strain Level ( $\mu\epsilon$ )	Load time (min)	Load no cycle	Rest time (min)	Rest no cycle	Initial Stiffness $E_0$ (Mpa)	$N_{f50\%}$
160	-	-	-	-	16805	59000
160	400	10000	400	10000	17762	58800
160	400	10000	4000	100000	15641	73400
160	400	10000	1200	30000	16351	77300
160	40	1000	400	10000	17207	148002
160	400	10000	2000	50000	17051	62801
160	800	20000	400	10000	17054	70501
160	400	10000	400	10000	16255	80000
160	400	10000	800	30000	15596	70001
160	400	10000	3000	75000	16537	75002
160	1200	30000	400	10000	17058	64901
160	400	10000	2000	50000	15922	79901
160	400	10000	1000	25000	11066	25000

**Table B13** ITFT test at 10°C in stress control mode

Stress Level (KPa)	Initial Stiffness E <sub>0</sub> (Mpa)	Nf (fracture)
200	8931	640500
250	8250	199500
300	7895	246500
400	8880	68000
500	8145	16000
500	7642	35166
600	8103	9300

**Table B14** ITFT test at 20°C in stress control mode

Stress Level (KPa)	Initial Stiffness E <sub>0</sub> (Mpa)	Nf (fracture)
100	2288	56000
200	3344	12500
300	3256	3000
400	3092	1000

**Table B15** ITFT test at 10°C in strain control mode

Strain Level (µε)	Initial Stiffness E <sub>0</sub> (Mpa)	Nf <sub>50%</sub>
80	7593	239500
100	8132	167500
120	7022	57000
140	7077	33500
160	7965	17000
170	7403	12000
180	8322	18500

**Table B16** ITFT Healing test at 10°C in strain control mode

Strain Level (µε)	Load time (min)	Load no Pulse	Rest time (min)	Rest no cycle	Initial Stiffness E <sub>0</sub> (Mpa)	Nf <sub>50%</sub>
160	-	-	-	-	7965	17000
160	126	15000	84	10000	7300	20500
160	84	10000	84	10000	7037	27000
160	42	5000	84	10000	8718	22500
160	42	5000	42	5000	8255	18000
160	126	15000	42	5000	7920	22000
160	42	5000	9	1000	8129	22500
160	84	10000	42	5000	8082	14730
160	126	15000	126	15000	7272	26000
160	42	5000	126	15000	7994	21500
160	84	10000	126	15000	8813	16000

## Data for 20mm DBM

**Table B17** Air Void and dimensions of trapezoidal specimens (2PB)

Specimen ID	Air void (%)	e (mm)	B (mm)	b (mm)	h (mm)
10-2230	5.3	25.2	68.9	25.3	250.3
10-2226	5.7	25	68.5	24.4	251
10-1823	6.2	24.9	69.7	25.2	252.7
10-1820	5.4	25.4	69.9	25.1	252.1
10-1804	5.7	25.5	70	24.6	250.1
10-1803	5.0	25.3	70	25.7	249.8
10-2232	5.4	24.9	68.5	25.2	250.5
10-2231	5.5	25.4	68.5	25.1	251
10-1807	5.2	25.7	69.6	24.9	250.5
10-1819	5.2	25.3	69.6	25.3	251.8
10-1810	5.4	25.4	69.7	25.4	250.4
10-1808	6.2	25.6	69.9	25.2	250.4
10-1796	5.7	25.5	69.8	25.5	250.1
10-1800	5.8	25.5	70	25.2	250.3
10-1793	5.1	25.4	70	25.4	249
10-1806	5.3	25.4	69.5	25.5	250.2
10-1798	5.0	25.3	69.6	25	250
10-1799	6.5	25.5	69.7	25.2	250.3

**Table B18** Air Void and Dimensions of cylindrical specimens (ITFT)

Specimen ID	Bulk Density (Kg/m <sup>3</sup> )	Target Density (Kg/m <sup>3</sup> )	Air Void (%)	Diameter (mm)	Thickness (mm)
11-863	2373	2600	9	99	39.2
11-872	2401	2600	8.3	98.9	39.8
11-870	2376	2600	8.3	99	40.6
11-857	2385	2600	8.2	99.1	39.7
11-868	2420	2600	7.4	99	40.3
11-877	2400	2600	7.5	98.9	39.1
11-850	2415	2600	7.4	98.9	39.5
11-864	2450	2600	6	99	39.7
11-860	2375	2600	9	98.9	40
11-869	2438	2600	6.4	99	40.4
11-865	2412	2600	7.2	99	40.1
11-852	2402	2600	8	98.9	39.2
11-851	2405	2600	7.6	99	40.2
11-855	2384	2600	8.1	99	40.5
11-849	2387	2600	8.7	98.9	41.5
11-856	2373	2600	8.8	98.9	40.3
11-859	2364	2600	8.9	99.1	40.5
11-858	2353	2600	9.8	99	40.8

**Table B19** 2PB stiffness test

Temperature (°C)	Frequency (Hz)	E*  (MPa)	Phase Angle (°)
-20	1	26752	3.1
-20	2	27285	2.8
-20	5	27950	2.4
-20	10	28466	2.0
-20	15	28587	1.8
-20	20	28849	2.3
-20	25	28964	2.2
-20	30	29046	2.1
-15	1	25381	3.8
-15	2	26041	3.4
-15	5	26801	2.9
-15	10	27413	2.6
-15	15	27547	2.3
-15	20	27870	2.7
-15	25	28087	2.6
-15	30	28208	2.5
-10	1	22693	5.5
-10	2	23585	4.9
-10	5	24650	4.1
-10	10	25432	3.4
-10	15	25667	3.4
-10	20	26065	3.6
-10	25	26357	3.5
-10	30	26435	3.4
-5	1	19935	7.5
-5	2	21040	6.7
-5	5	22376	5.6
-5	10	23290	5.0
-5	15	23697	4.5
-5	20	24066	4.8
-5	25	24380	4.8
-5	30	24631	4.5
0	1	16410	10.7
0	2	17653	9.5
0	5	19248	8.0
0	10	20427	7.0
0	15	20972	6.5
0	20	21423	6.7
0	25	21807	6.5
0	30	22094	6.2
5	1	12632	15.5
5	2	13978	13.7
5	5	15827	11.4
5	10	17182	10.1
5	15	17865	9.2
5	20	18366	9.3
5	25	18827	9.0
5	30	19154	8.6
10	1	8968	22.0

10	2	10403	19.3
10	5	12307	16.1
10	10	13791	14.2
10	15	14600	12.9
10	20	15205	12.8
10	25	15692	12.4
10	30	16022	11.8
15	1	5668	30.3
15	2	6942	26.8
15	5	8849	22.6
15	10	10346	19.7
15	15	11194	18.1
15	20	11838	17.7
15	25	12347	17.1
15	30	12753	16.4
20	1	3269	38.7
20	2	4256	35.4
20	5	5860	30.4
20	10	7237	26.8
20	15	8057	24.8
20	20	8657	24.2
20	25	9146	23.4
20	30	9584	22.6
25	1	1720	46.3
25	2	2367	43.5
25	5	3582	38.7
25	10	4664	34.9
25	15	5372	32.6
25	20	5886	32.0
25	25	6378	30.9
25	30	6756	30.1
30	1	857	50.2
30	2	1225	49.2
30	5	2005	46.1
30	10	2782	42.9
30	15	3325	40.9
30	20	3713	40.4
30	25	4062	40.1
30	30	4375	39.7

**Table B20** IT-CY stiffness test (University of Nottingham, UK)

Temperature (°C)	Stiffness (Mpa)
10	10582
10	10206
10	10231
10	11081
10	10220
10	9828
10	10089
10	9245
10	9928
10	9133
10	9913
10	12539
10	10329
10	9713
10	10900
10	10361
10	9660
10	10976

**Table B21** 2PB fatigue test at 10 °C and 25 Hz in strain control mode

Strain Level ( $\mu\epsilon$ )	Initial Stiffness $E_0$ (Mpa)	$N_{f50\%}$
75	15888	1084300
75	16518	686900
84	15581	943900
85	16225	888950
99	15663	373900
105	15158	1354950
122	15459	154900
123	15796	254700
140	16067	162100
183	15630	29900

**Table B22** 2PB fatigue test at 10 °C and 25 Hz in stress control mode

Stress Level (kPa)	Initial Stiffness $E_0$ (Mpa)	$N_{f50\%}$
1153	16071	702883
1167	16329	1184813
1268	17106	1026122
1269	16322	841377
1523	16131	164249
1524	15788	450981
1777	16789	212218
1778	15511	108008

**Table B23** ITFT test at 10 °C in stress control mode

<b>Strees Level (kPa)</b>	<b>Initial Stiffness E<sub>0</sub> (Mpa)</b>	<b>Nf (fracture)</b>
600	12776.52	41217
650	13943.2	34851
700	14641.51	41908
750	14712.94	22213
800	13878.97	15179
850	14465.25	5709
900	12858.78	10751
1000	15221.39	3668
1200	13650.76	1009

**Table B24** ITFT test at 10 °C in strain control mode

<b>Strain Level (με)</b>	<b>Initial Stiffness E<sub>0</sub> (Mpa)</b>	<b>Nf<sub>50%</sub></b>
125	10900	149243
135	10329	126500
145	11081	88923
155	10231	42613
165	10220	49383
175	10582	22393
185	9828	30963
200	9928	18683
220	9245	17773